

FIG. 1

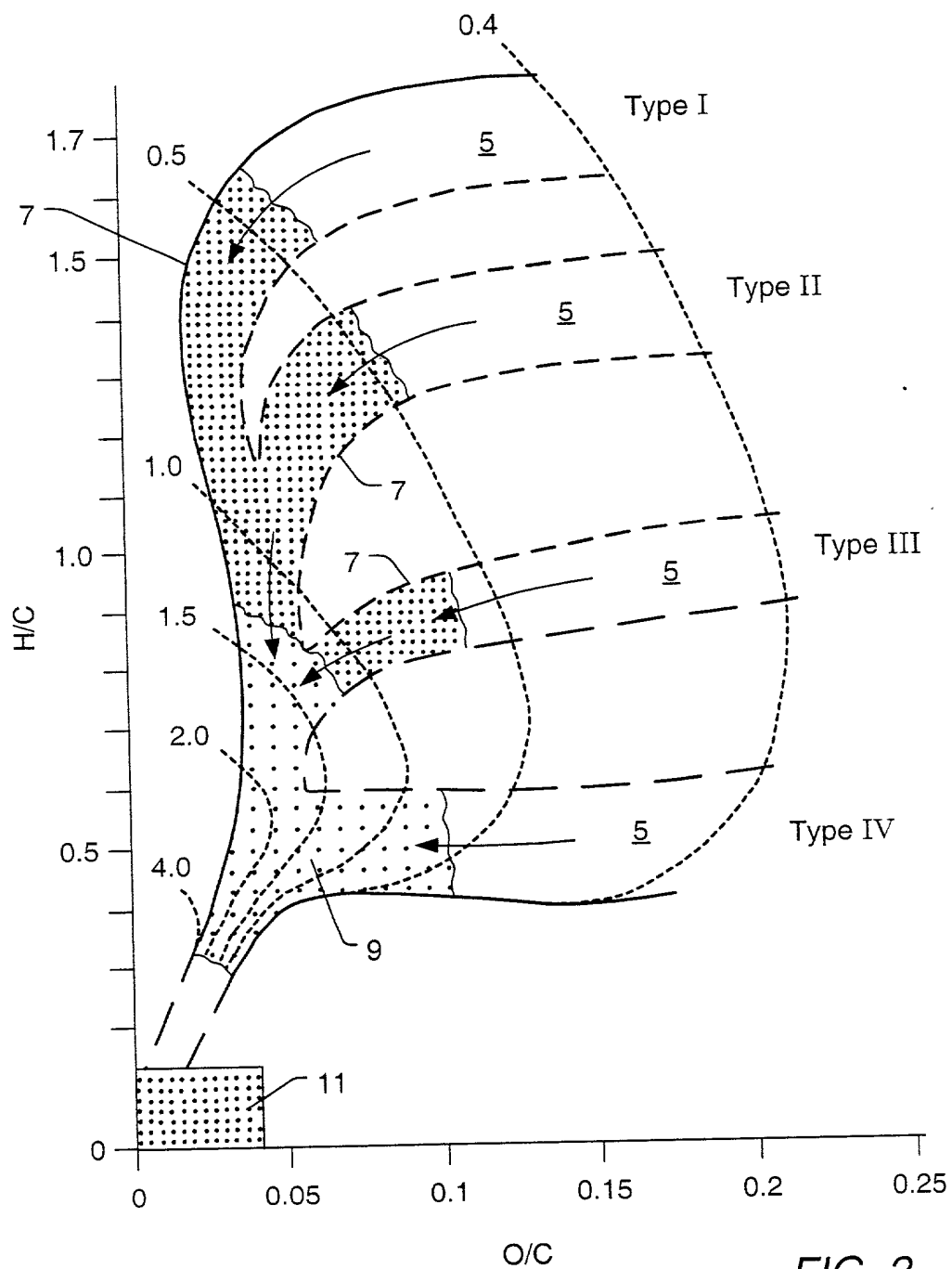


FIG. 2

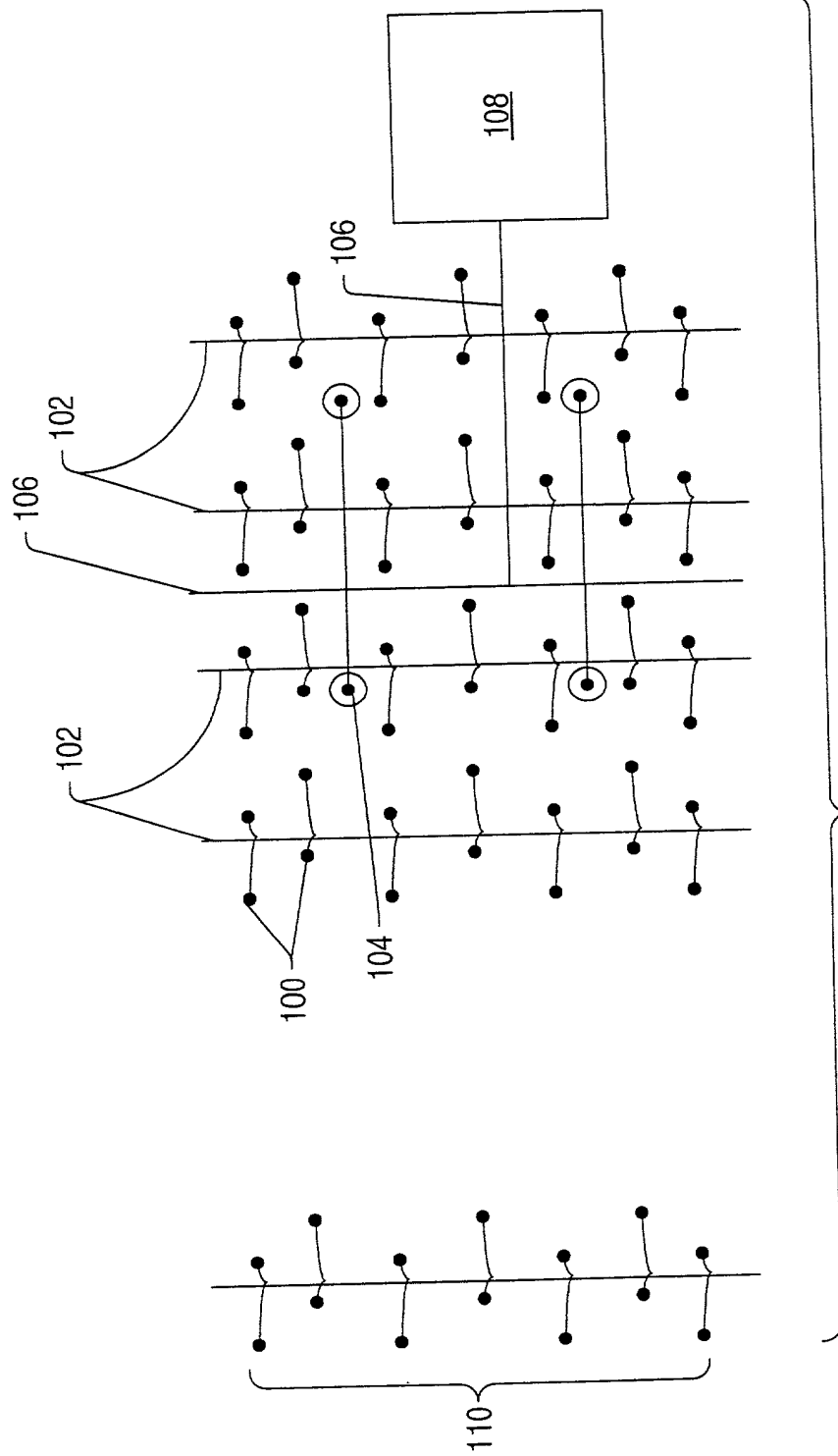


FIG. 3

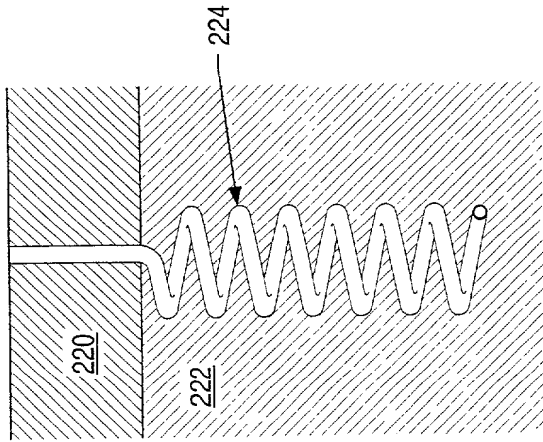


FIG. 3a

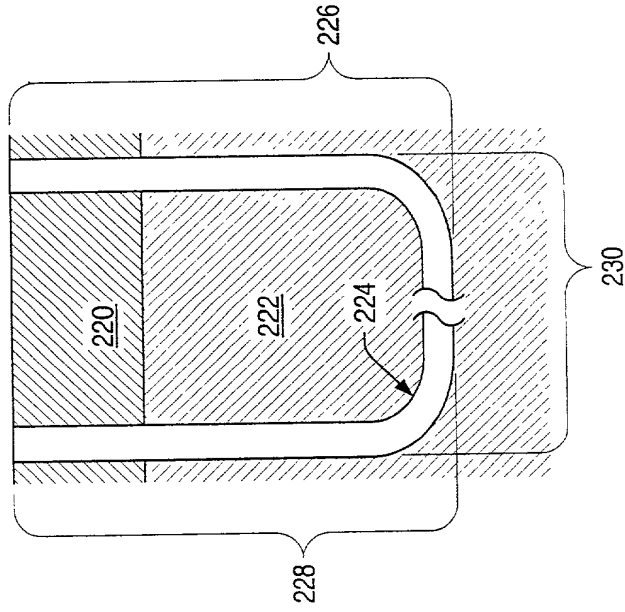


FIG. 3b

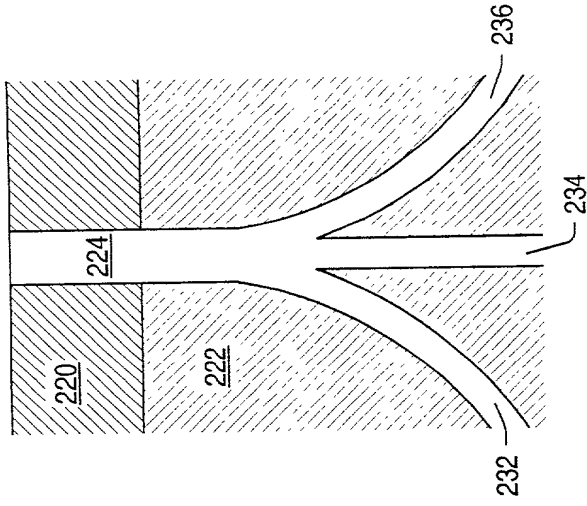
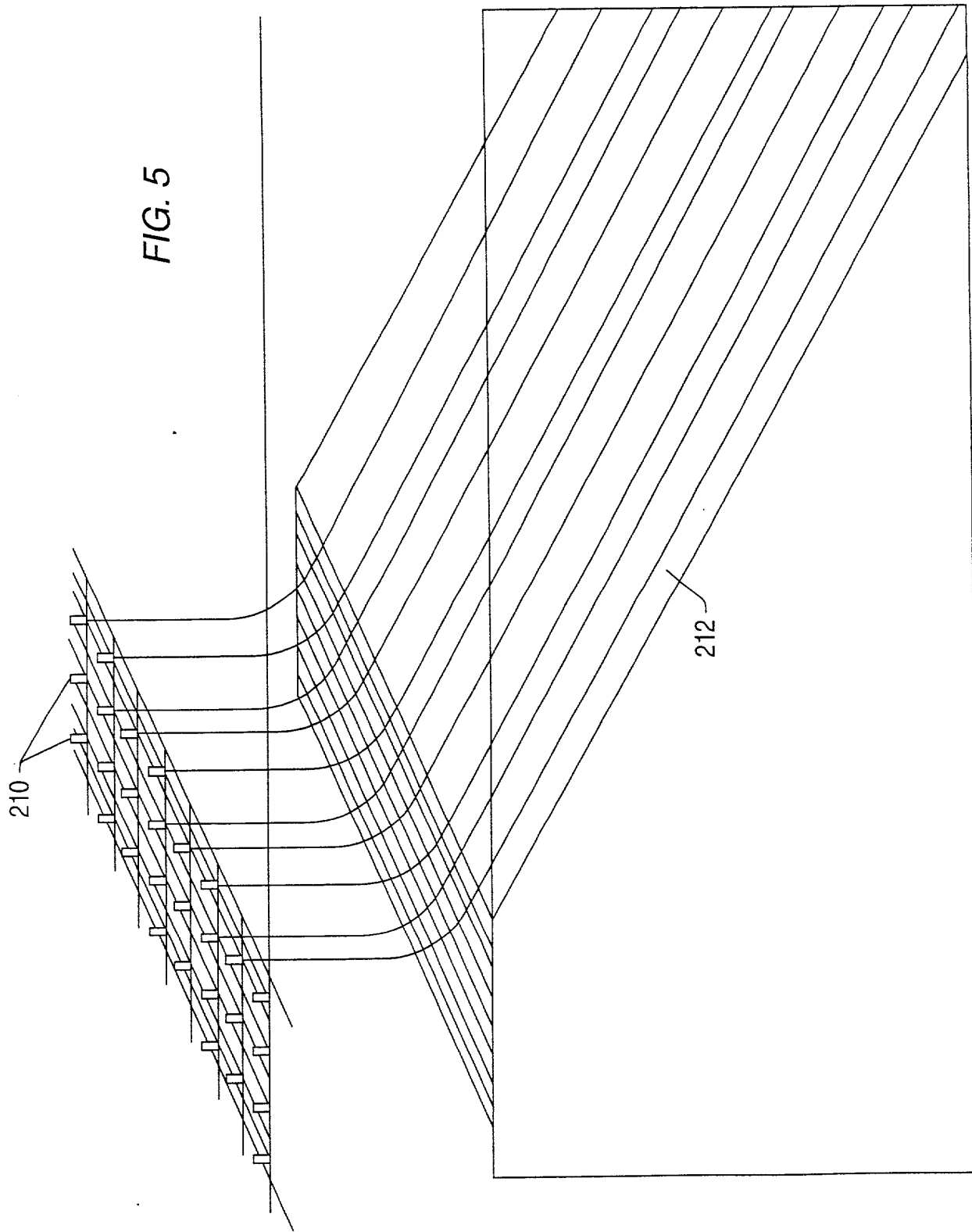


FIG. 3c

200



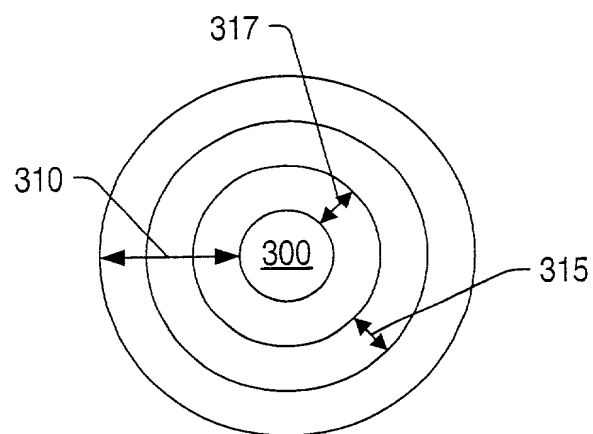


FIG. 6

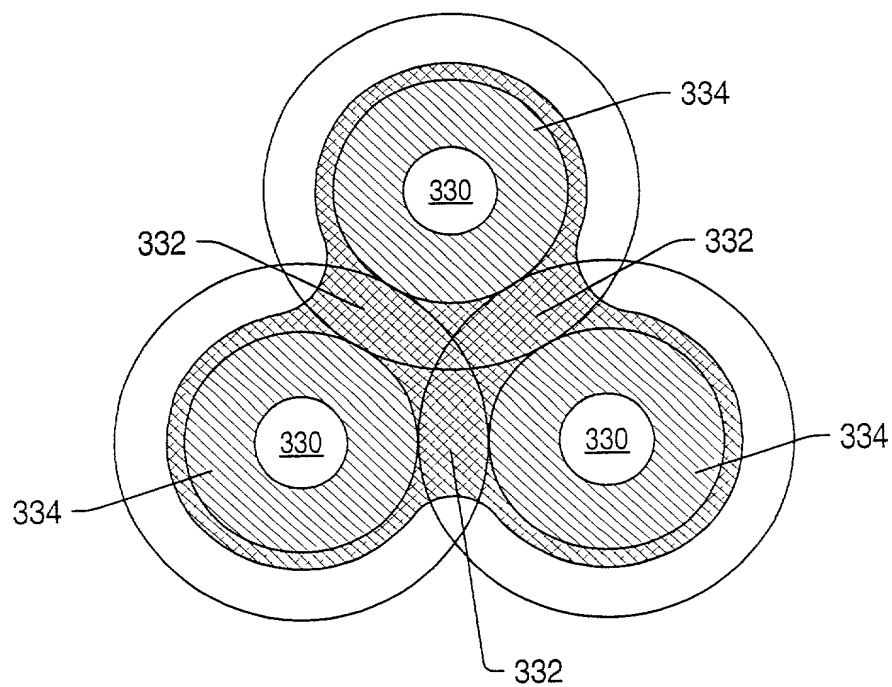


FIG. 7

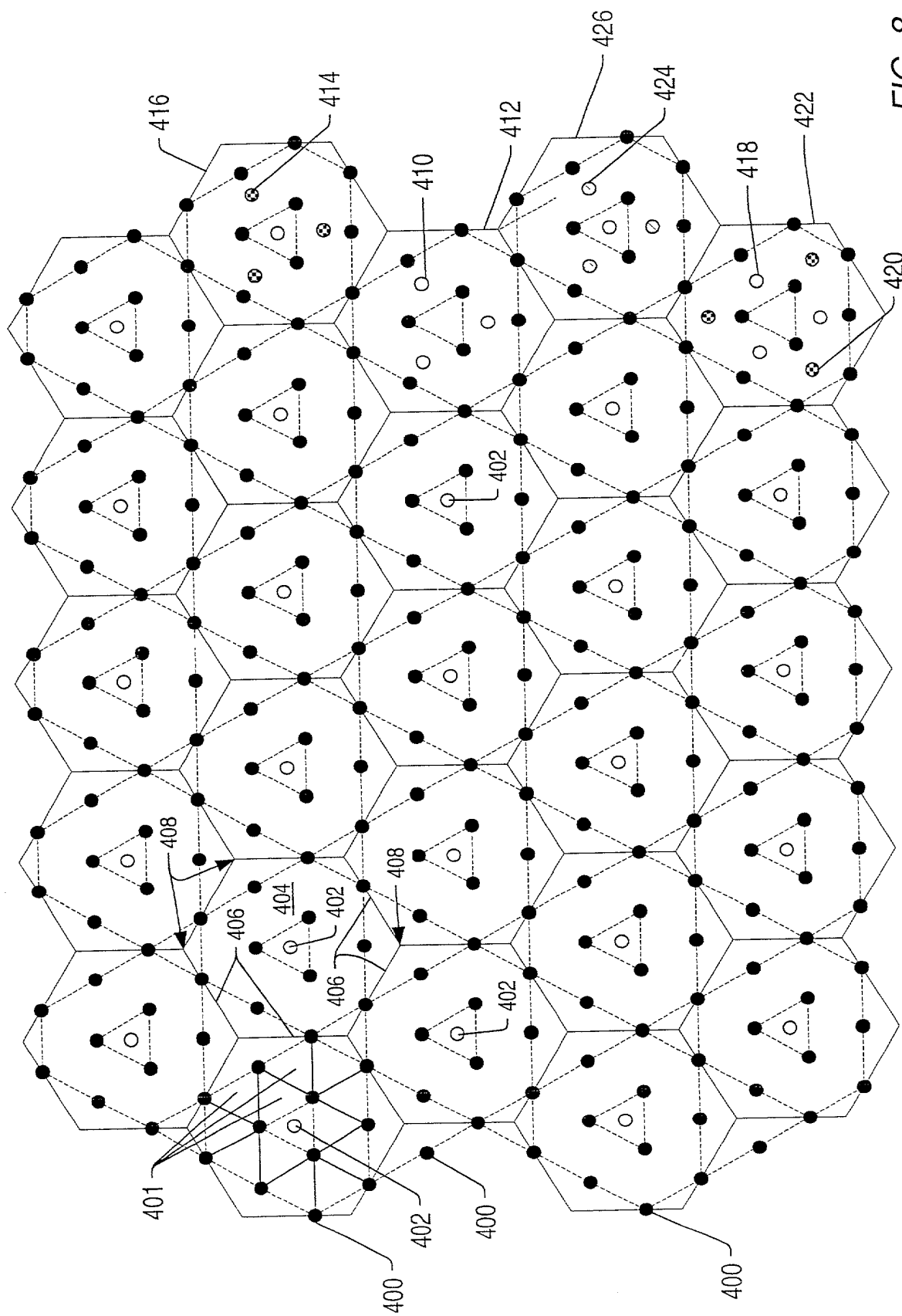


FIG. 8



FIG. 9 is a schematic diagram of a hexagonal lattice structure 400. The lattice is composed of a central hexagon 402 and six surrounding hexagons 404. The vertices of the central hexagon are labeled 400a and 400b. The vertices of the surrounding hexagons are labeled 400a and 400b. The lattice is shown in a perspective view.

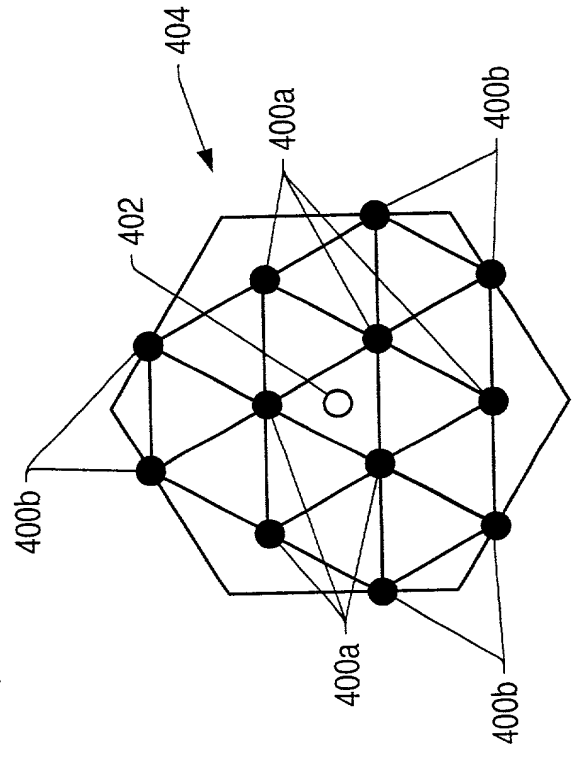


FIG. 9



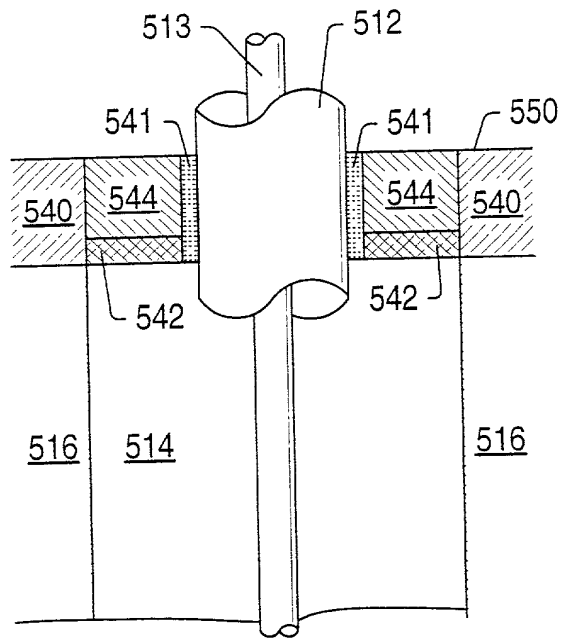


FIG. 11

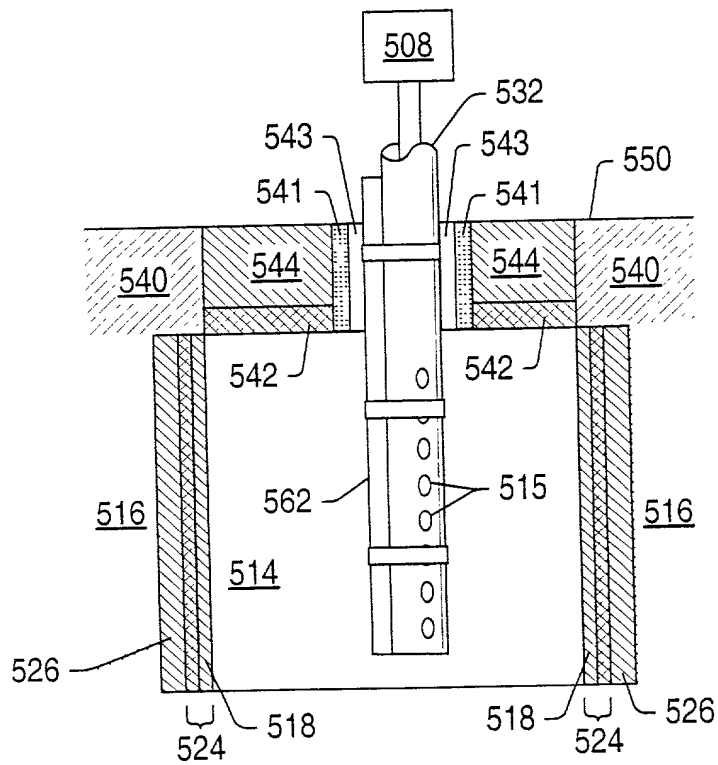
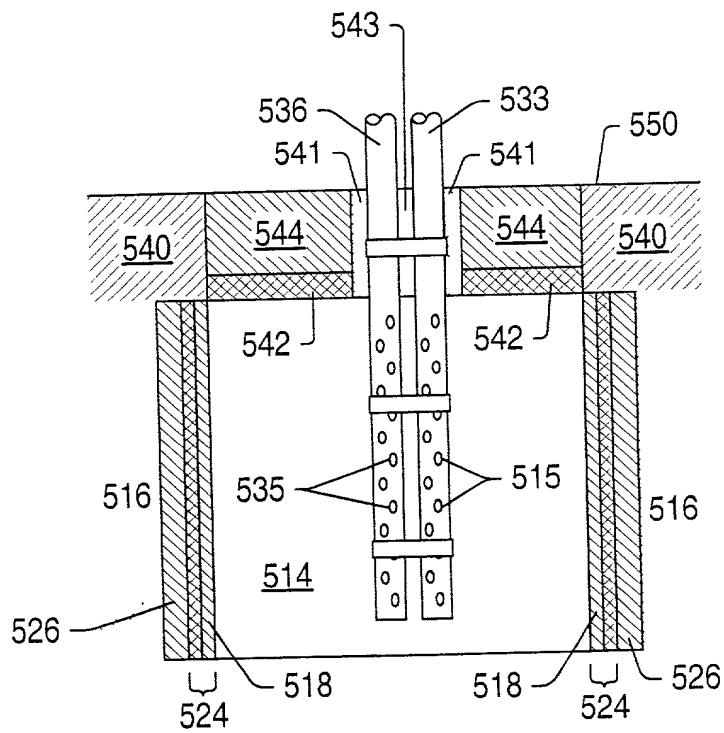


FIG. 12



*Fig. 13*

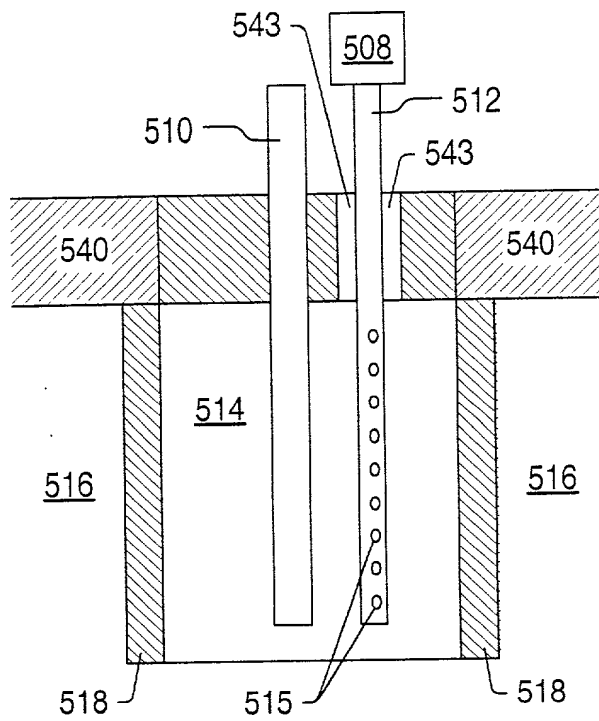


FIG. 14

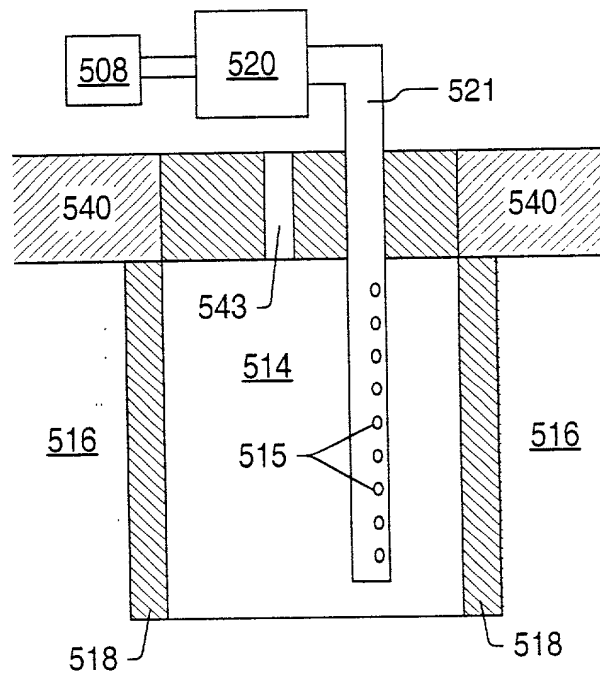


FIG. 15

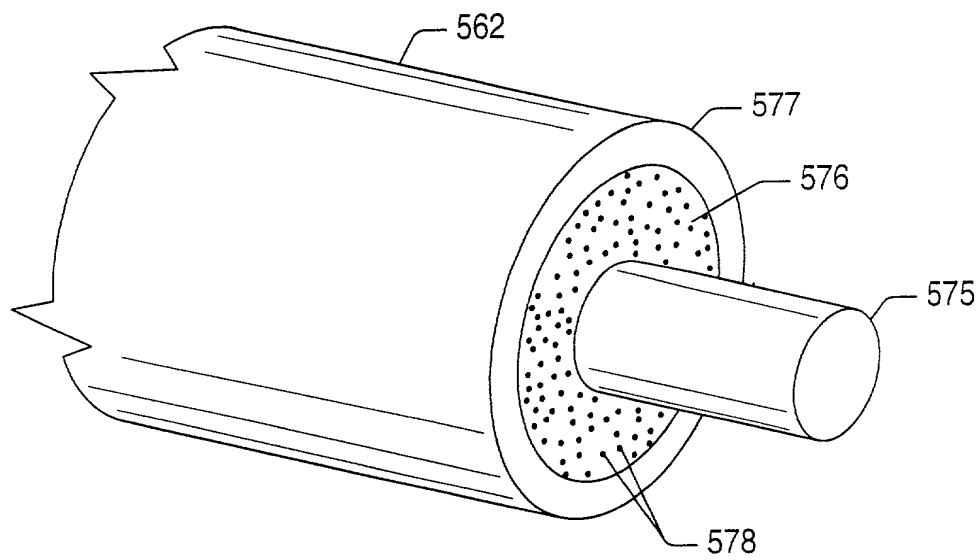


FIG. 16

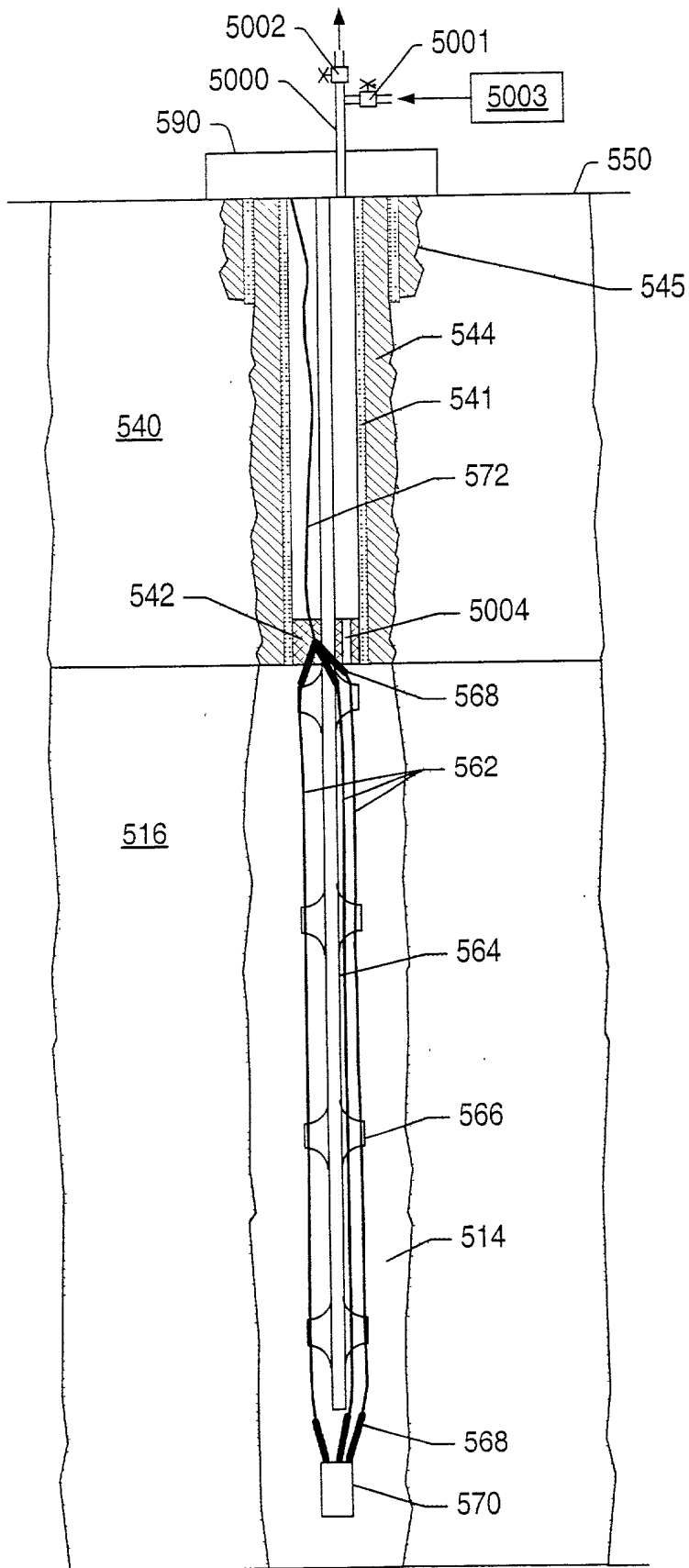


FIG. 17

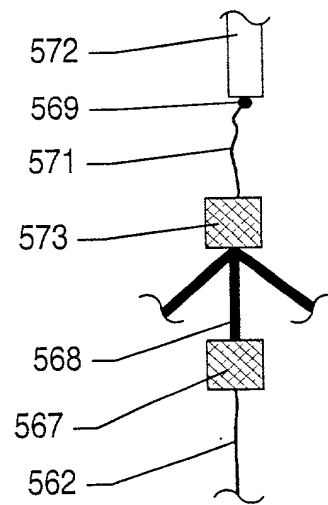


FIG. 17A

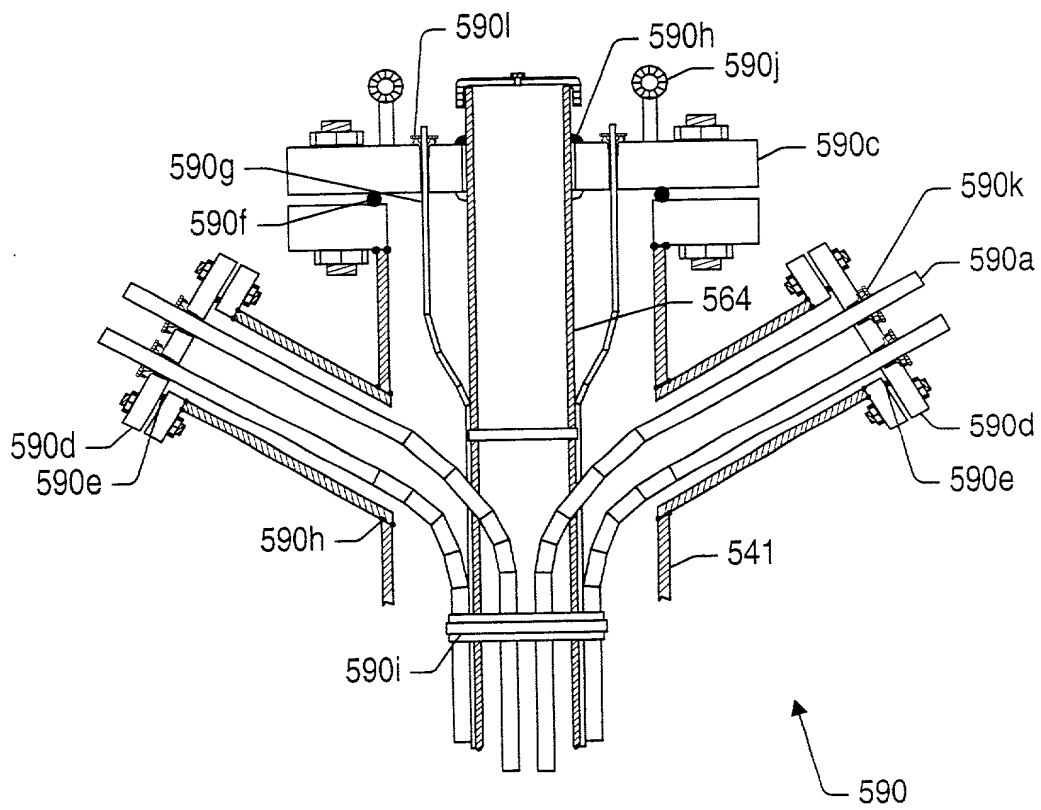


FIG. 18



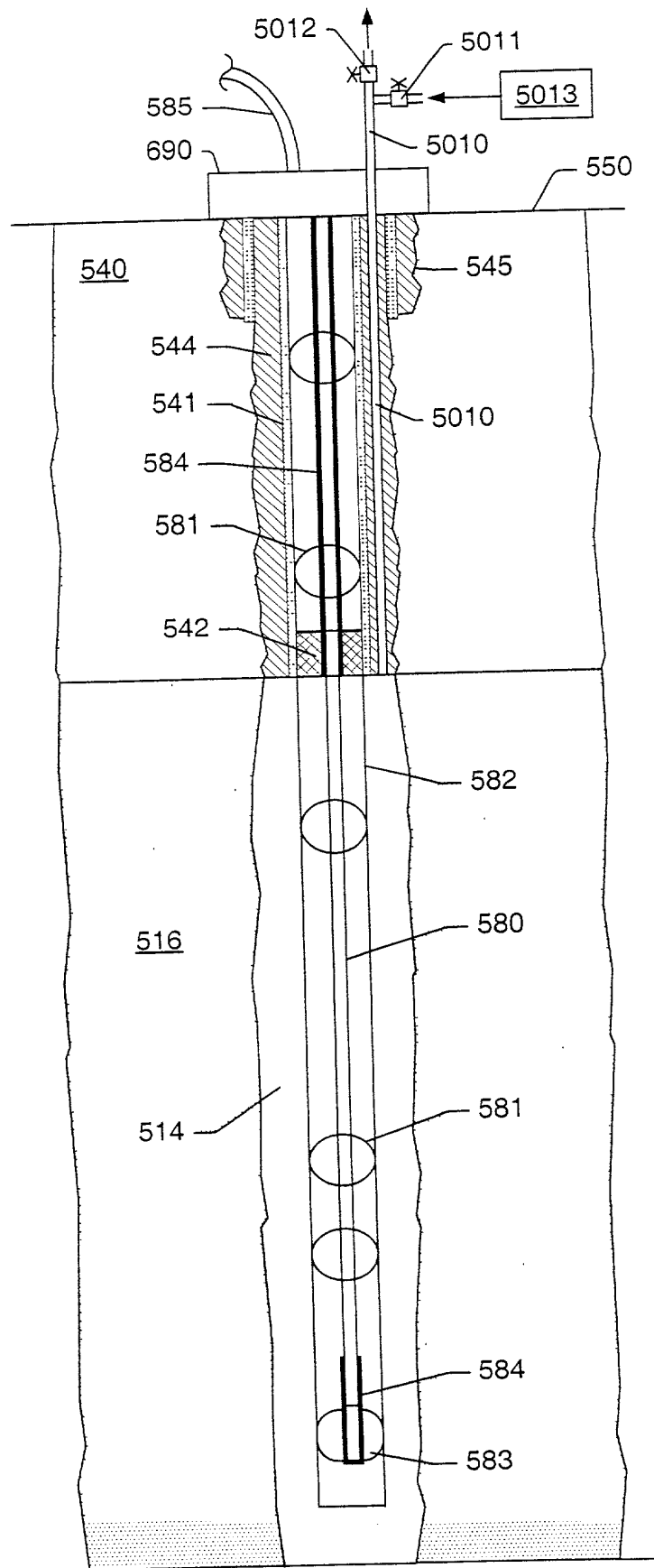


FIG. 19

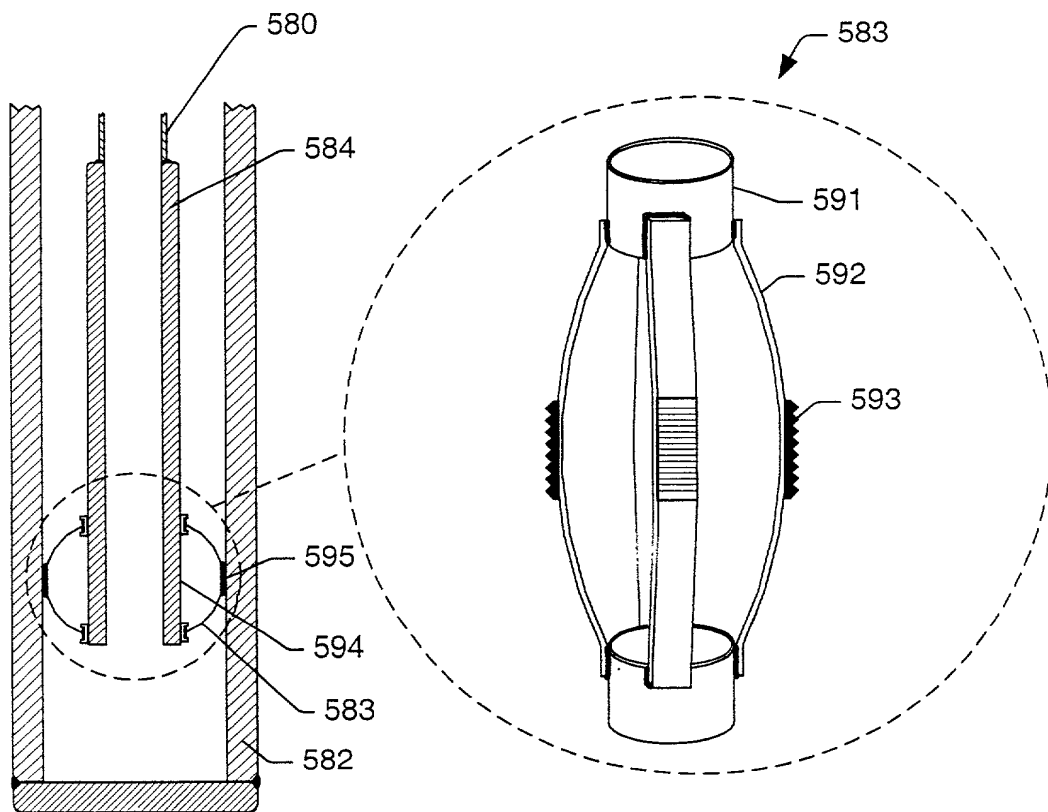


FIG. 20

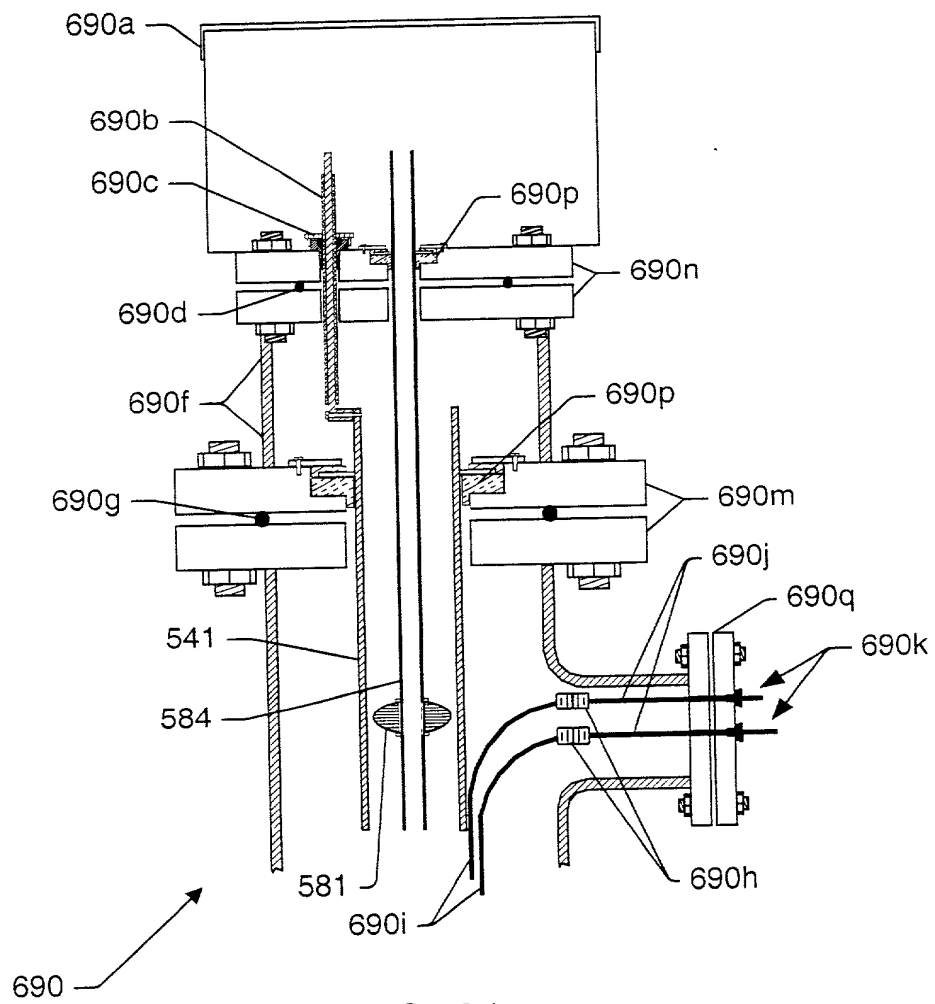


FIG. 21

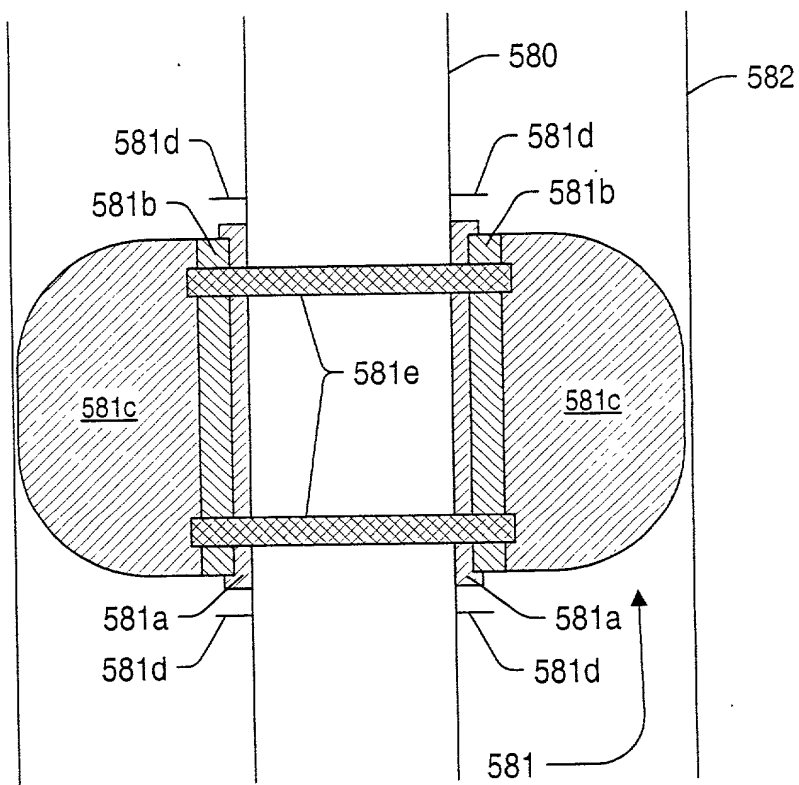


FIG. 22

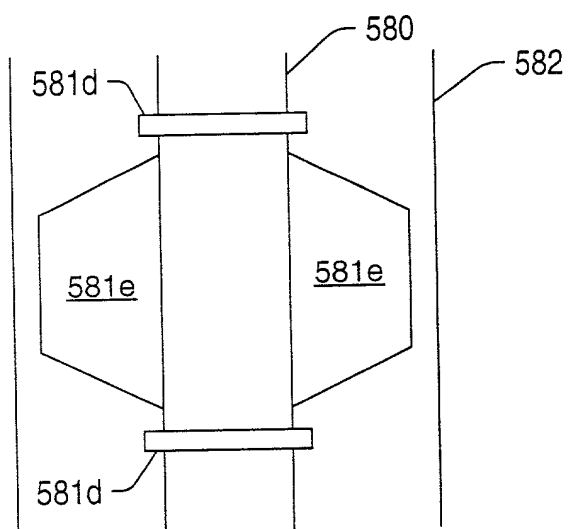


FIG. 23a

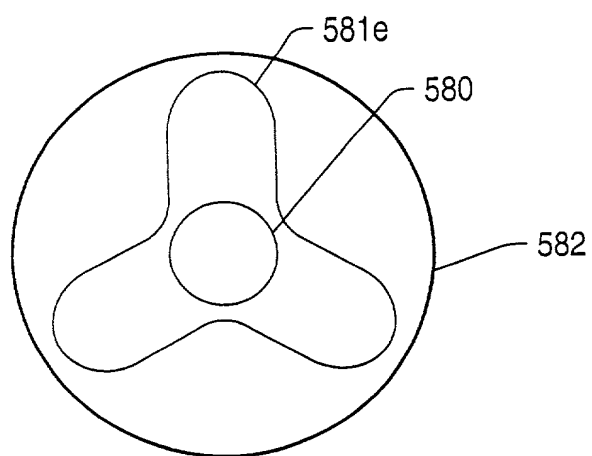


FIG. 23b

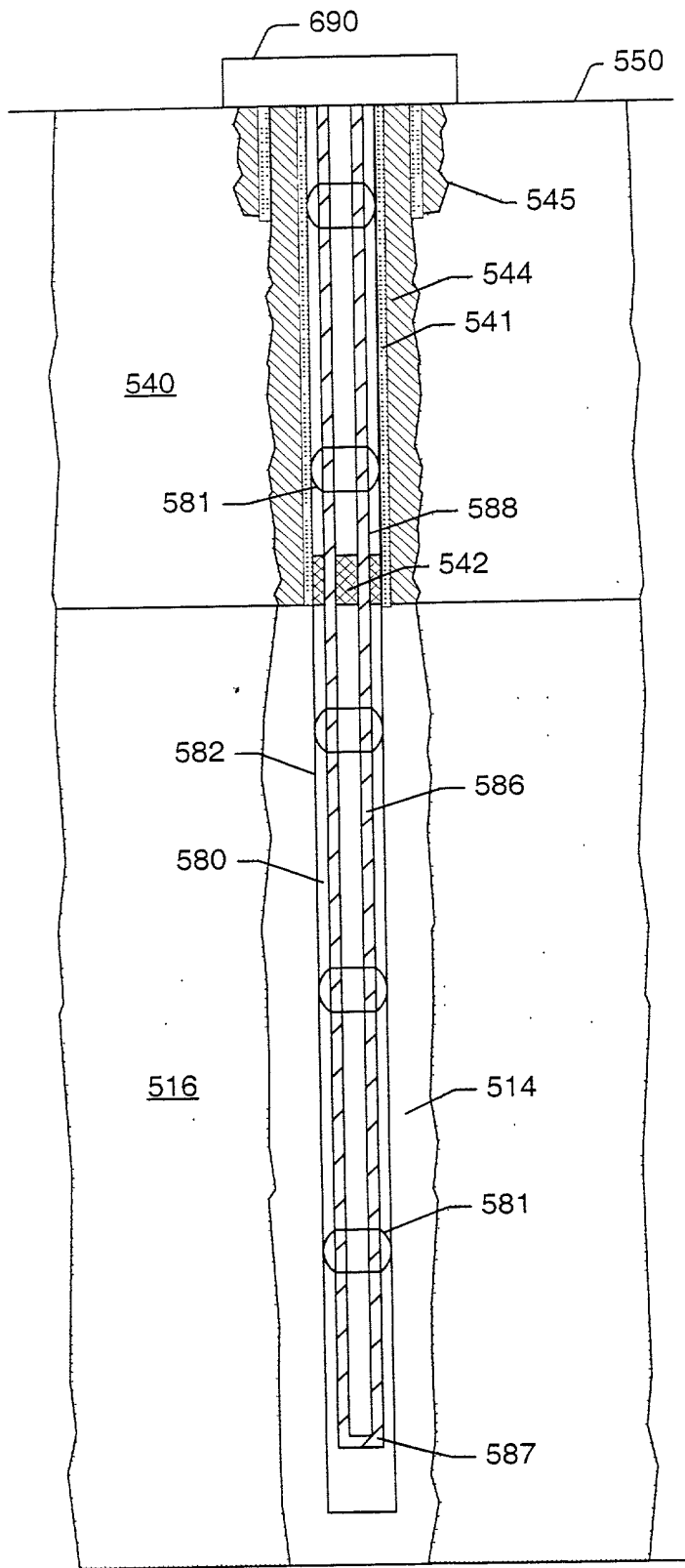


Fig. 24

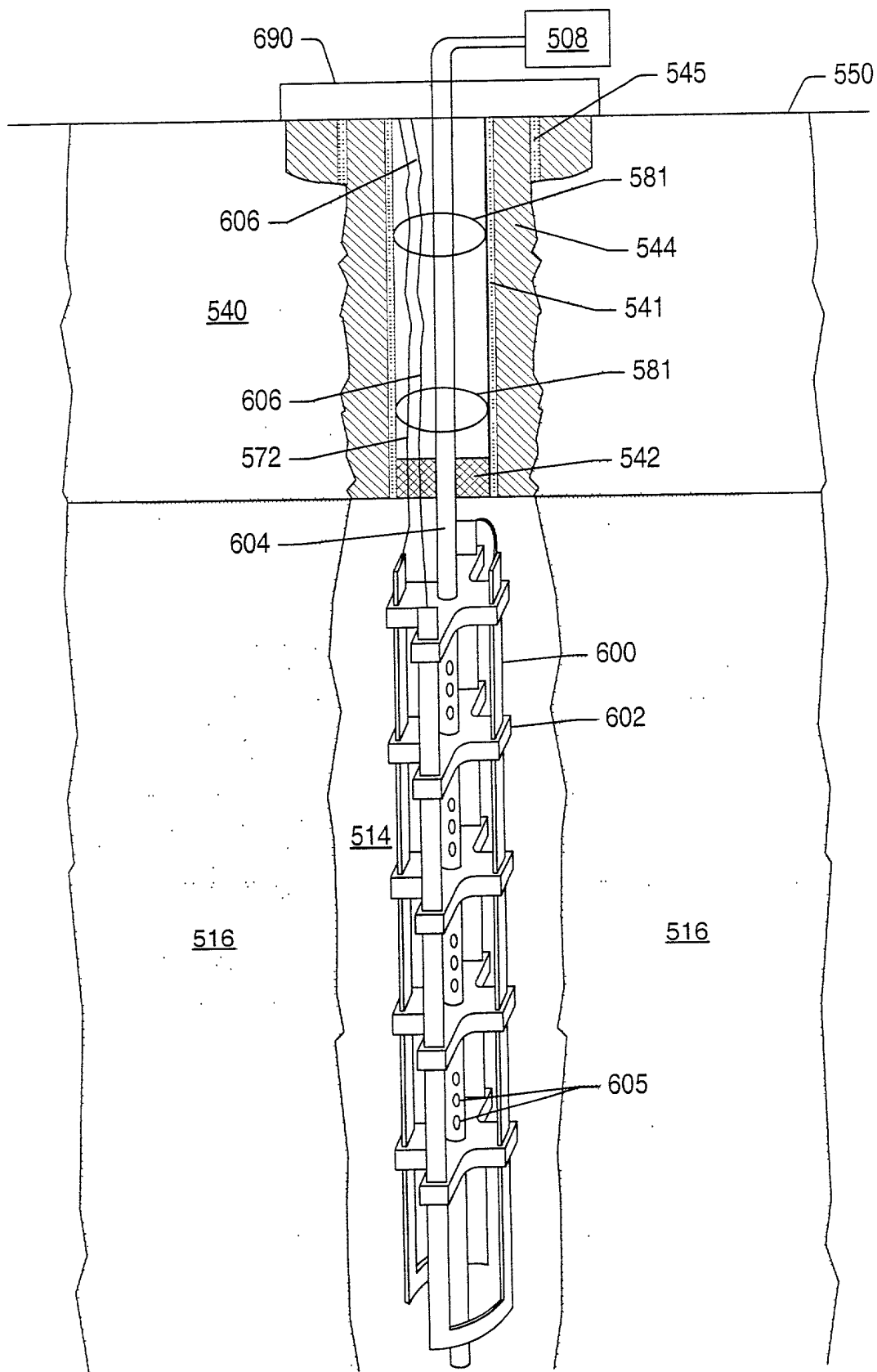


FIG. 25

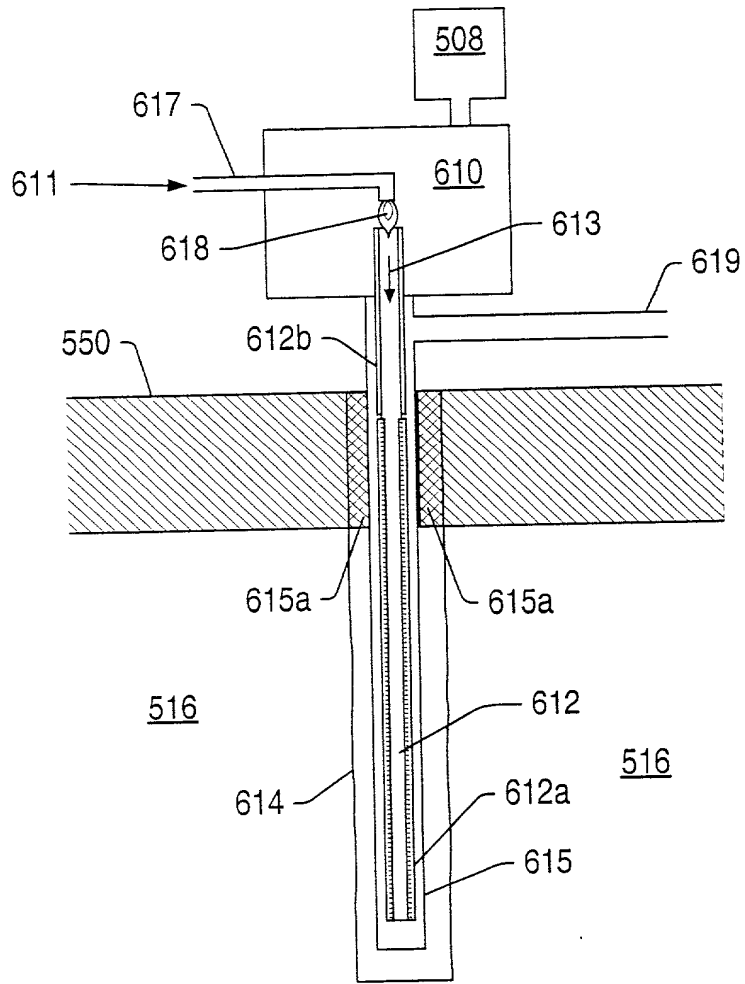


FIG. 26

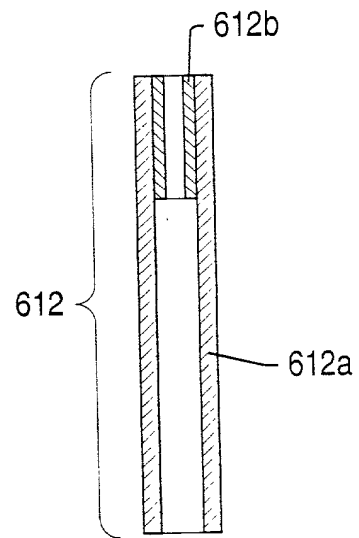


FIG. 27



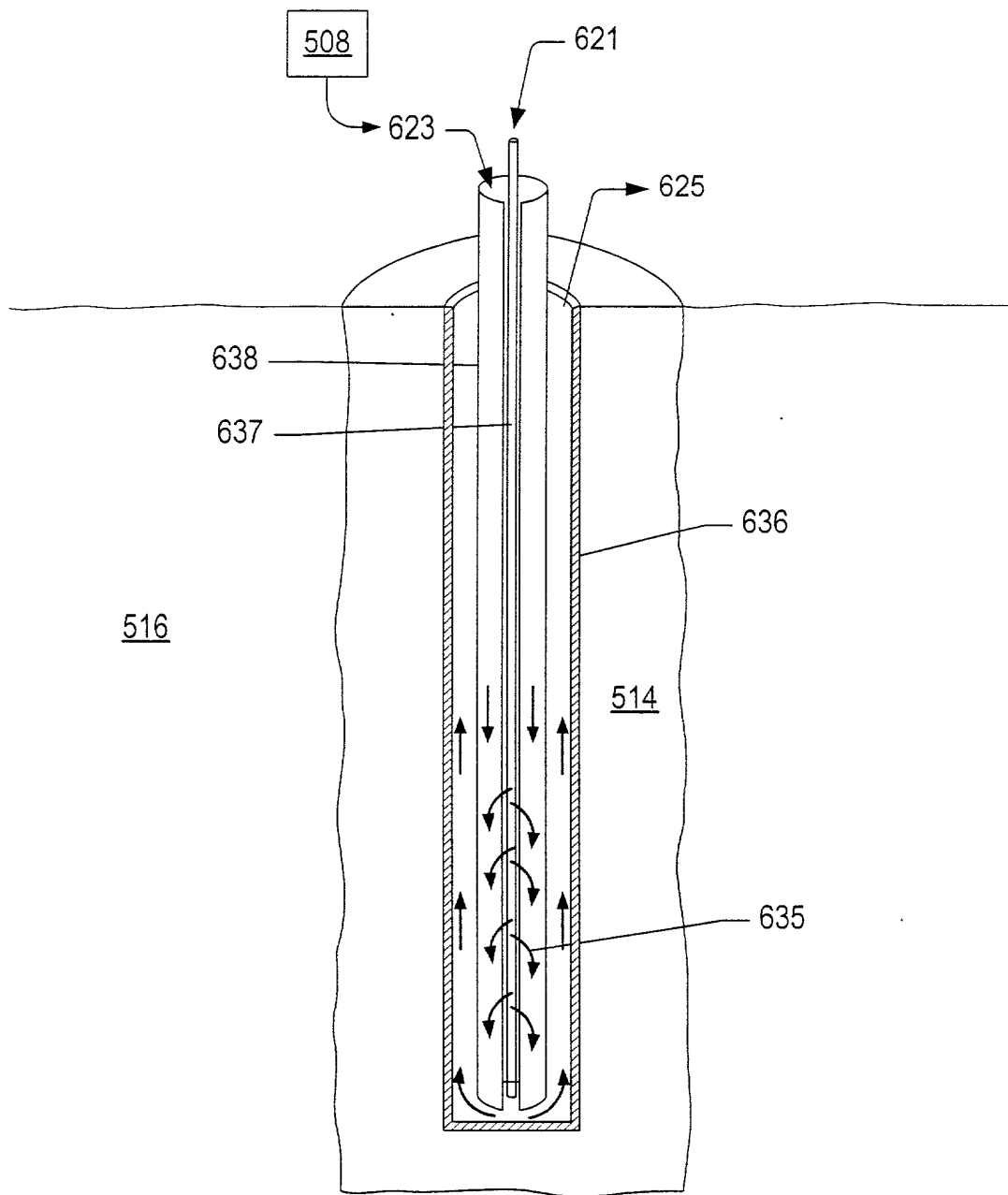


FIG. 28

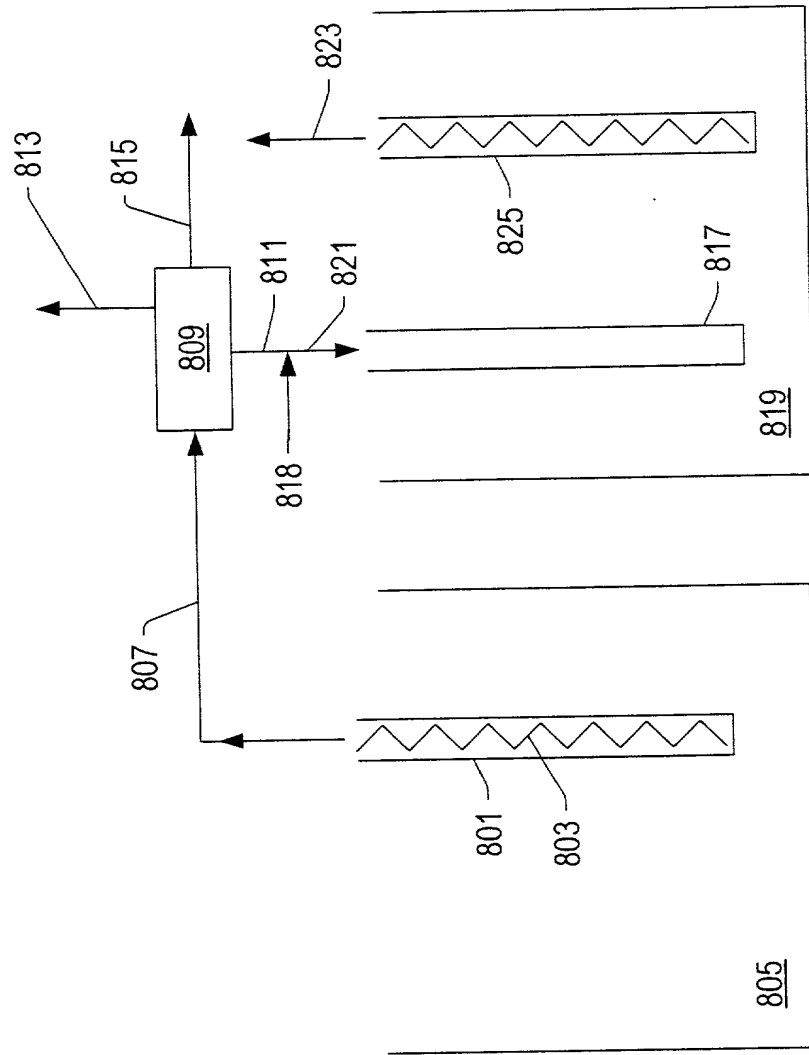


FIG. 29



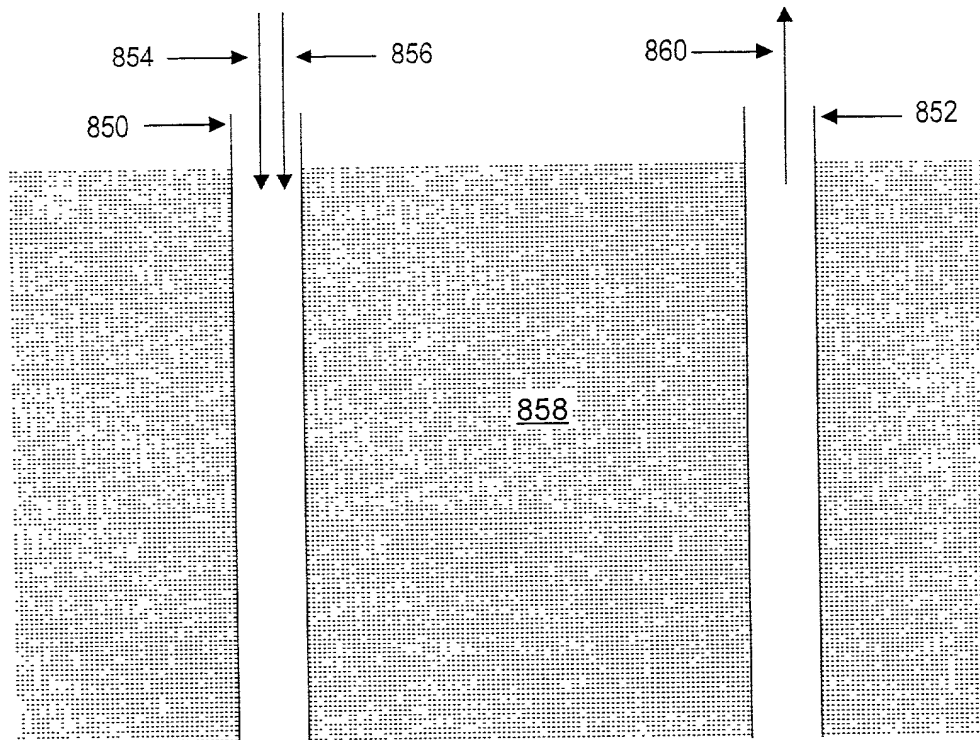


FIG. 31

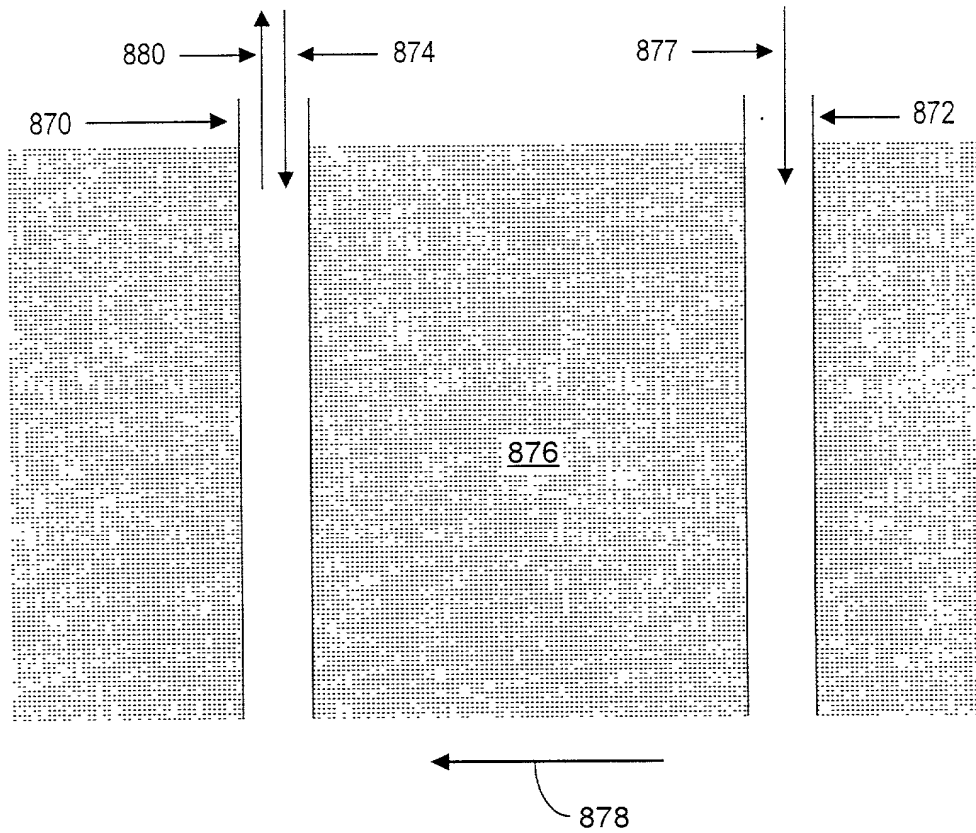


FIG. 32

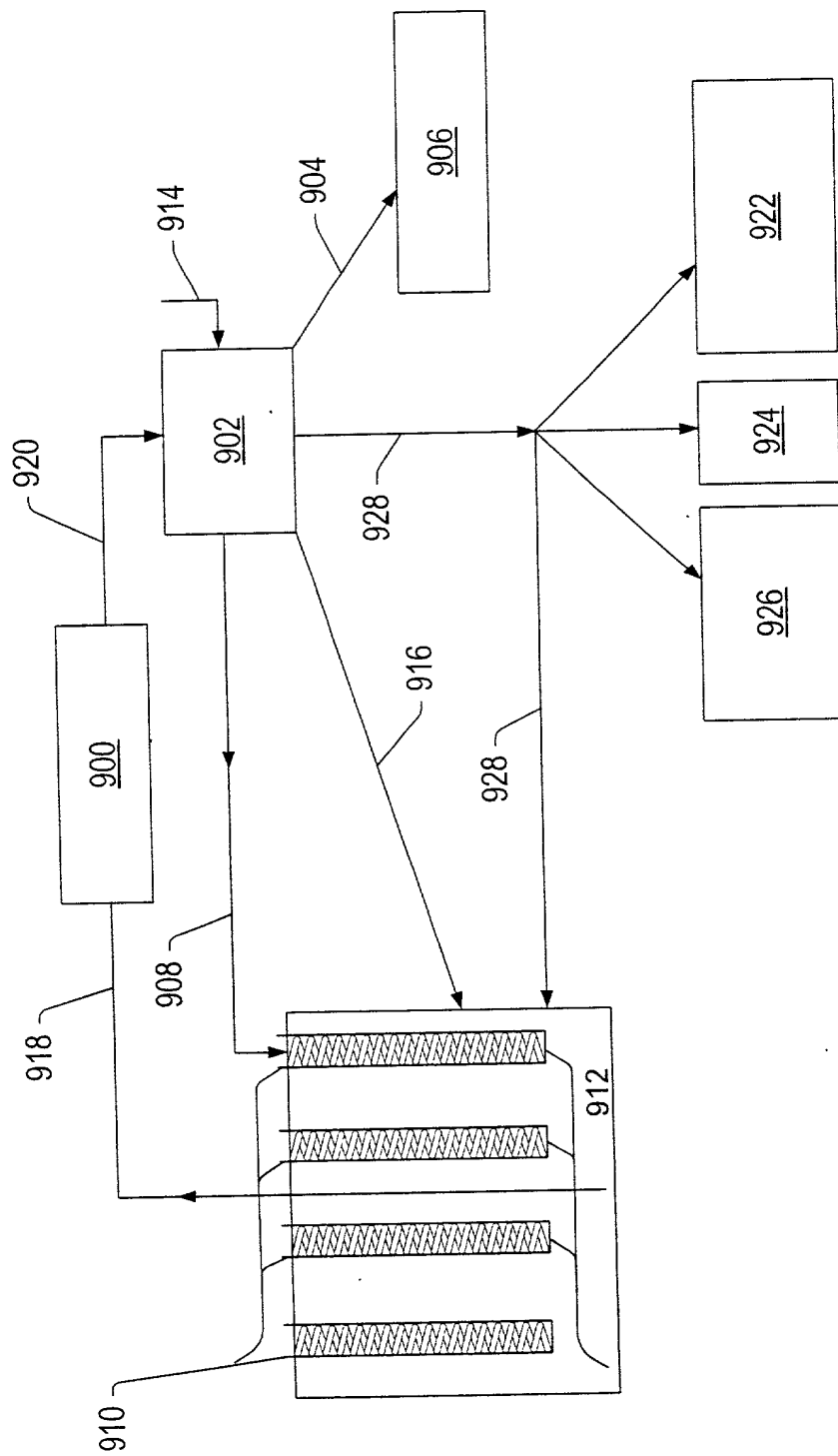


FIG. 33

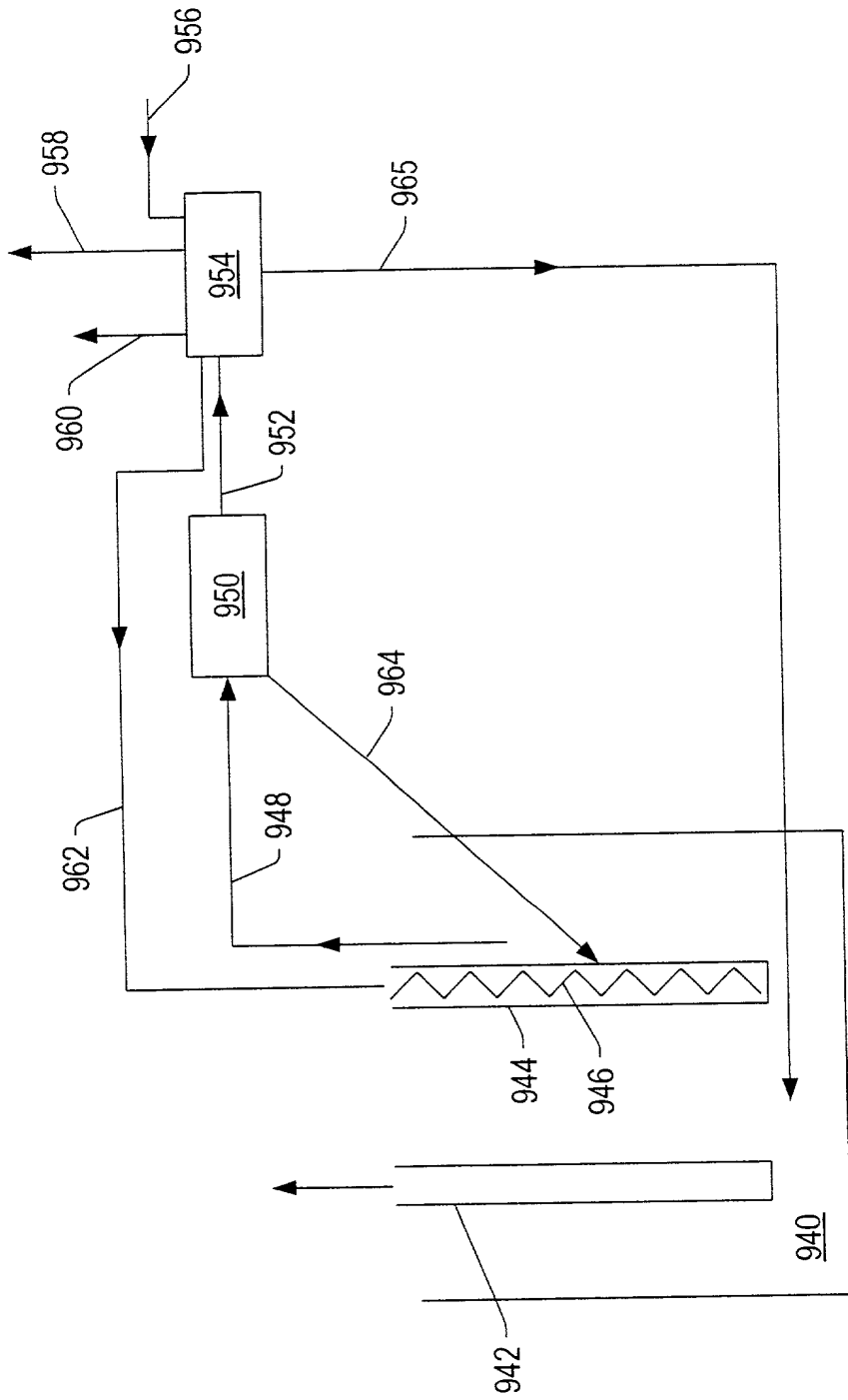


FIG. 34

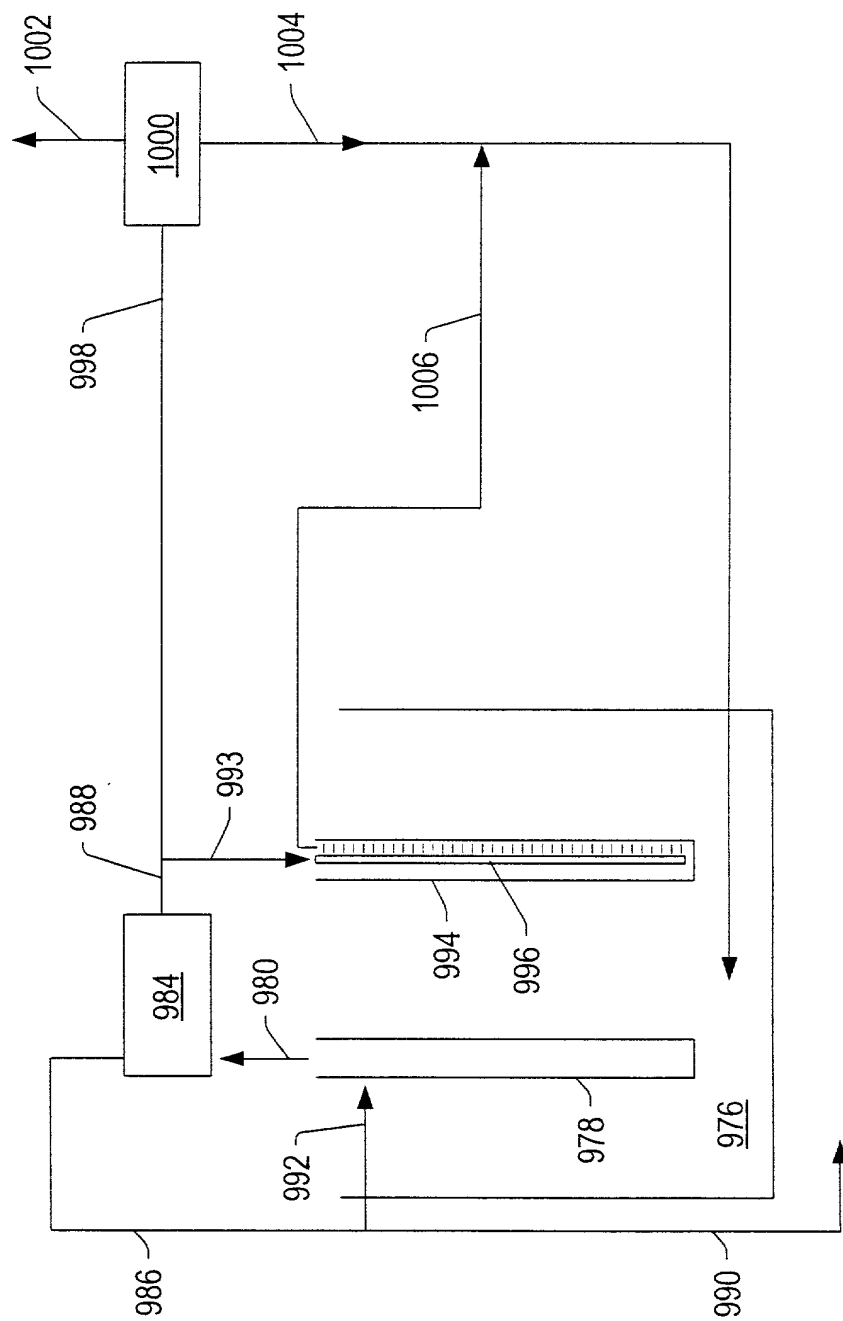
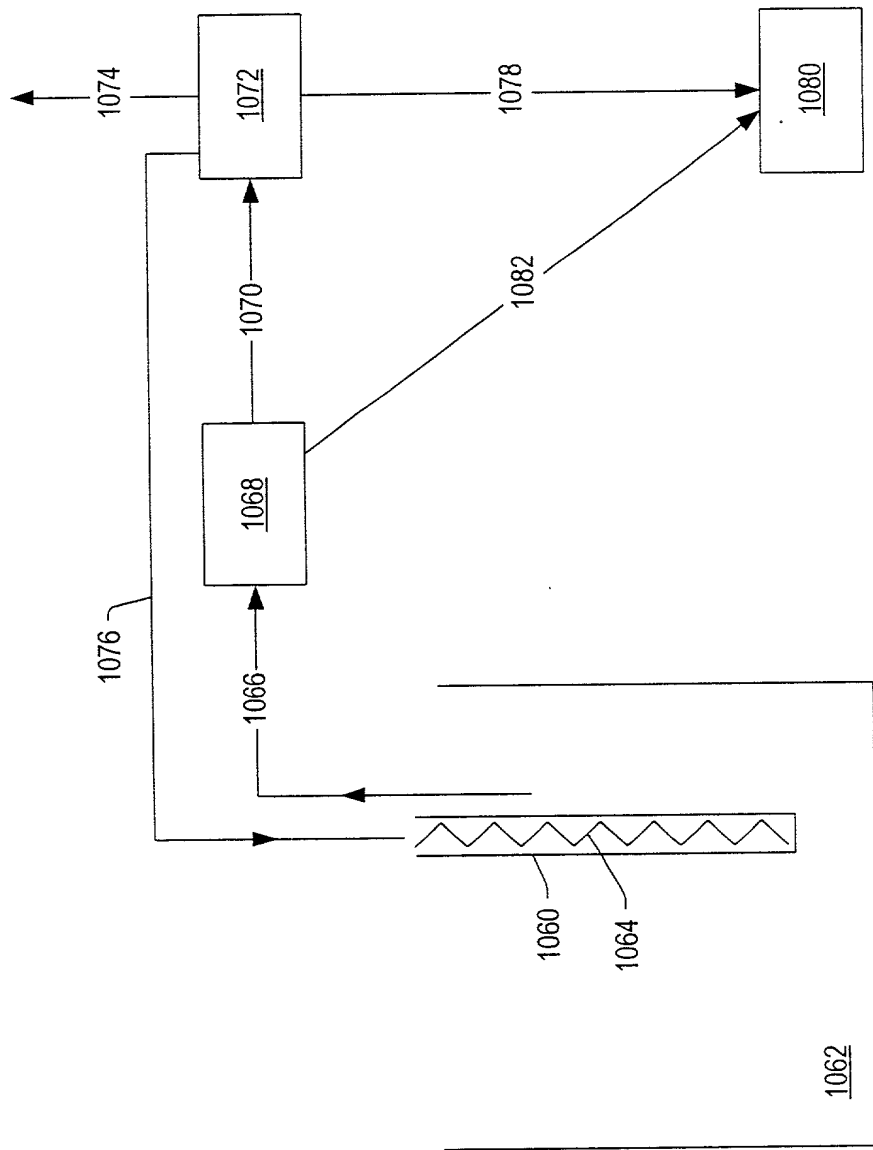


FIG. 35







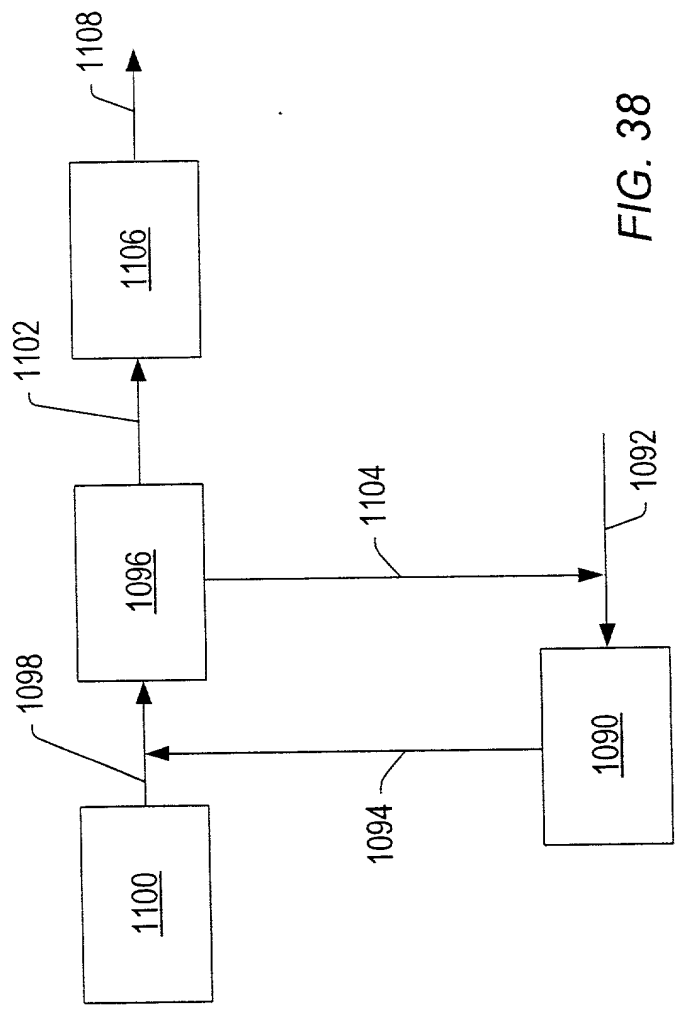


FIG. 38

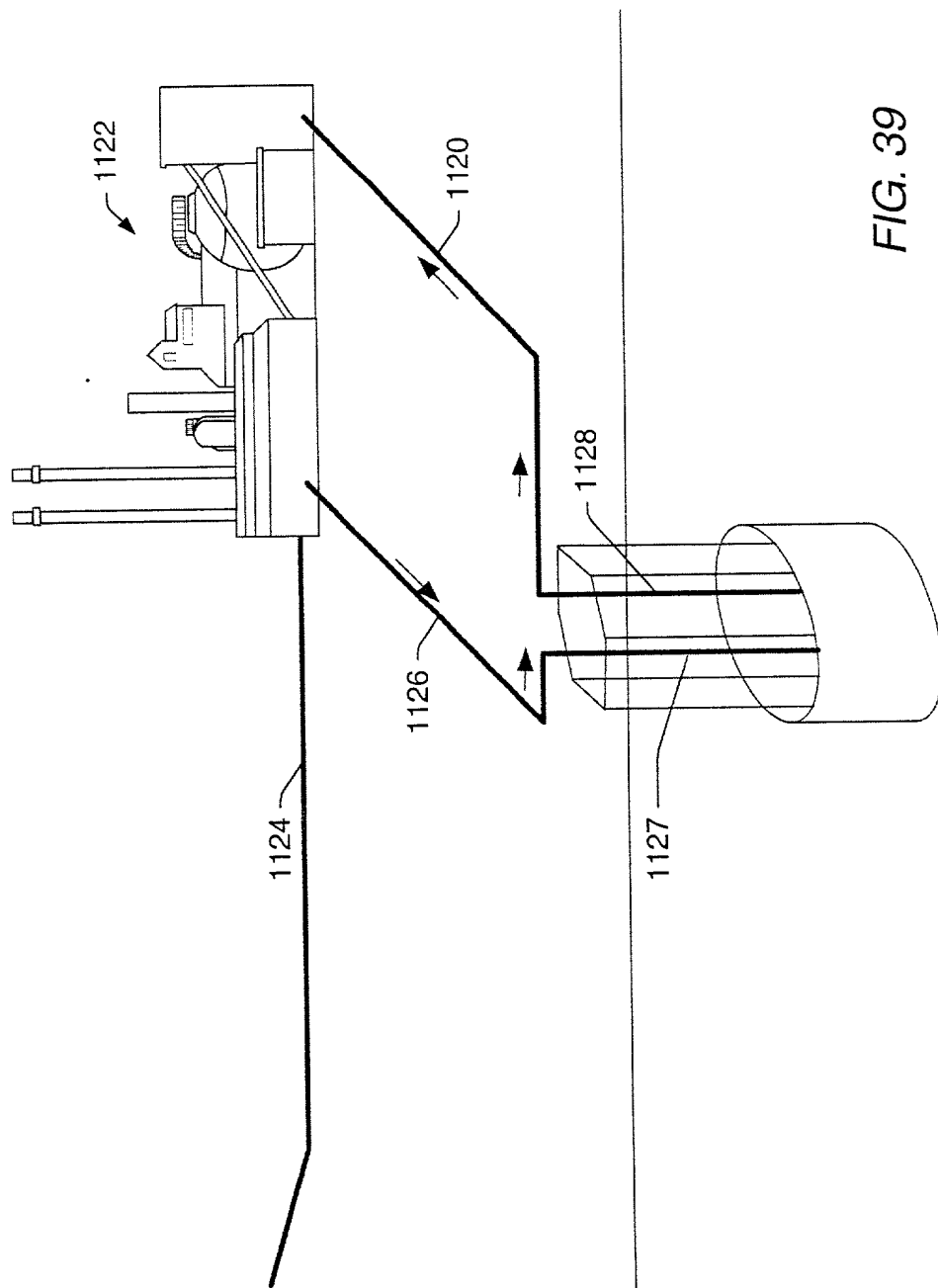


FIG. 39

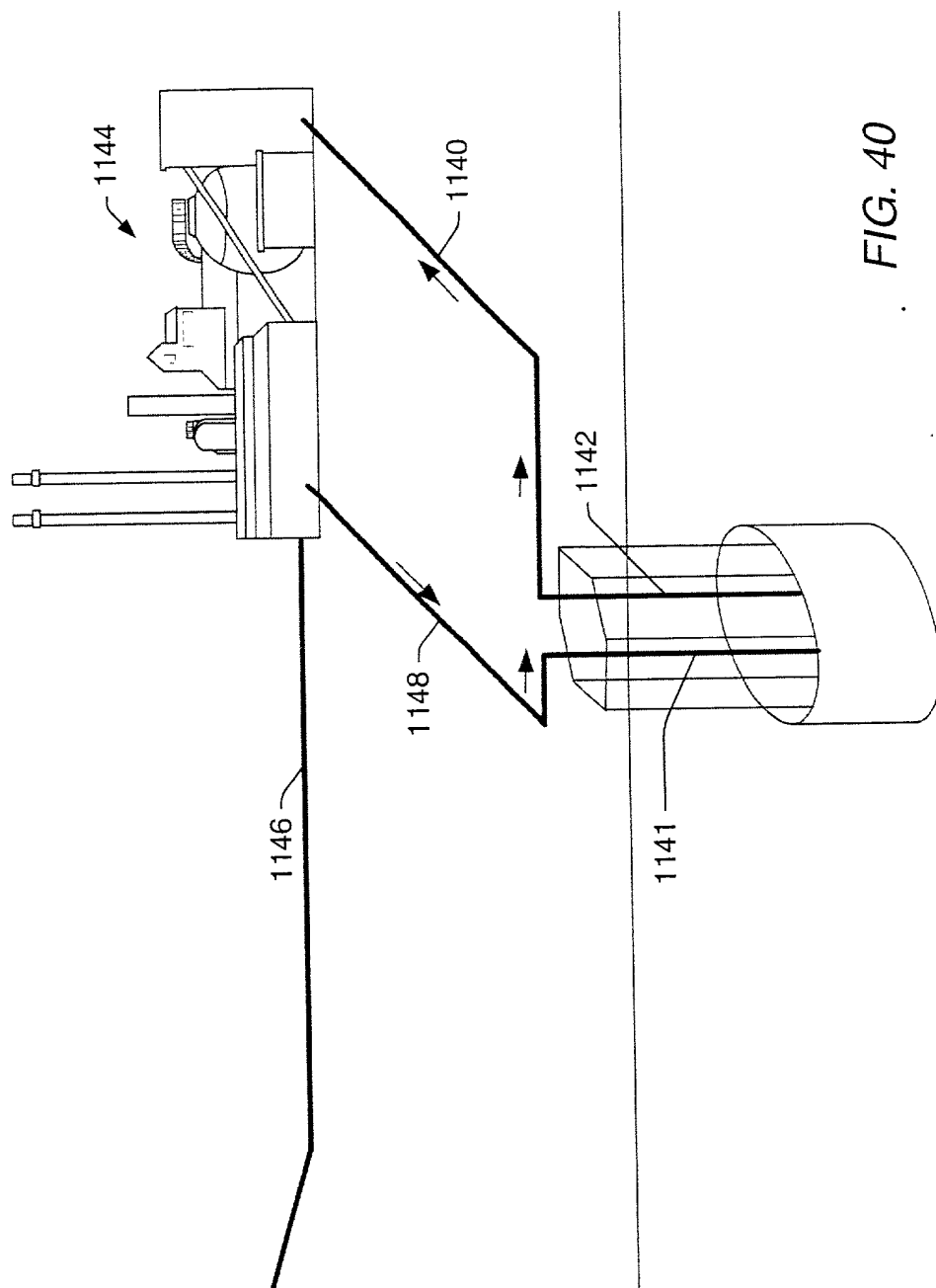


FIG. 40

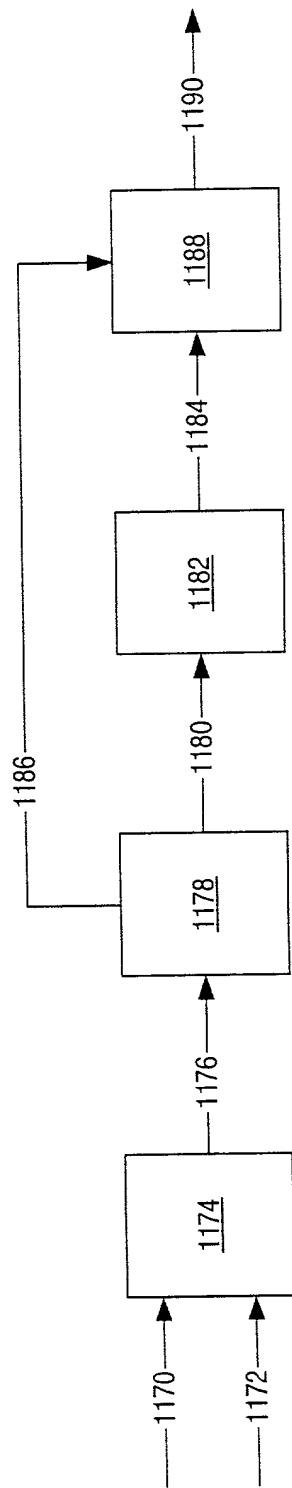


FIG. 41

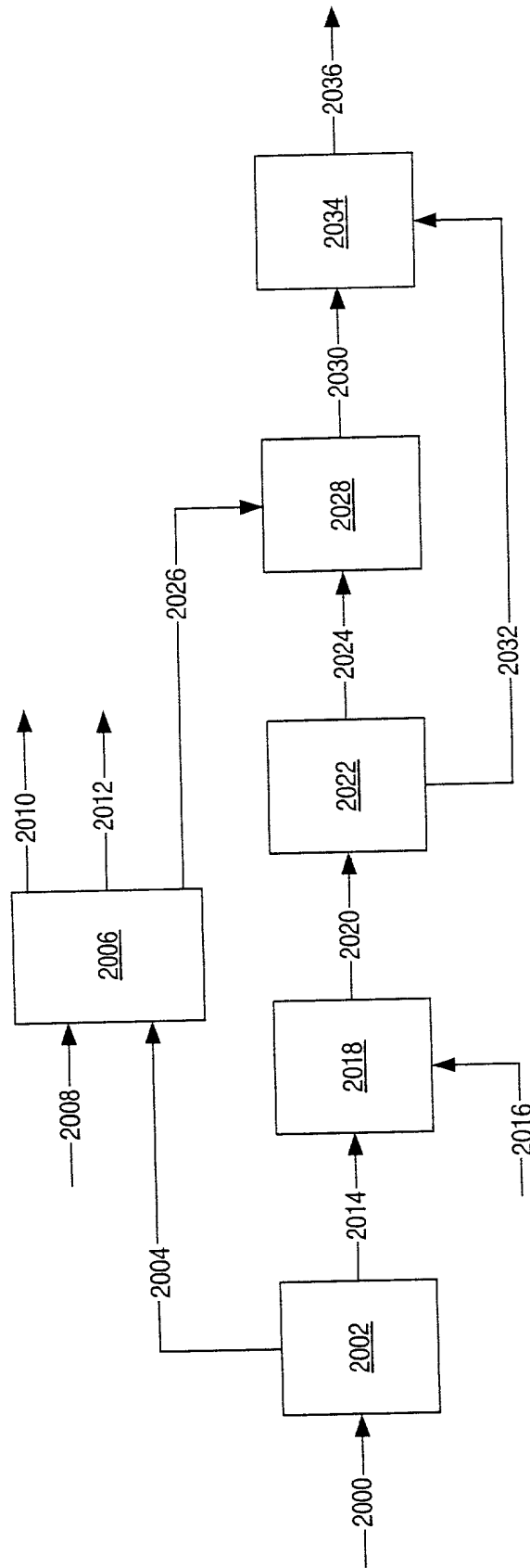
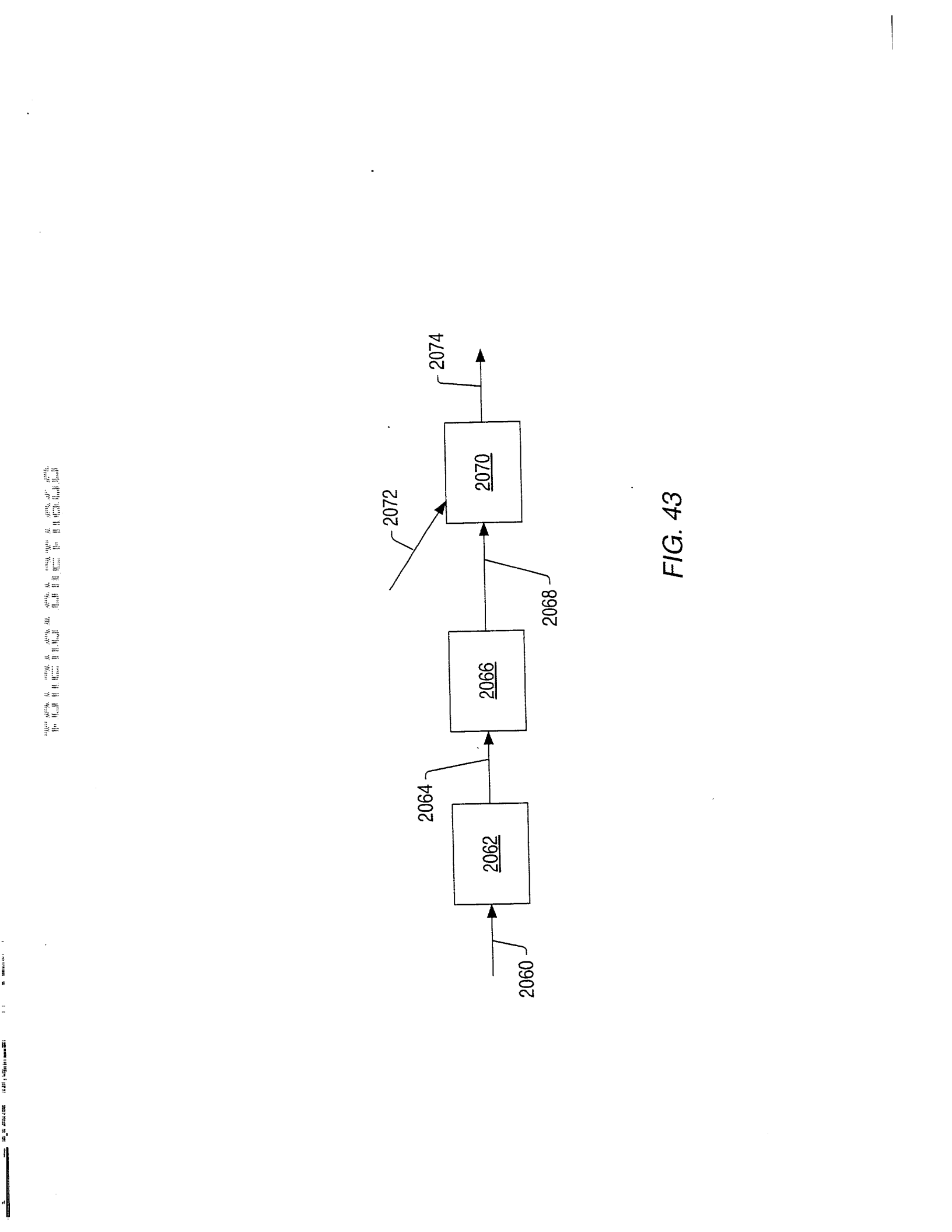


FIG. 42





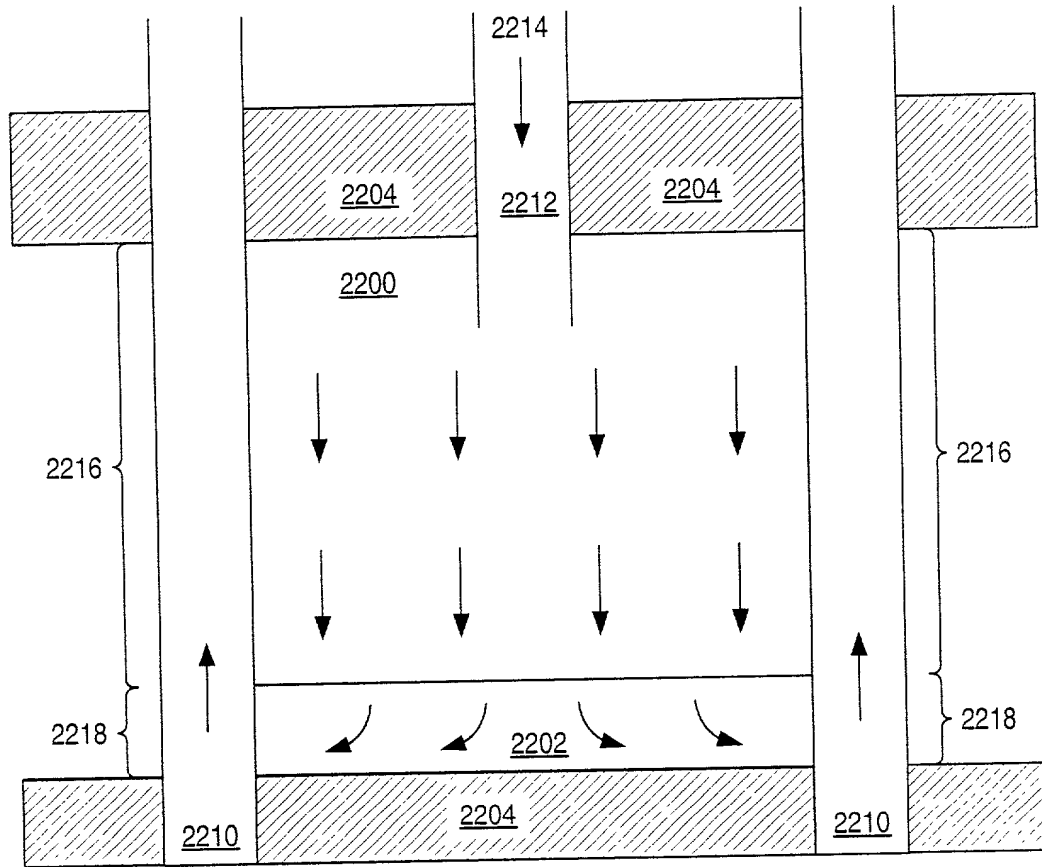


FIG. 44

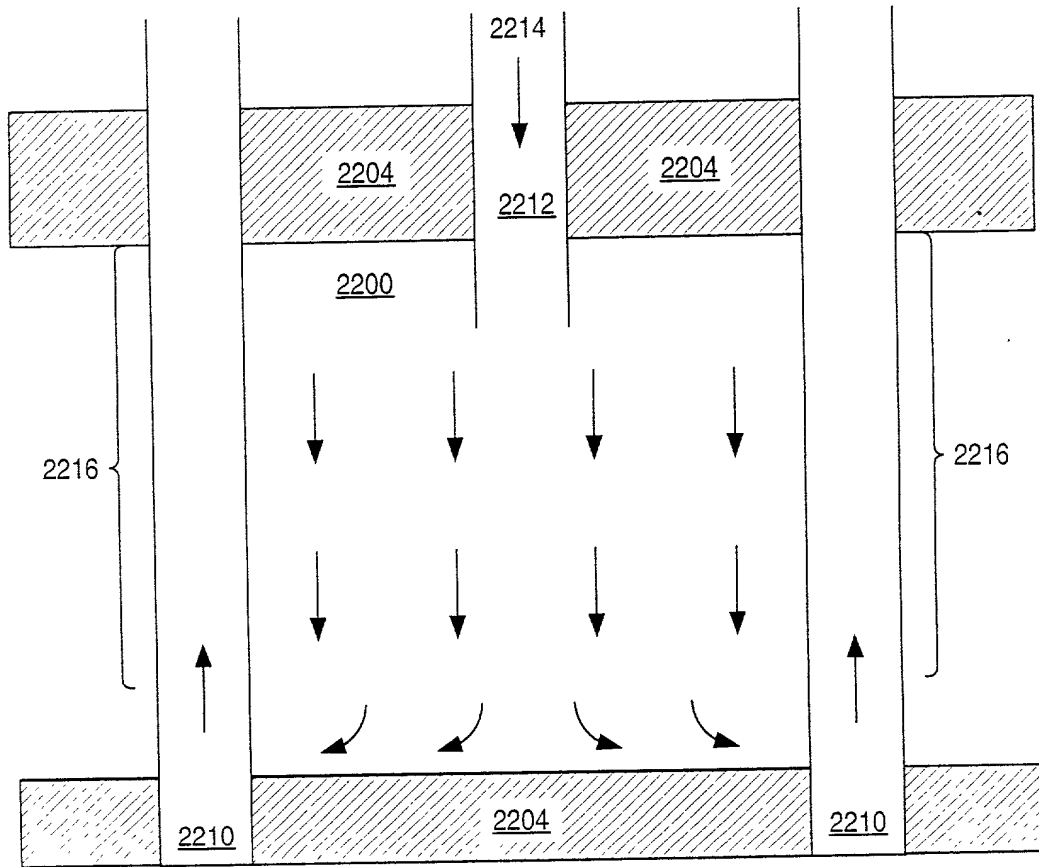


FIG. 45

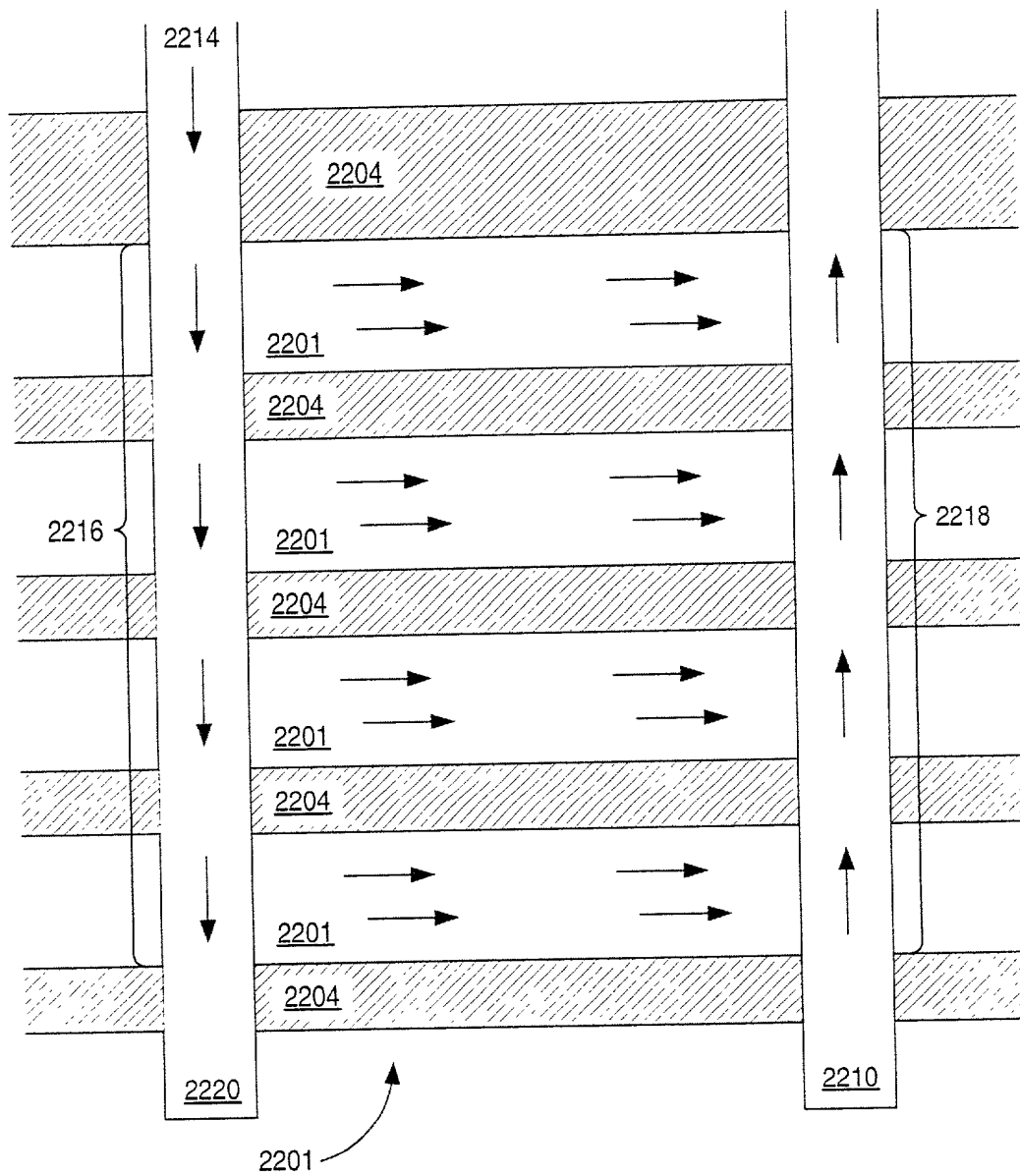


FIG. 46

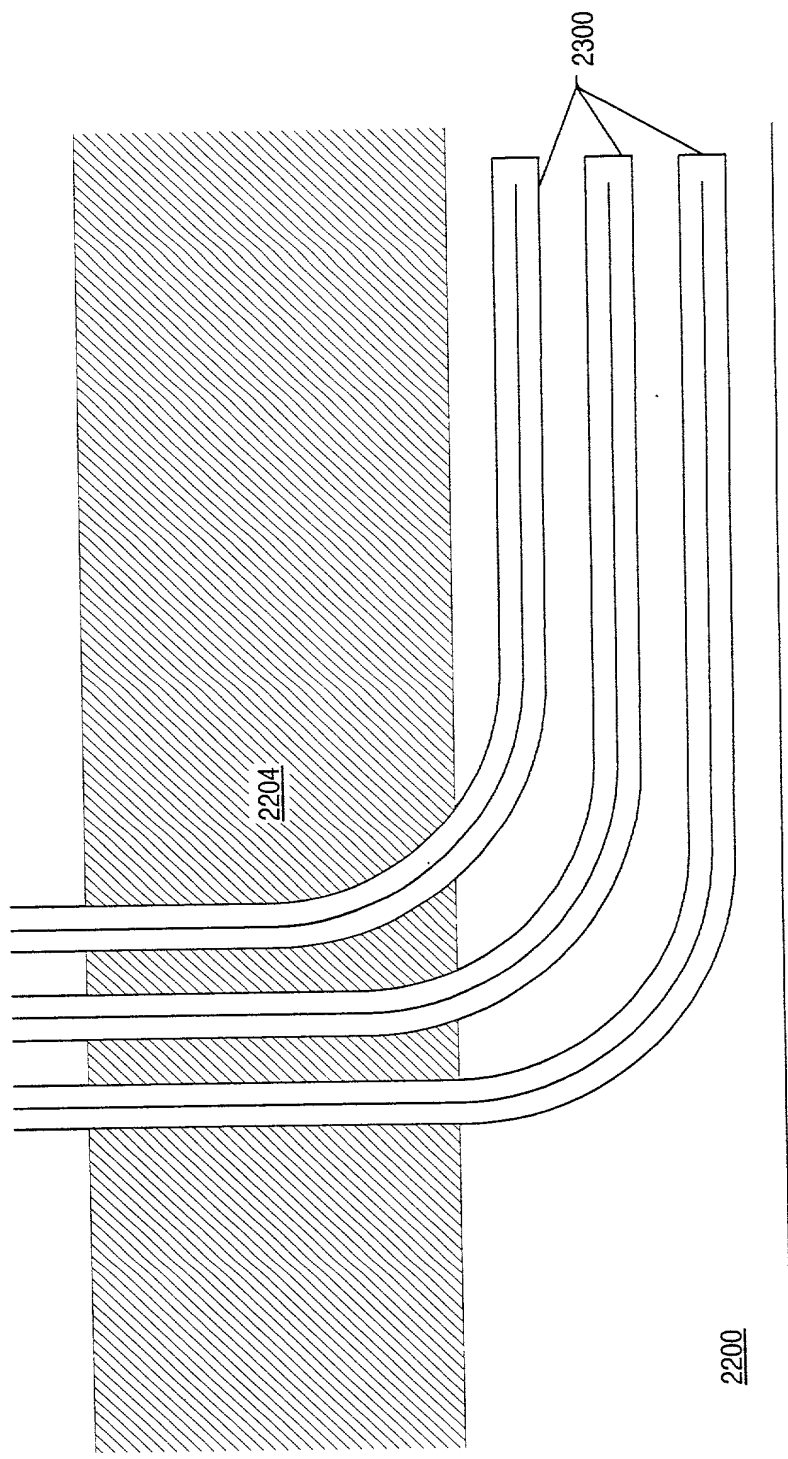


FIG. 47

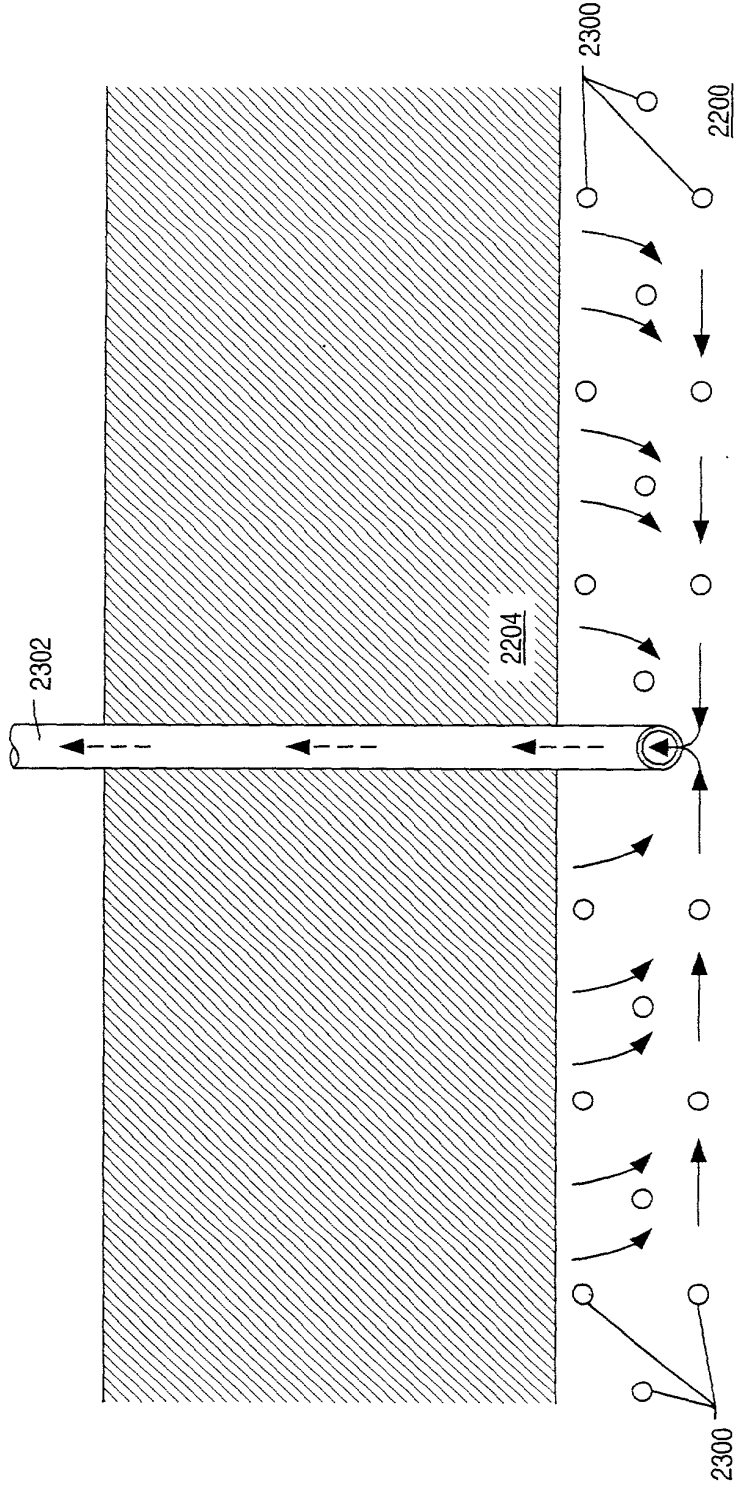


FIG. 48

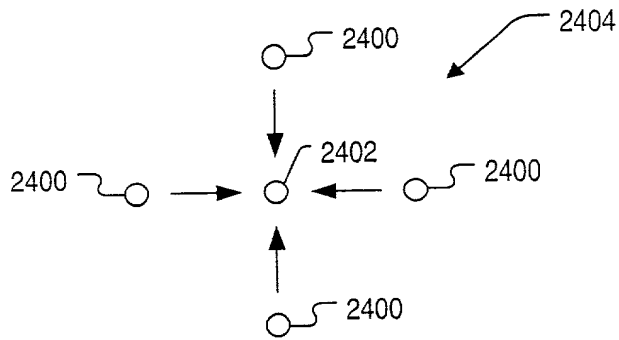


FIG. 49

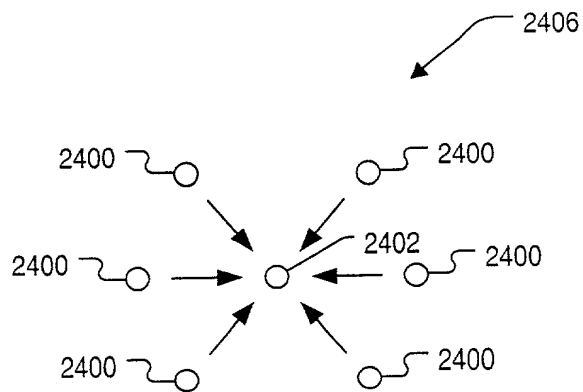


FIG. 50

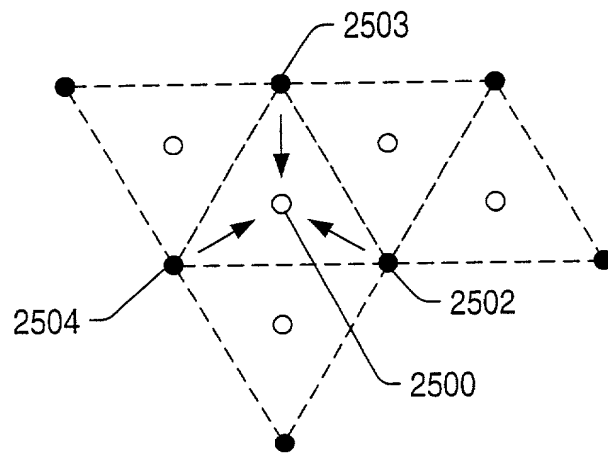


FIG. 51

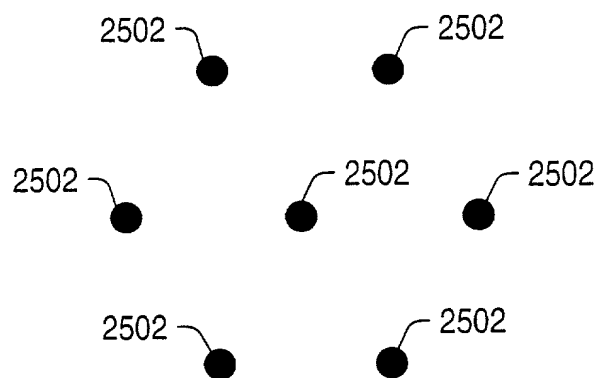


FIG. 52

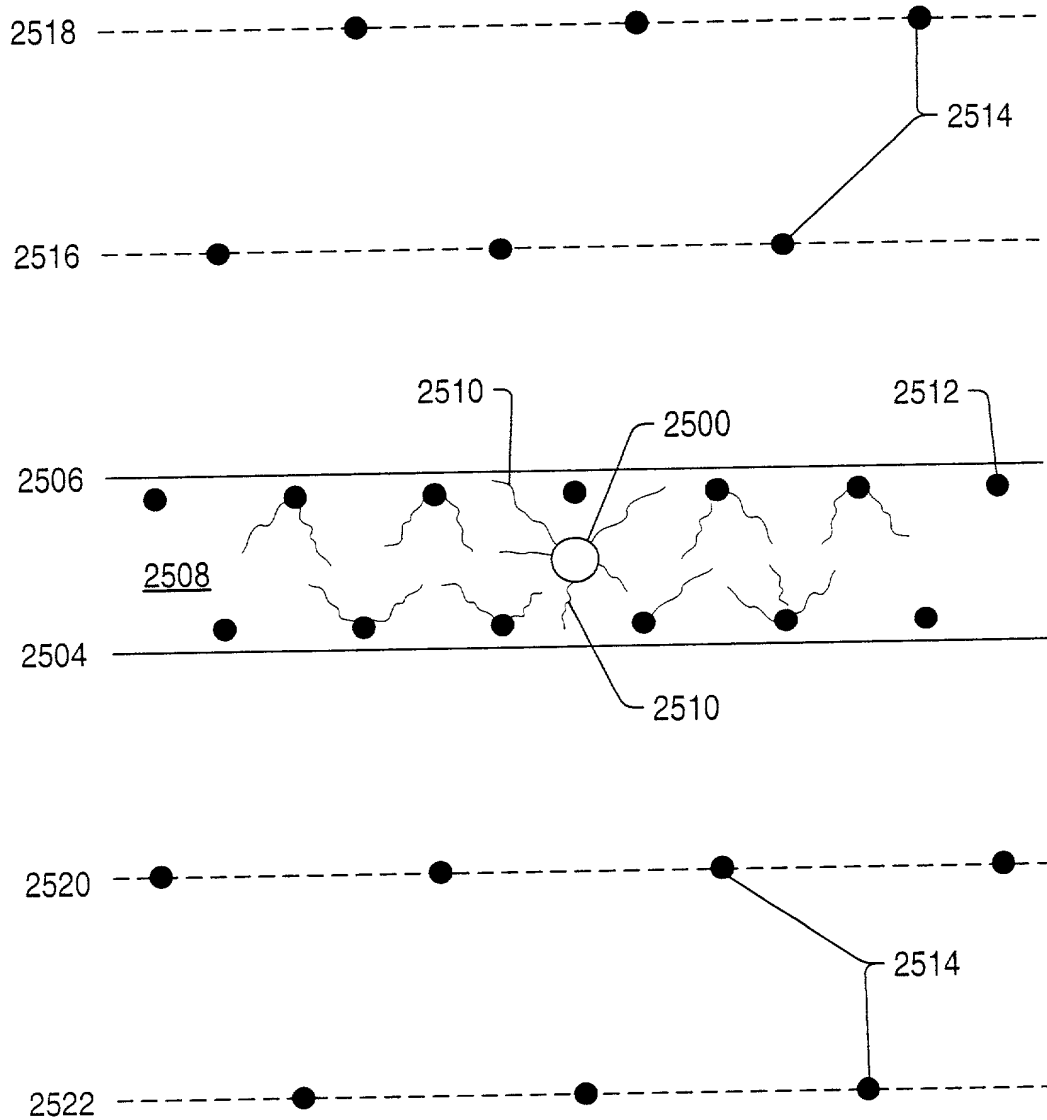


FIG. 53



FIG. 54 is a schematic diagram of a system 2500, including a plurality of components 2540, 2542, 2544, 2548, 2550, 2552, and 2554, arranged in a linear fashion along a dashed line.

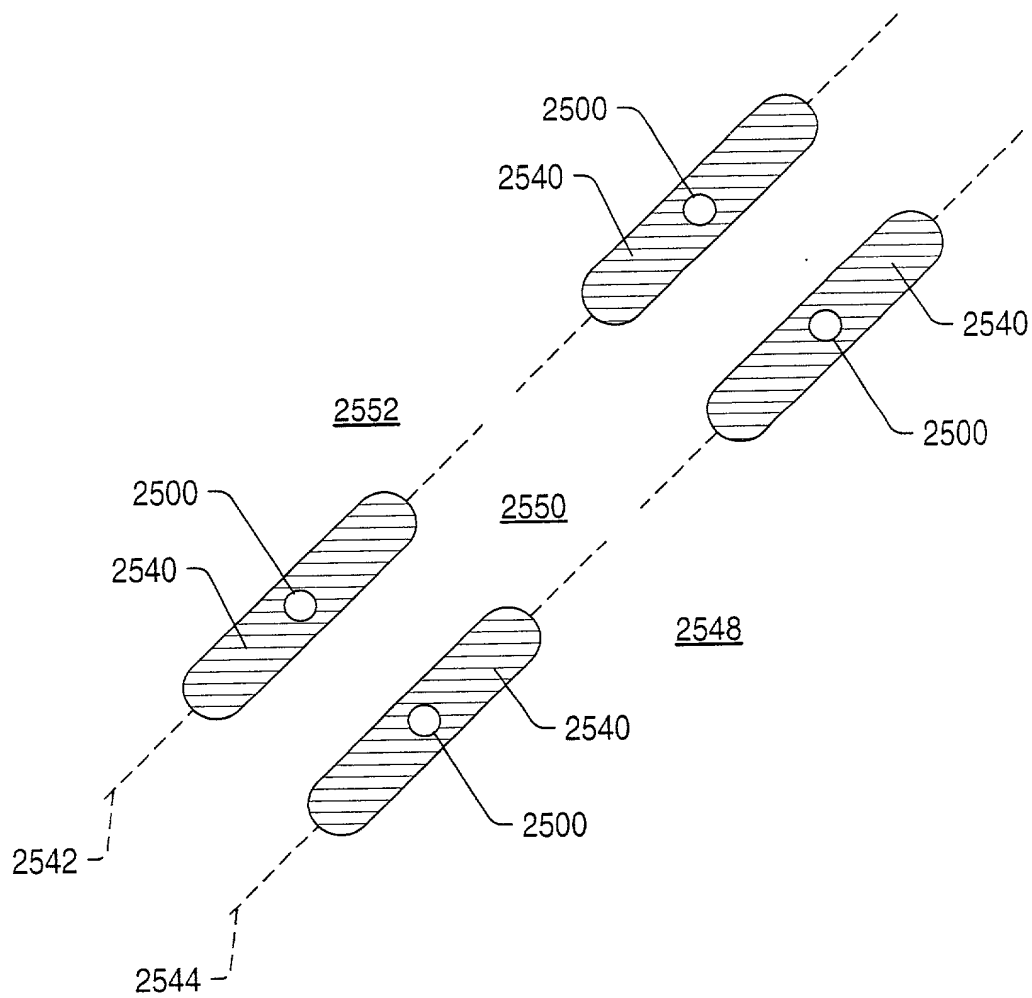


FIG. 54

FIG. 55 is a schematic diagram of a system 2600 for controlling a vehicle 2602. The system 2600 includes a processor 2604 and a memory 2606. The processor 2604 is configured to receive sensor data 2608 from a sensor 2610 and to control the vehicle 2602 based on the sensor data 2608. The memory 2606 is configured to store the sensor data 2608 and the control data 2612. The sensor 2610 is configured to sense the environment of the vehicle 2602 and to output the sensor data 2608. The control data 2612 is configured to control the vehicle 2602. The system 2600 is configured to control the vehicle 2602 based on the sensor data 2608 and the control data 2612.

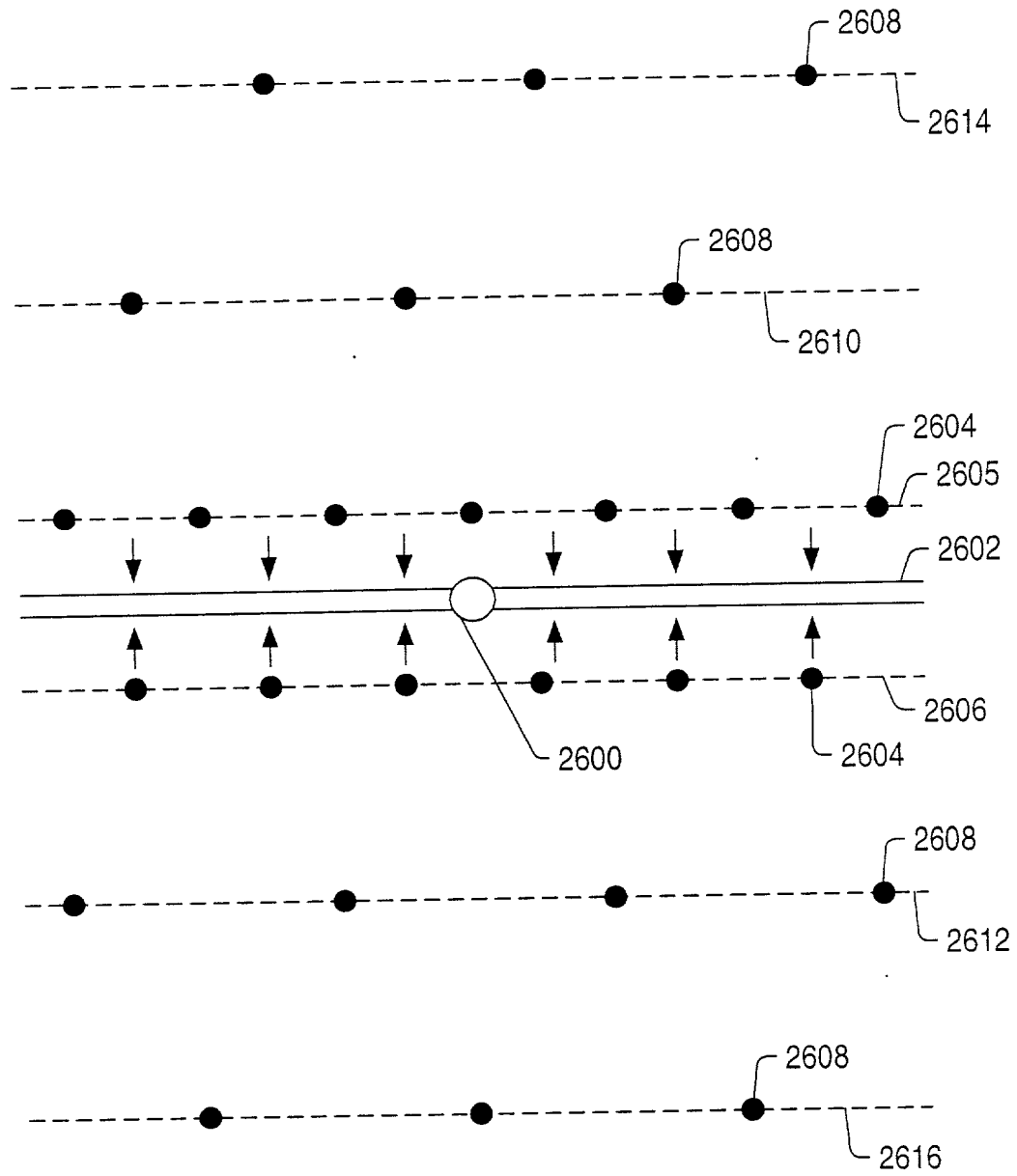


FIG. 55

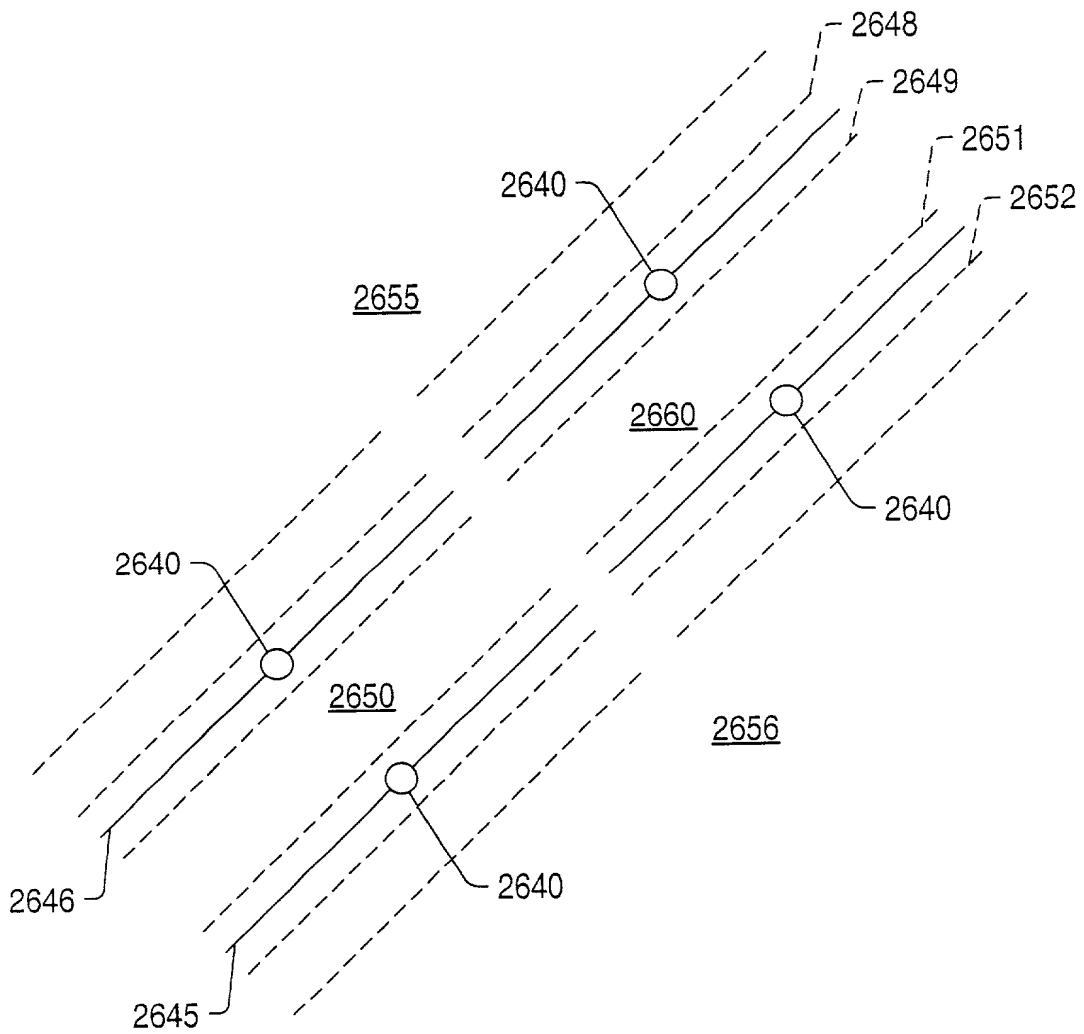


FIG. 56

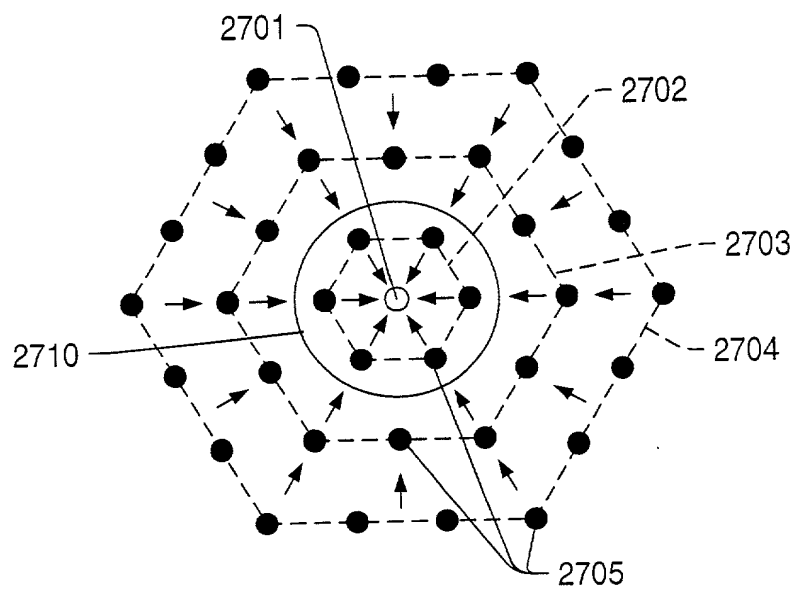


FIG. 57

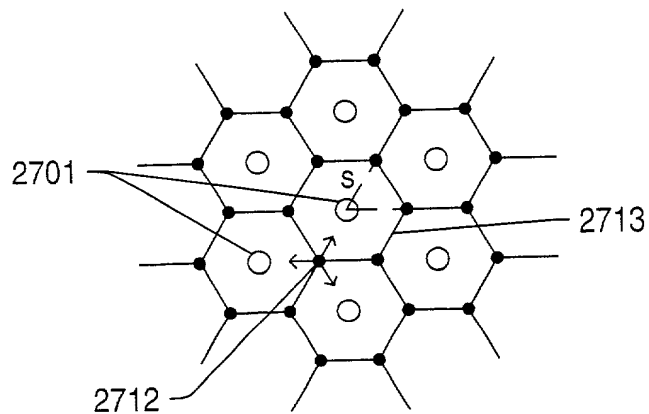


FIG. 58

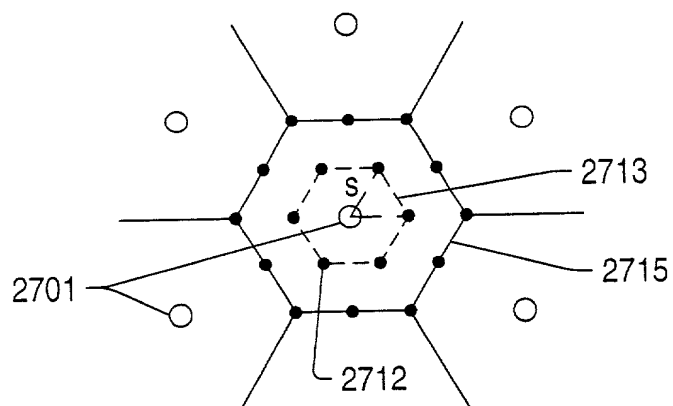


FIG. 59

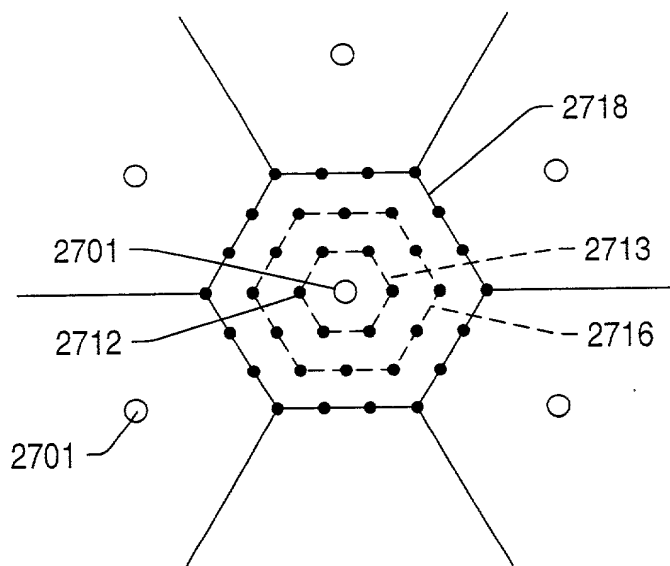


FIG. 60

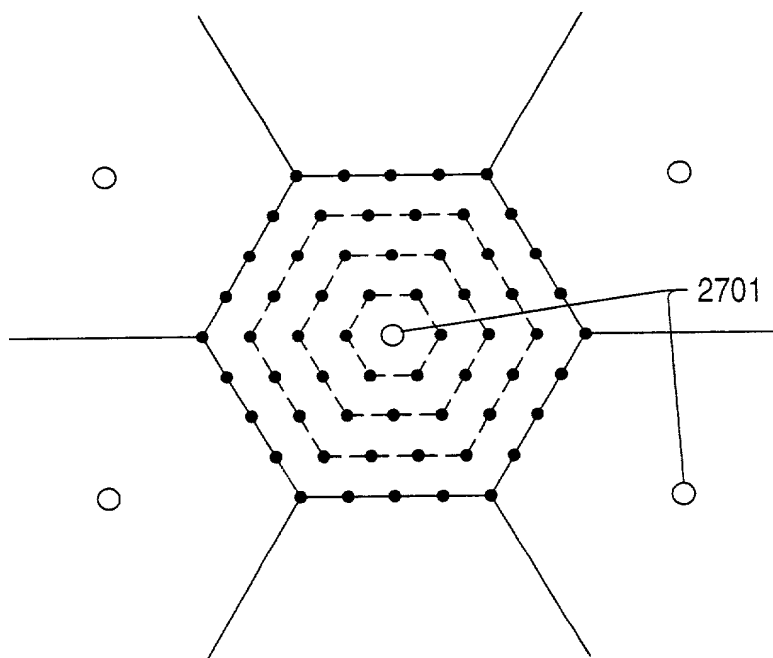


FIG. 61

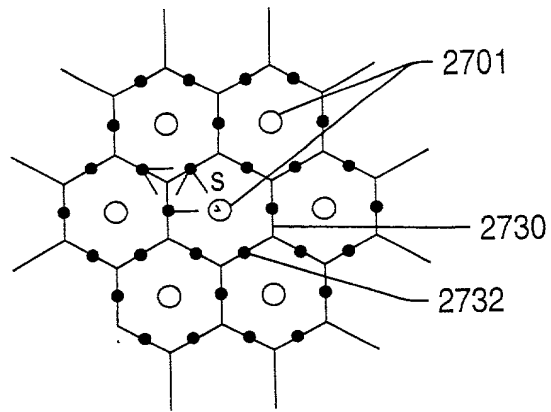


FIG. 62

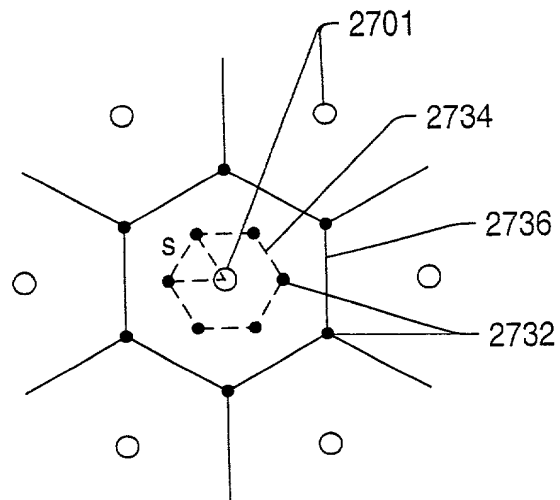


FIG. 63

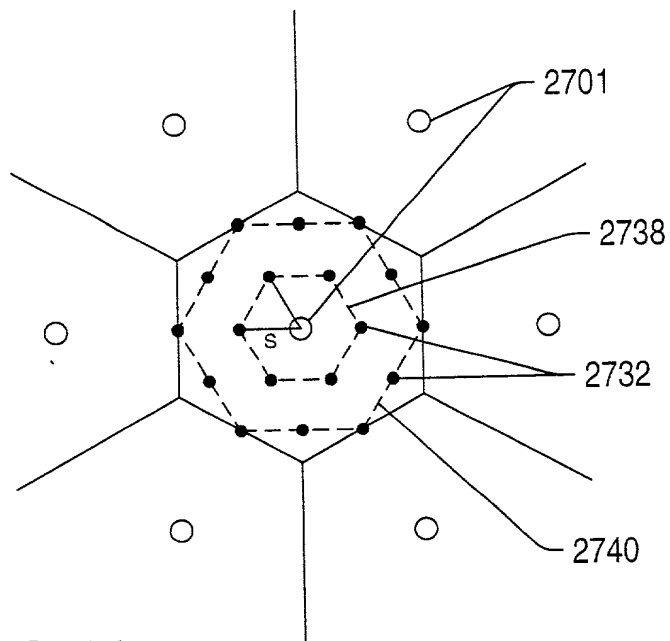


FIG. 64

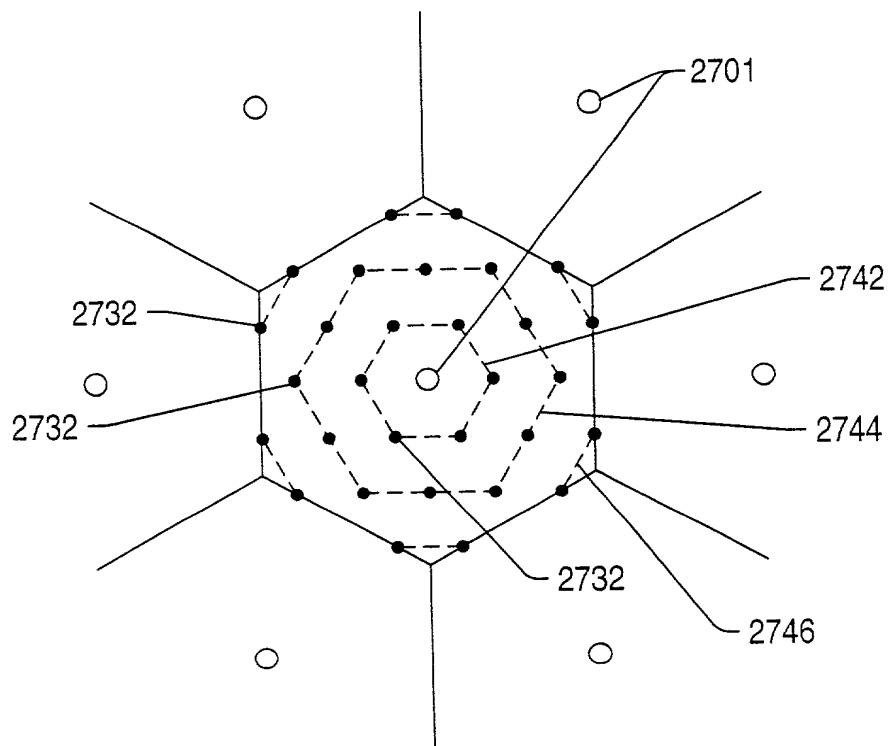


FIG. 65



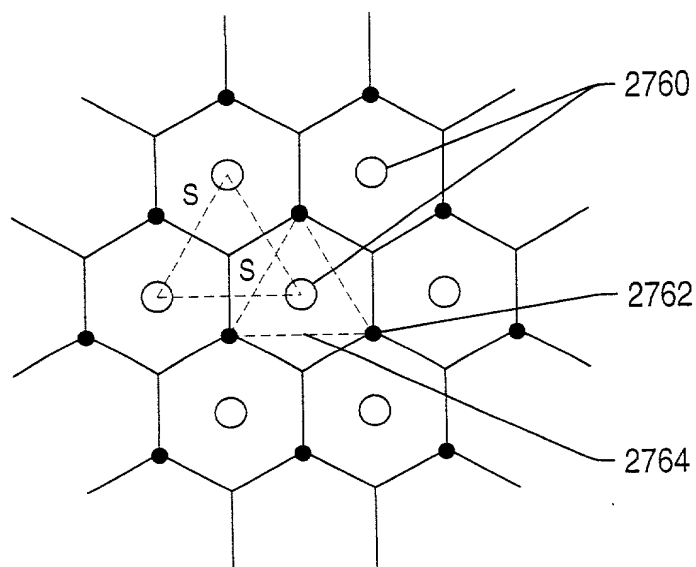


FIG. 66

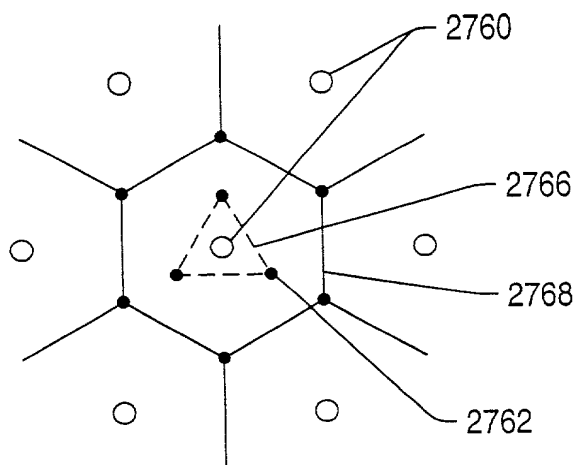


FIG. 67

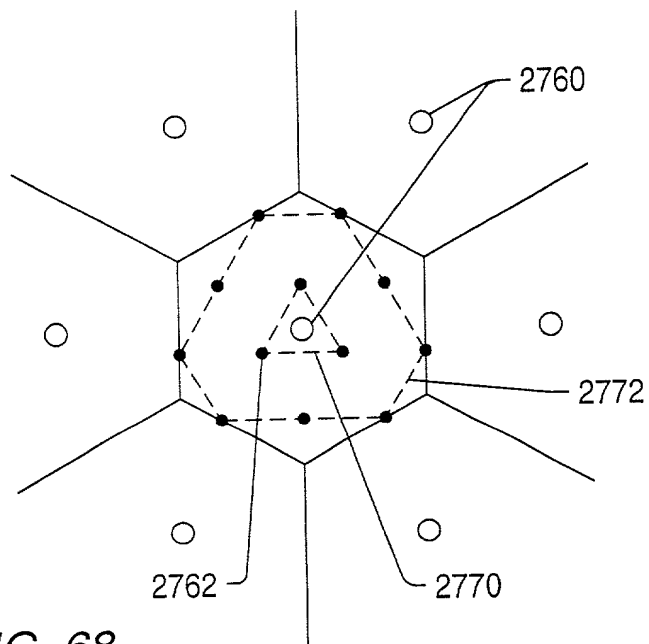


FIG. 68

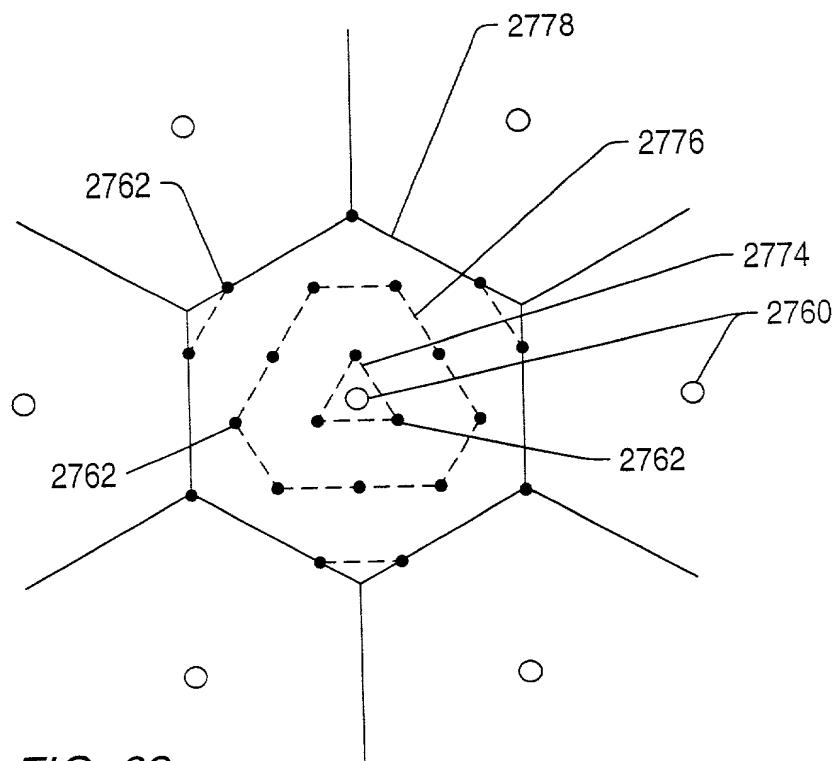


FIG. 69

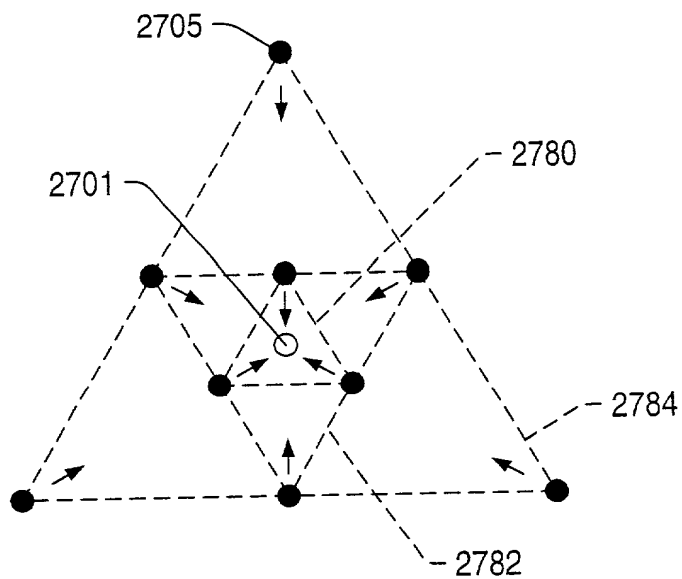


FIG. 70

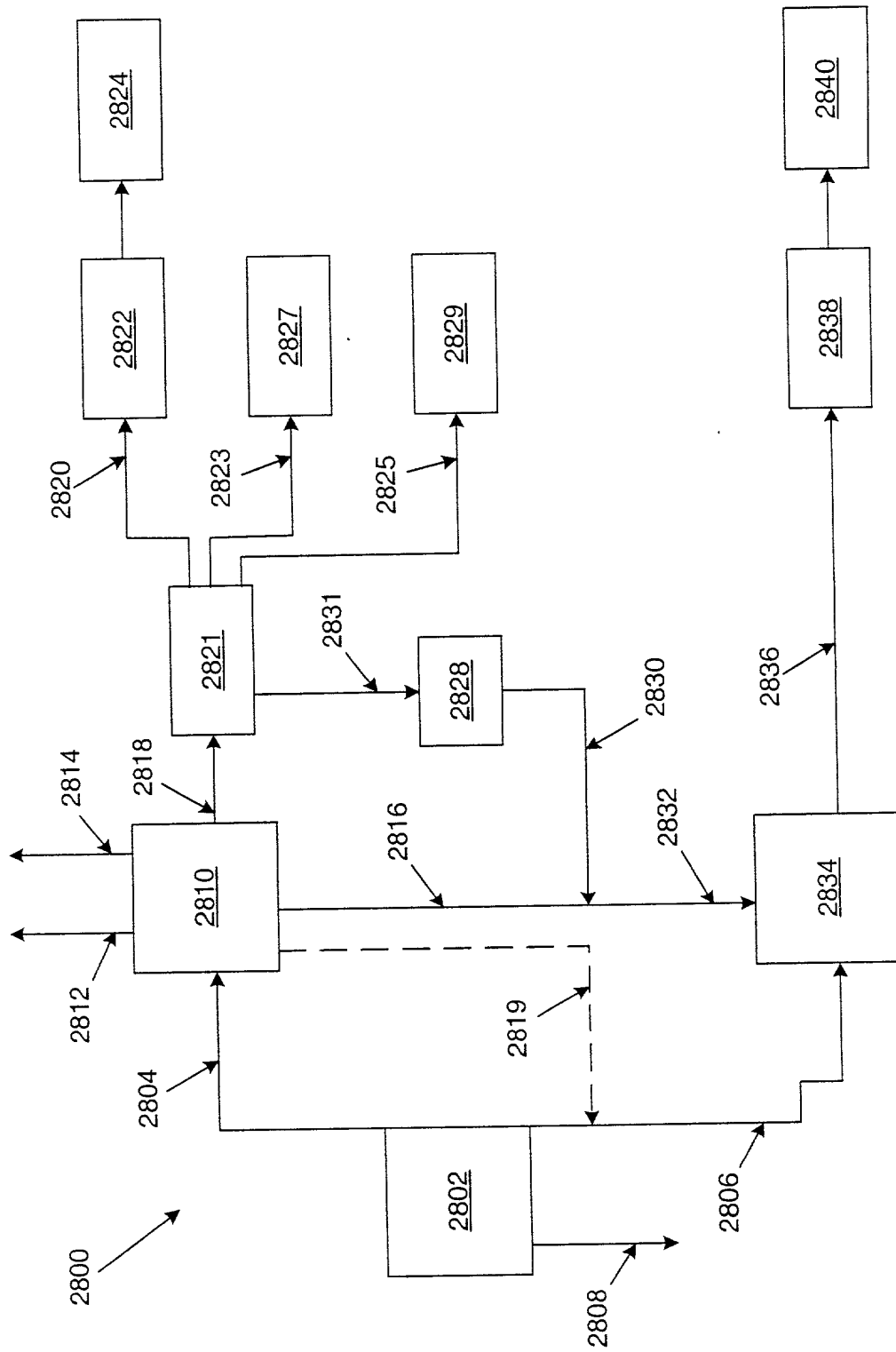


Fig. 71

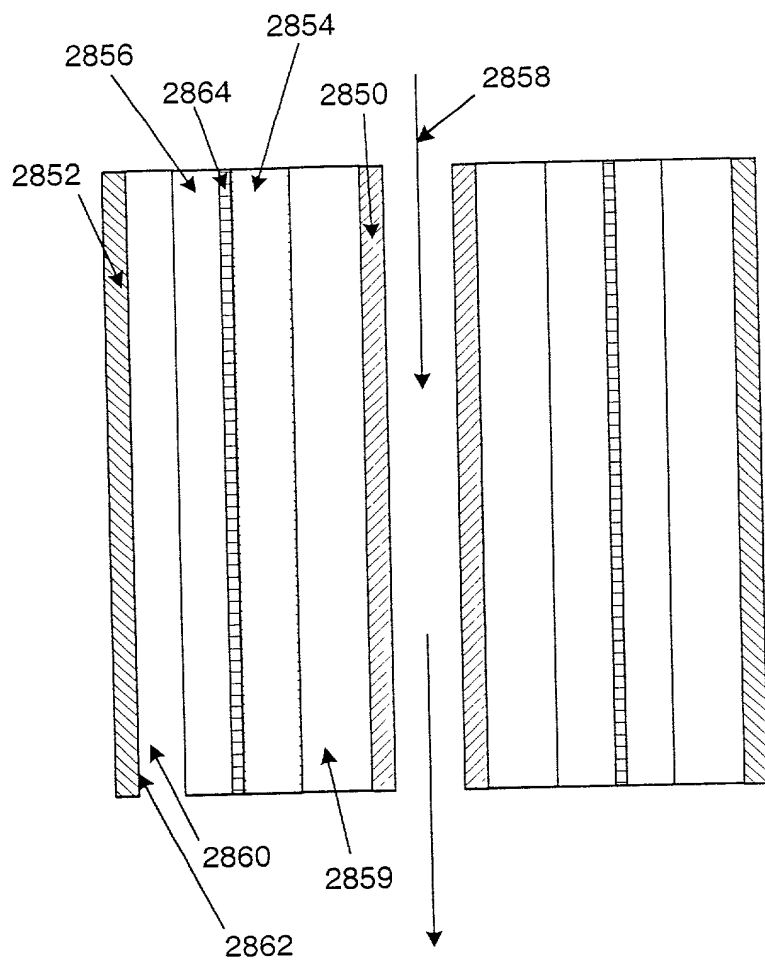


Fig. 72

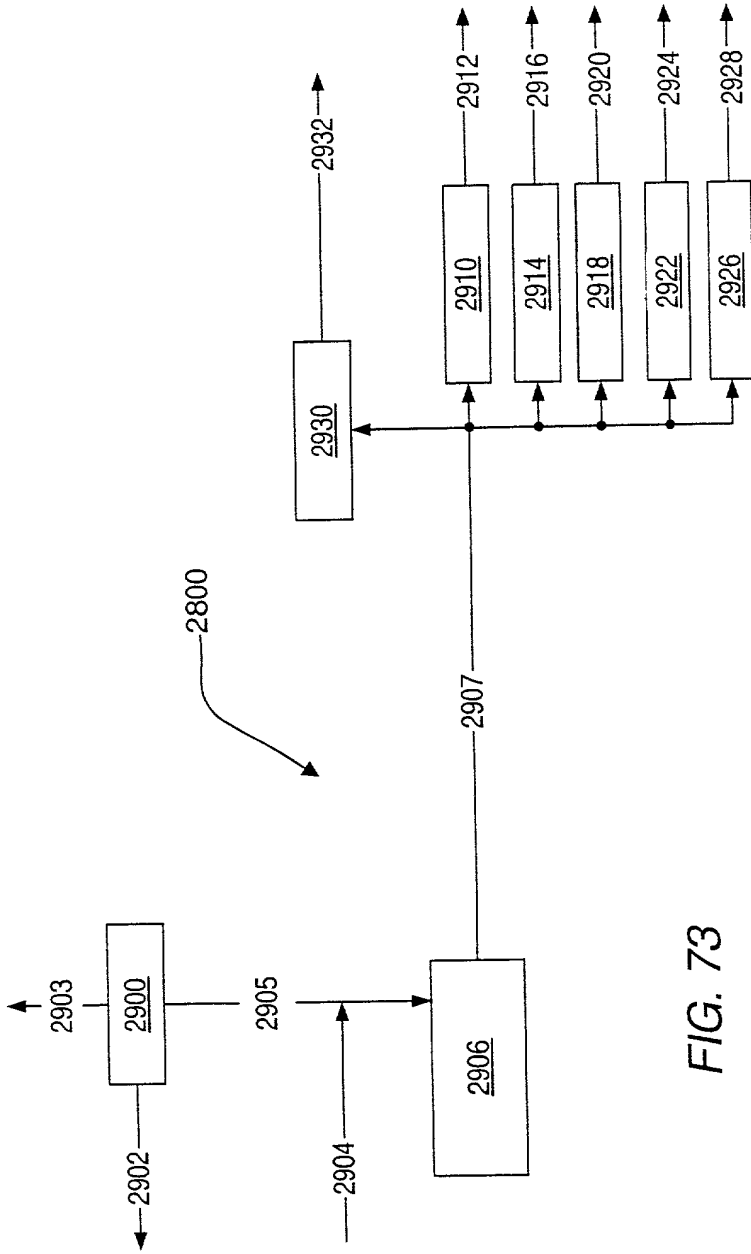


FIG. 73

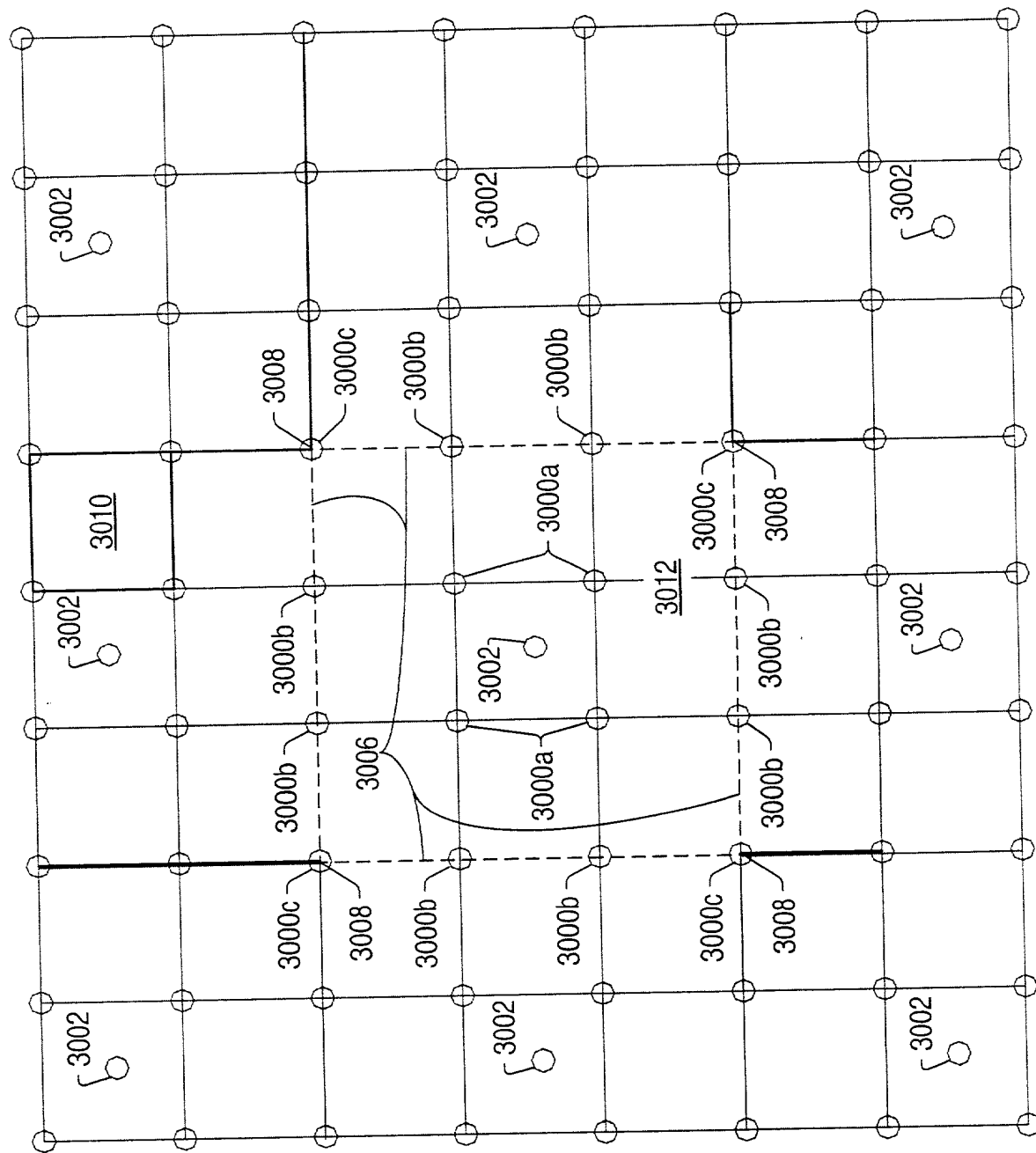


FIG. 74

FIG. 75 is a schematic diagram of a hexagonal lattice structure. The lattice is composed of hexagonal cells. A central hexagonal cell is labeled 3000. It is surrounded by six other hexagonal cells, each labeled 3002. These six cells are further surrounded by a ring of twelve hexagonal cells, each labeled 3006. The outermost ring consists of twelve hexagonal cells, each labeled 3008. The diagram illustrates a hierarchical structure where the central cell 3000 is connected to the inner ring of cells 3002, which are in turn connected to the middle ring of cells 3006, and finally to the outer ring of cells 3008. The connections are shown as solid lines between adjacent cells and dashed lines between cells in different rings.

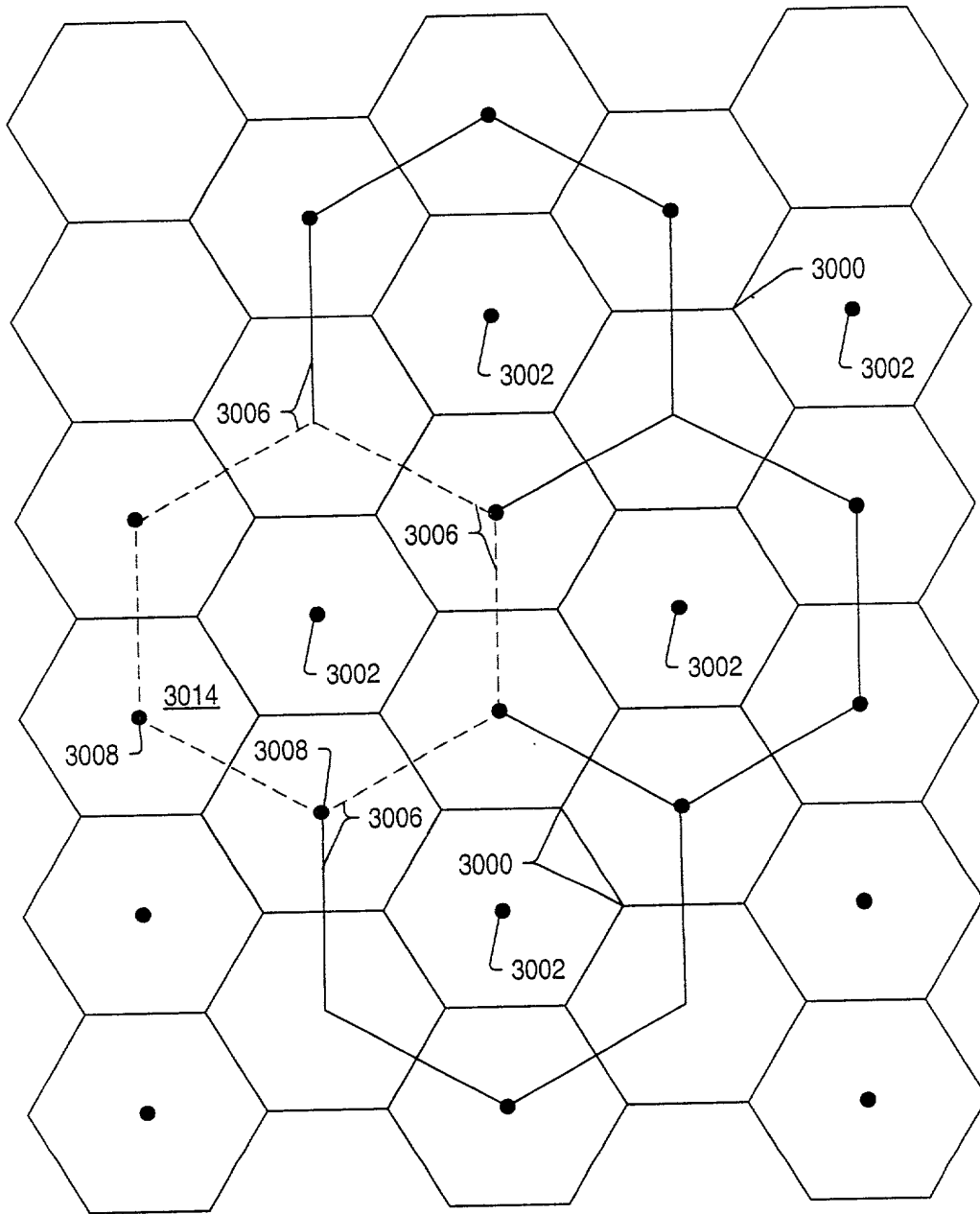


FIG. 75



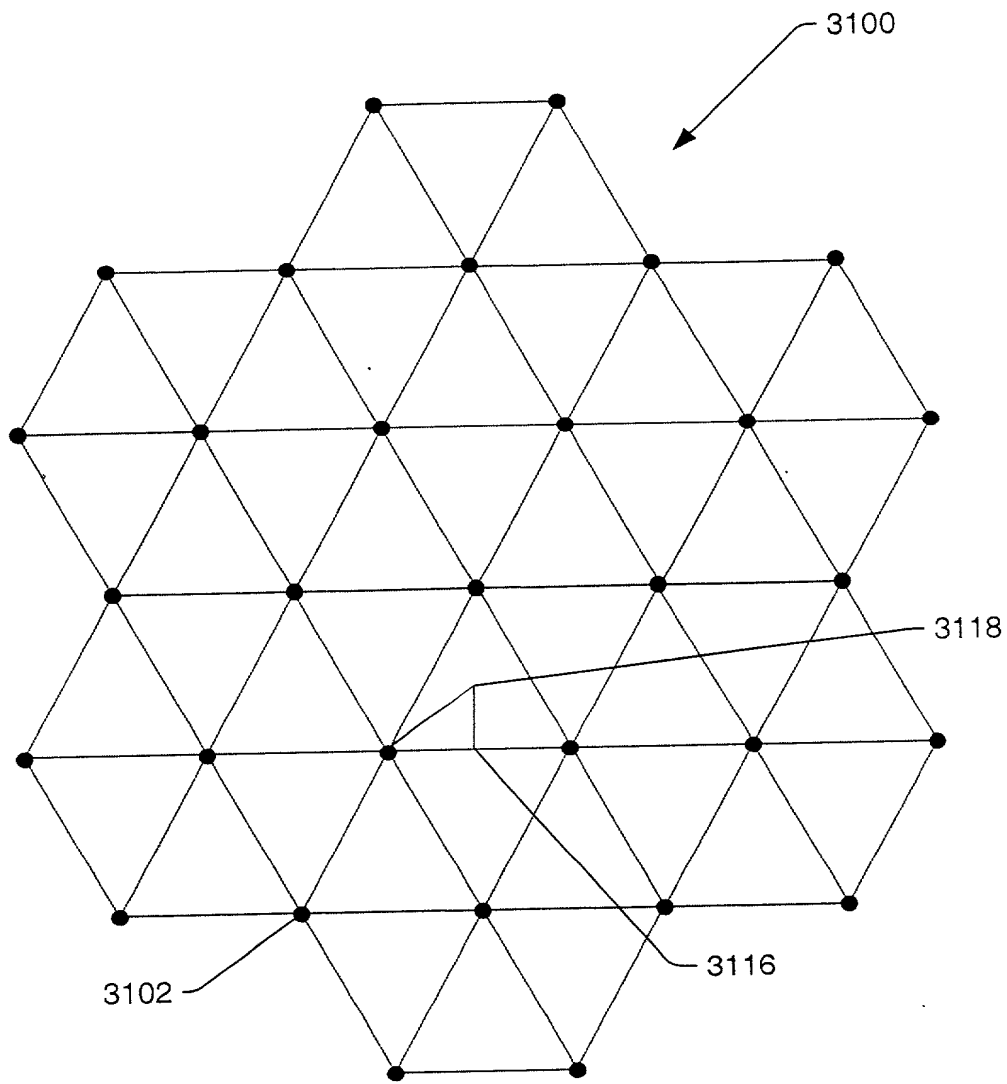


FIG. 76

FIG. 76a

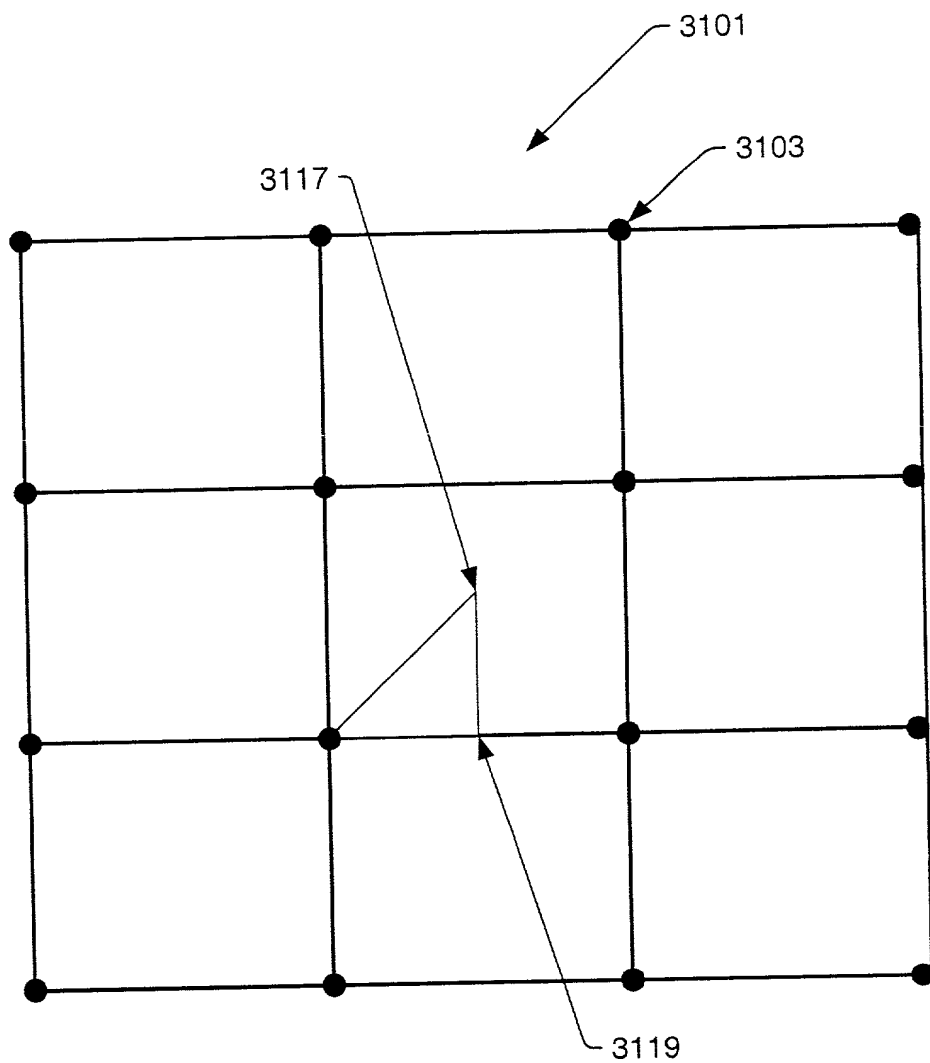


FIG. 76a

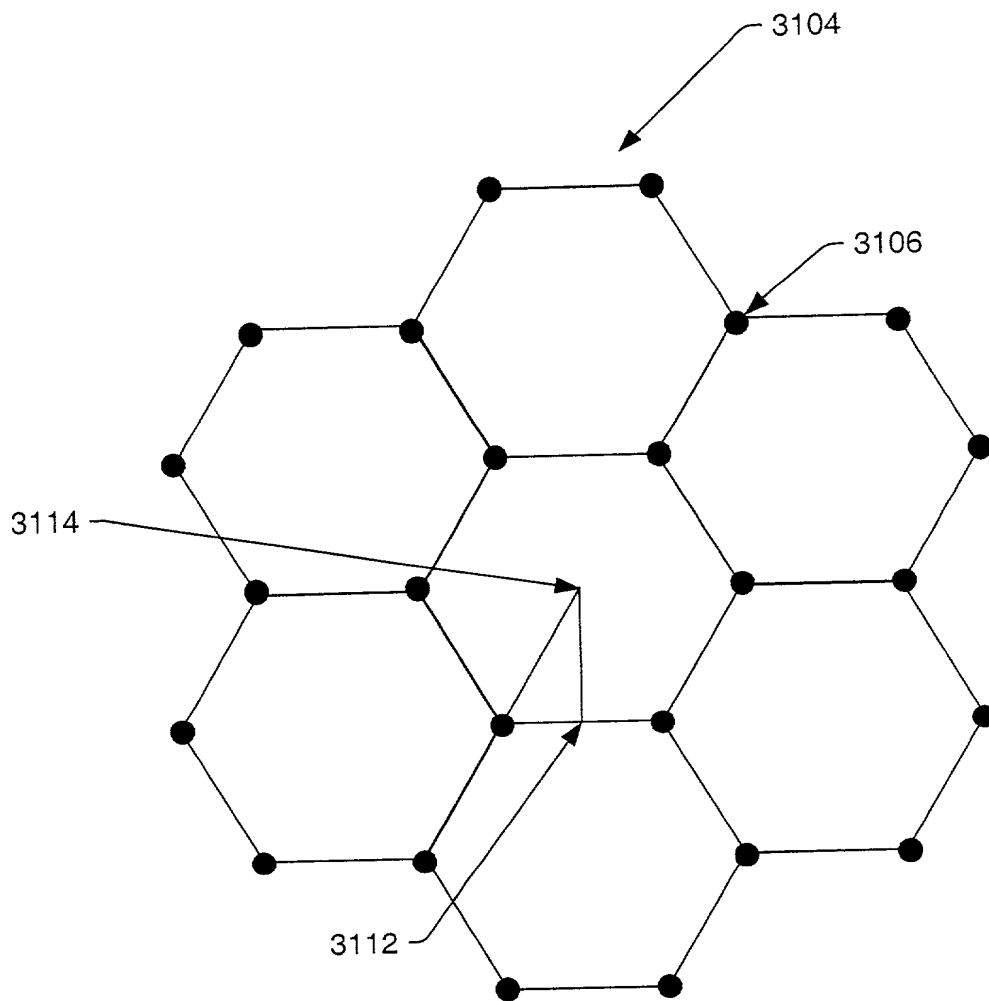


FIG. 77

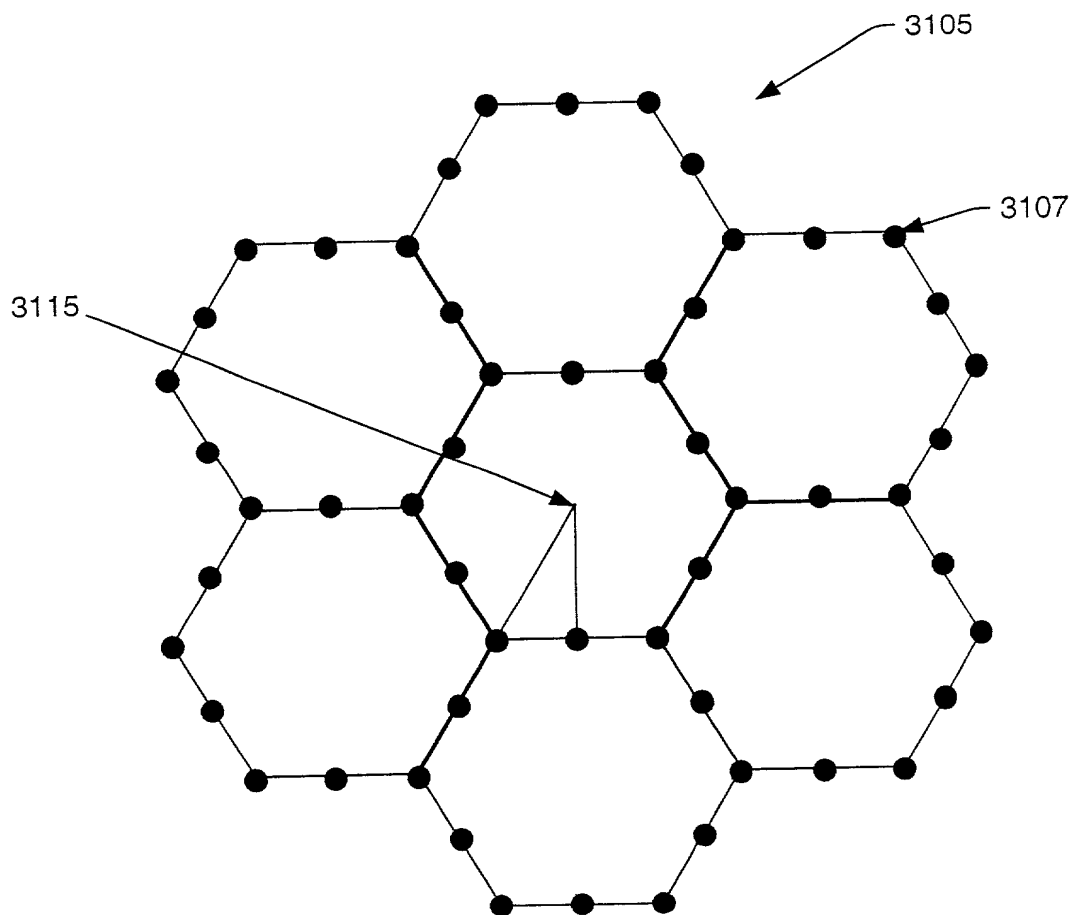


FIG. 77a

FIG. 78 is a 3D surface plot of the temperature distribution T (°C) as a function of the spatial coordinates x and y. The plot shows a complex, multi-peaked surface, indicating significant variations in temperature across the domain. The x and y axes range from -10 to 10, and the temperature T ranges from 500 to 600 °C.

3110

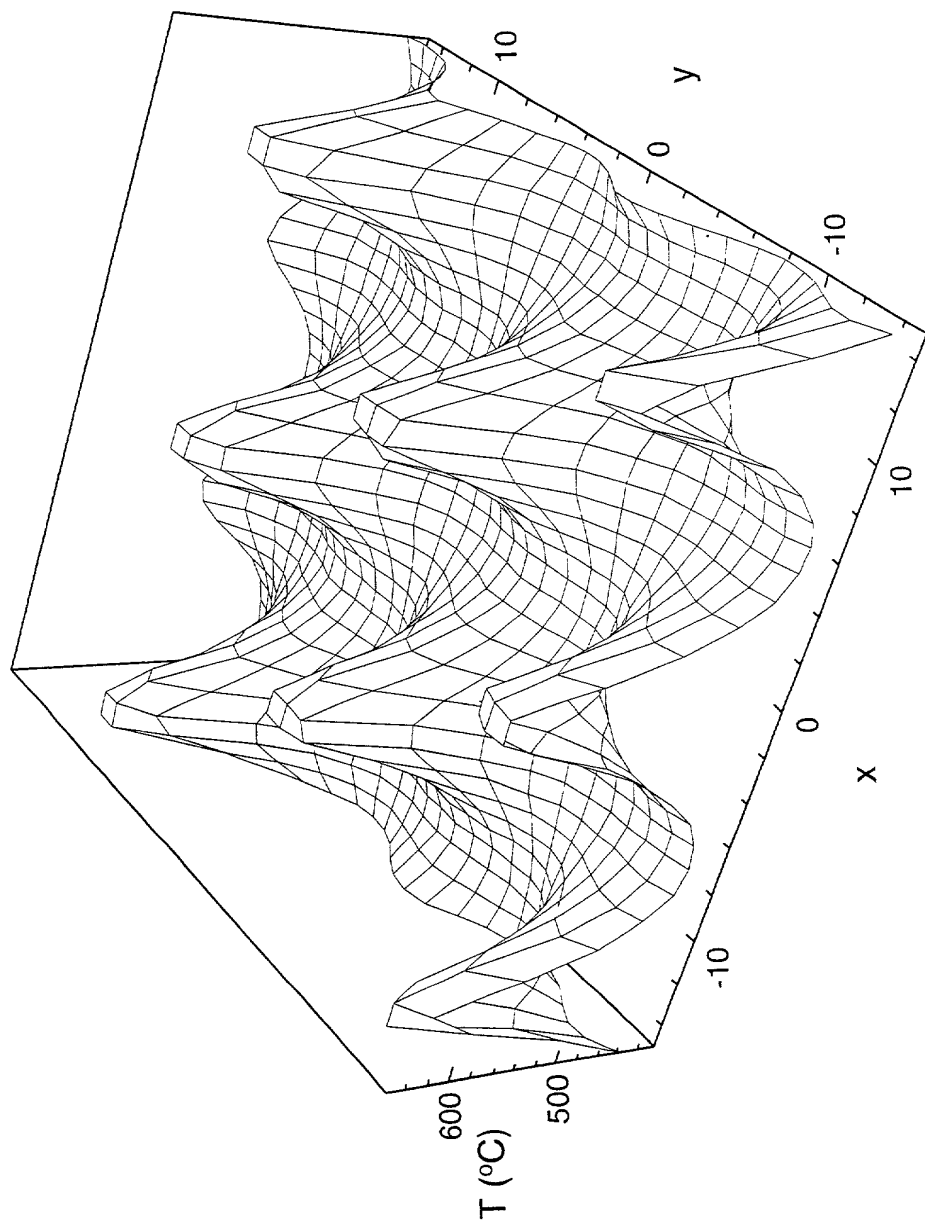


FIG. 78

FIG. 79 is a 3D surface plot showing the temperature distribution T (°C) as a function of position (x, y). The plot displays a complex, wavy surface with multiple peaks and valleys, indicating significant temperature variations across the domain. The x and y axes range from -10 to 10, and the temperature T (°C) ranges from 400 to 550.

3108

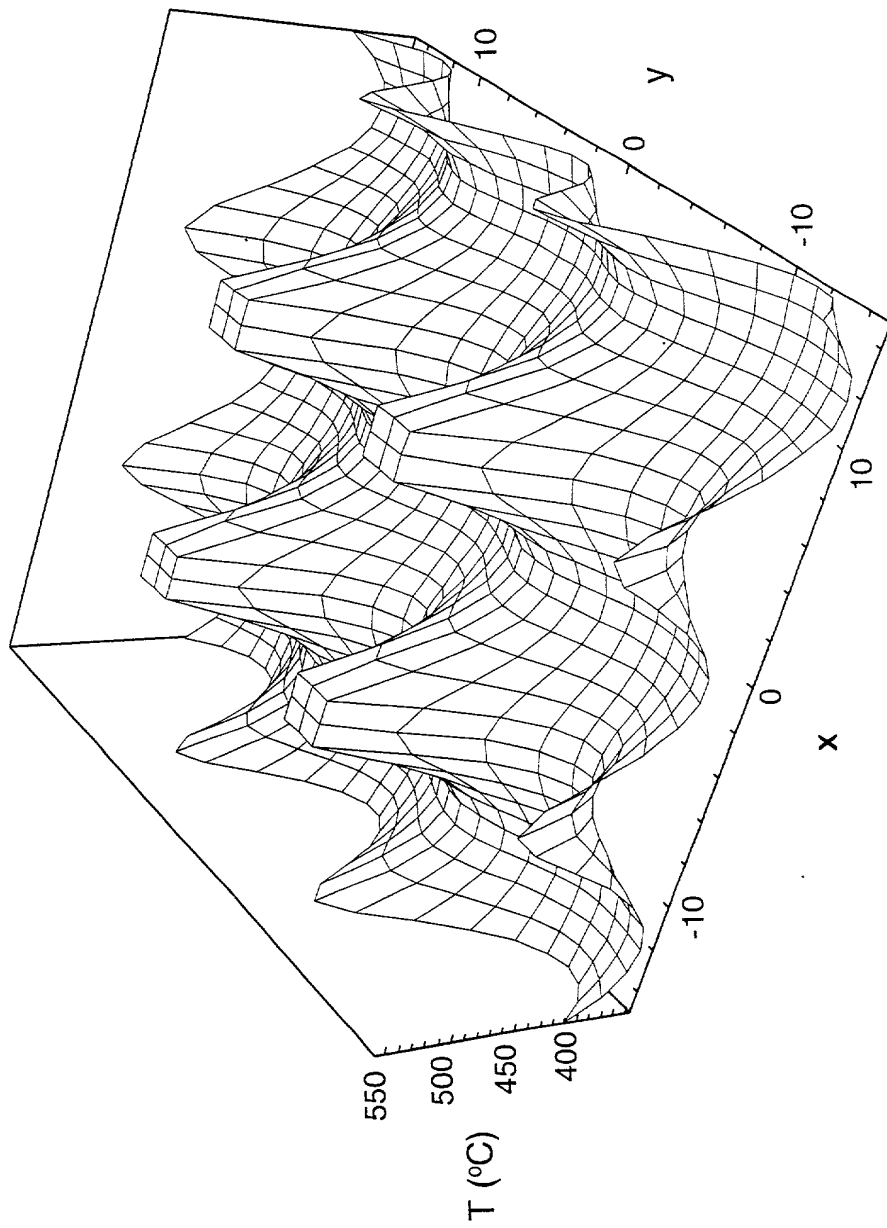


FIG. 79

3109

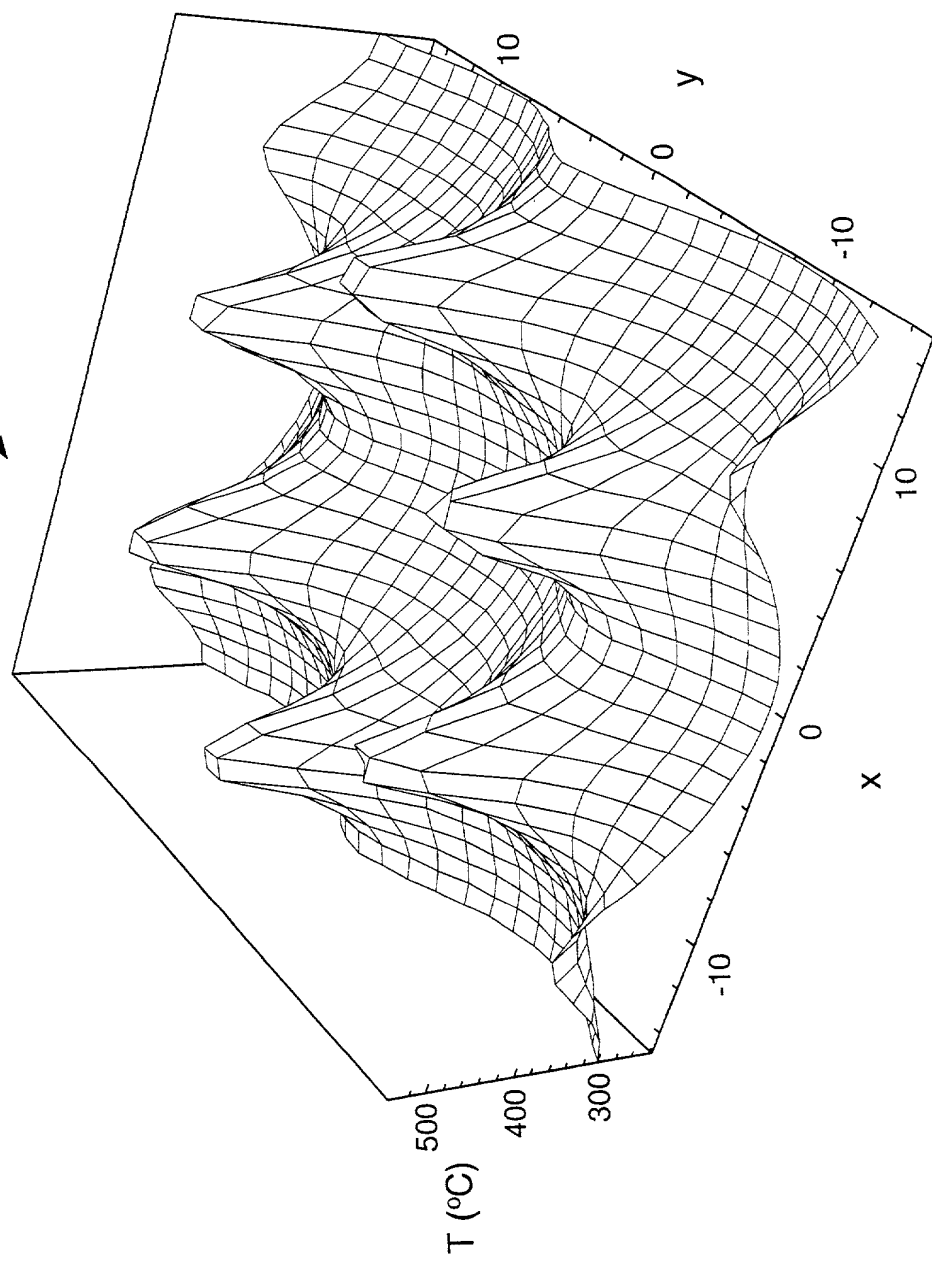


FIG. 79a

FIG. 80

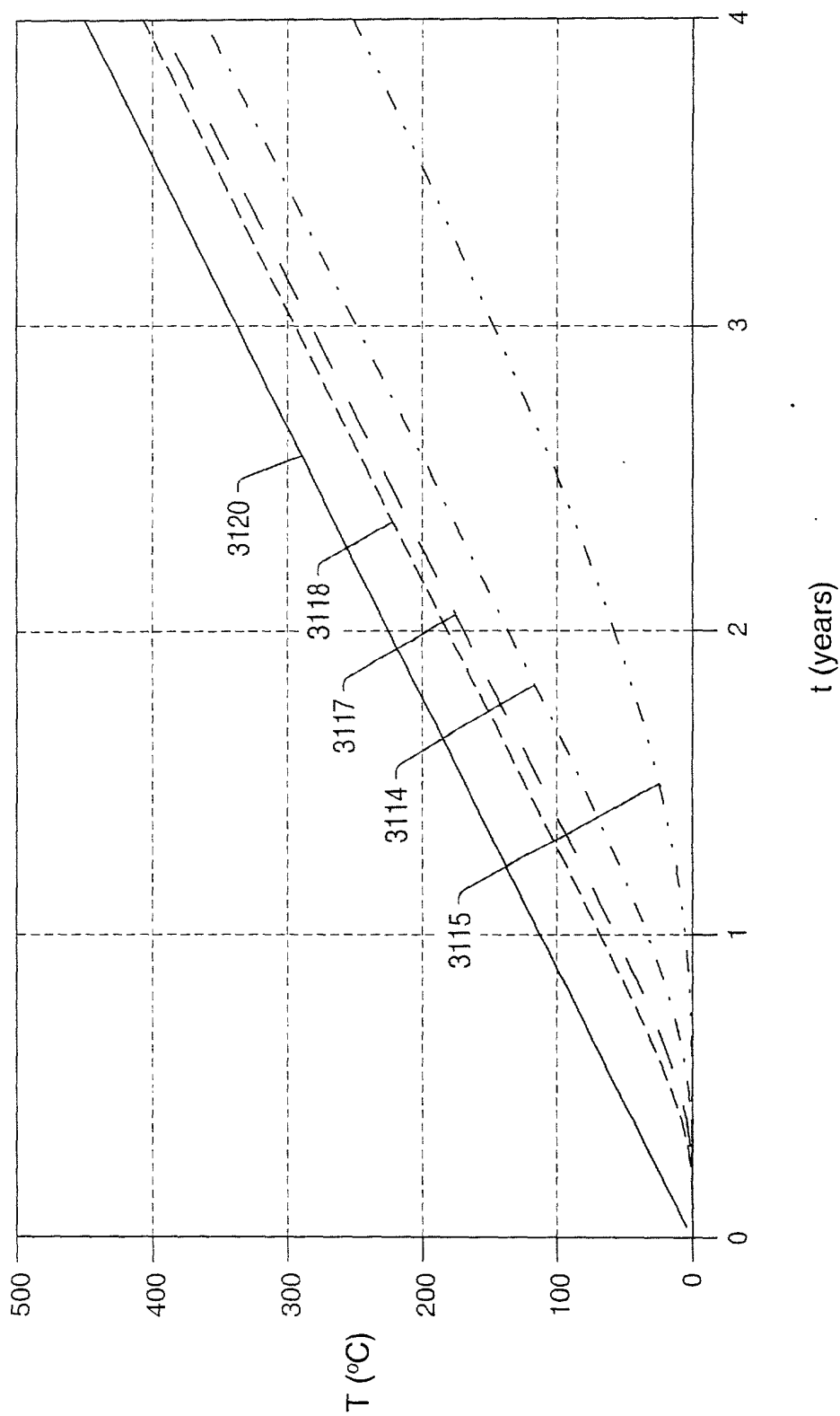


FIG. 80



$\frac{d\theta}{dt} = \frac{1}{C} \left( \frac{dQ}{dt} - \frac{dQ_{loss}}{dt} \right)$   
 $\theta = \frac{1}{C} \left( Q - Q_{loss} \right)$

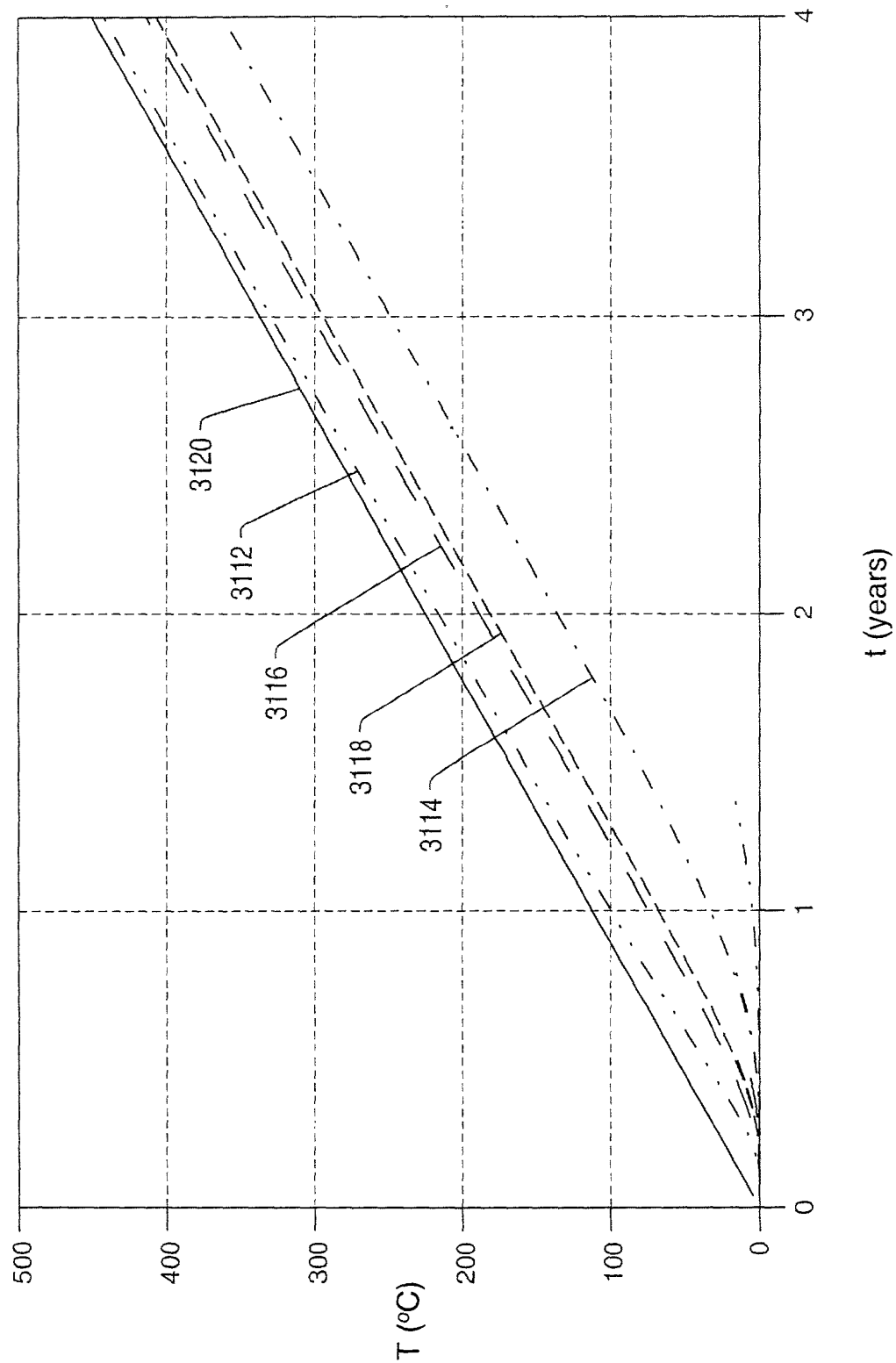


FIG. 81

FIG. 81a

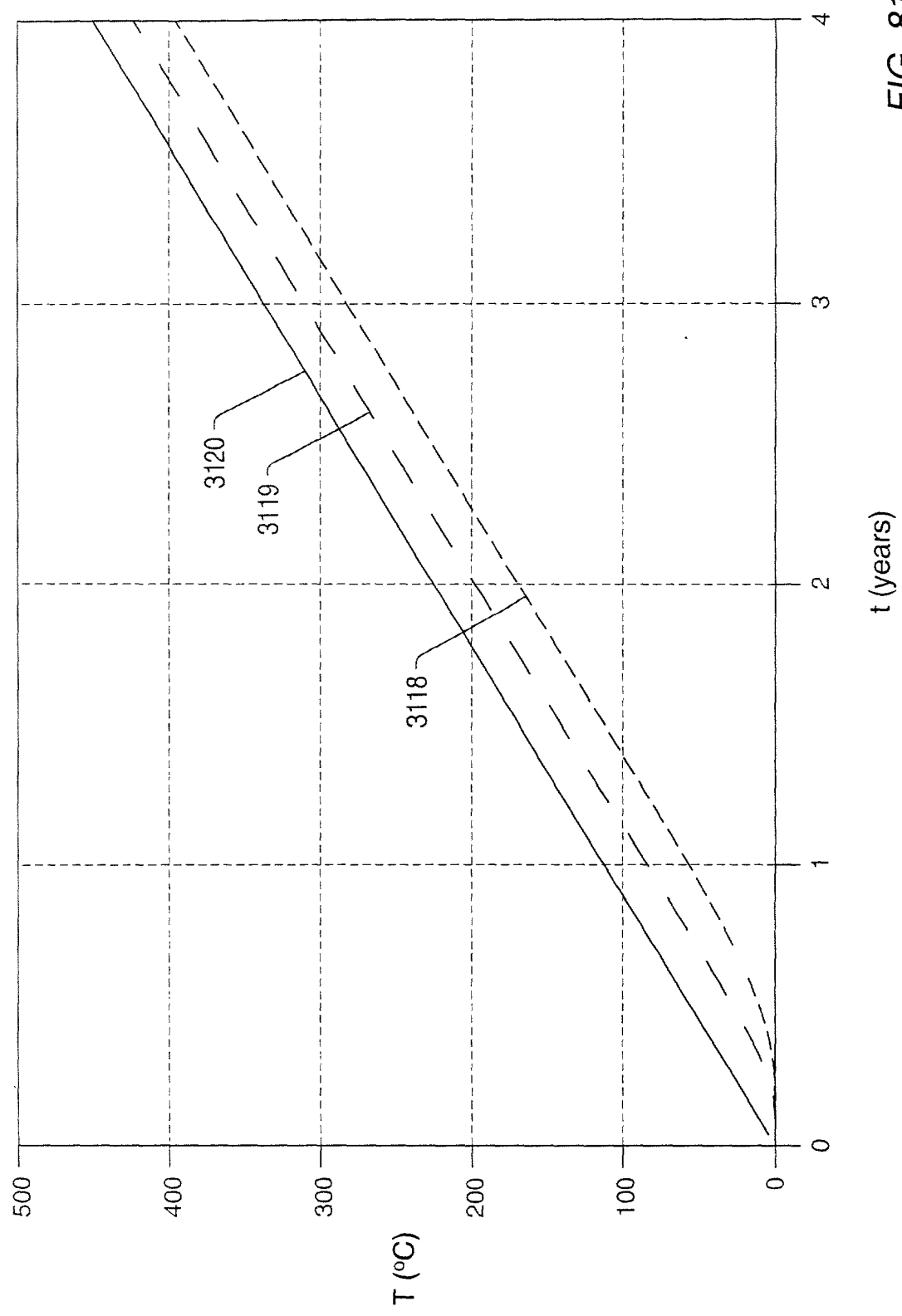


FIG. 81a

FIG. 81b

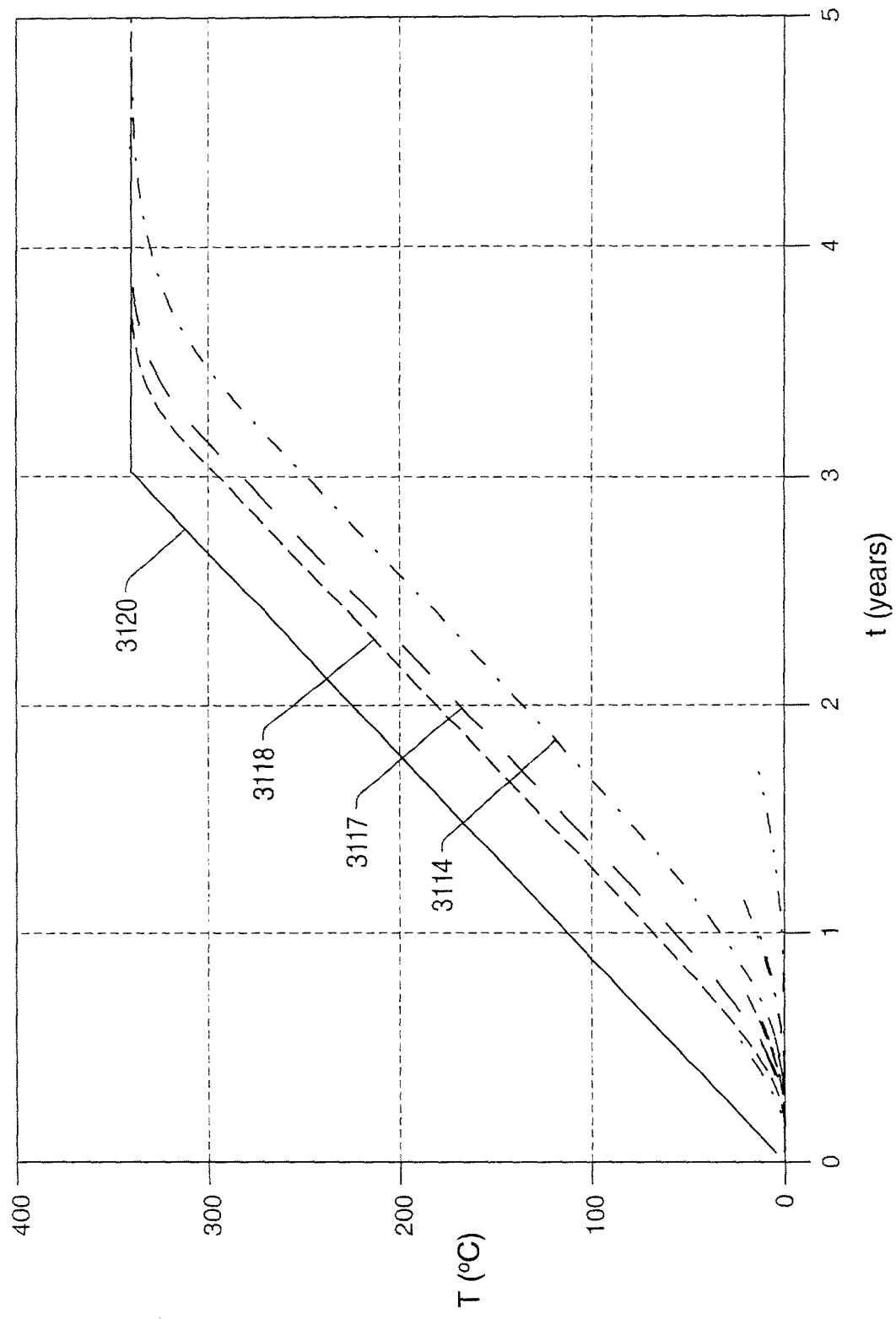
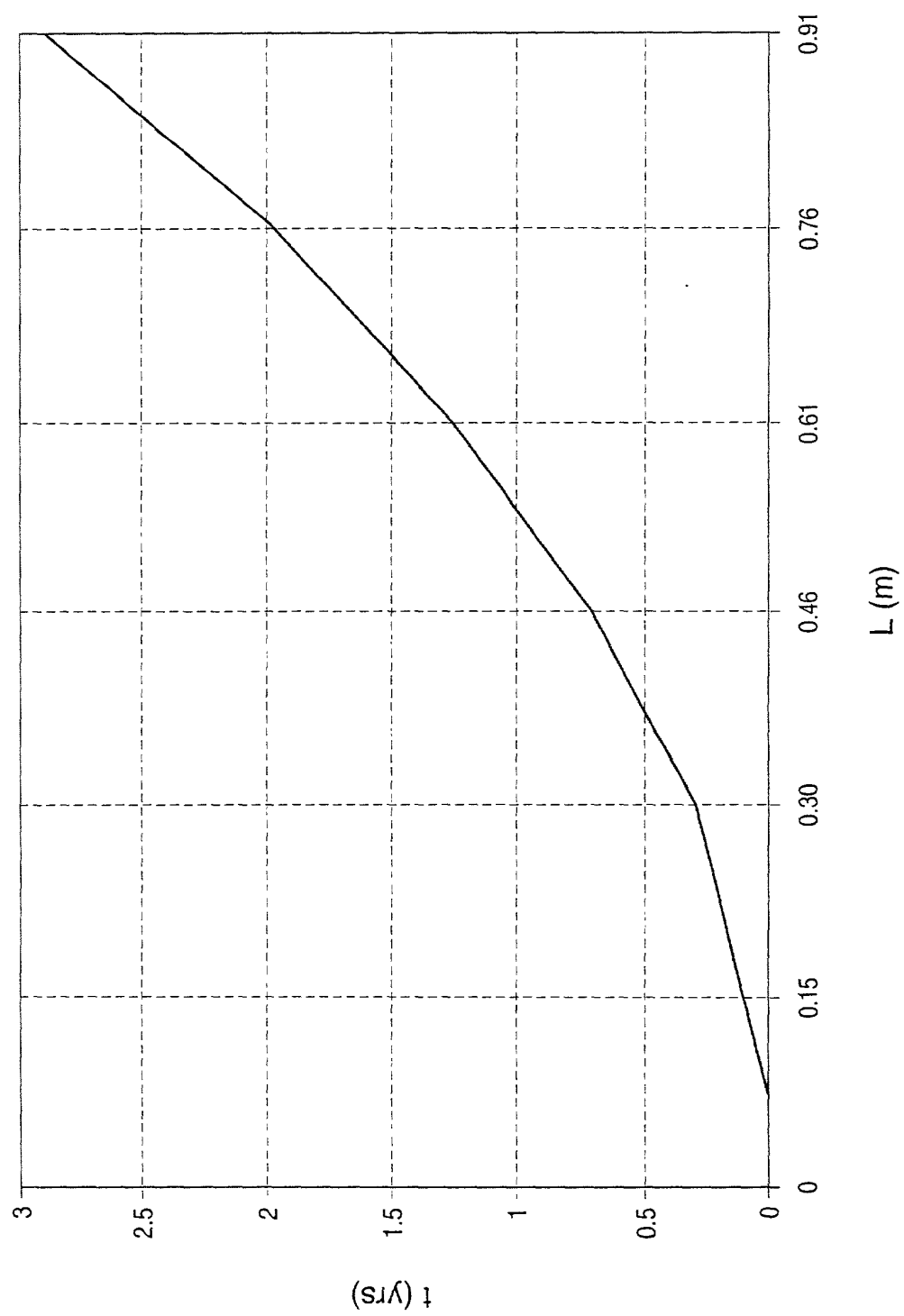
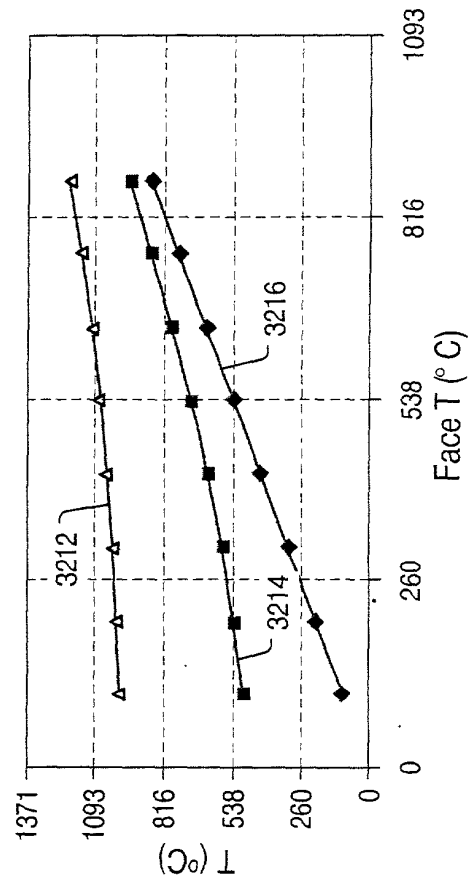
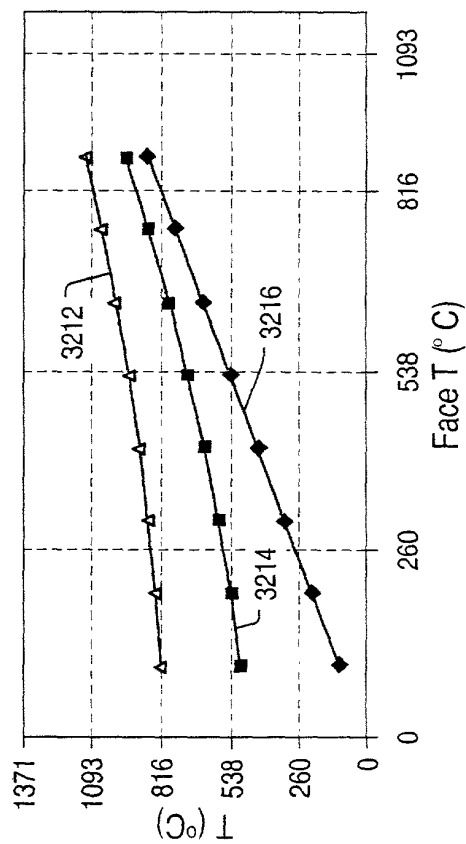
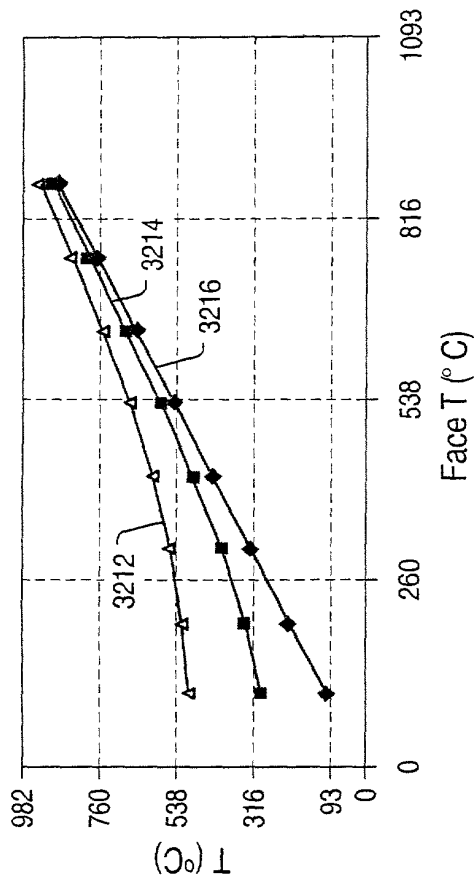
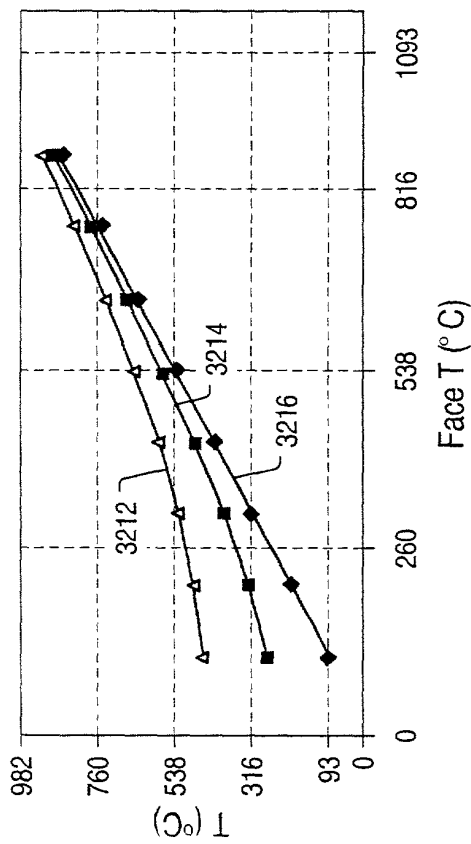


FIG. 81b









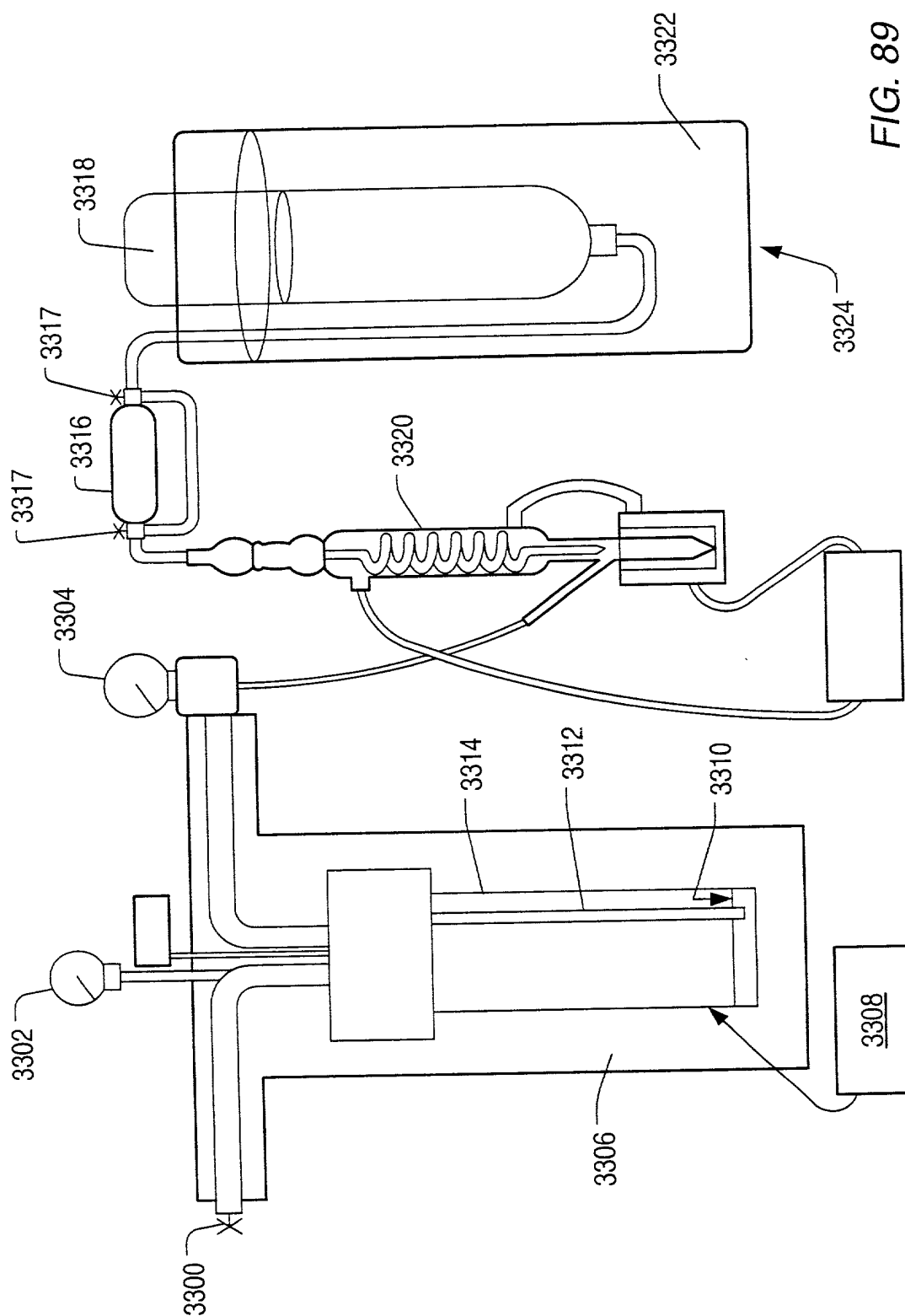




Fig. 90. The temperature dependence of the vapor pressure of the liquid phase of the system  $\text{H}_2\text{O}-\text{H}_2\text{O}_2$  at various concentrations of  $\text{H}_2\text{O}_2$  in the liquid phase.

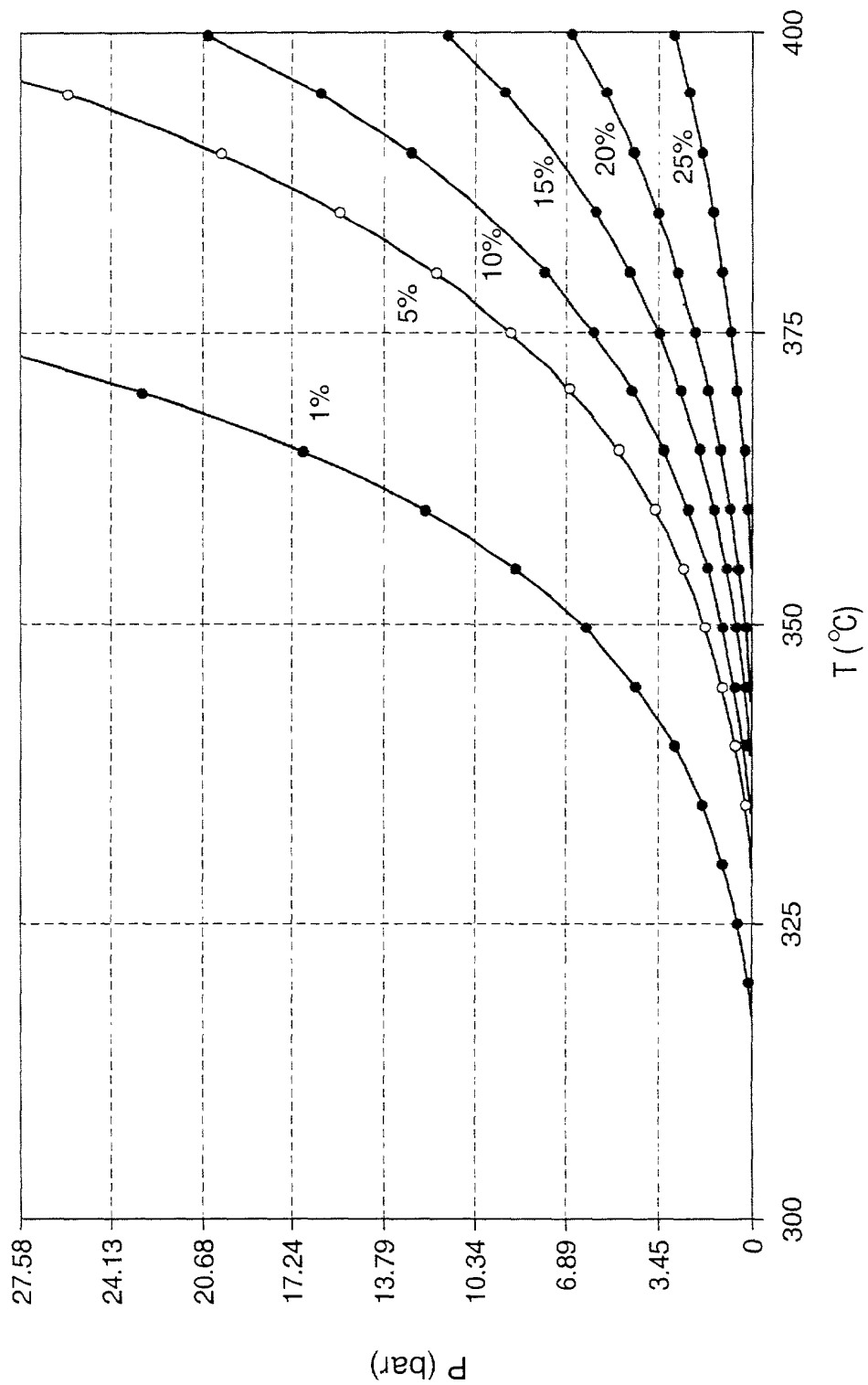


FIG. 90

$\frac{dP}{dT} = \frac{H_{vap} - H_{liq}}{T \Delta V}$   $\frac{dP}{dT} = \frac{H_{vap} - H_{liq}}{T \Delta V}$   $\frac{dP}{dT} = \frac{H_{vap} - H_{liq}}{T \Delta V}$   $\frac{dP}{dT} = \frac{H_{vap} - H_{liq}}{T \Delta V}$

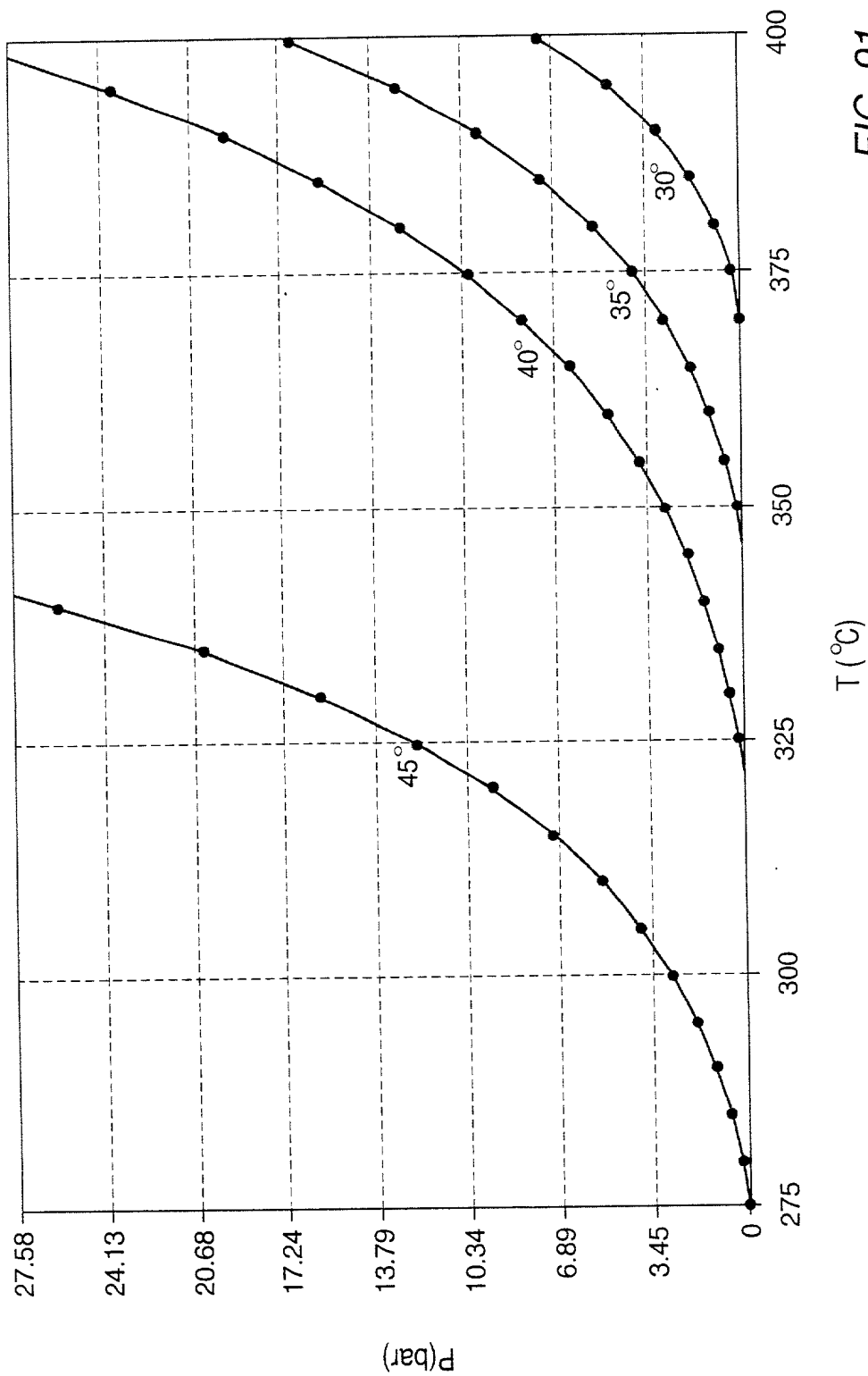


FIG. 91

$\frac{dP}{dT} = \frac{H_{vap} - H_{liq}}{T \Delta V}$

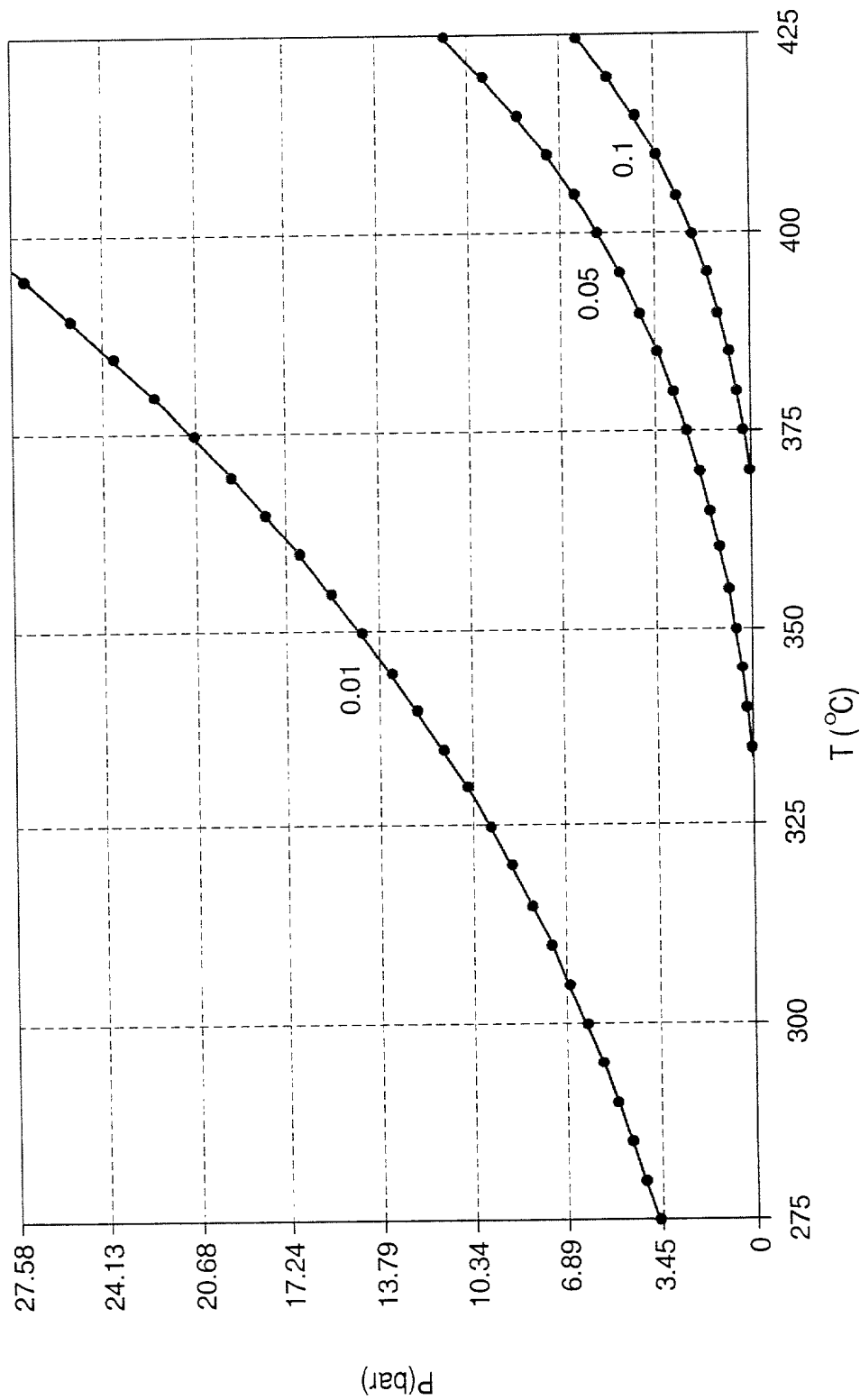


FIG. 92



Figure 1 is a graph showing the pressure dependence of the glass transition temperature  $T_g$  for poly(vinylidene fluoride). The y-axis represents pressure  $P$  in bar, ranging from 0 to 27.58. The x-axis represents temperature  $T$  in  $^{\circ}\text{C}$ , ranging from 275 to 400. Four curves are plotted, labeled 3350, 3352, 3354, and 3356, representing different samples. The curves show that  $T_g$  increases with increasing pressure. Curve 3350 is the lowest, followed by 3352, 3354, and 3356 is the highest.

 $T(^{\circ}\text{C})$

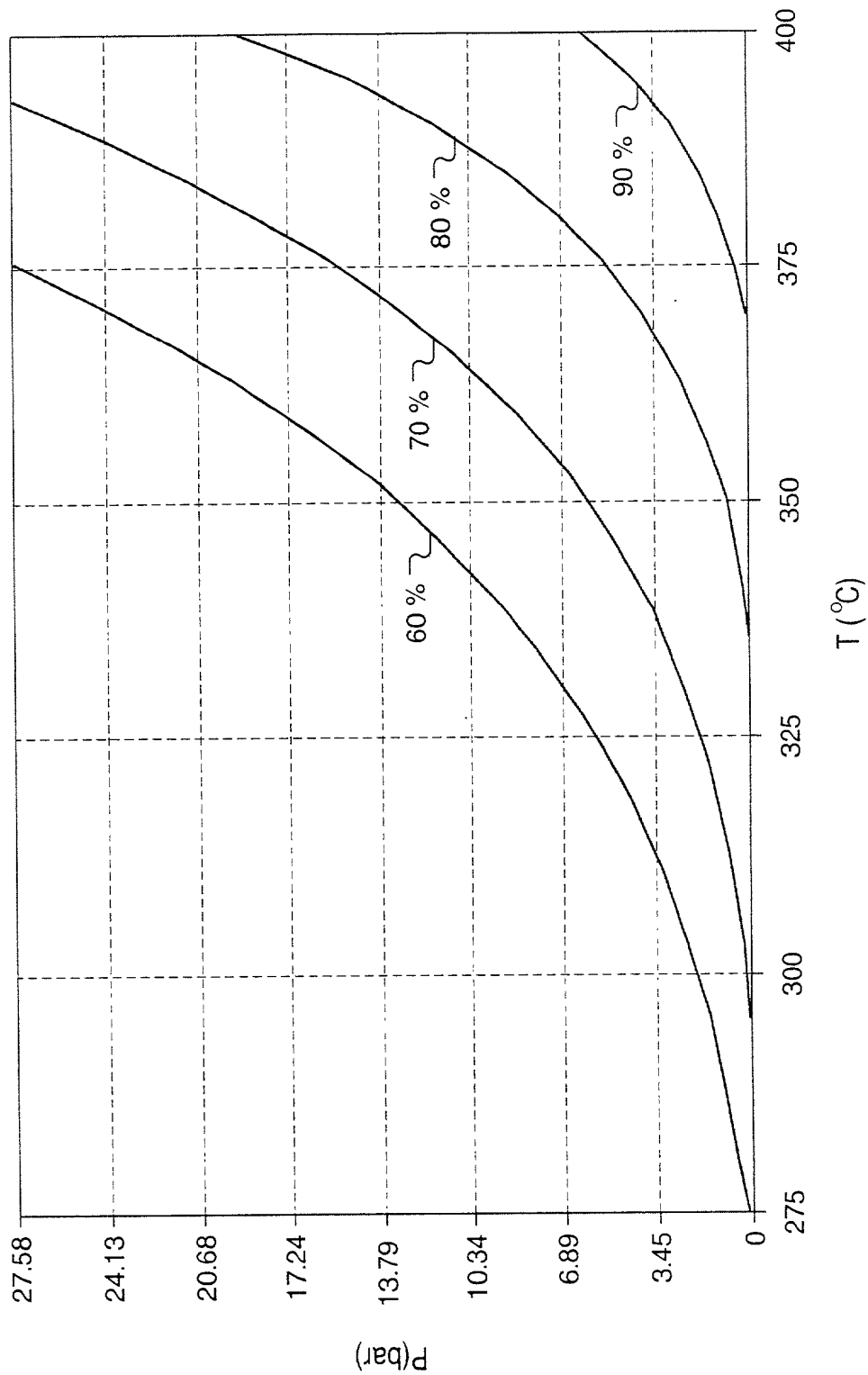


FIG. 95

FIG. 96 is a graph showing the relationship between the pressure P (bar) and the temperature T (°C) for a system. The graph includes three curves labeled 1.8, 1.9, and 1.99, representing different conditions or parameters. The pressure P (bar) is plotted on the vertical axis, and the temperature T (°C) is plotted on the horizontal axis. The curves show that as temperature increases, the pressure also increases, with the rate of increase being more pronounced at higher temperatures.

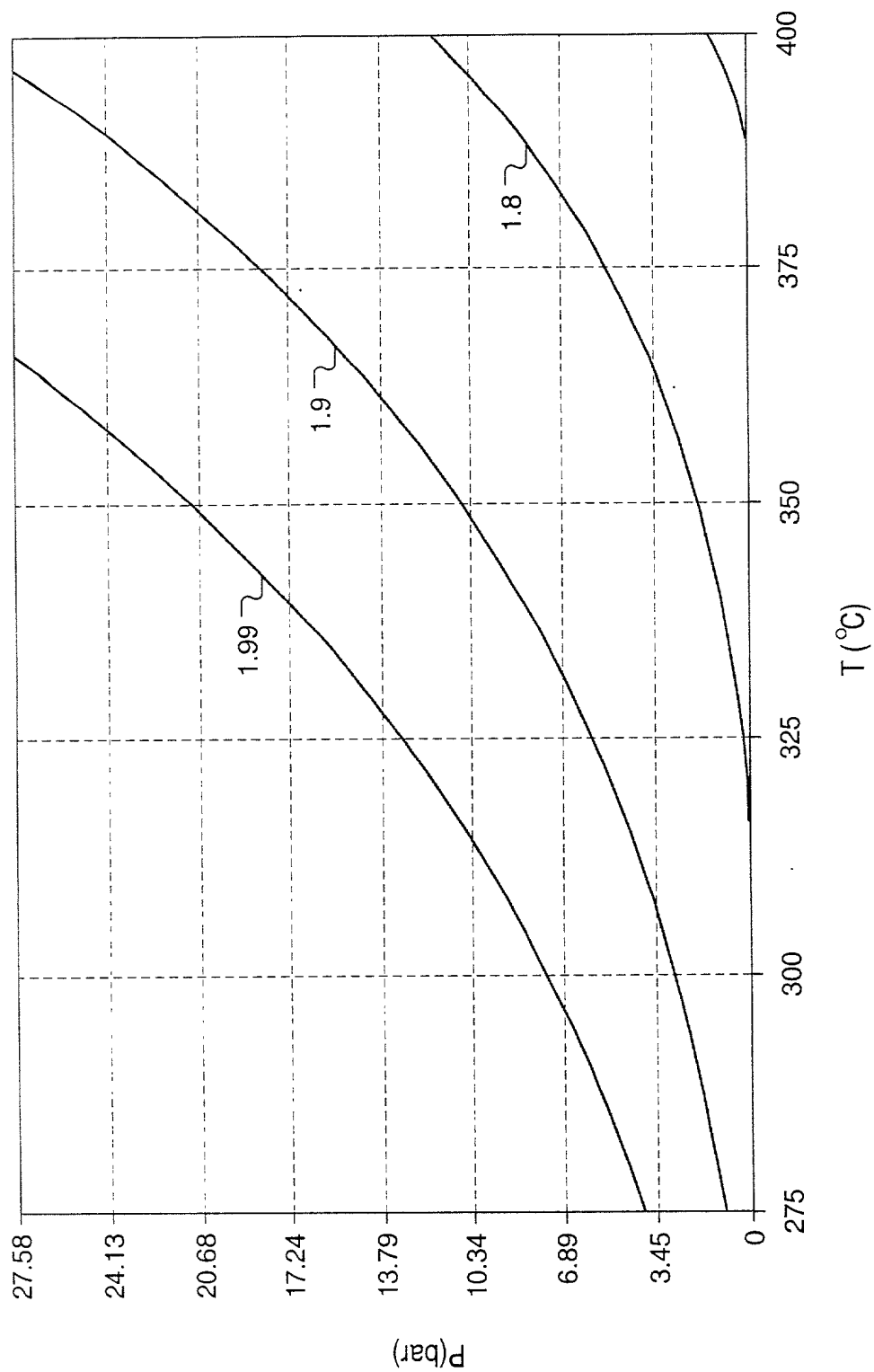


FIG. 96

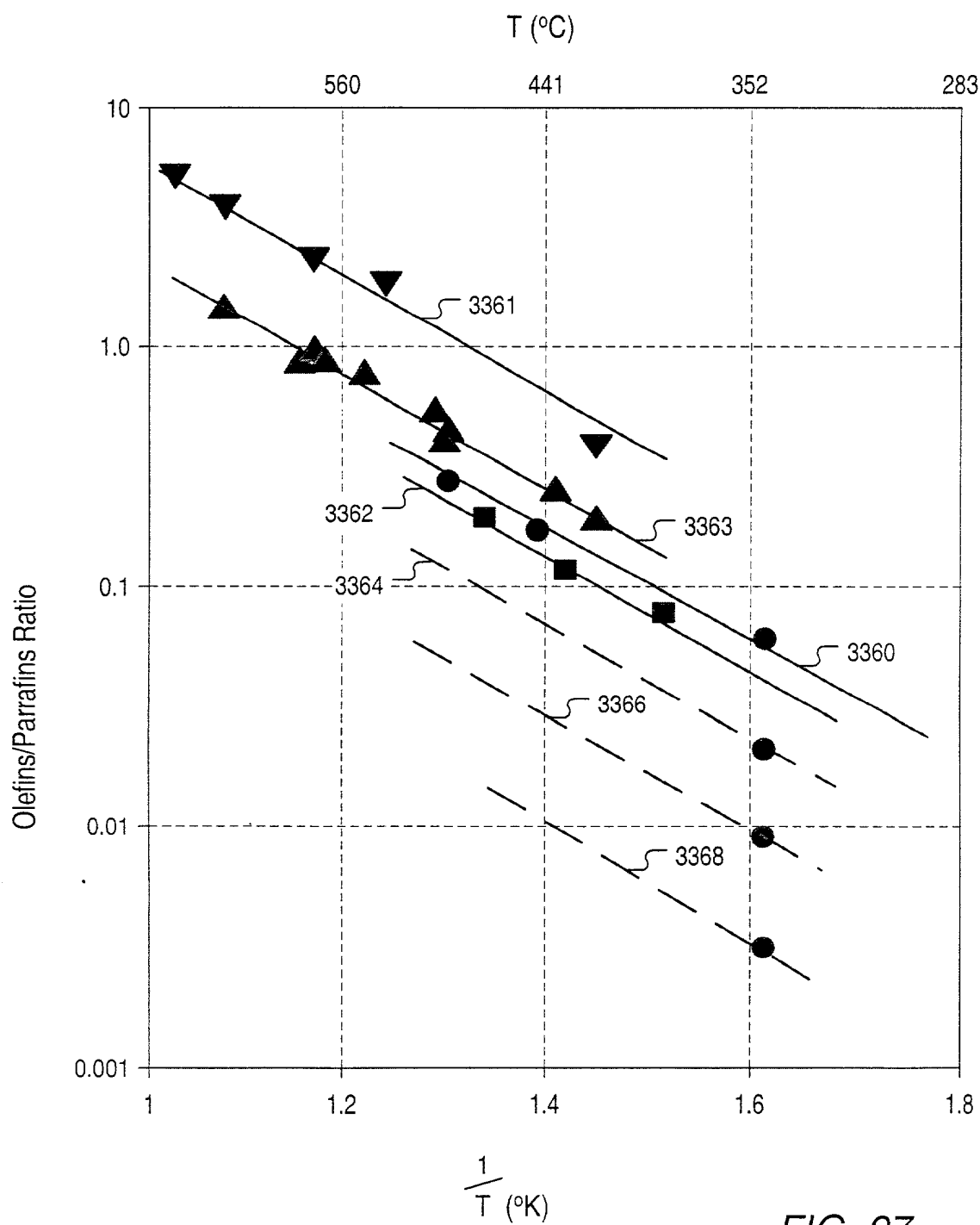


FIG. 97



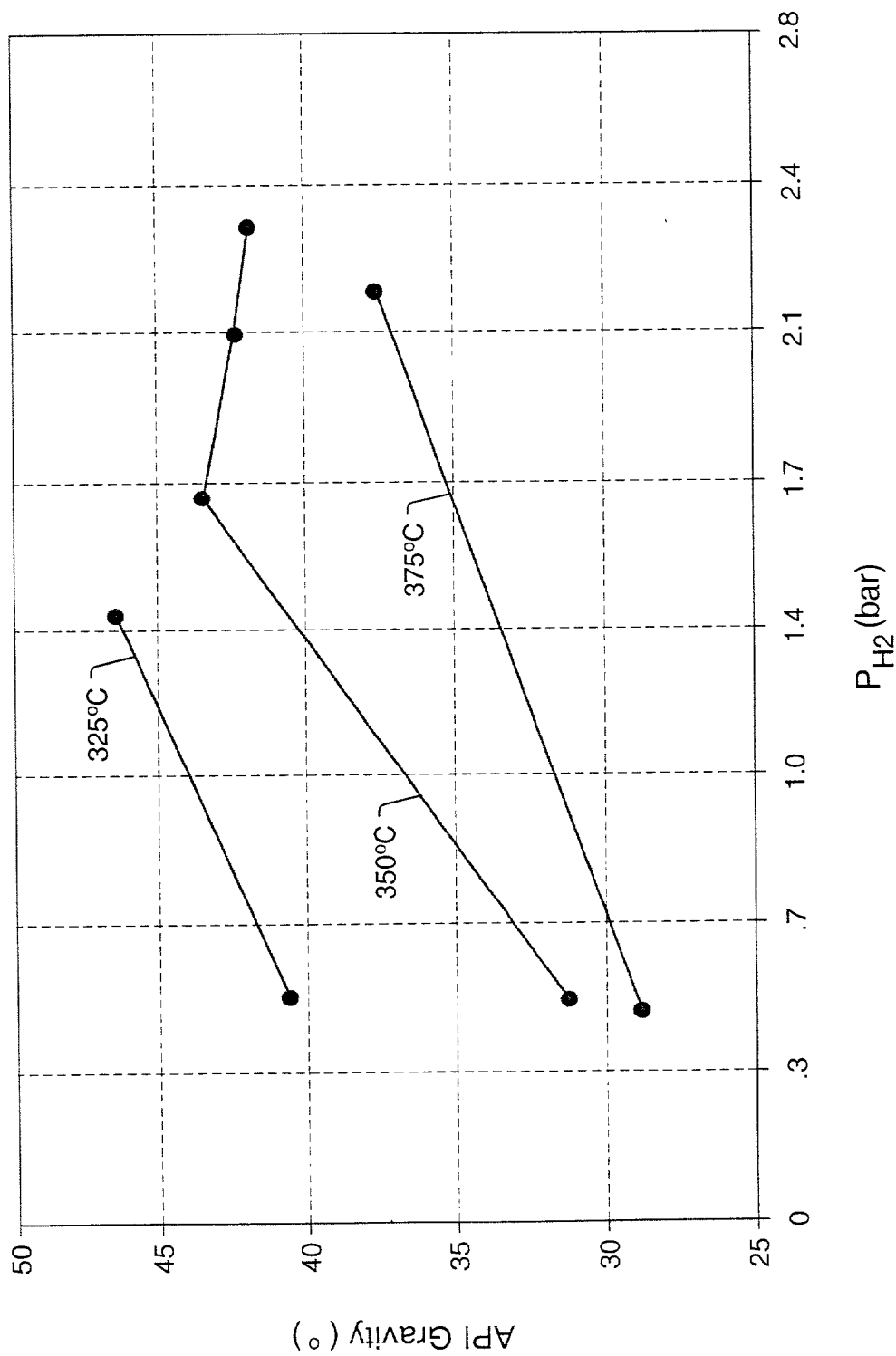


FIG. 98

FIG. 99 is a graph showing the relationship between the pressure of hydrogen gas (P<sub>H2</sub>) and the oil yield (m<sup>3</sup>/kg) for three different temperatures: 325°C, 350°C, and 375°C.

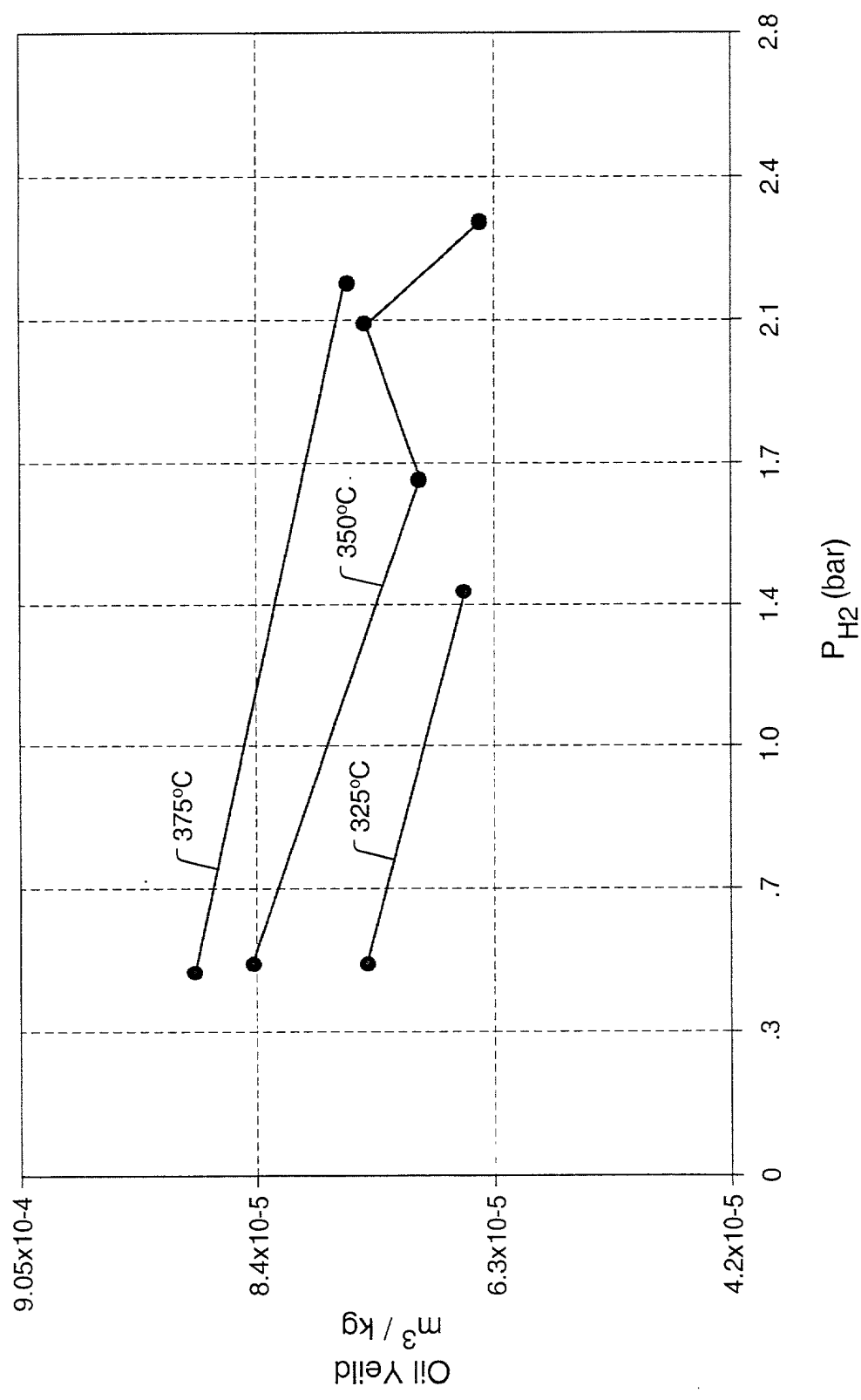


FIG. 99

FIG. 100

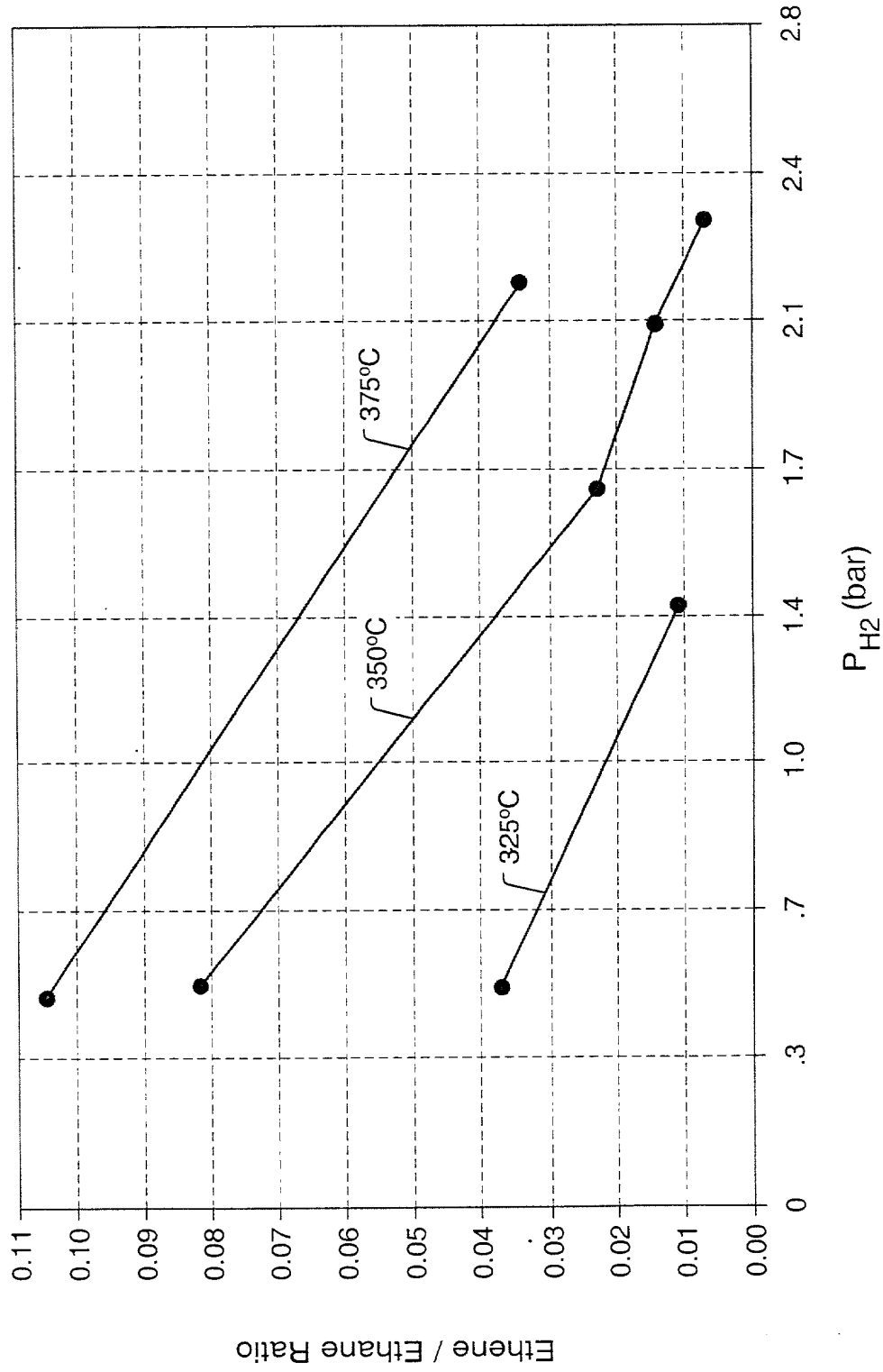


FIG. 100

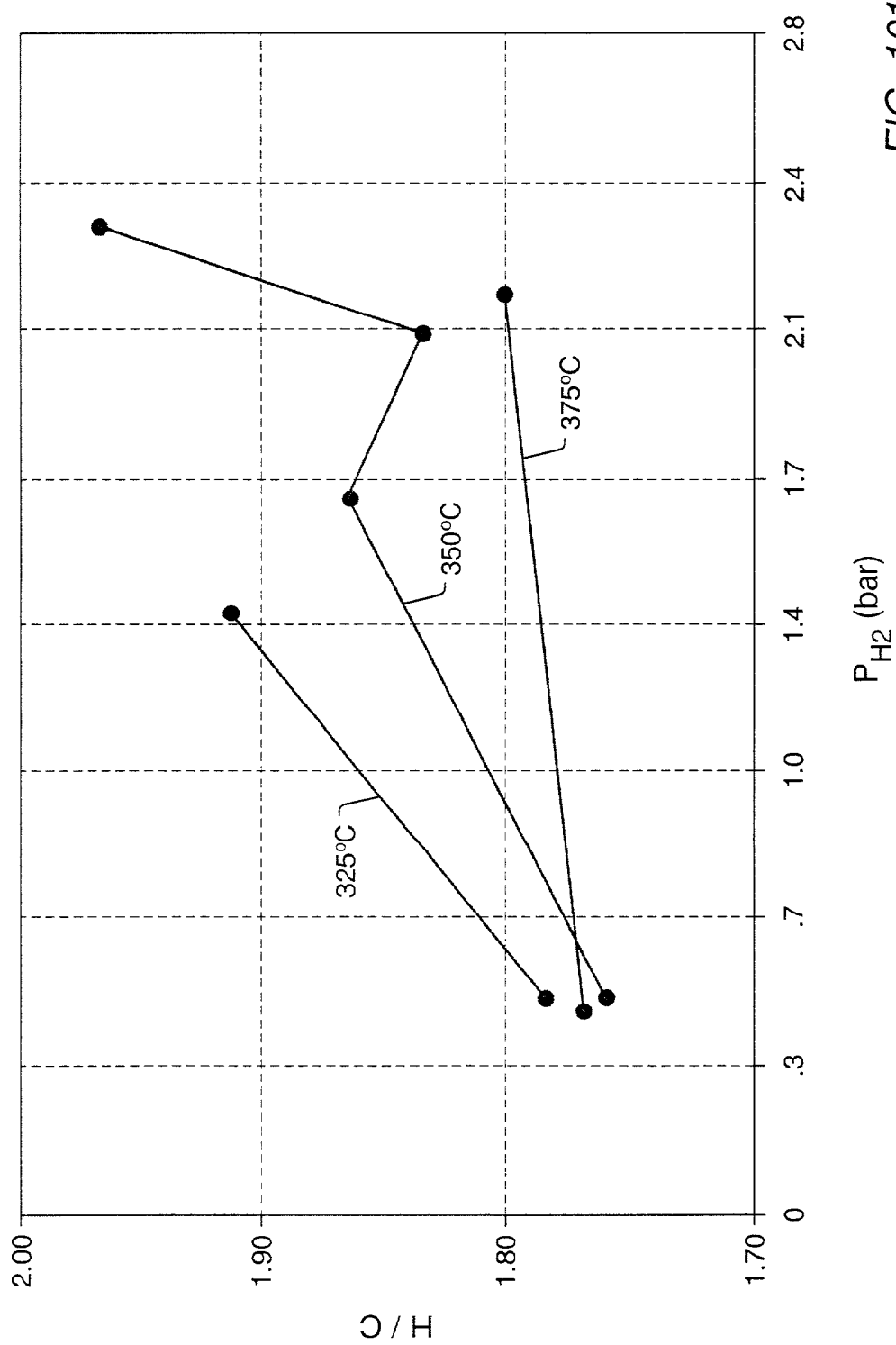


FIG. 101

FIG. 102 is a schematic diagram of a system for processing a material. The system includes a material source 3400, a processing chamber 3402, a heating element 3404, a gas inlet 3406, a gas outlet 3408, a gas flow controller 3410, a gas detector 3412, a gas filter 3414, and a gas purifier 3416. The material source 3400 is connected to the processing chamber 3402 via a gas inlet 3406. The processing chamber 3402 is connected to a gas outlet 3408. The gas outlet 3408 is connected to a gas flow controller 3410. The gas flow controller 3410 is connected to a gas detector 3412. The gas detector 3412 is connected to a gas filter 3414. The gas filter 3414 is connected to a gas purifier 3416. The gas purifier 3416 is connected to a gas inlet 3406. The heating element 3404 is connected to the processing chamber 3402. The gas inlet 3406 is connected to the processing chamber 3402. The gas outlet 3408 is connected to the processing chamber 3402. The gas flow controller 3410 is connected to the processing chamber 3402. The gas detector 3412 is connected to the processing chamber 3402. The gas filter 3414 is connected to the processing chamber 3402. The gas purifier 3416 is connected to the processing chamber 3402.

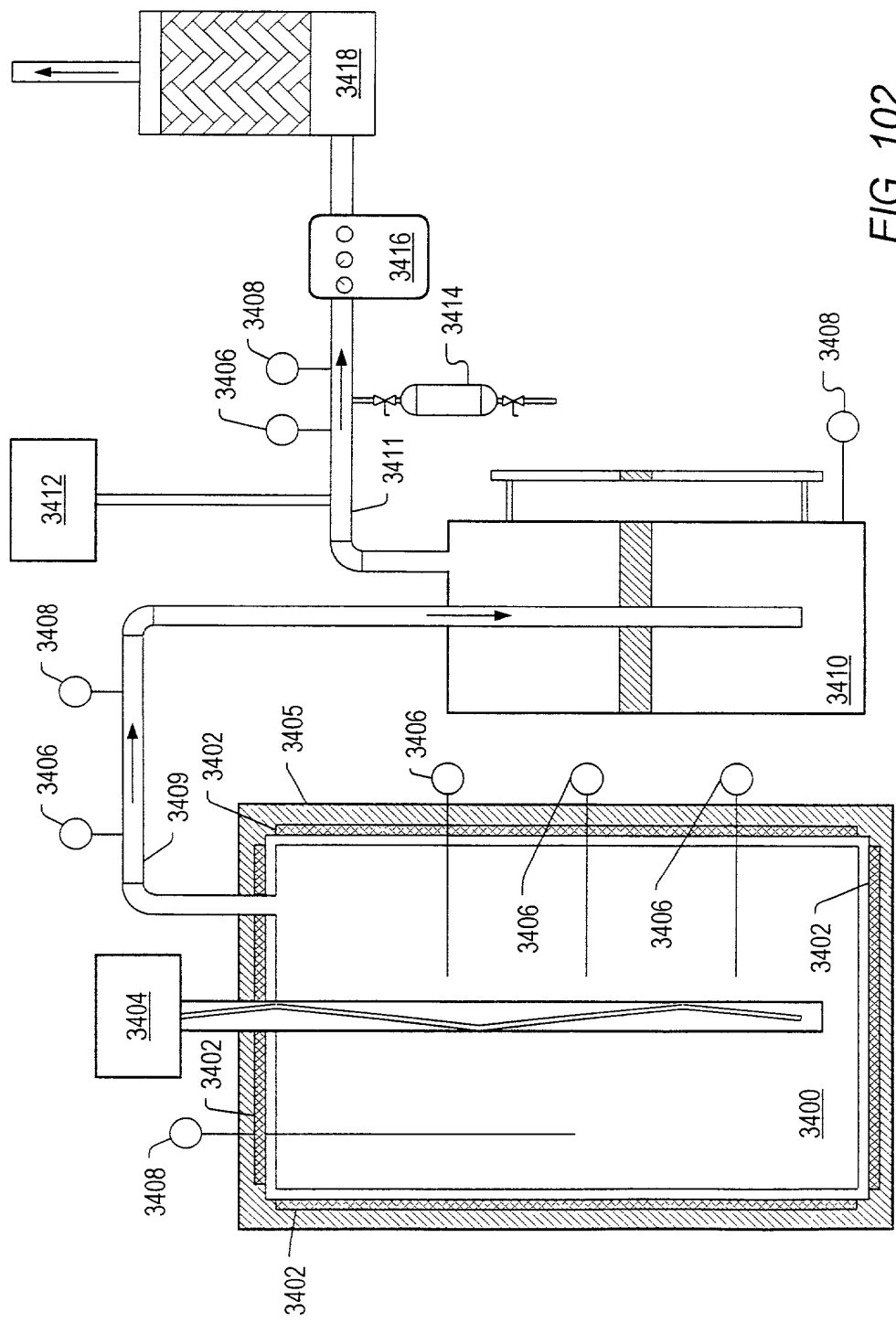


FIG. 102

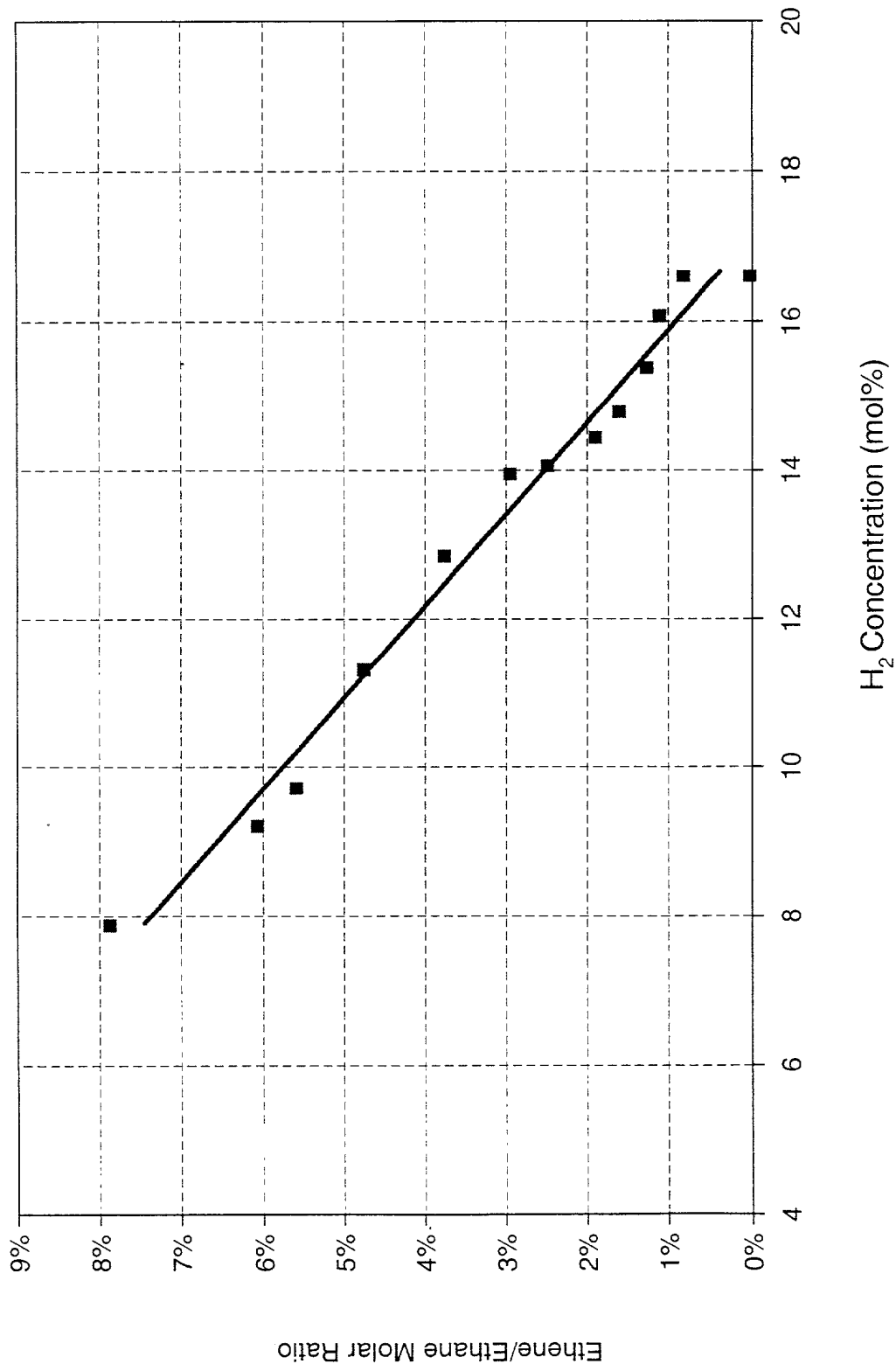
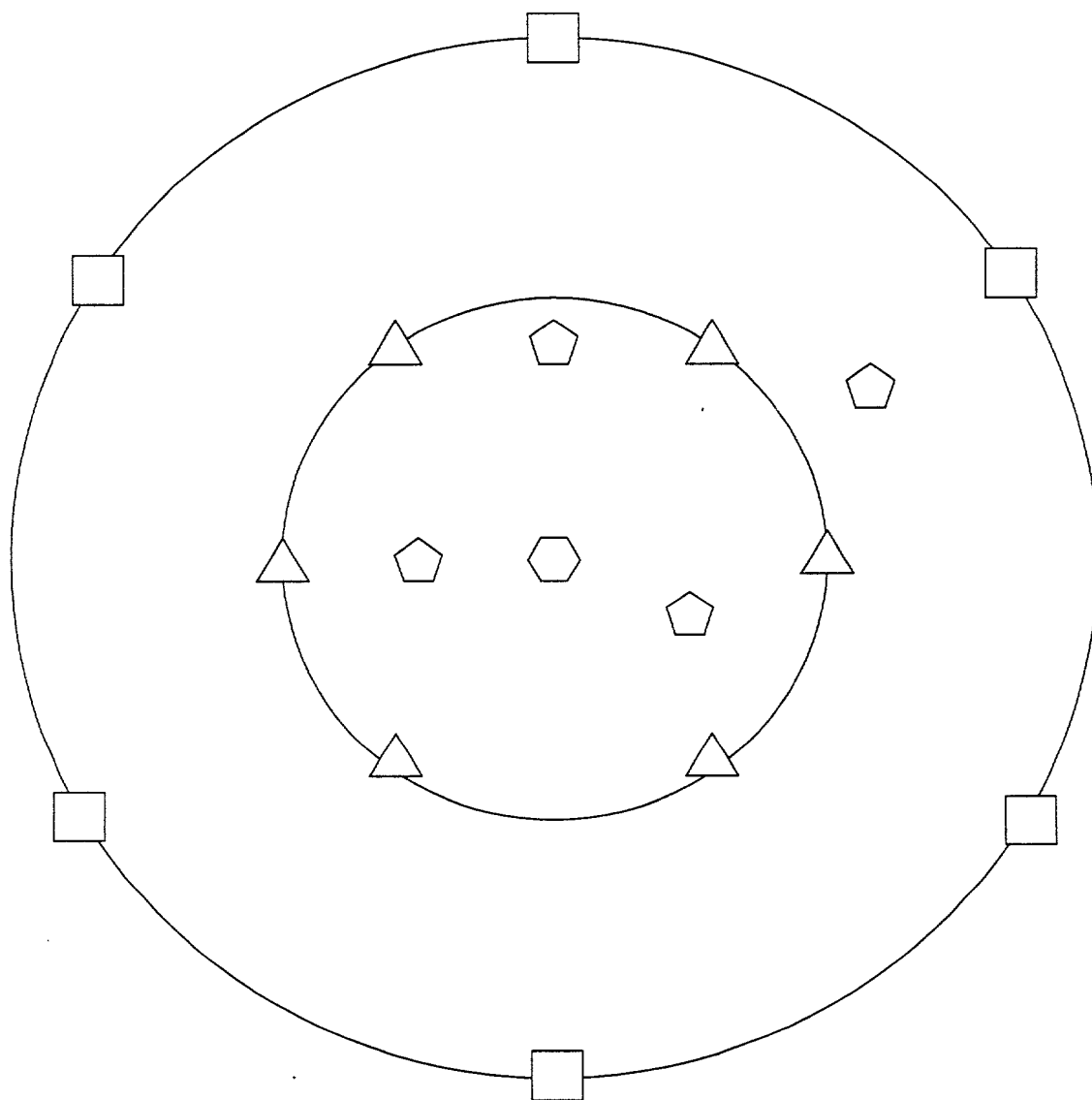


FIG. 103

FIG. 104 is a schematic diagram of a system 100. The system 100 includes a central processing unit 102, a memory unit 104, a network interface unit 106, a user interface unit 108, and a power supply unit 110. The central processing unit 102 is connected to the memory unit 104, the network interface unit 106, the user interface unit 108, and the power supply unit 110. The memory unit 104 is connected to the central processing unit 102. The network interface unit 106 is connected to the central processing unit 102. The user interface unit 108 is connected to the central processing unit 102. The power supply unit 110 is connected to the central processing unit 102.



△ - 3600

⬠ - 3603

□ - 3604

⬡ - 3602

FIG. 104

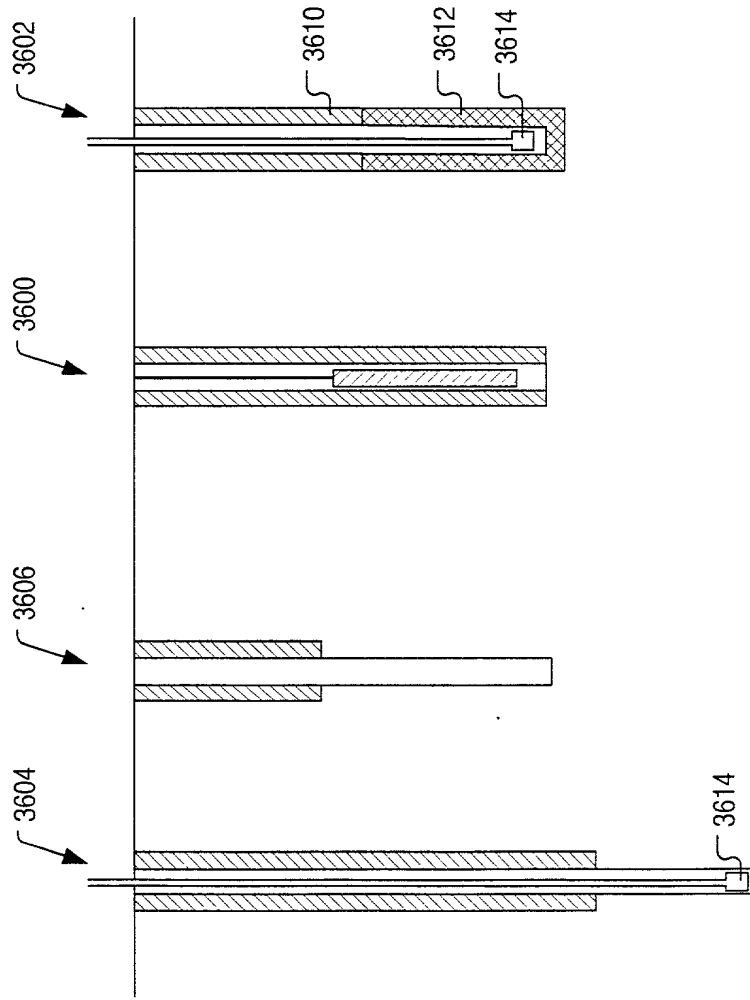


FIG. 105



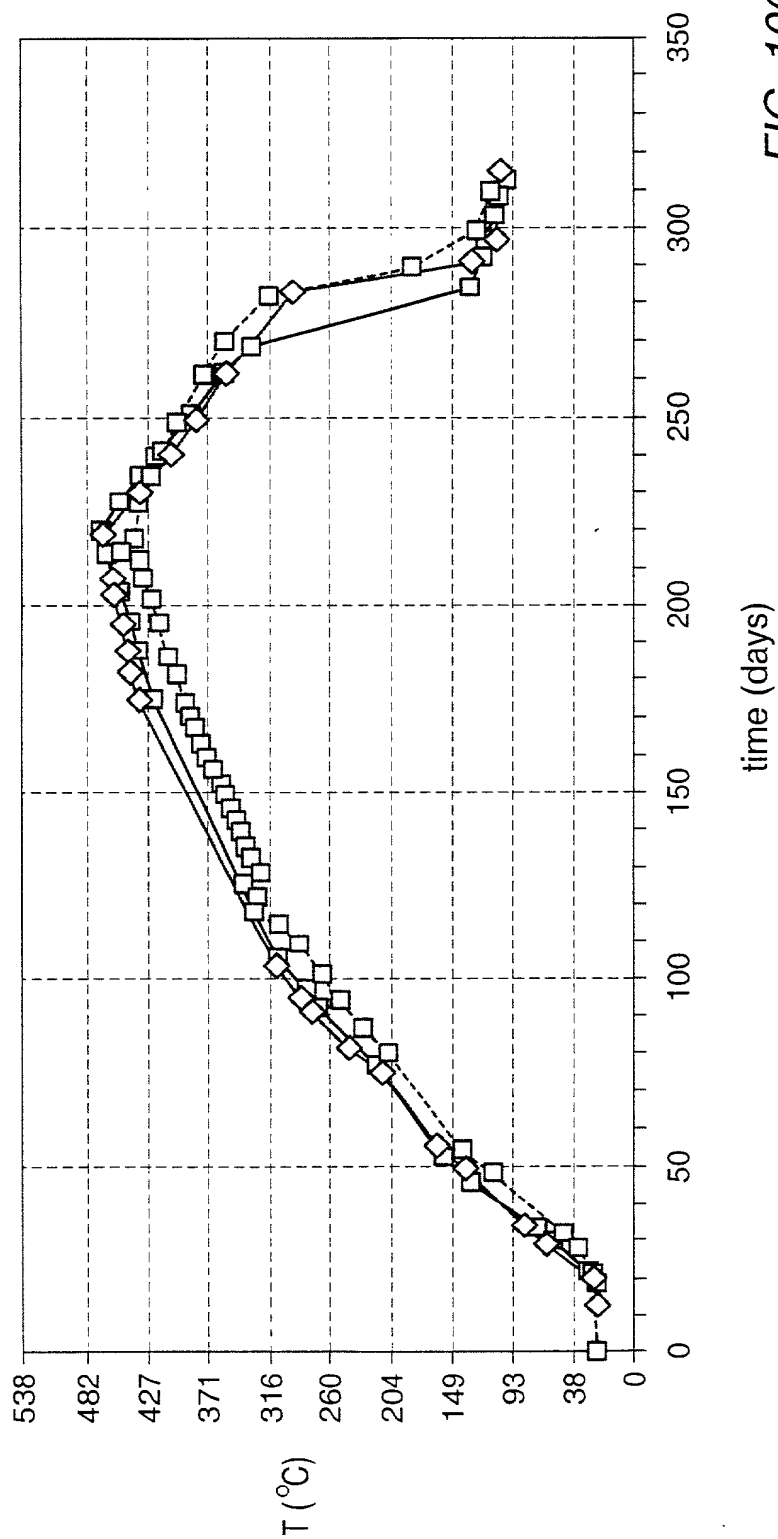


FIG. 106

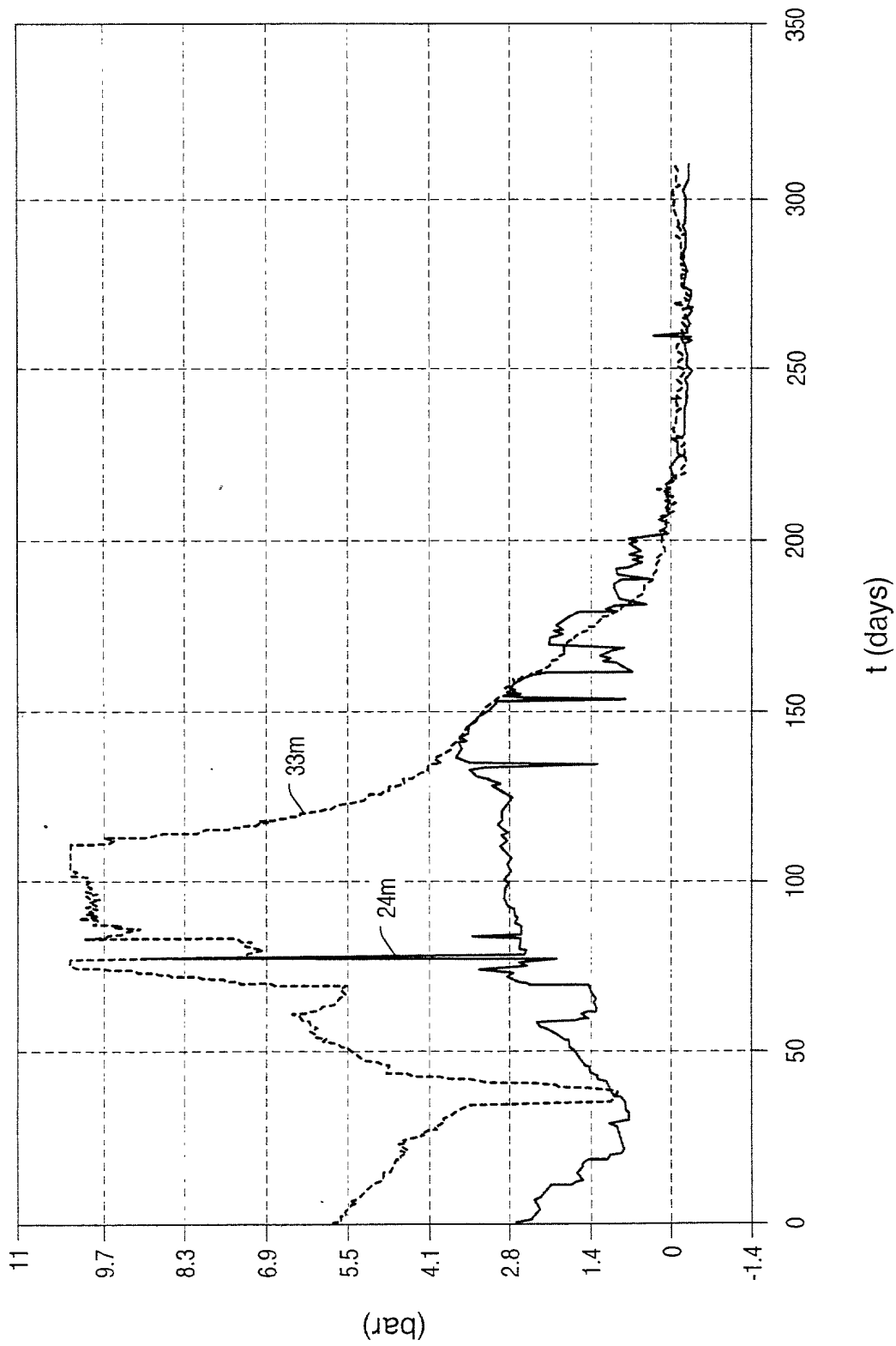


FIG. 107

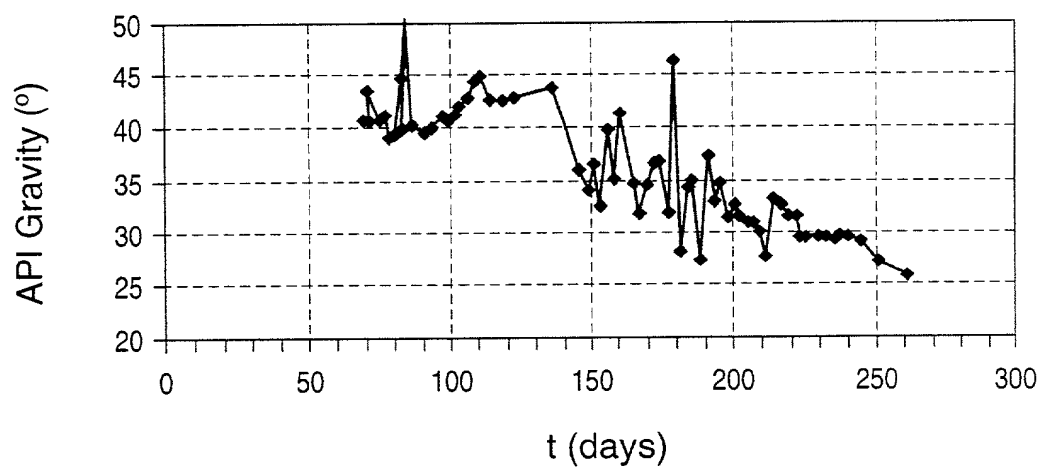


FIG. 108

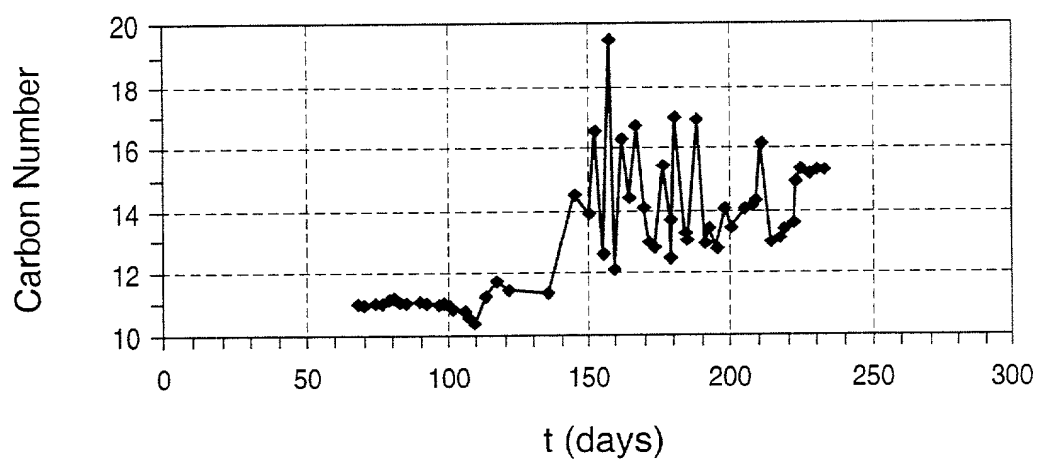


FIG. 109

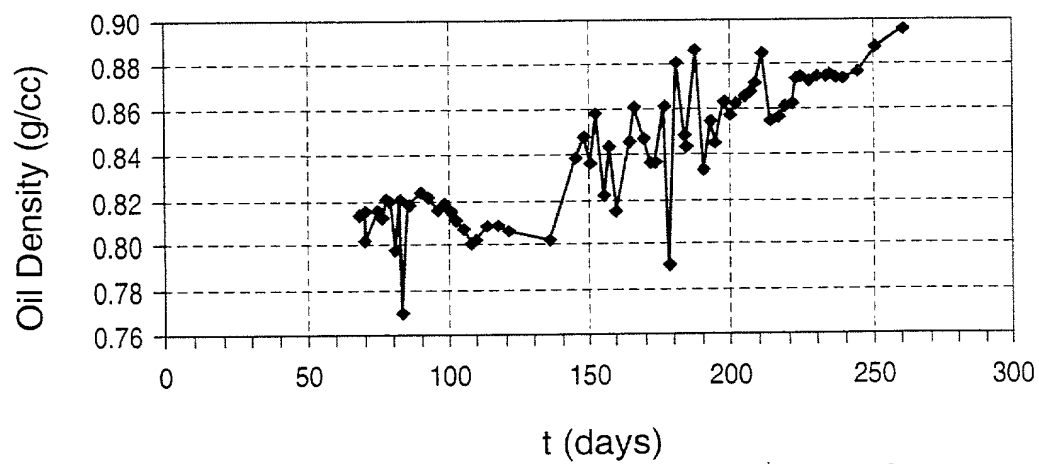


FIG. 110

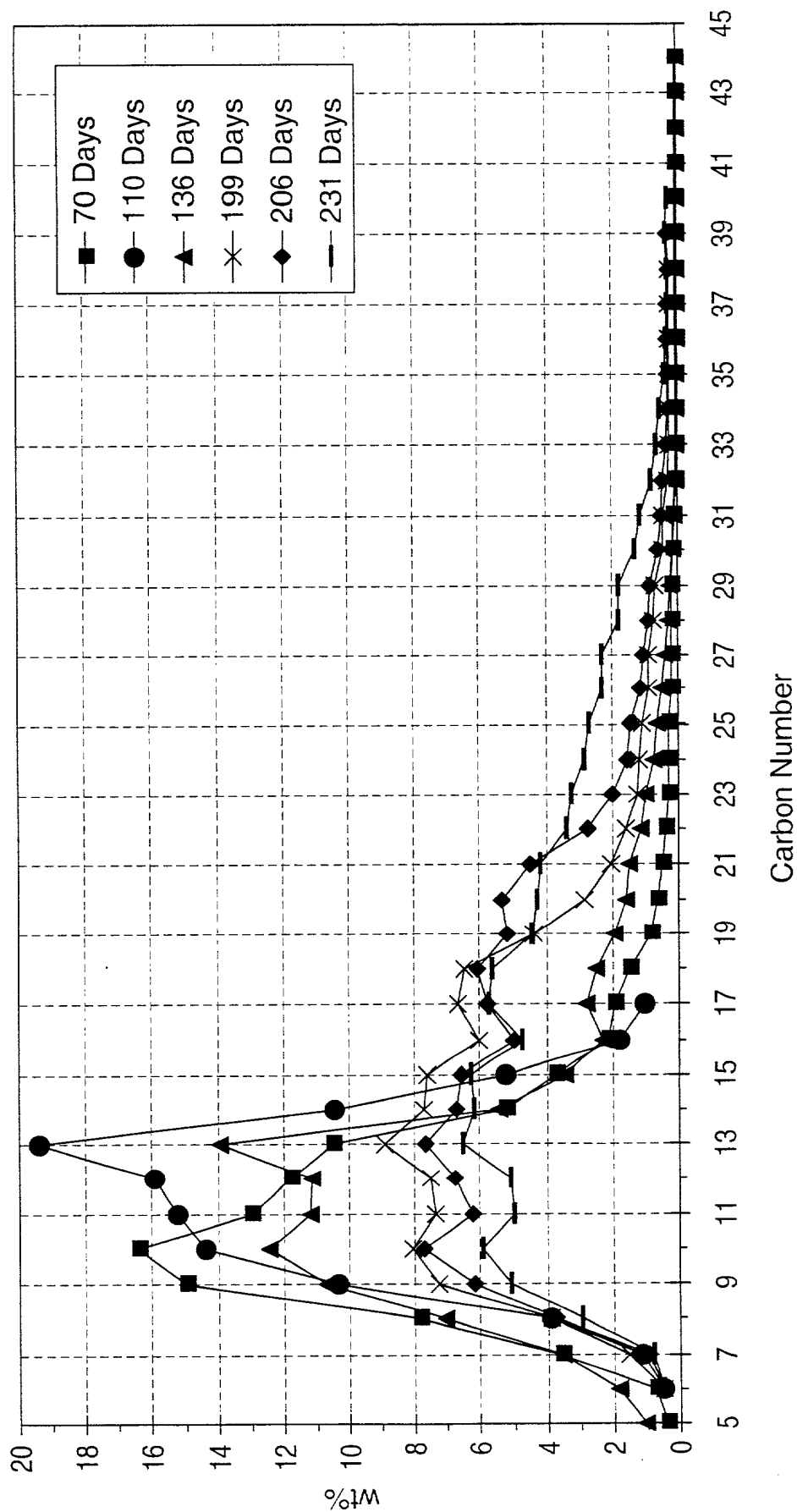


FIG. 111

Figure 112 is a graph showing the weight percentage of the various components of the polymer as a function of the carbon number (C#) of the polymer. The graph shows two curves, one for the polymer with a carbon number of 3620 and one for the polymer with a carbon number of 3622. The weight percentage of the polymer with a carbon number of 3620 is shown by the open circles and the weight percentage of the polymer with a carbon number of 3622 is shown by the filled squares. The graph shows that the weight percentage of the polymer with a carbon number of 3620 is generally higher than the weight percentage of the polymer with a carbon number of 3622, except for the carbon numbers 3620 and 3622 where the weight percentages are equal.

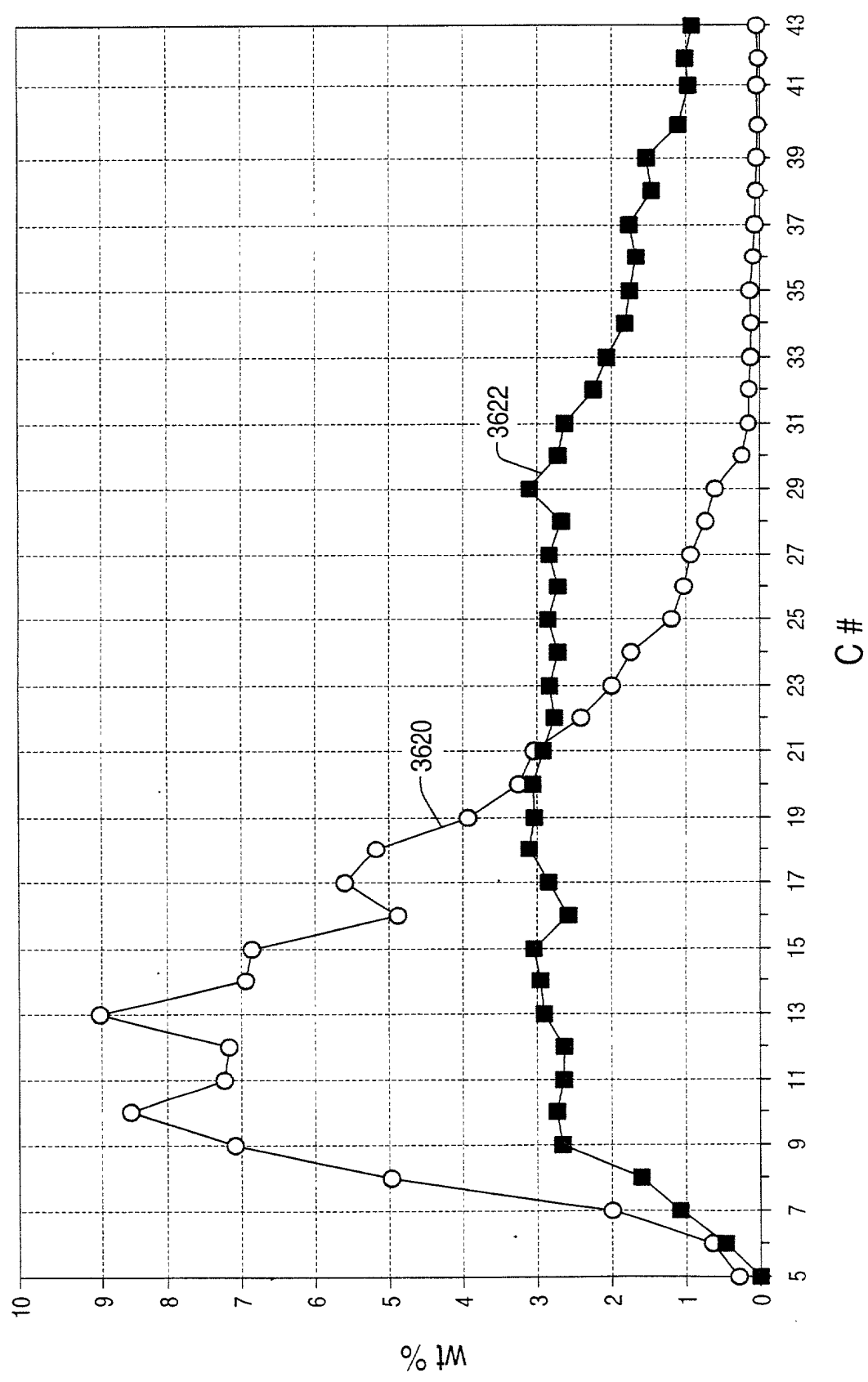


FIG. 112

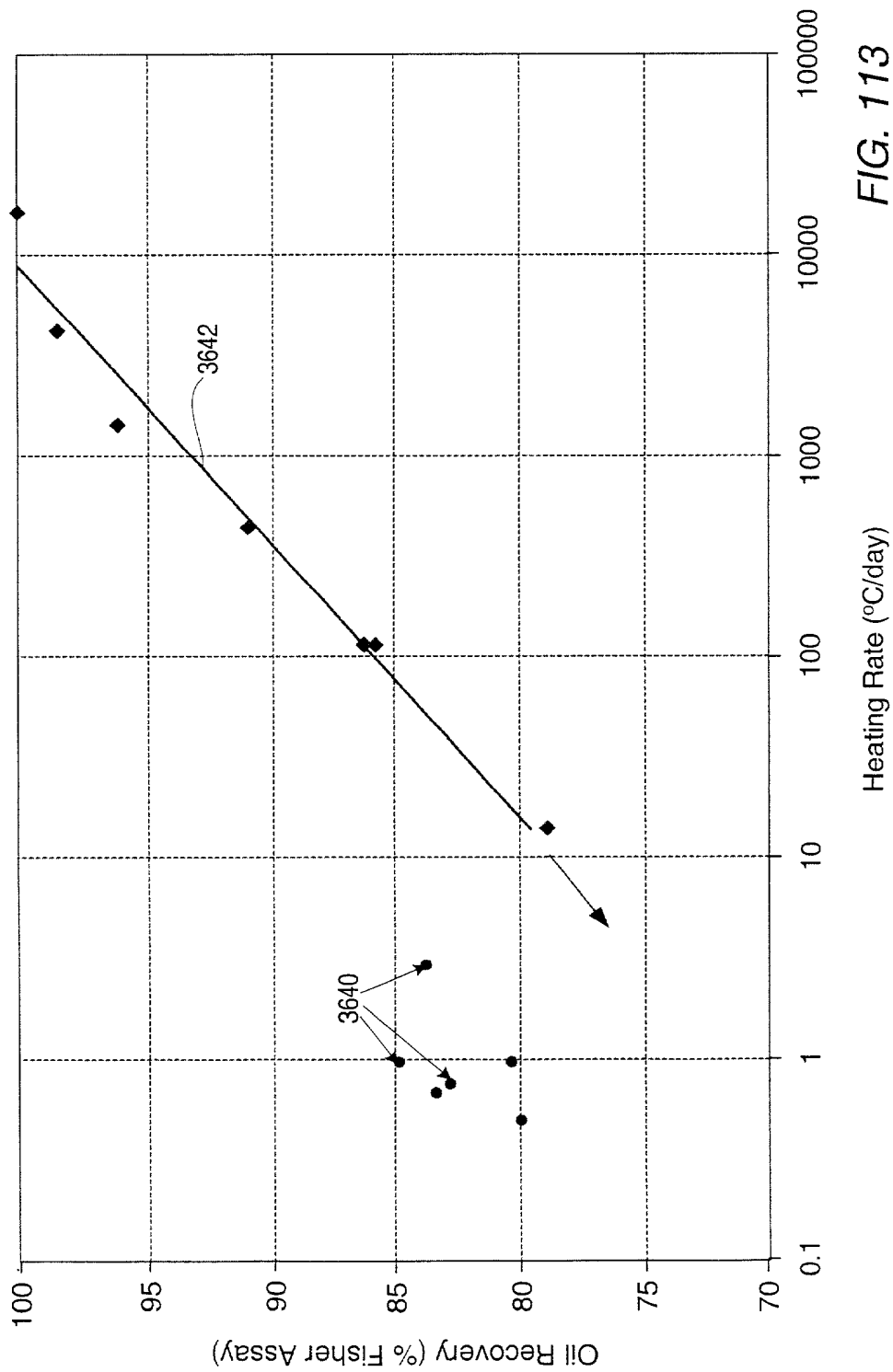


FIG. 113

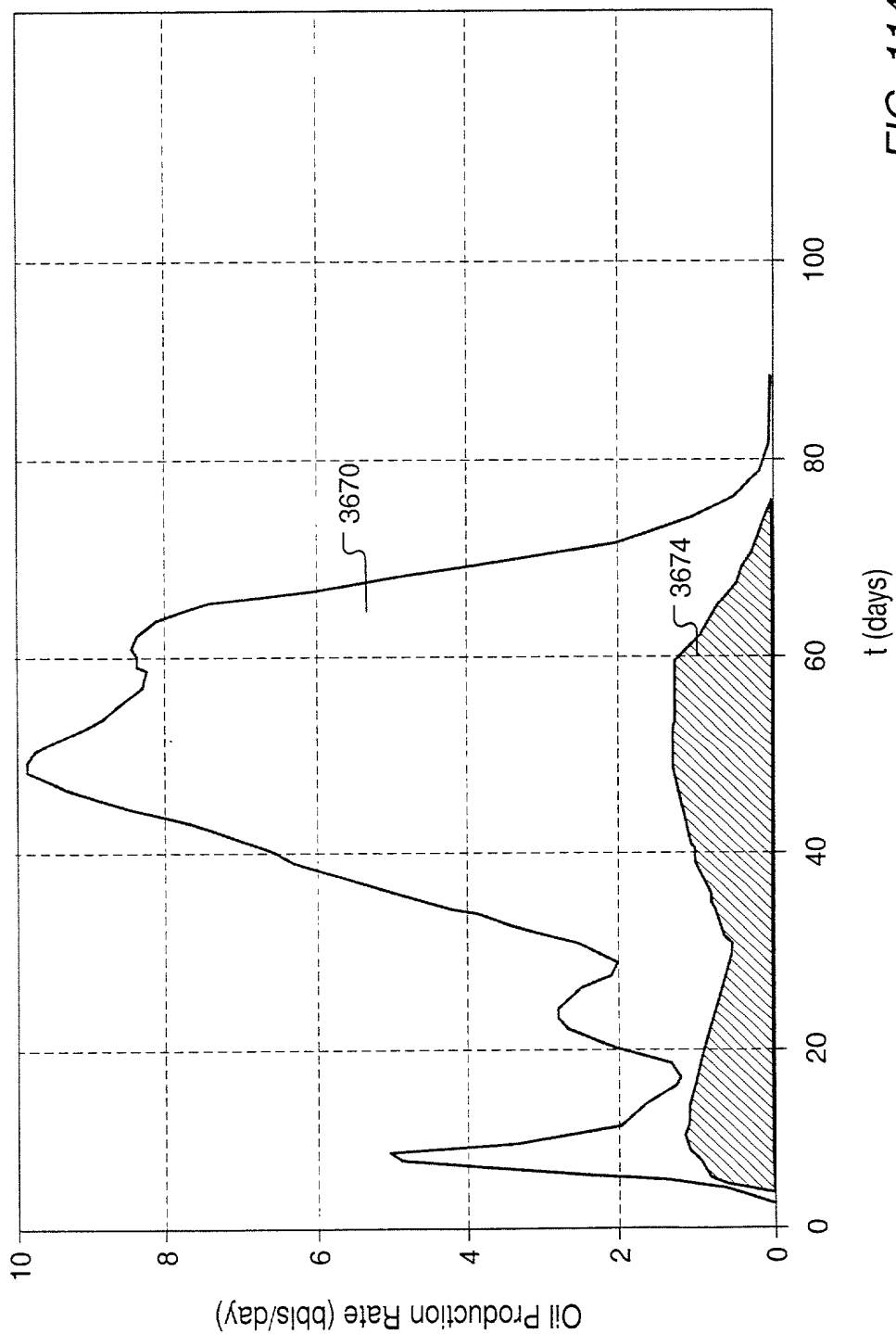


FIG. 114

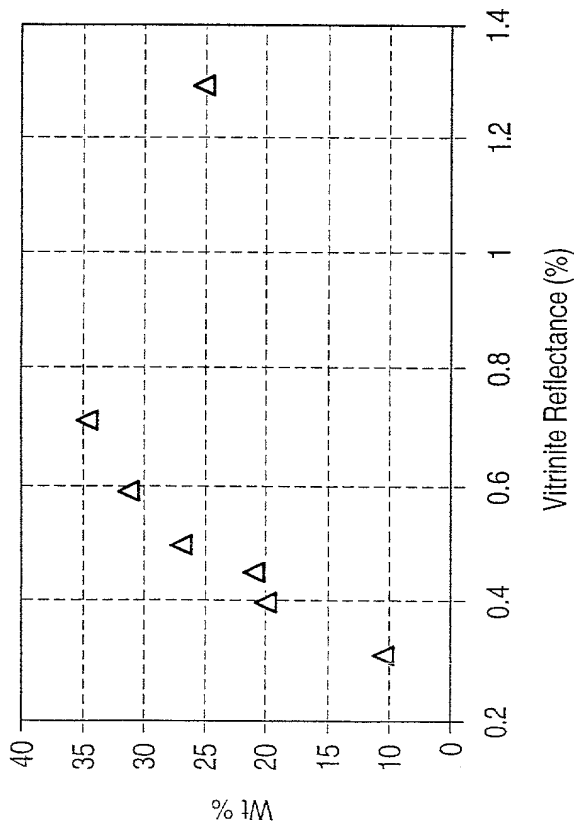


FIG. 115

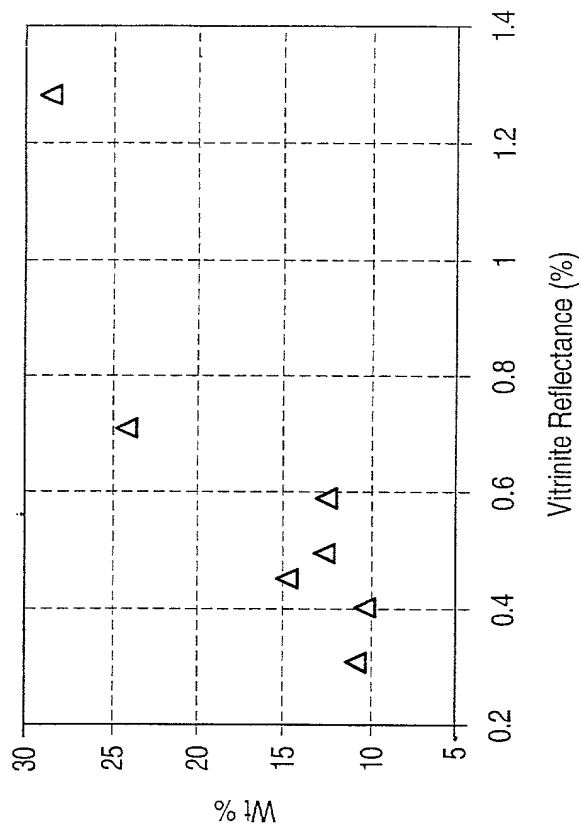


FIG. 116

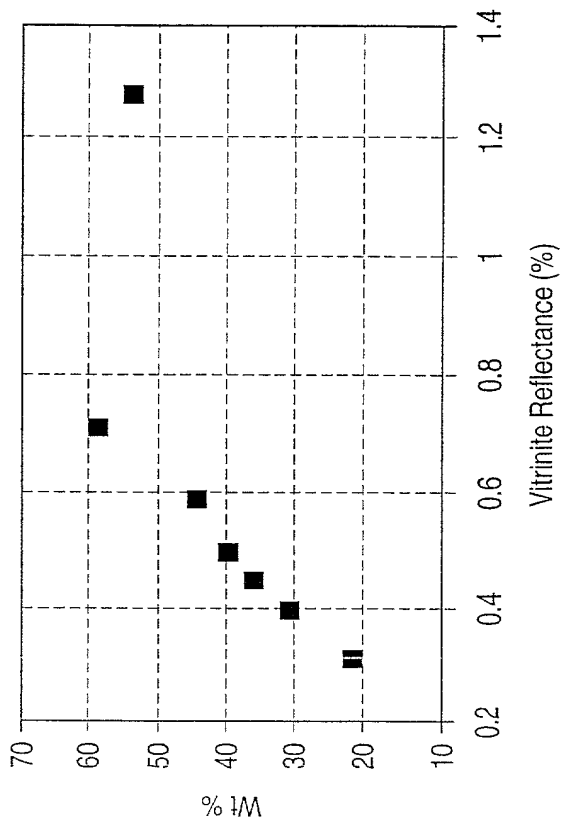


FIG. 117

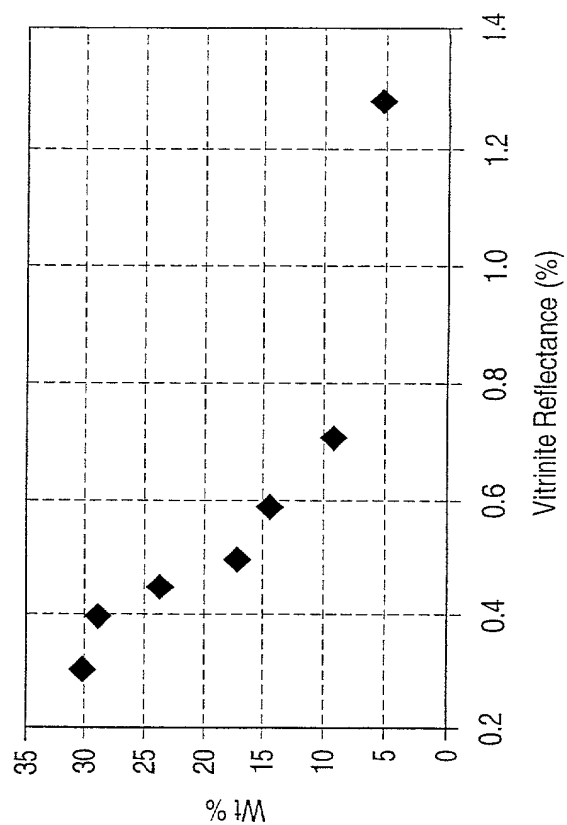


FIG. 118



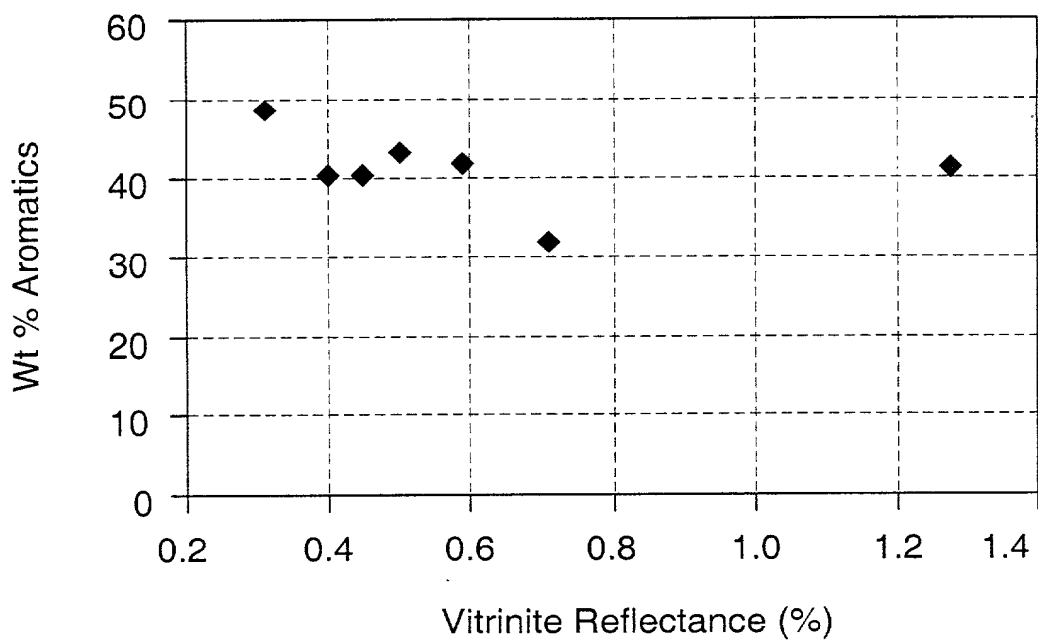


FIG. 119

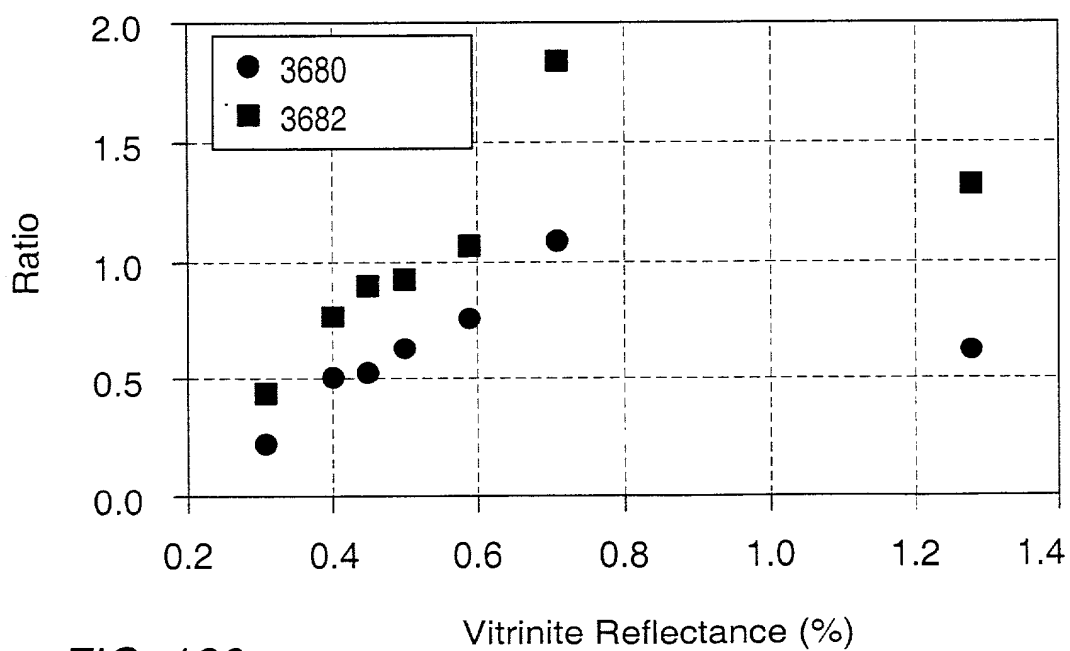


FIG. 120

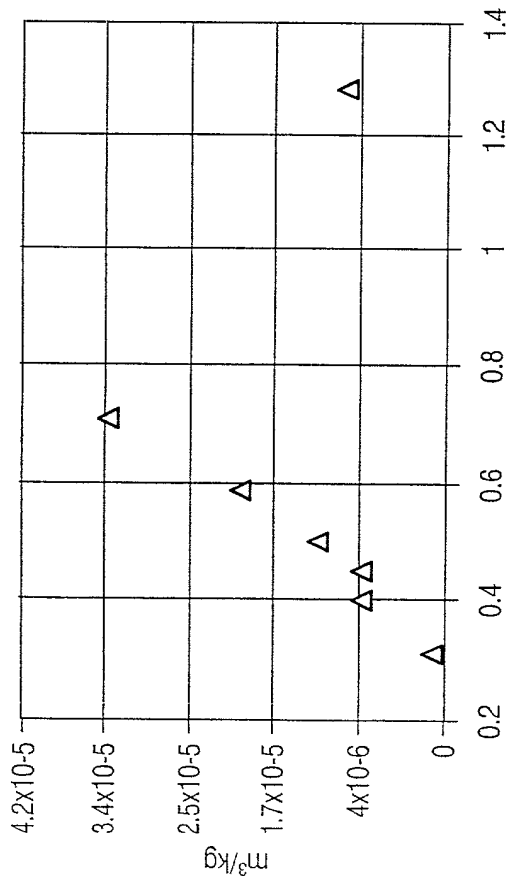


FIG. 121

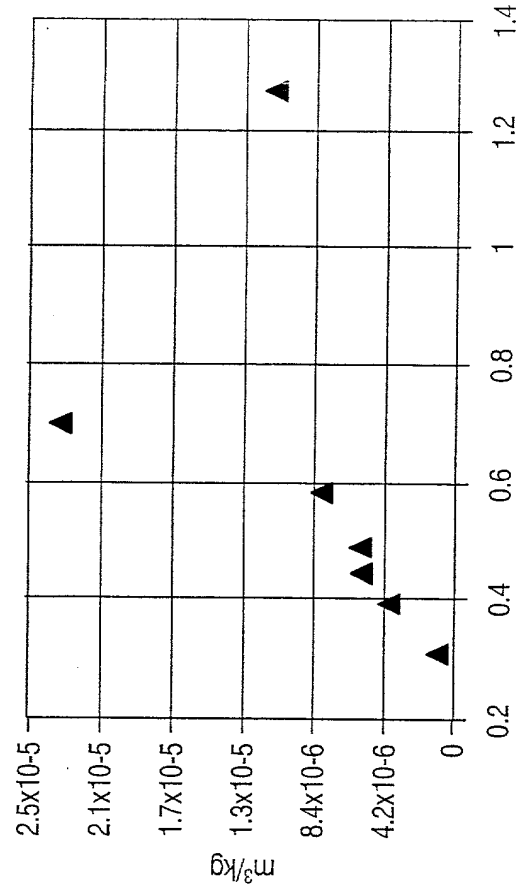


FIG. 122

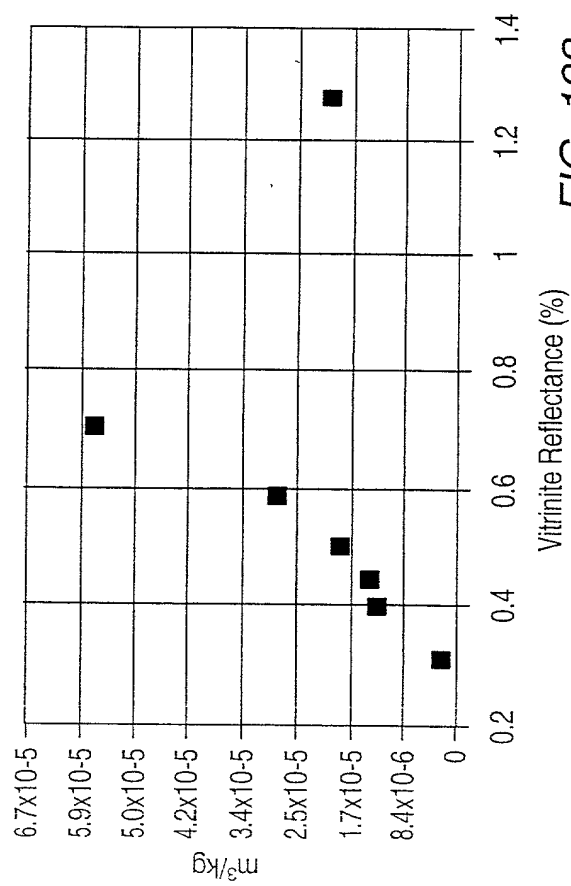


FIG. 123

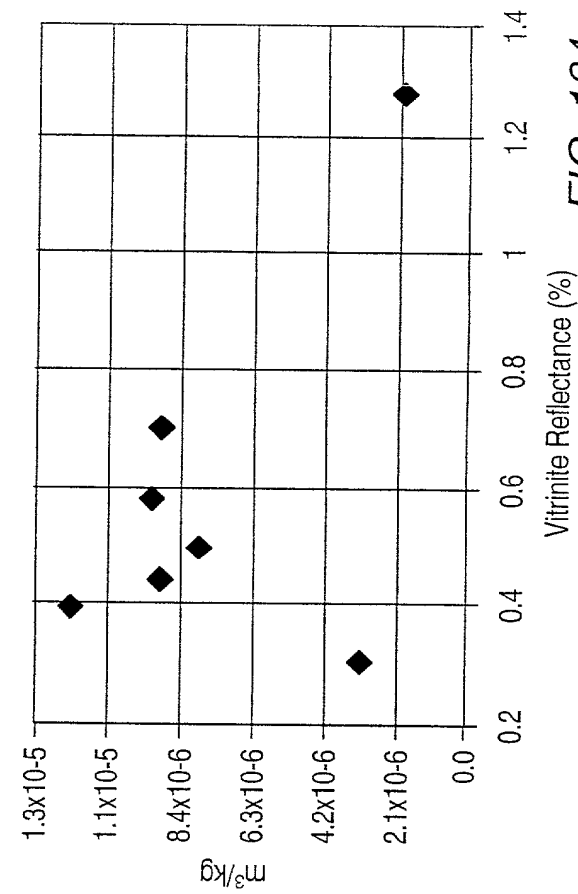


FIG. 124

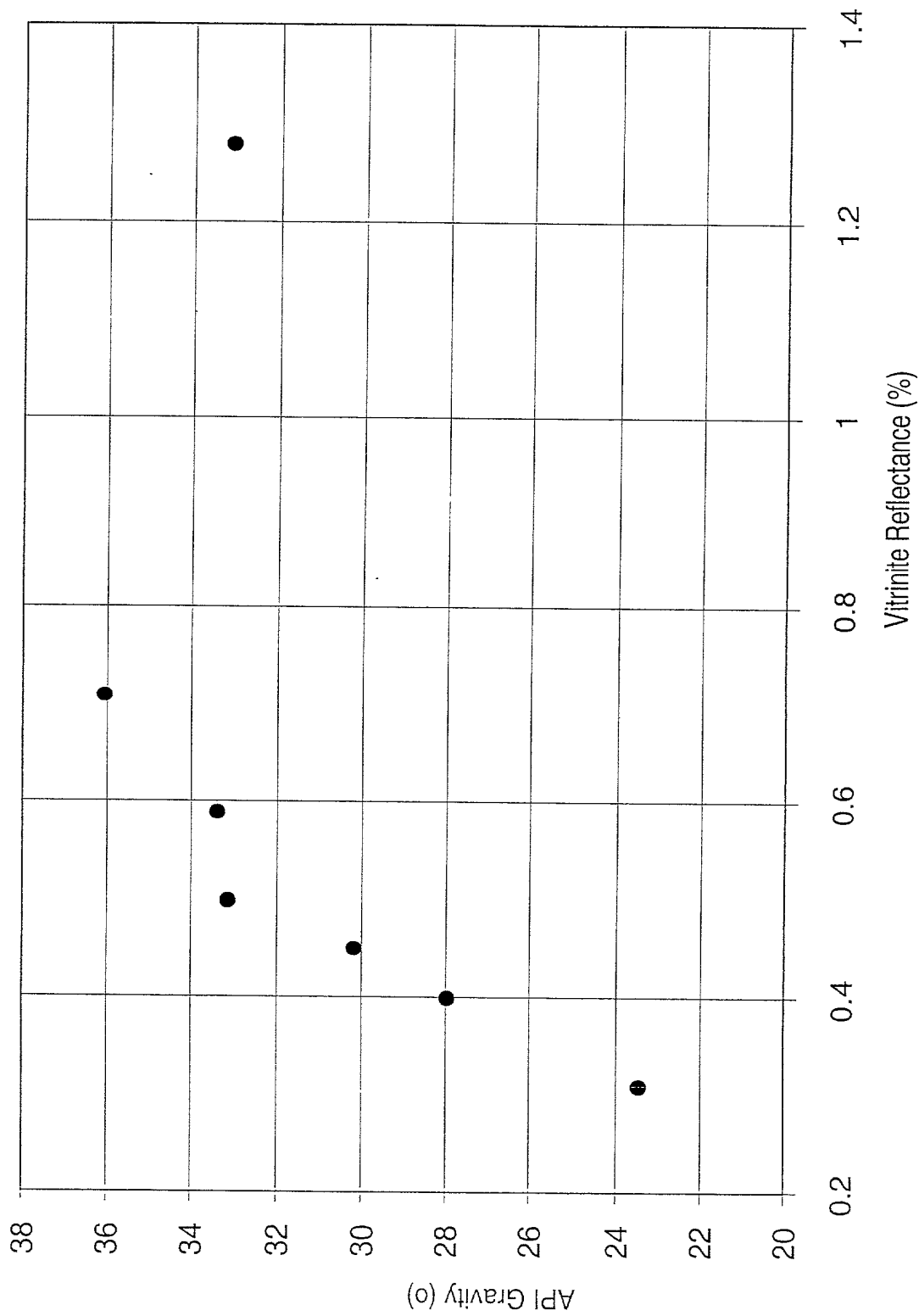
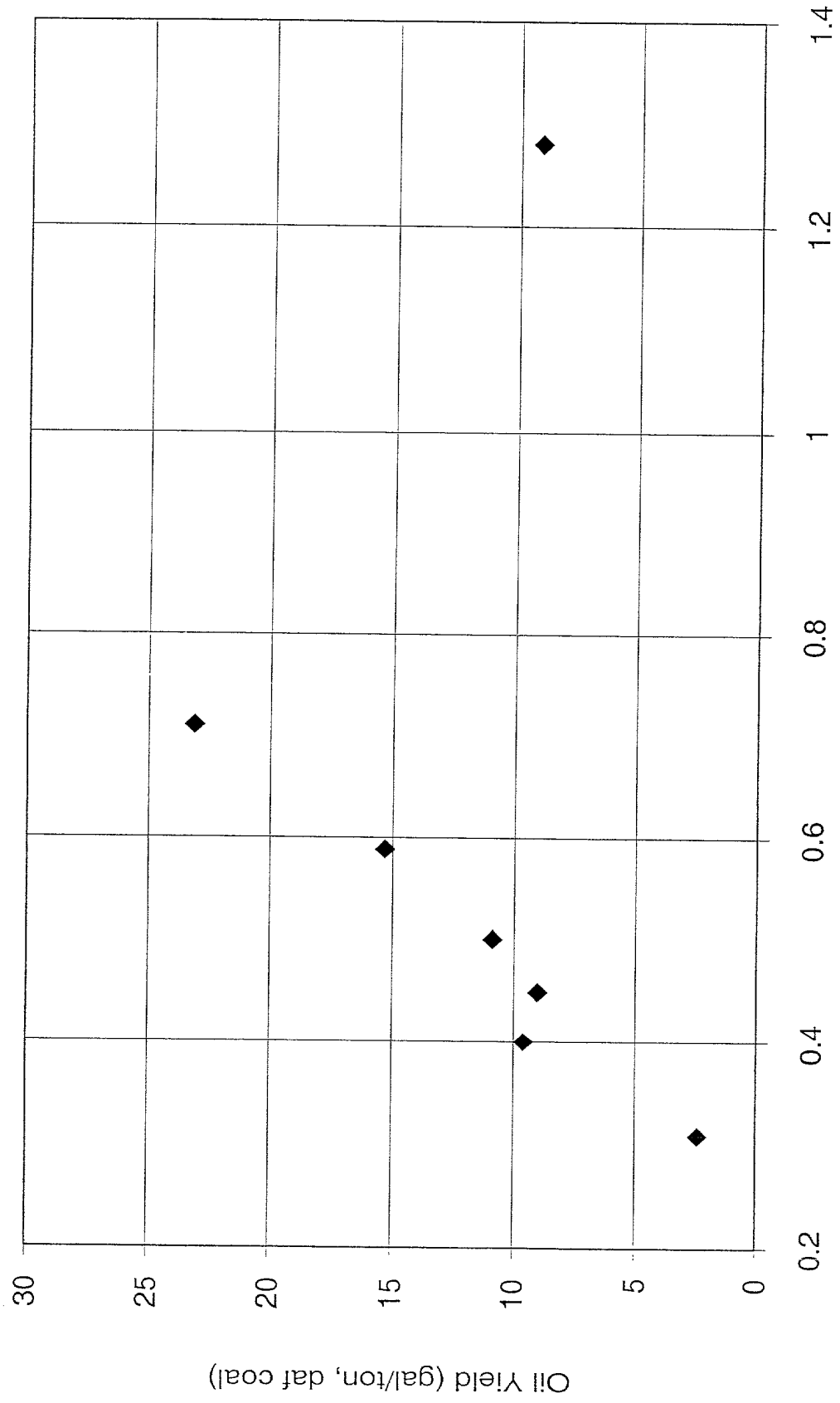


FIG. 125

Figure 126 is a scatter plot showing the relationship between Oil Yield (gal/ton, daf coal) on the Y-axis and Vitrinite Reflectance (%) on the X-axis. The Y-axis ranges from 0 to 30 in increments of 5. The X-axis ranges from 0.2 to 1.4 in increments of 0.2. There are seven data points plotted as solid diamonds.



Vitrinite Reflectance (%)

FIG. 126

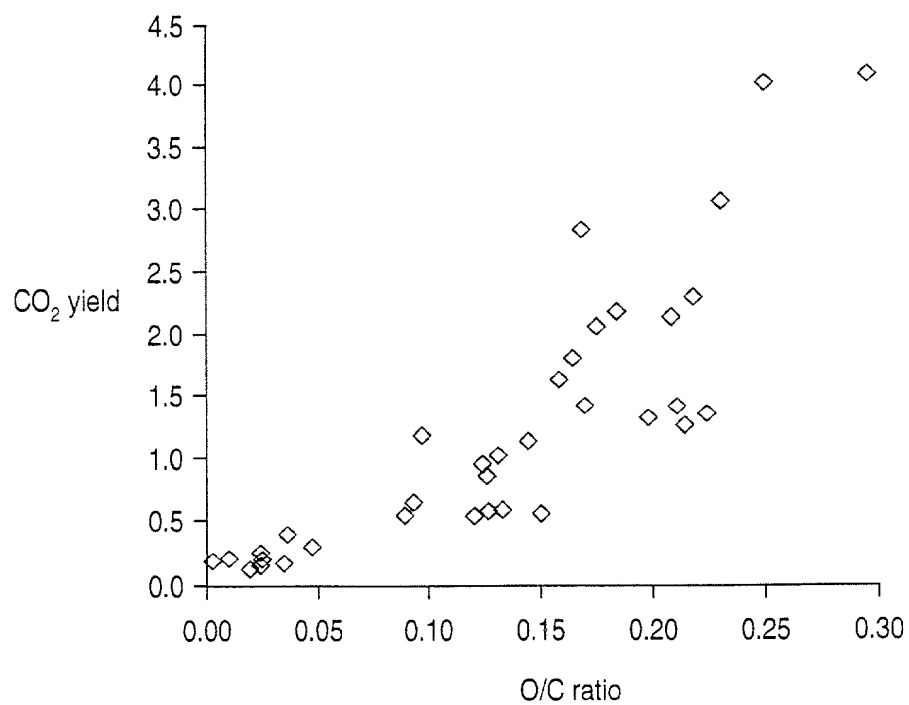
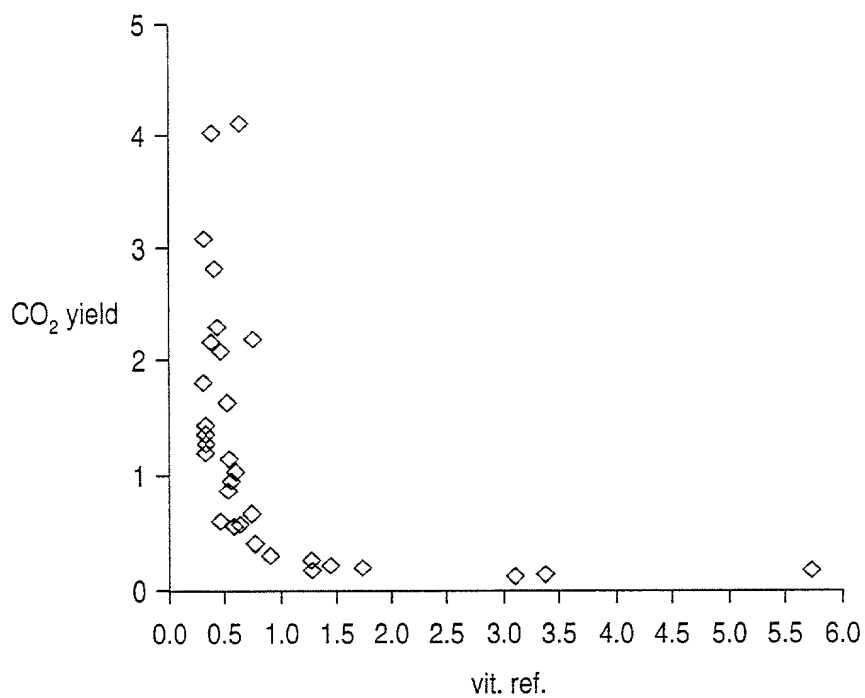




FIG. 130 is a graph showing the relationship between the depth of the water and the temperature of the water. The graph shows that the temperature of the water increases as the depth of the water increases, up to a certain point, and then decreases.

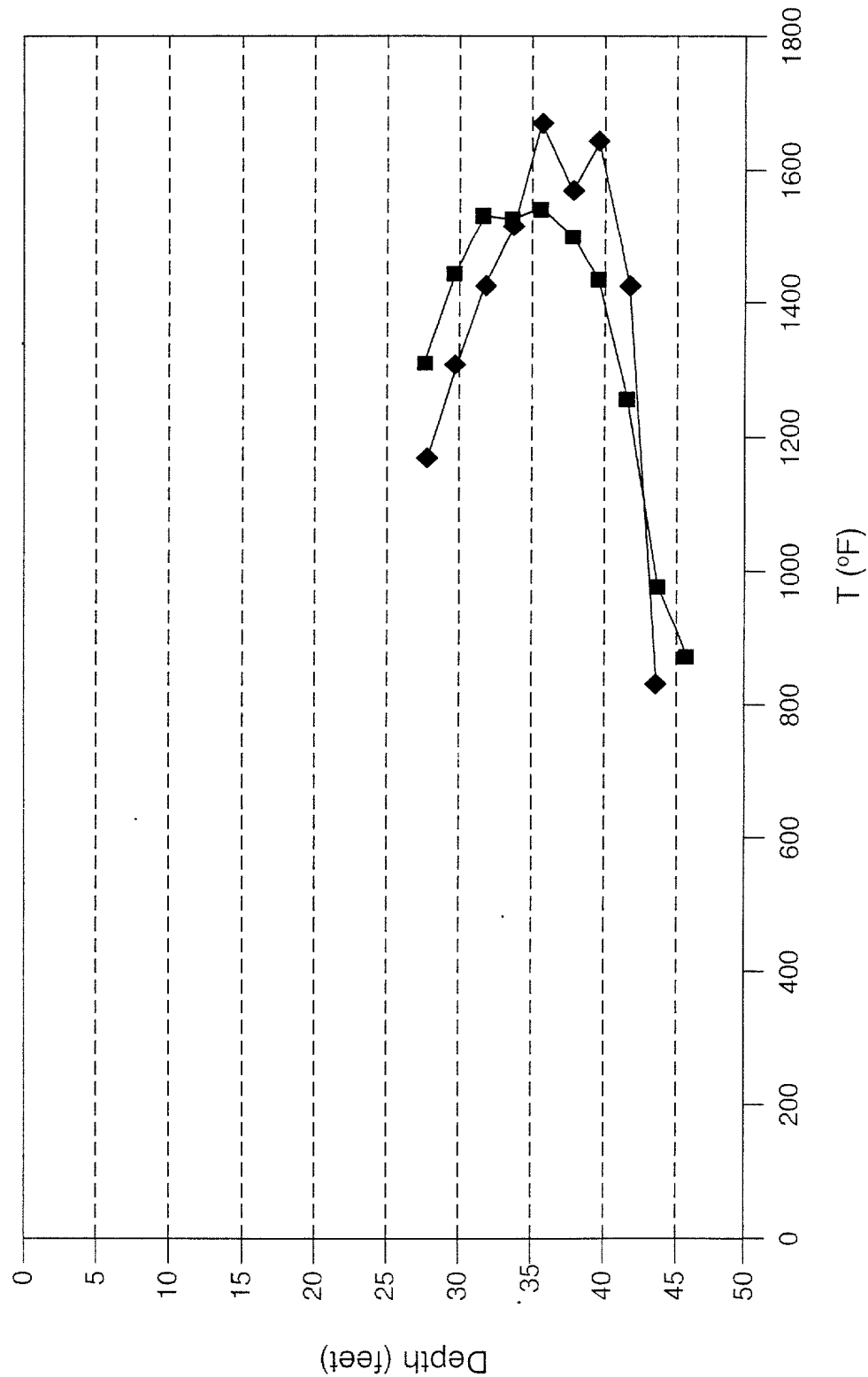


FIG. 130

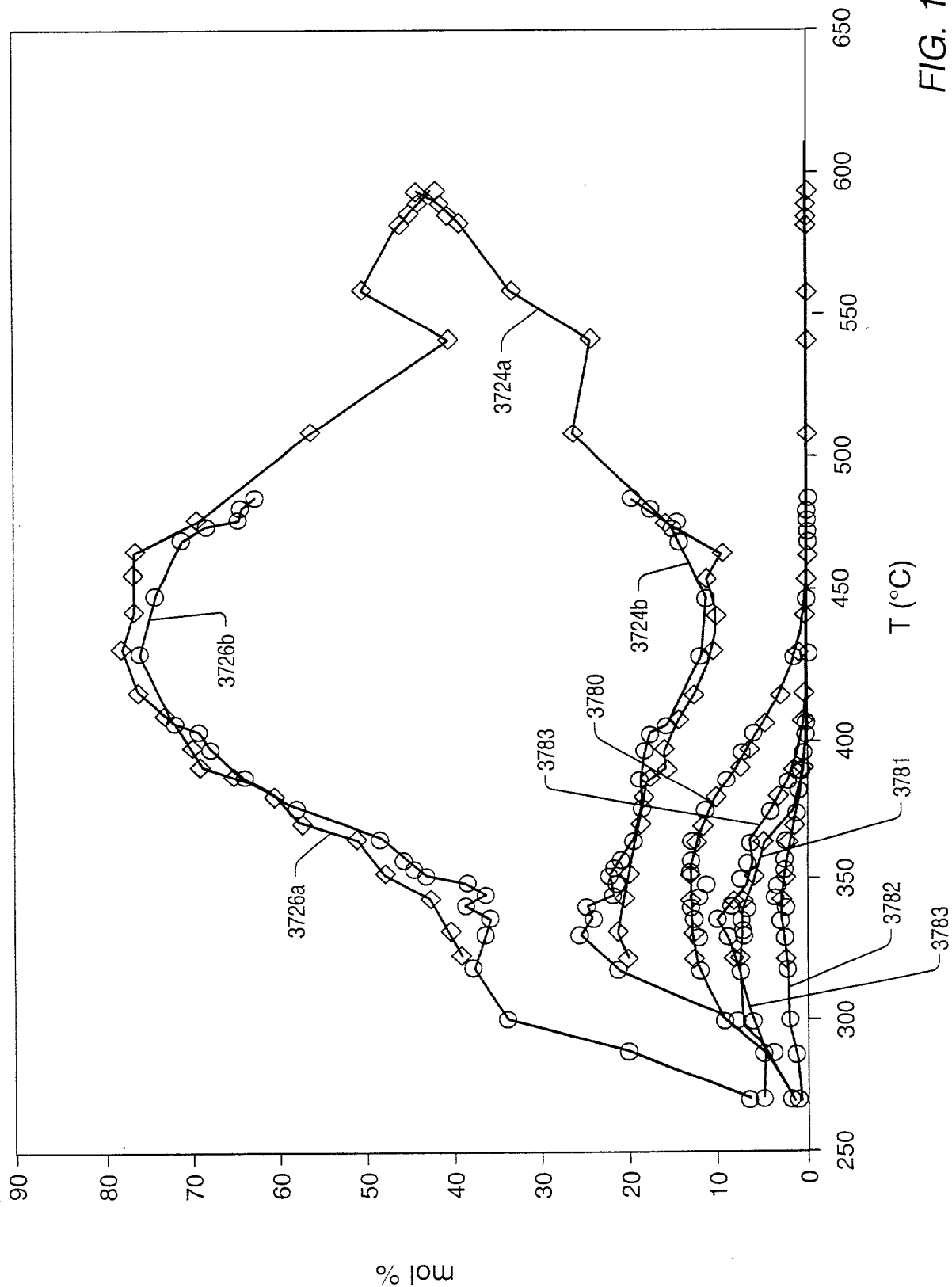


FIG. 131



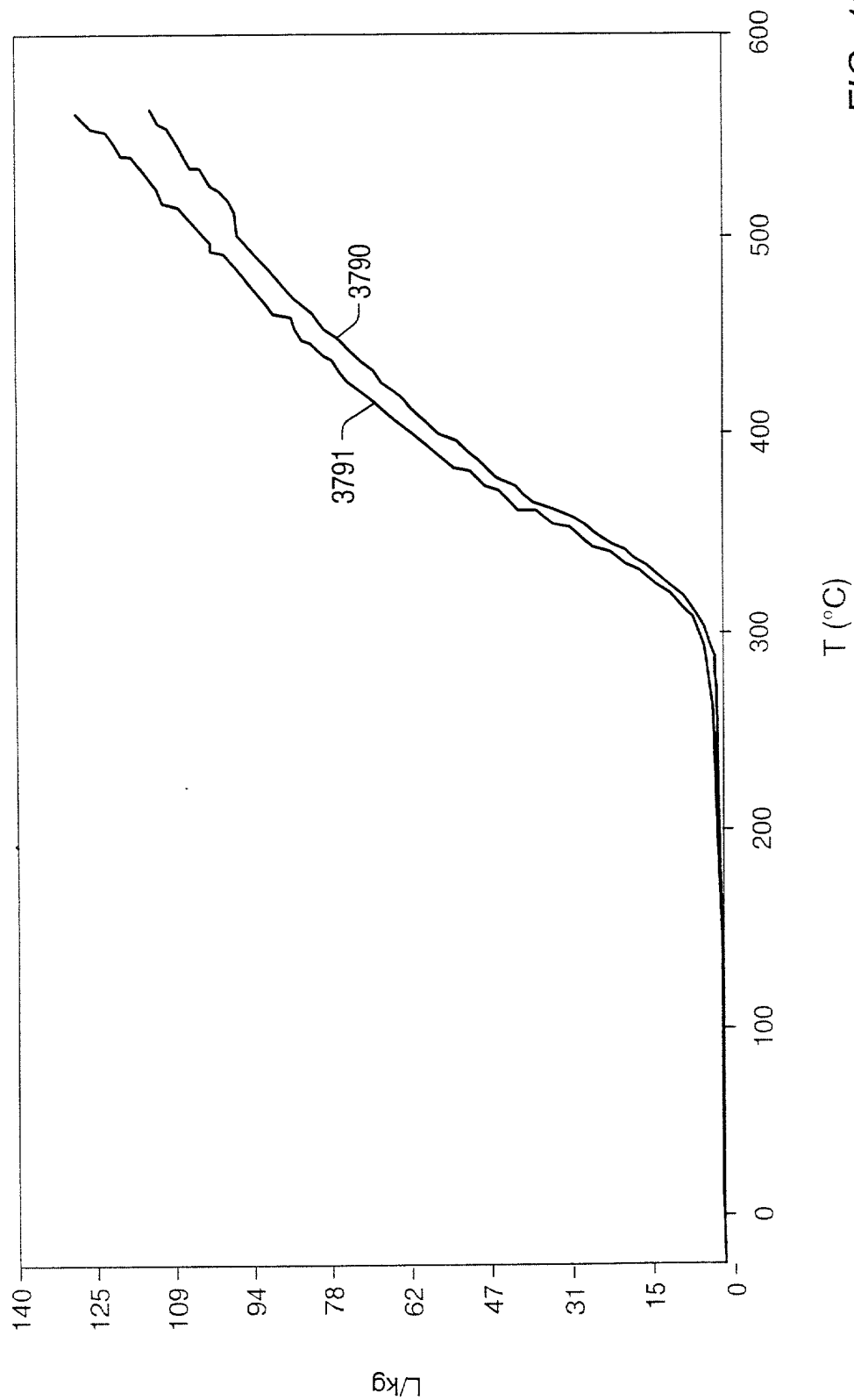
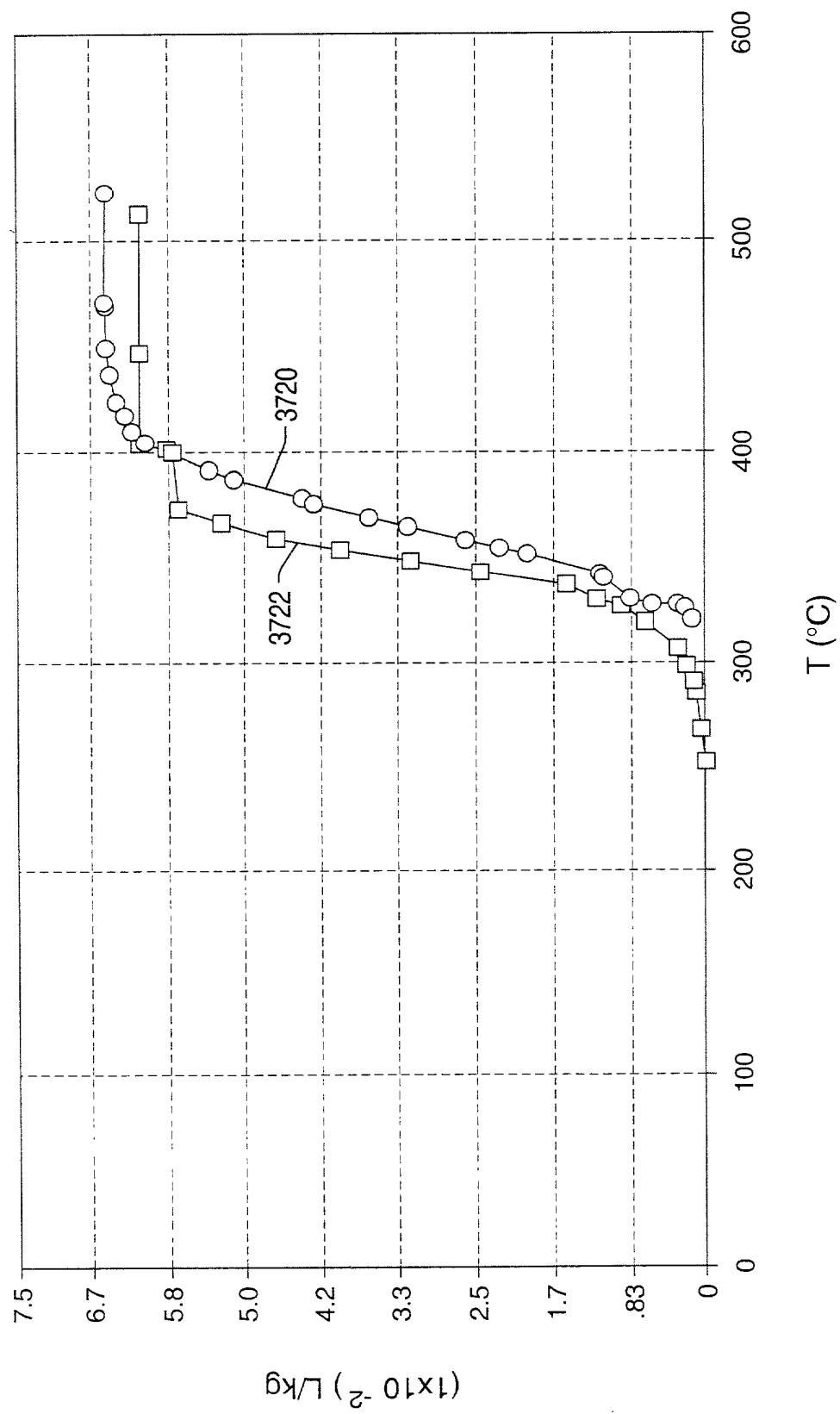


FIG. 132

[illegible]



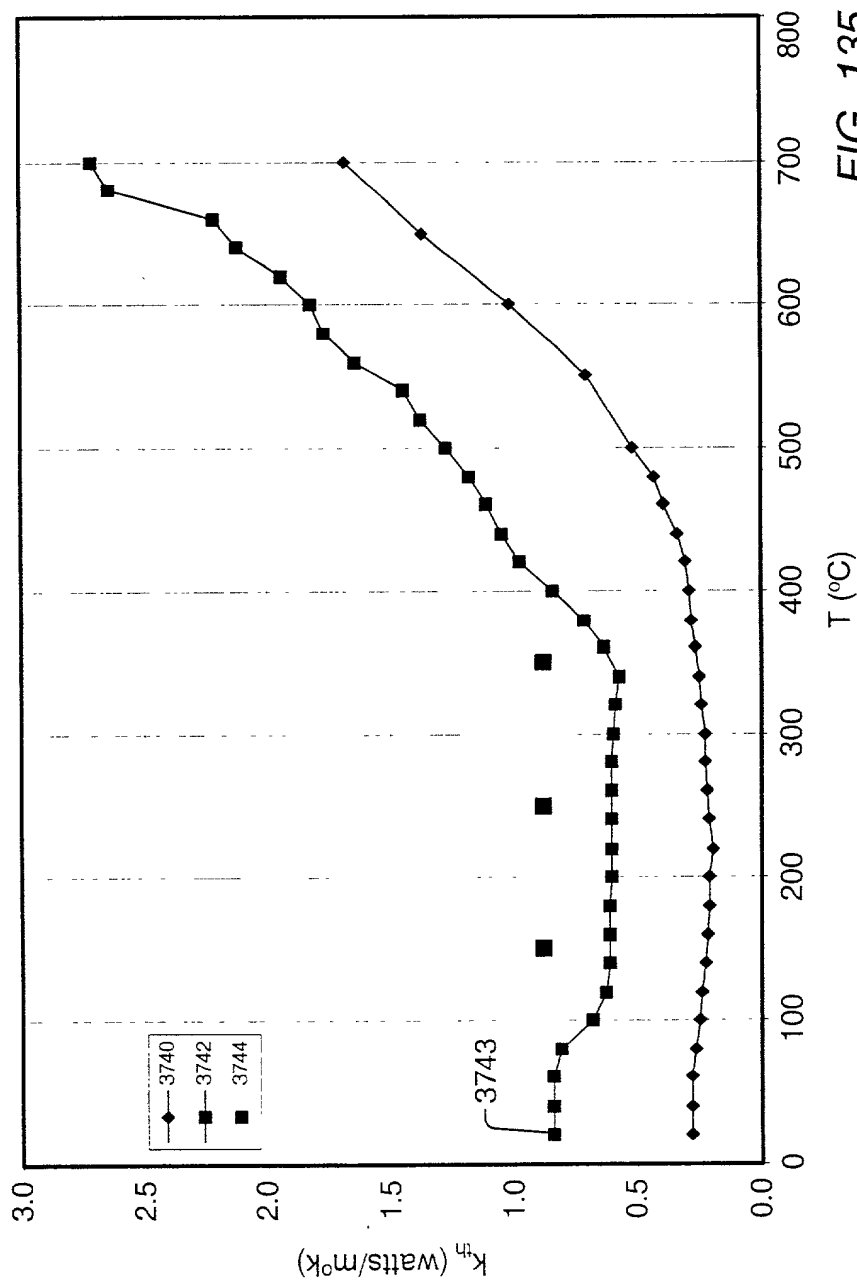


FIG. 135

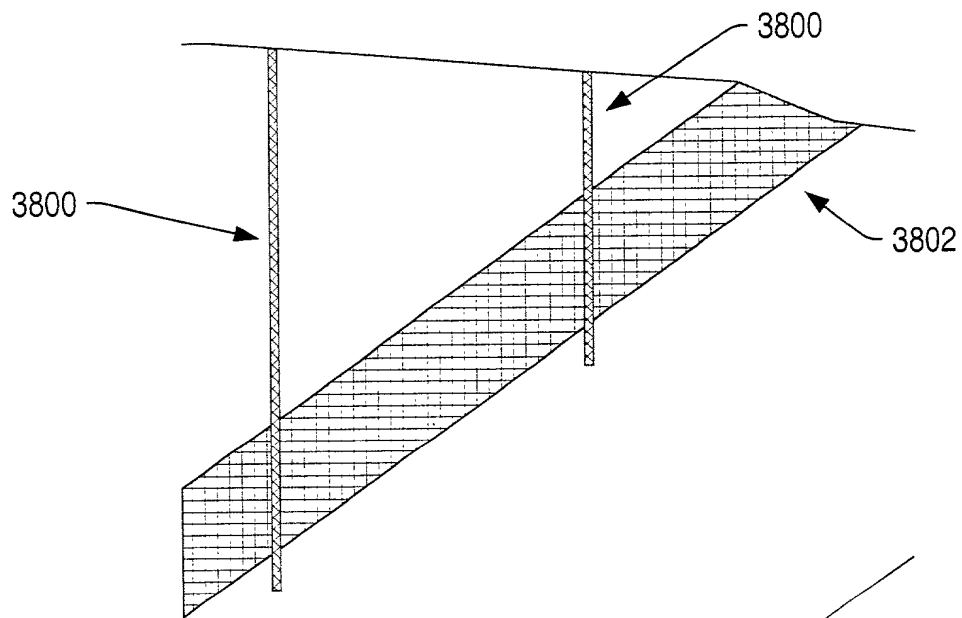


FIG. 136

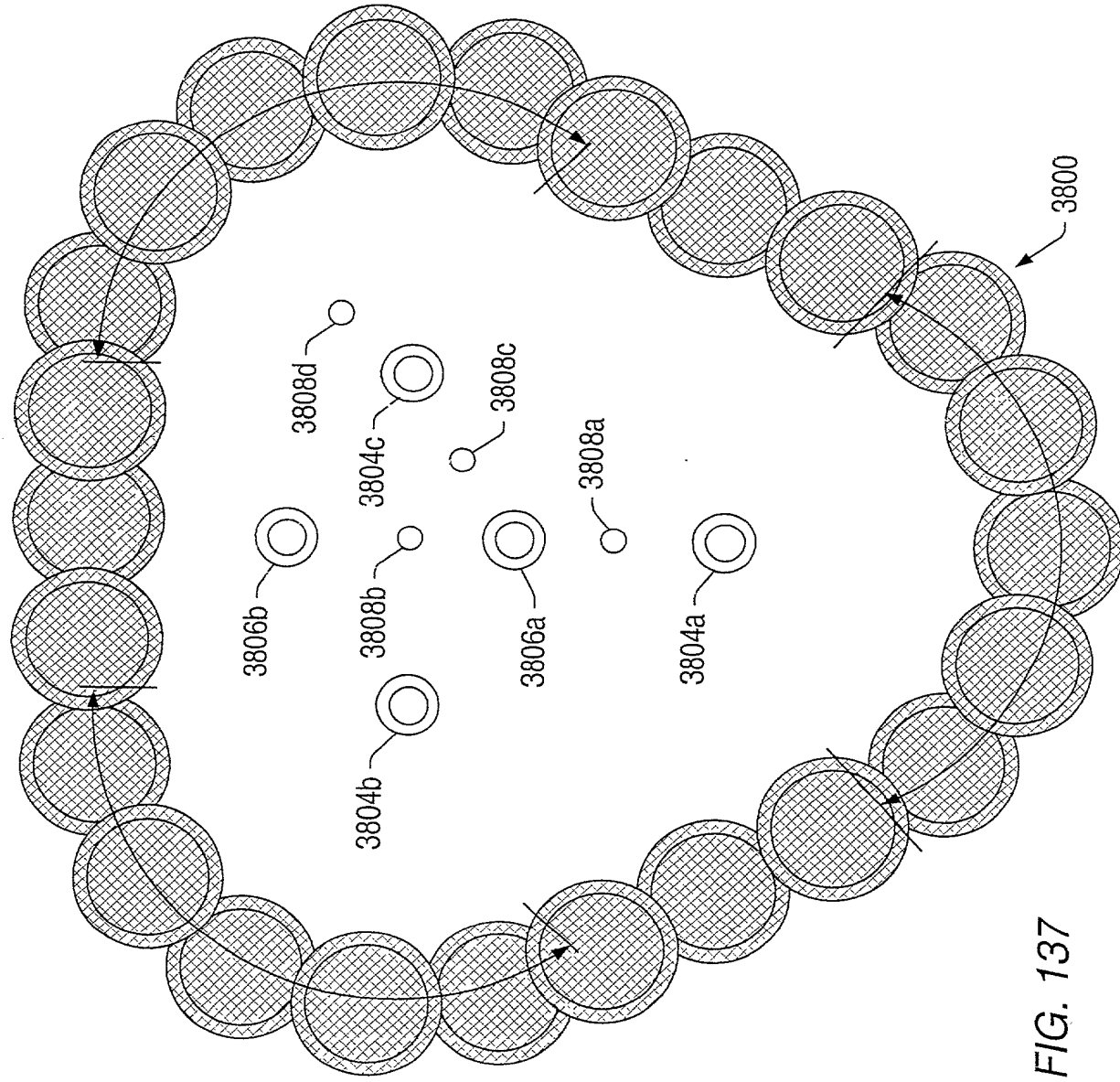
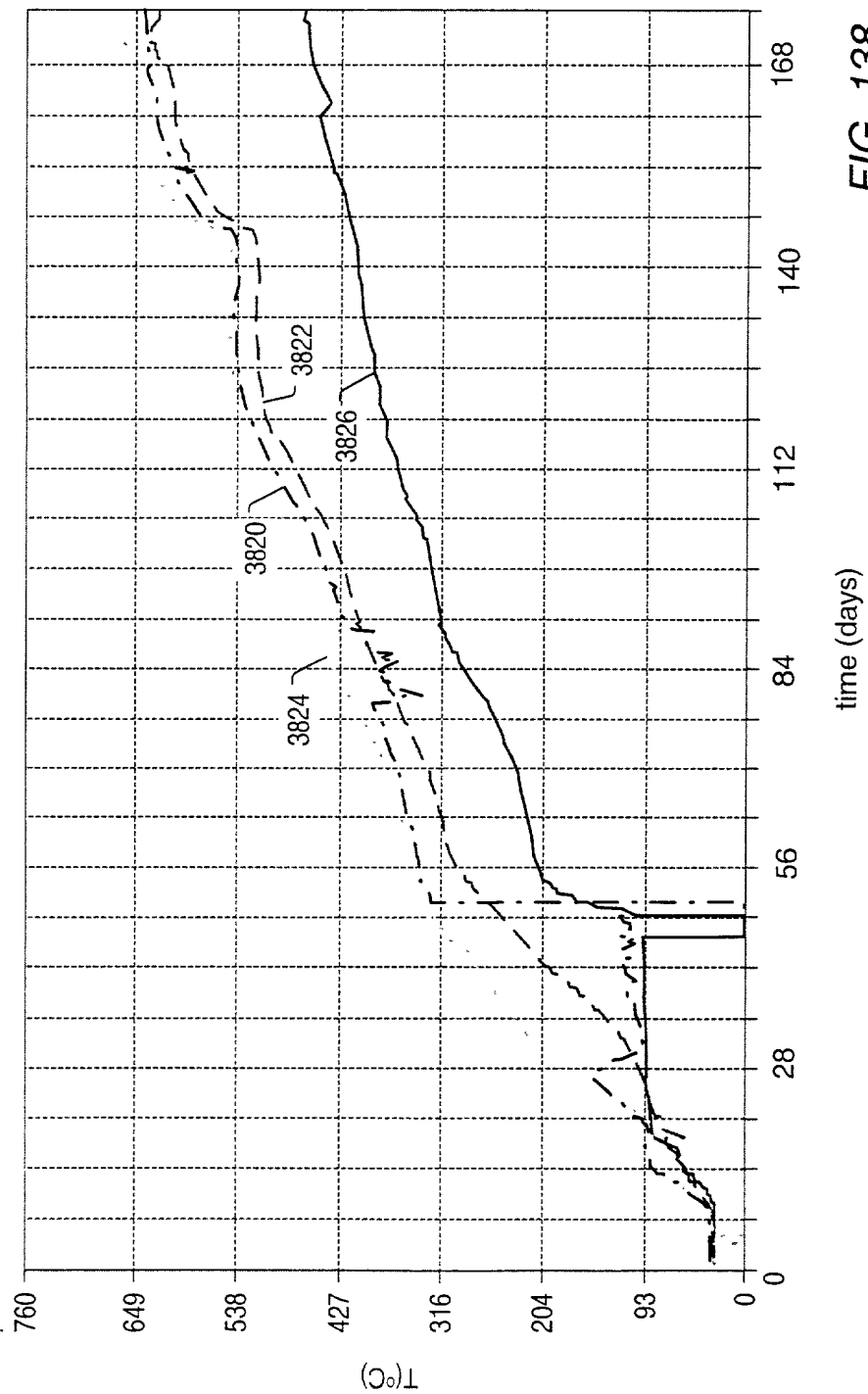
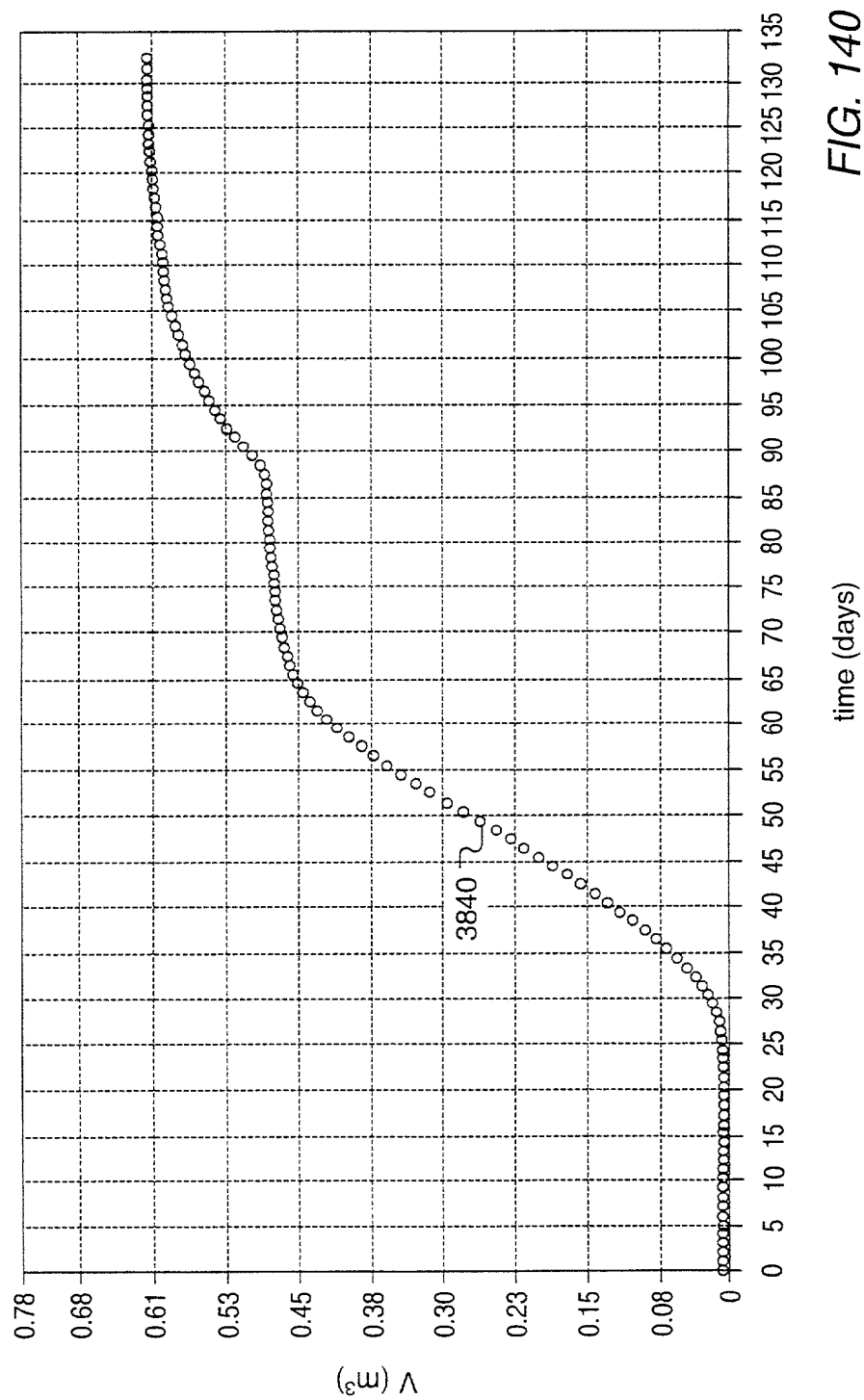


FIG. 137



time (days)





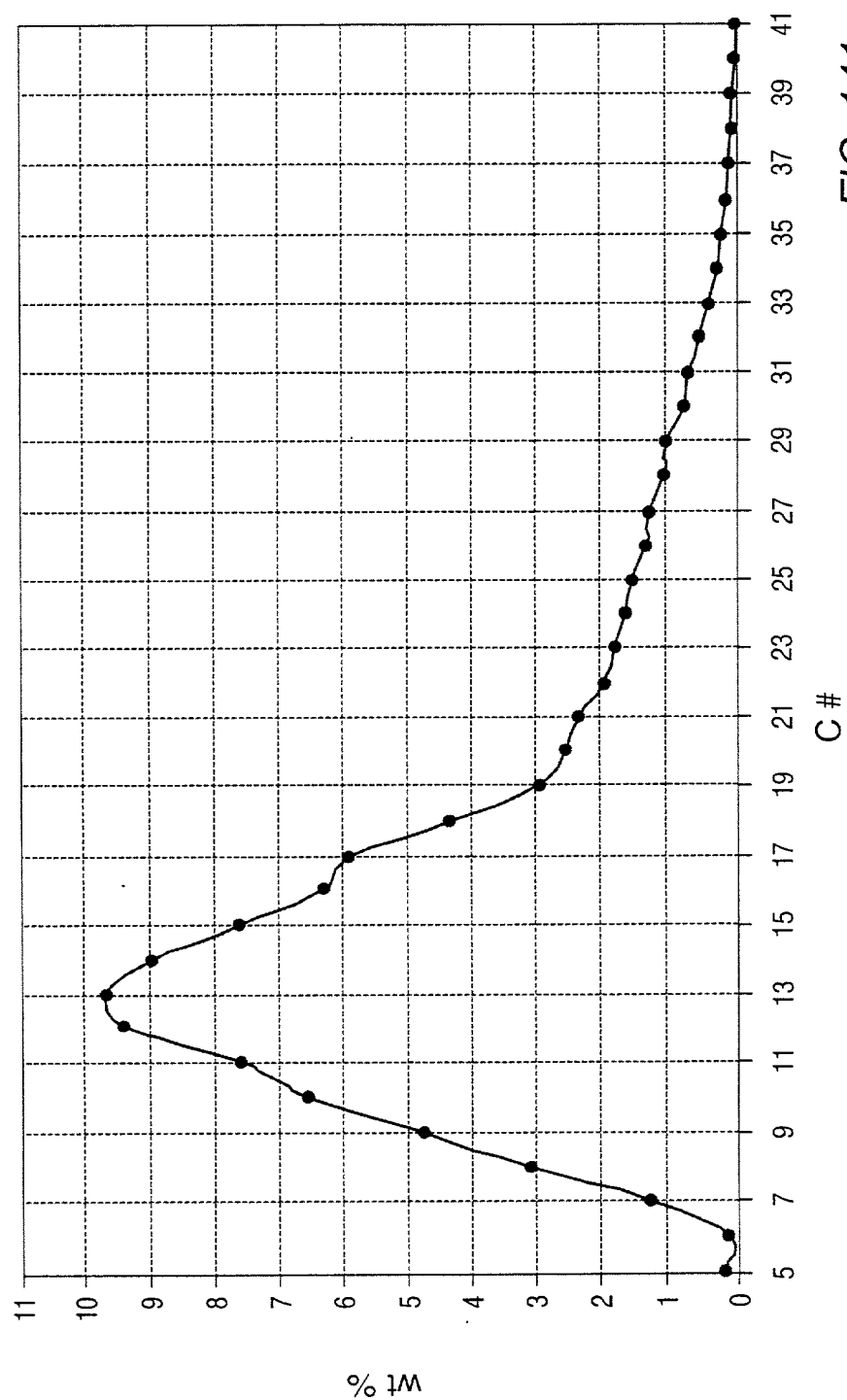


FIG. 141

Figure 142 shows the weight percentage of carbon in the residue as a function of carbon number for the two samples. The heating rate was 10°C/day.

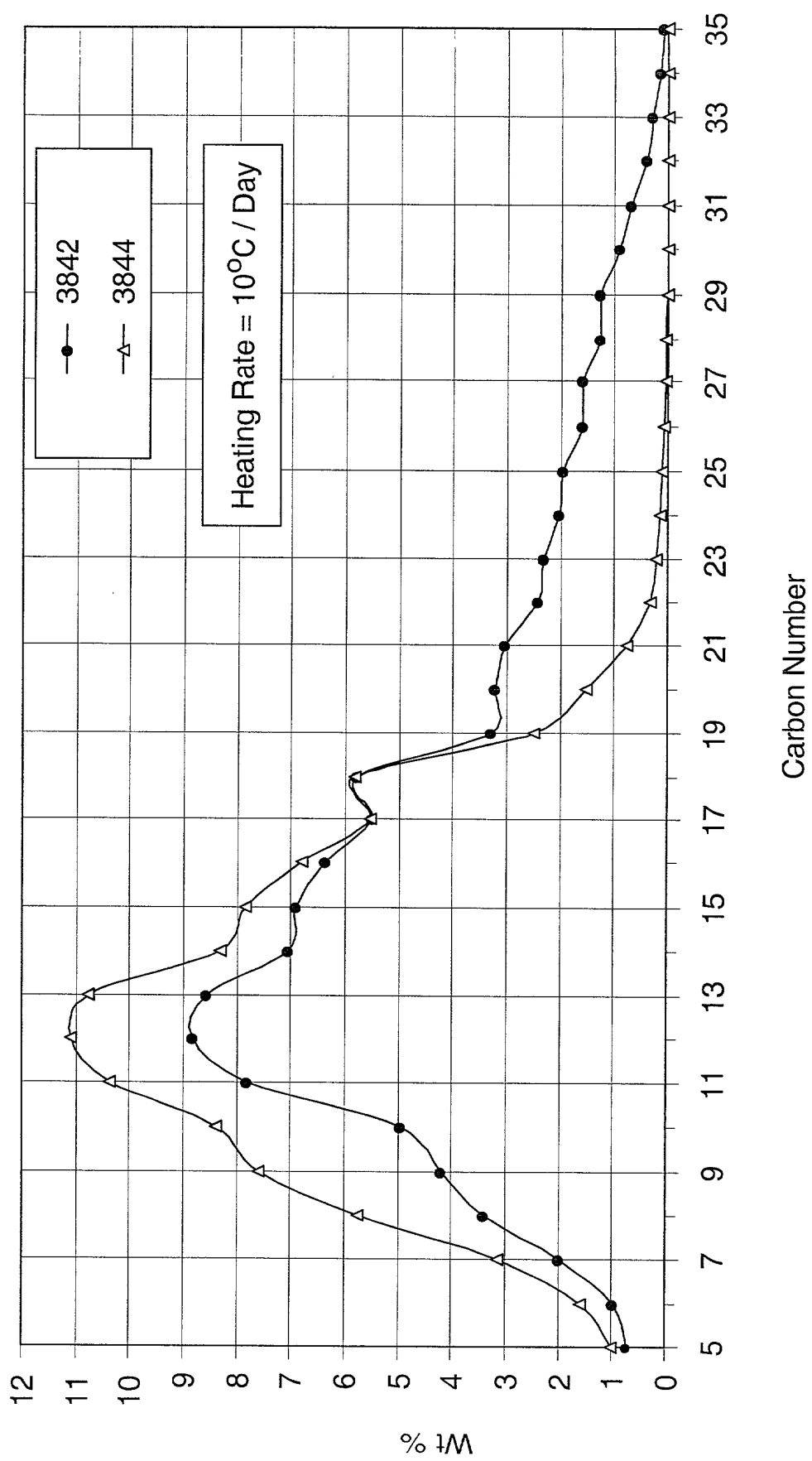


FIG. 142

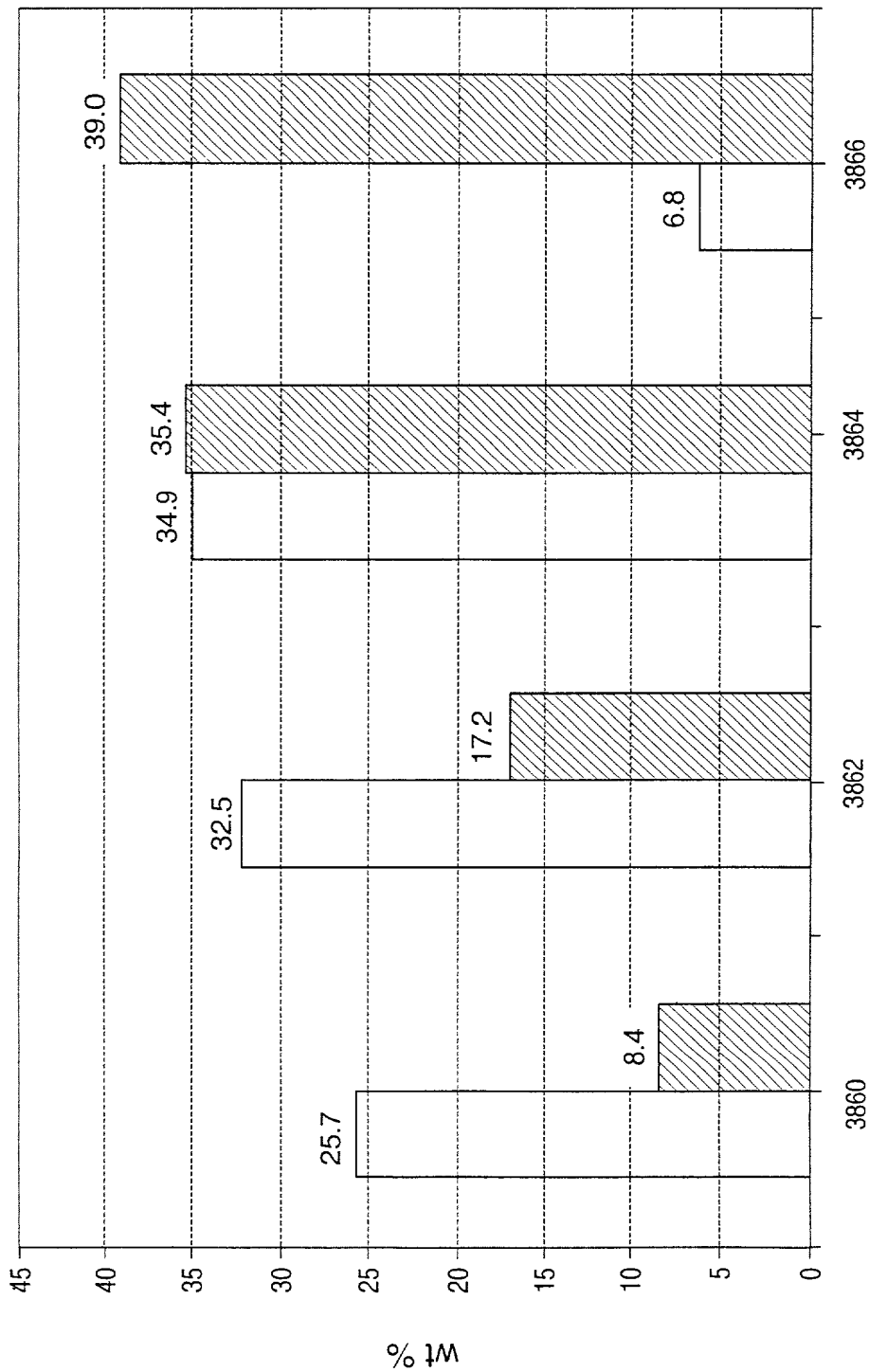


FIG. 143

Figure 144 is a graph showing the Ethene/Ethane Ratio versus the Heating Rate in °C/day. The Ethene/Ethane Ratio is plotted on the Y-axis (0% to 20%) and the Heating Rate is plotted on the X-axis (1 to 100,000 °C/day). The data points show a sharp increase in the Ethene/Ethane Ratio at a heating rate of approximately 10,000 °C/day, reaching a value of about 19%.

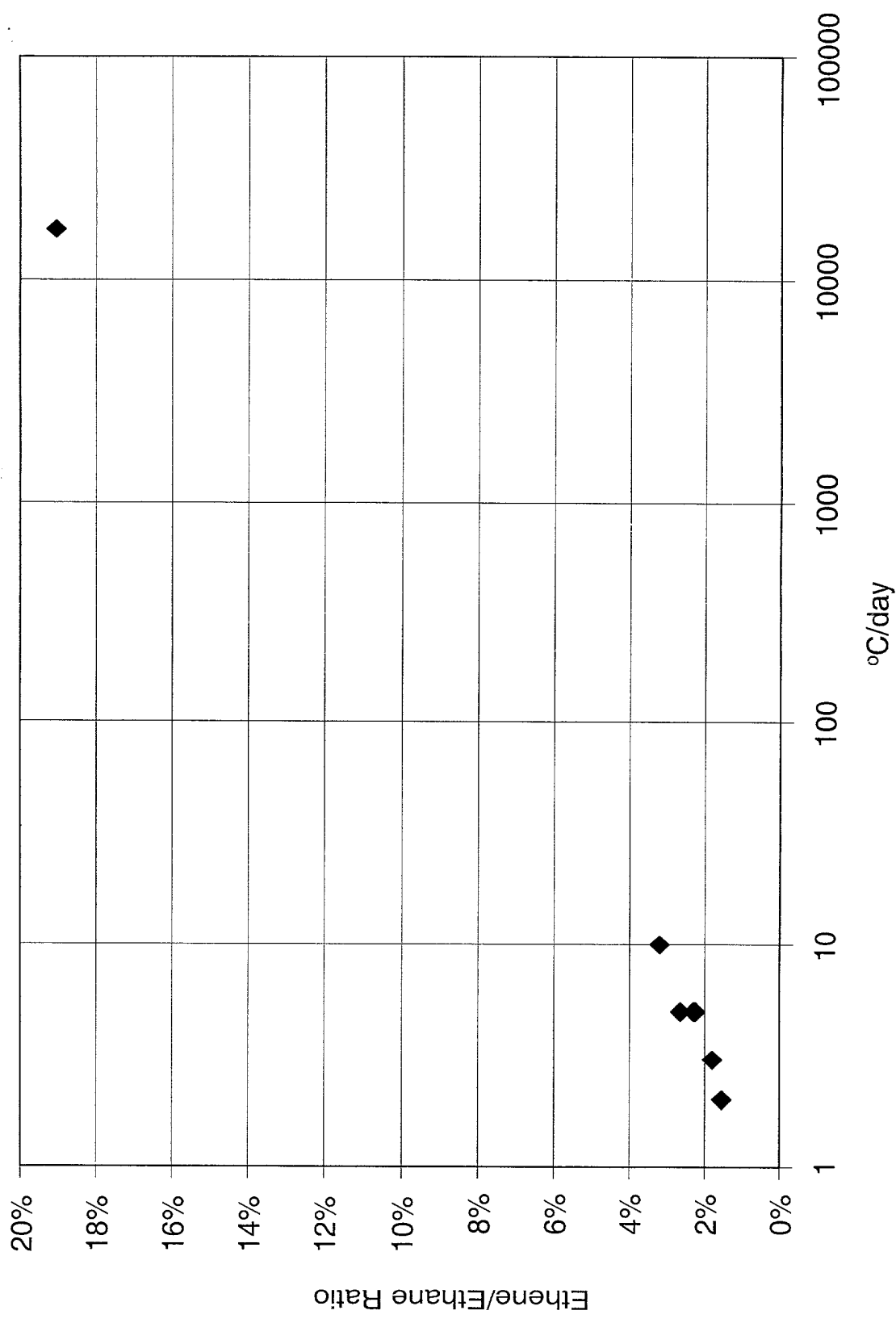


FIG. 144

Copyright © 2000 by the American Petroleum Institute. All rights reserved. Reproduction or translation without permission is prohibited.

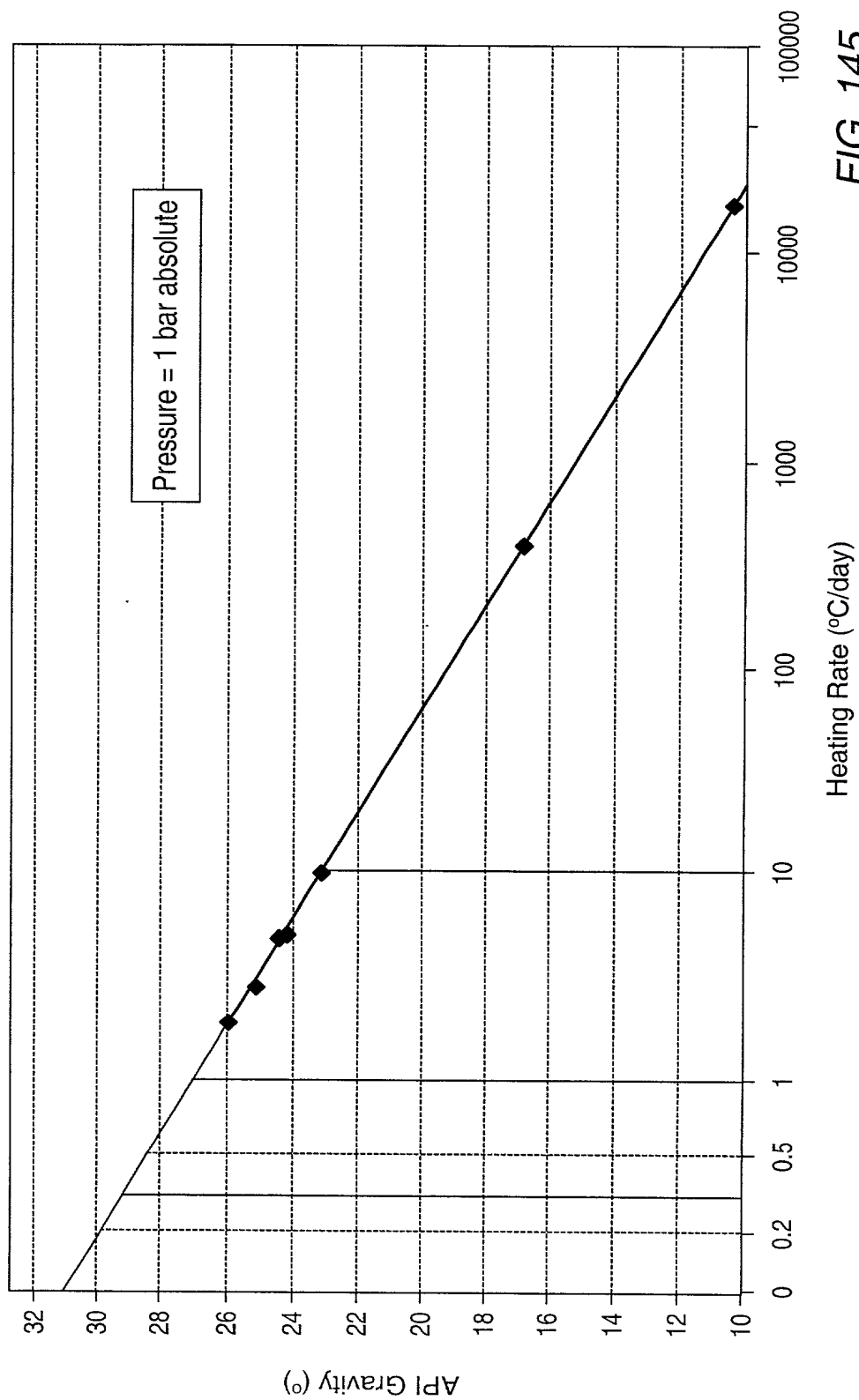


FIG. 145

Figure 146 shows the weight percentage of the various components in the various samples. The weight percentage of the various components is plotted against the sample number. The weight percentage of the various components is plotted against the sample number.

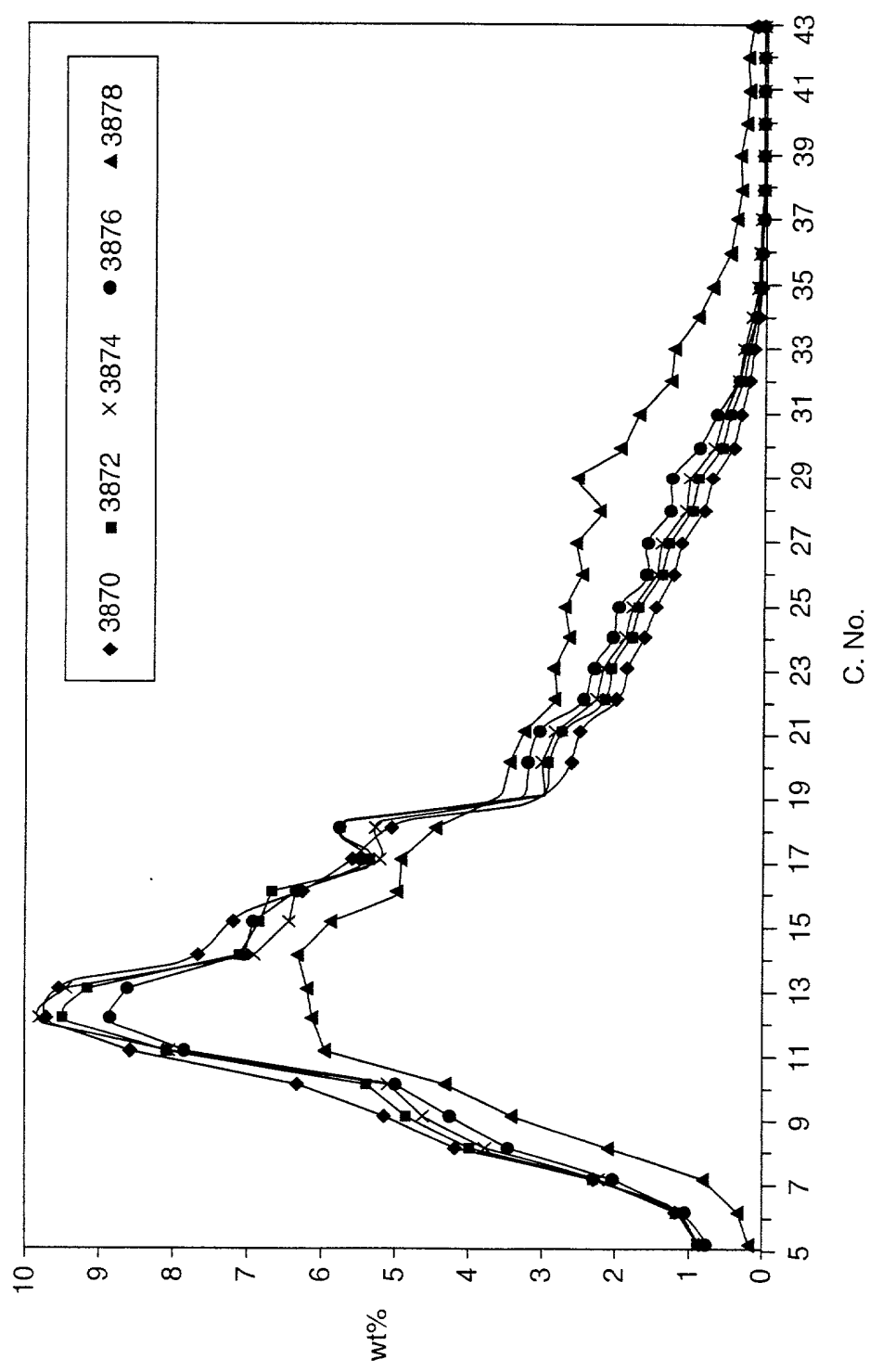


FIG. 146

CO<sub>2</sub> concentration (%) vs. time (minutes) for three different temperatures: 3904, 3902, and 3900.

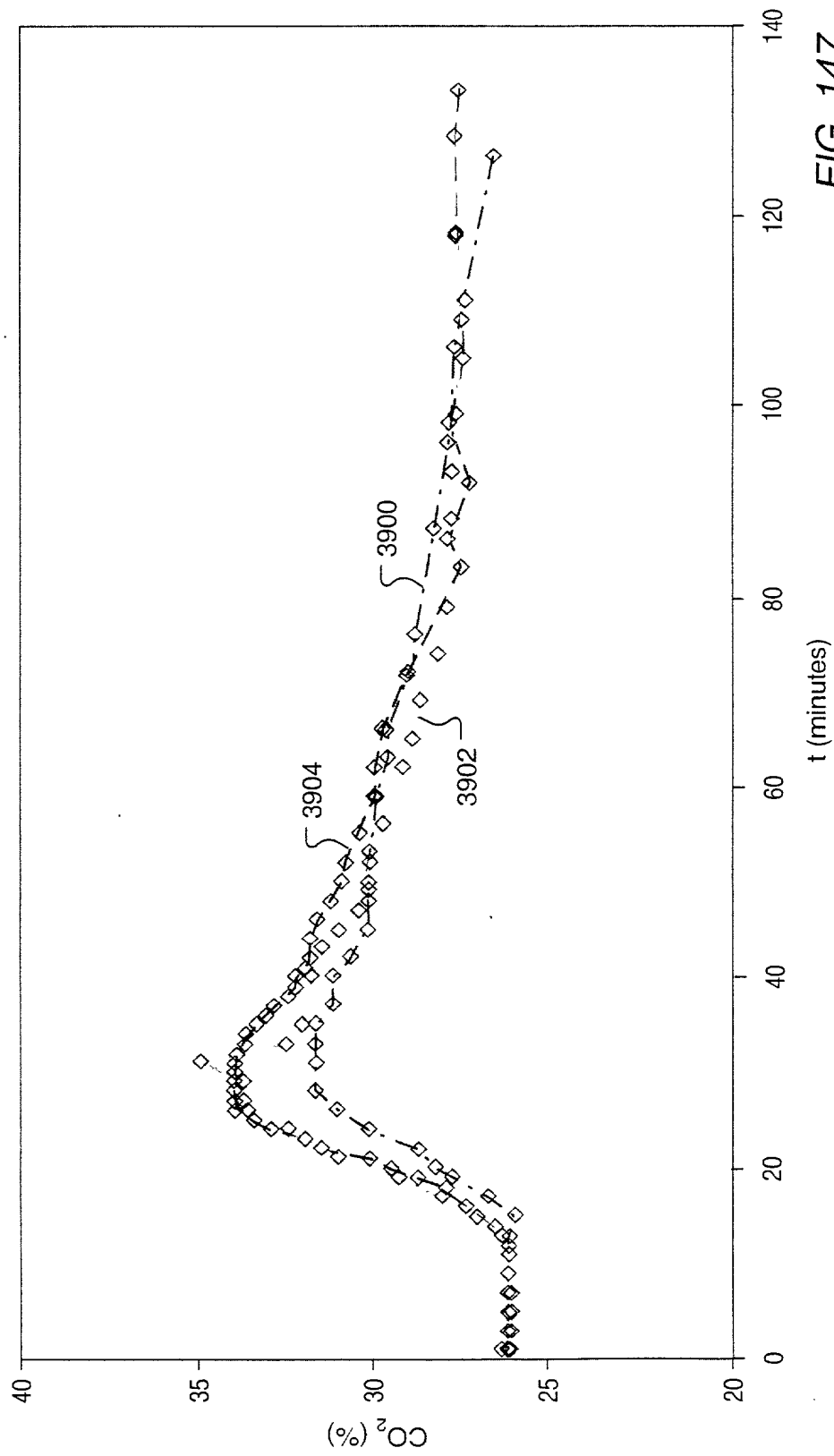


FIG. 147



Copyright © 1998 by the American Nuclear Society  
All rights reserved. No part of this publication may be reproduced, stored in a retrieval system, or transmitted, in any form or by any means, electronic, mechanical, photocopying, recording, or by any information storage and retrieval system, without permission in writing from the American Nuclear Society.

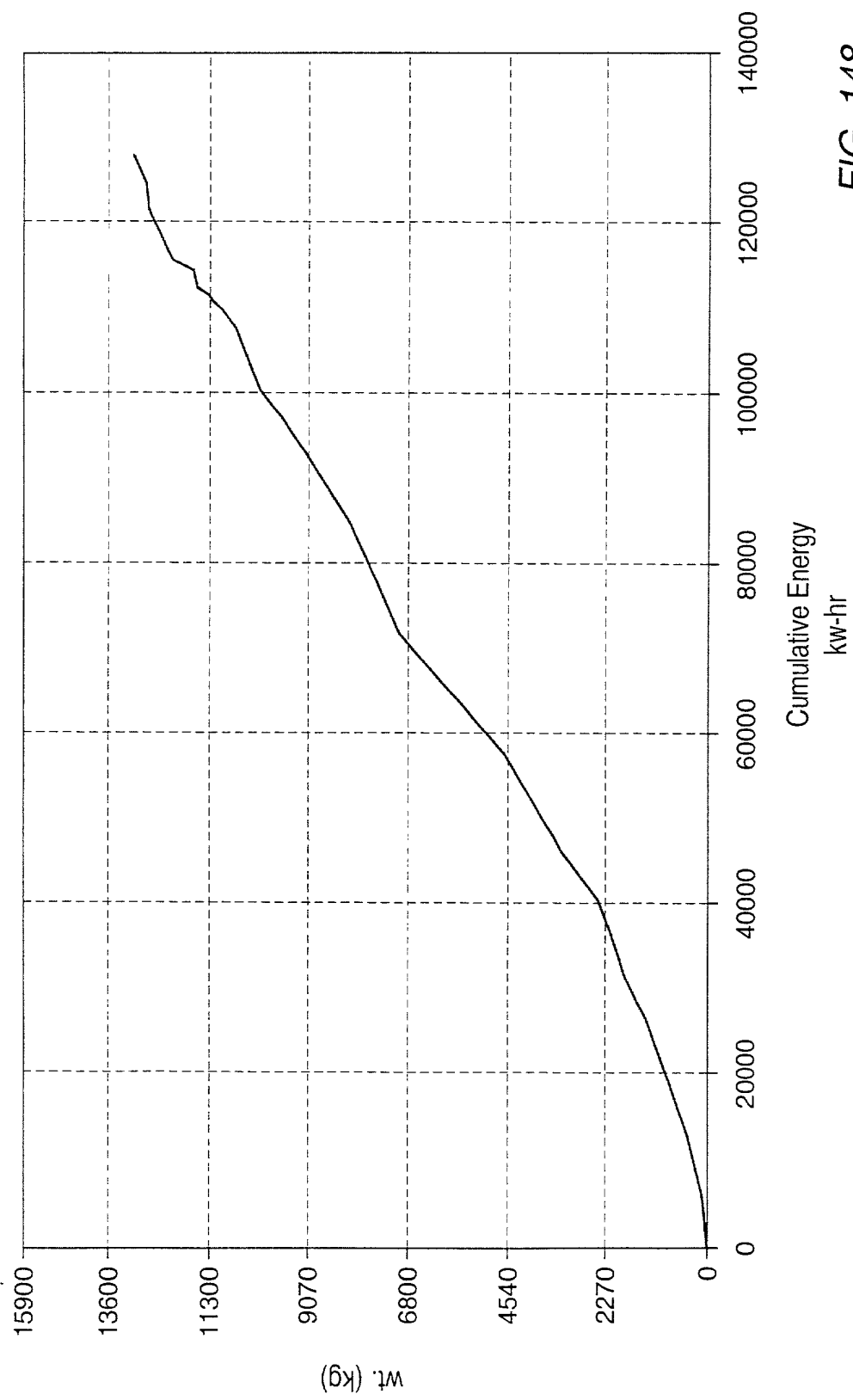


FIG. 148

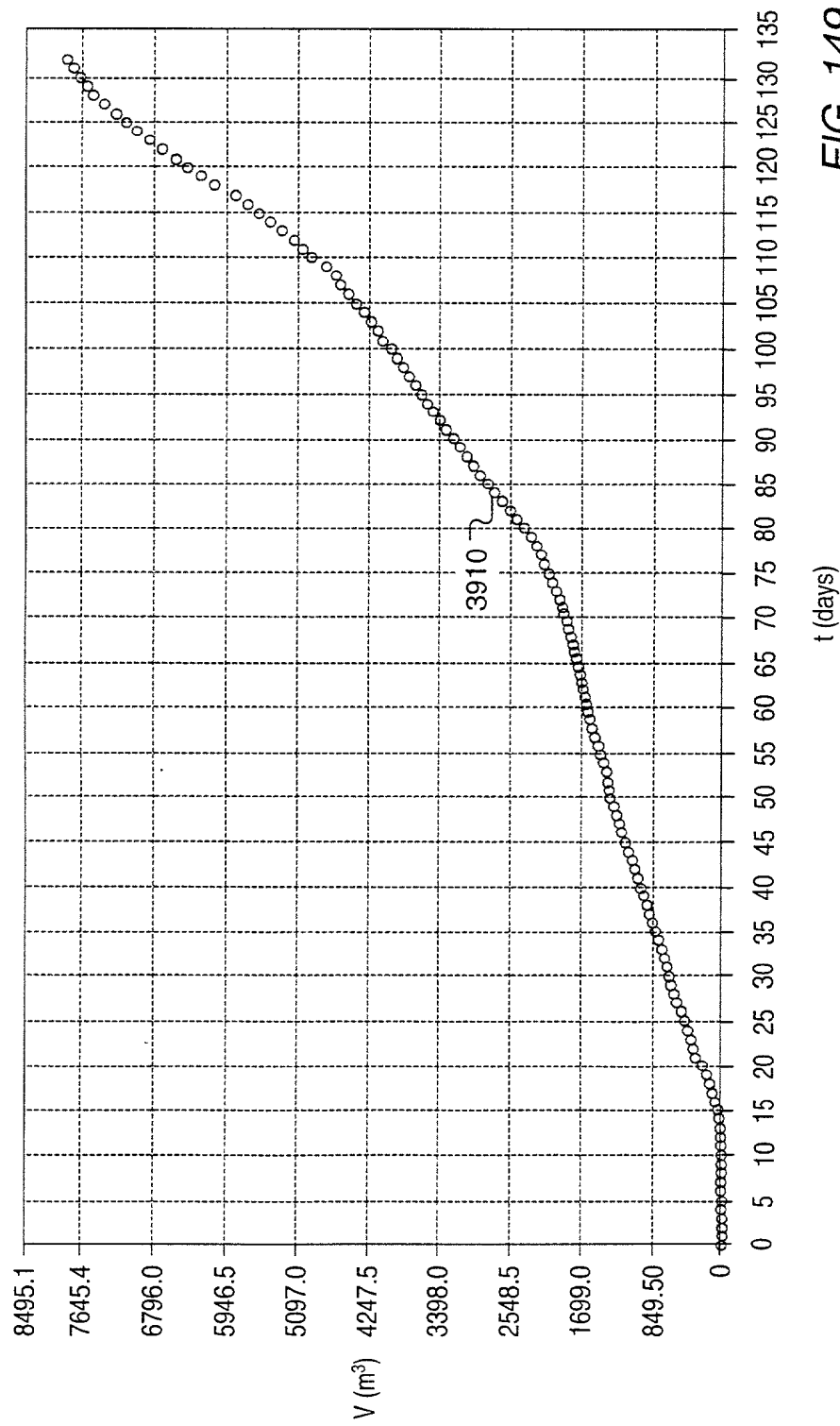


FIG. 149

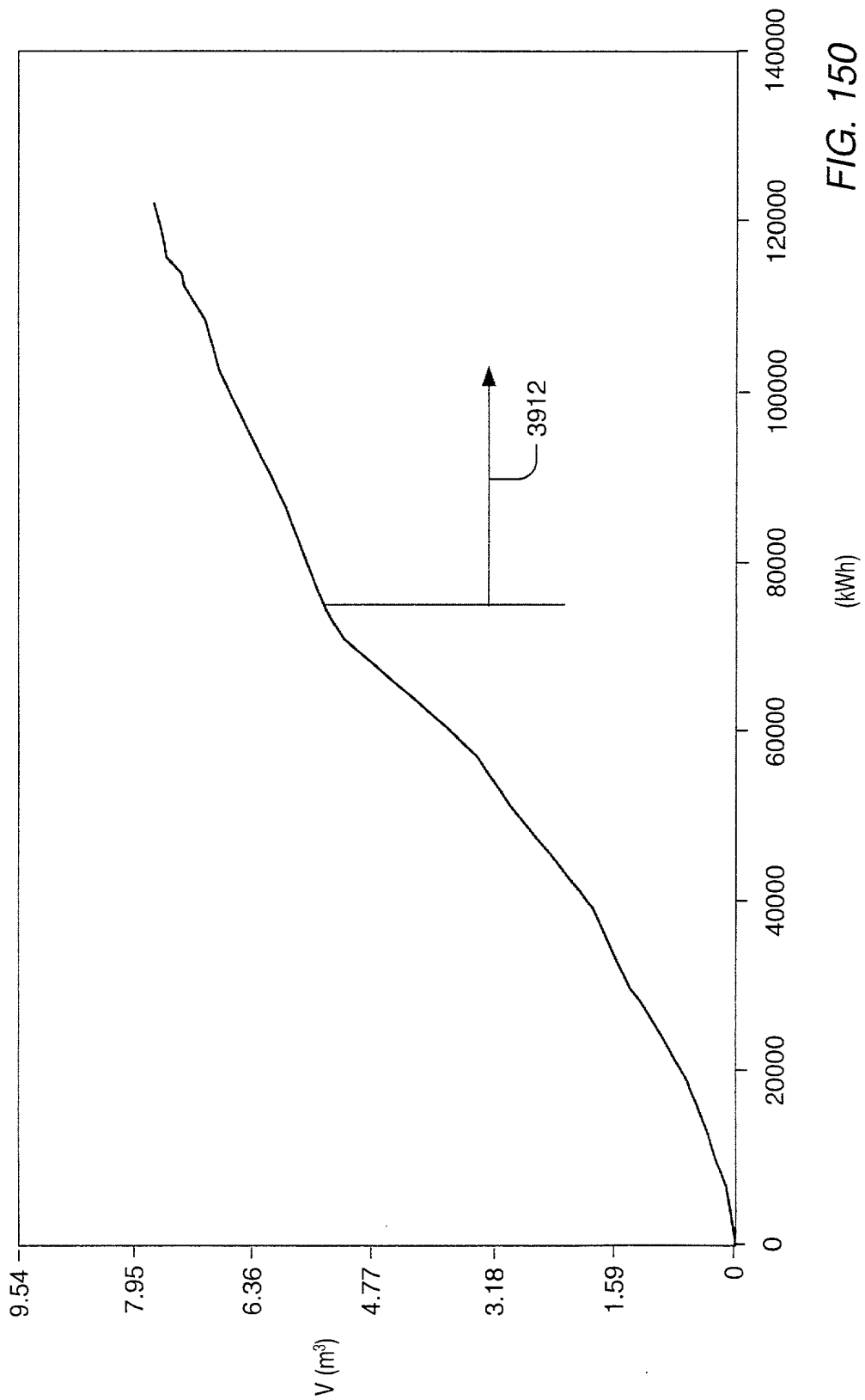


FIG. 150

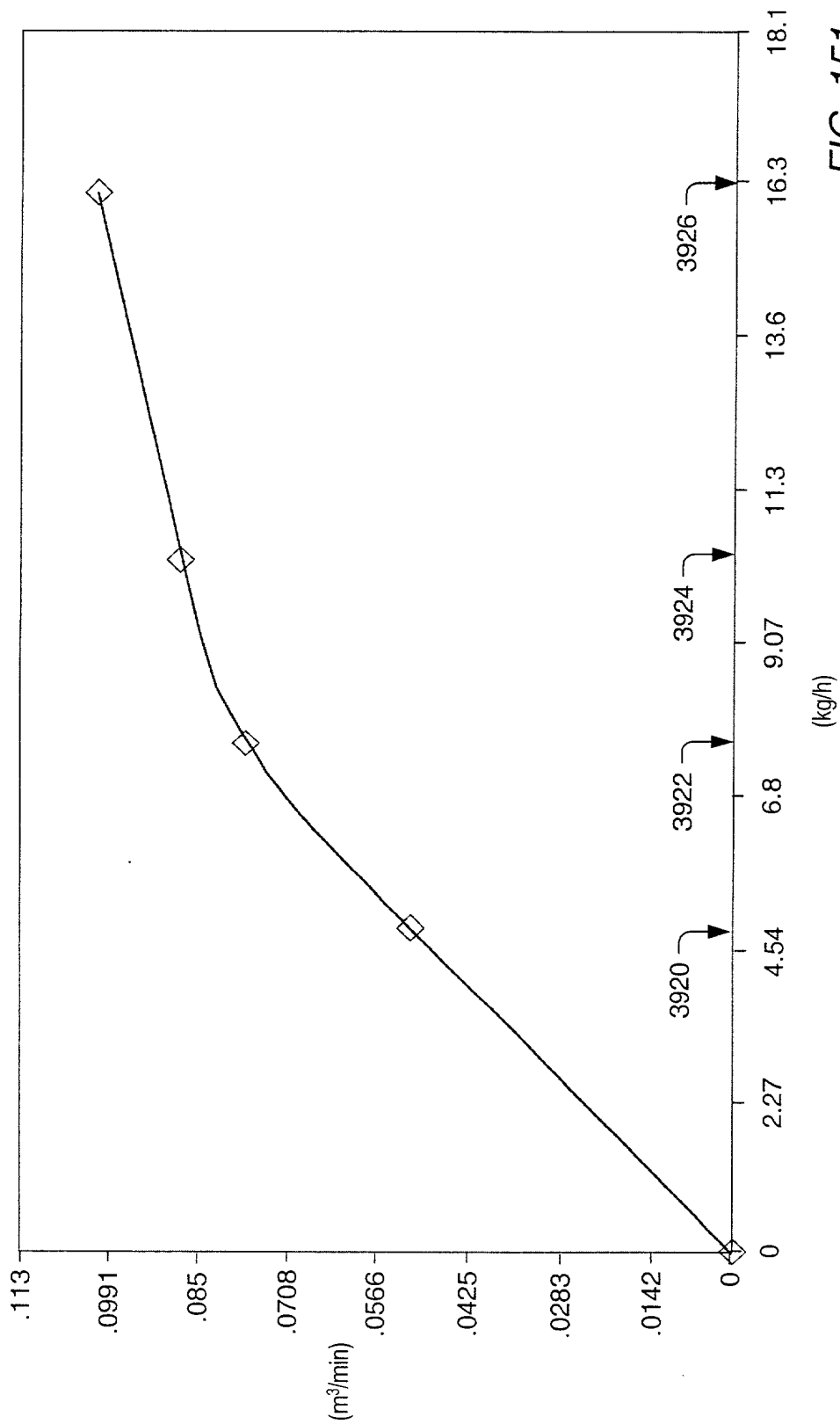


FIG. 151

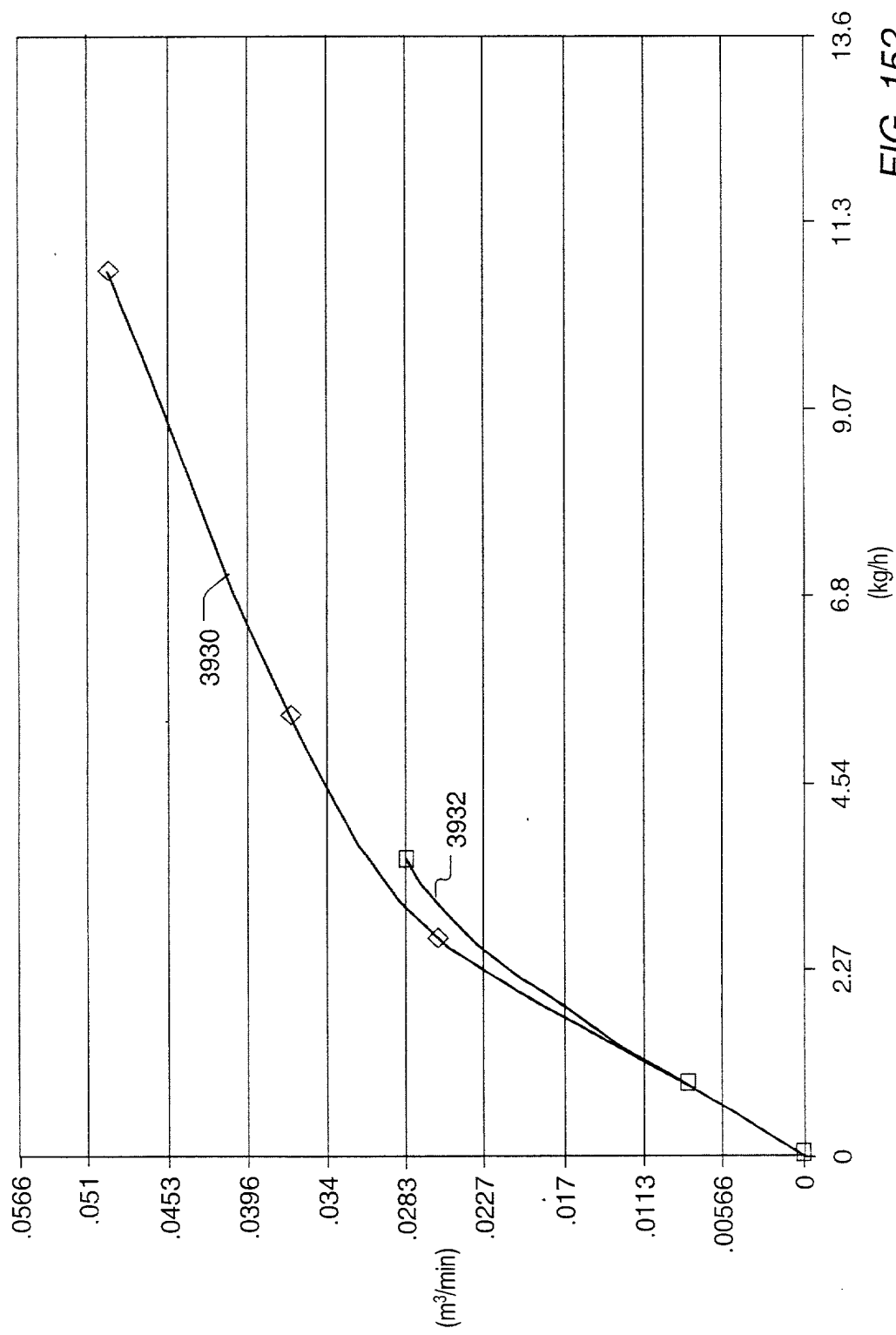


FIG. 152

Figure 153 is a scatter plot showing the relationship between Flow Rate (m³/hr) on the Y-axis and Methane Injection Rate (m³/hr) on the X-axis. The Y-axis ranges from 0 to 8.495 with major grid lines every 1.416 units. The X-axis ranges from 0 to 16.99 with major grid lines every 2.832 units. Data points are plotted for two series: 3940 (represented by squares) and 3942 (represented by diamonds). The data points for series 3940 are approximately (0, 0.5), (14.16, 7.079), and (14.16, 5.663). The data points for series 3942 are approximately (0, 1.416), (14.16, 5.663), and (14.16, 7.079).

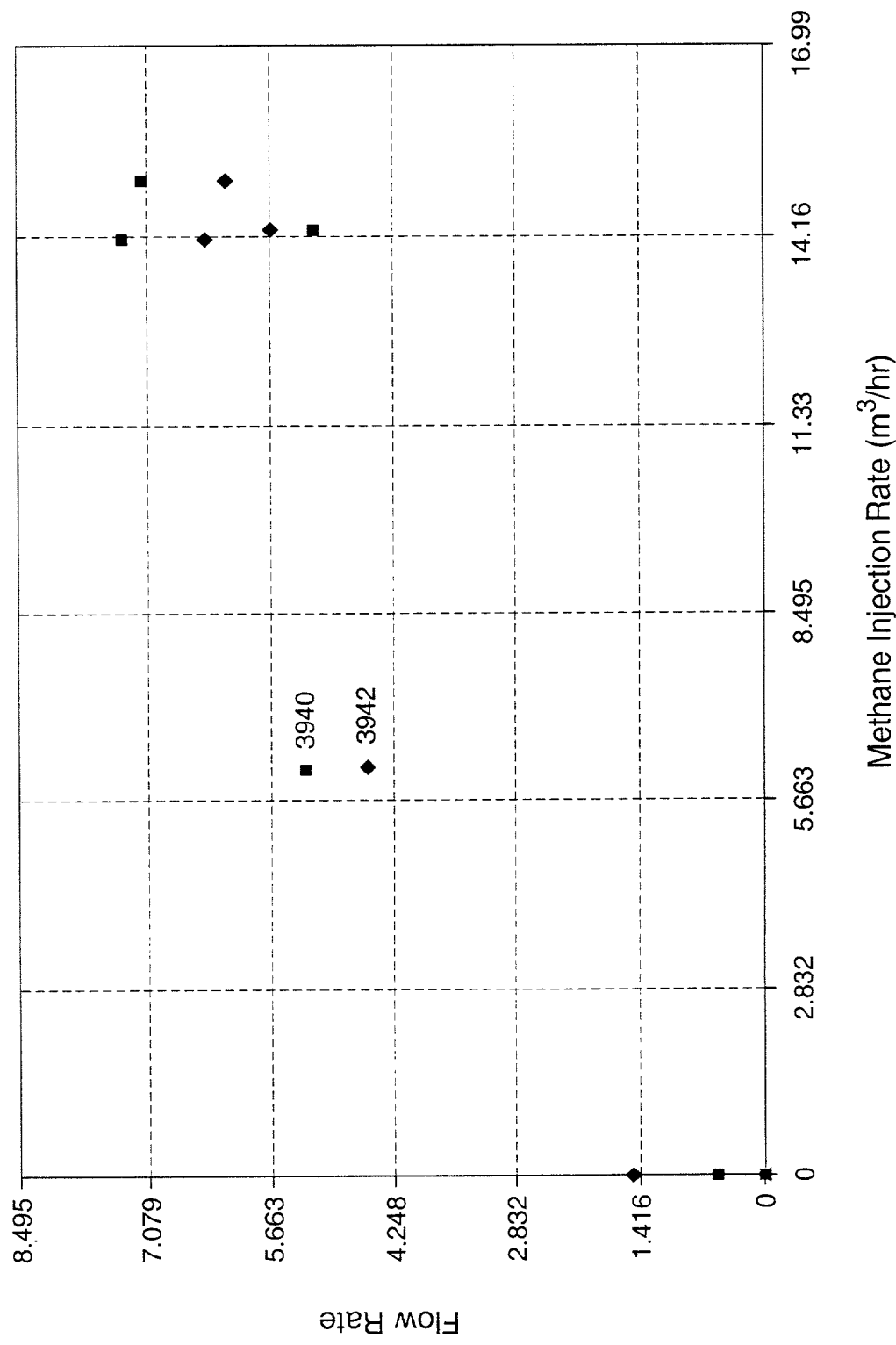


FIG. 153

Figure 154 is a scatter plot showing the relationship between Flow Rate (m³/hr) on the Y-axis and Ethane Injection Rate (m³/hr) on the X-axis. The data points are categorized by four different symbols: solid squares (3950), solid diamonds (3952), solid triangles (3954), and crosses (3956). The X-axis ranges from 0 to 14.16 m³/hr, and the Y-axis ranges from 0 to 11.33 m³/hr. The plot shows a general trend where Flow Rate increases with Ethane Injection Rate, with some scatter observed at higher injection rates.

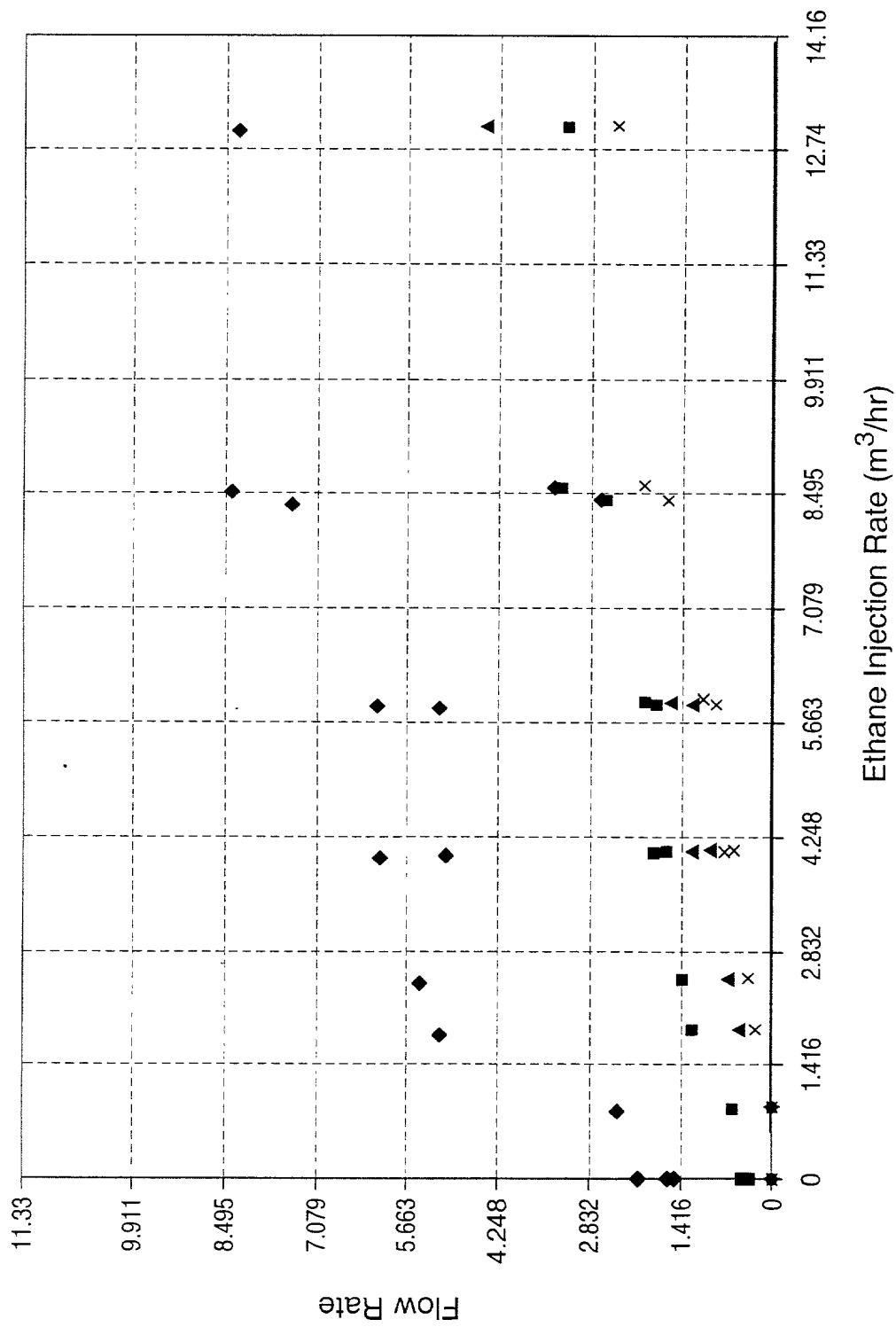


FIG. 154

Figure 155 is a scatter plot showing the relationship between Propane Injection Rate (m³/hr) on the X-axis and Flow Rate on the Y-axis. The X-axis ranges from 0 to 7.079 m³/hr, and the Y-axis ranges from 0 to 9.917. Data points are plotted for various propane injection rates, with symbols indicating different flow rates. The data points show a general trend of increasing flow rate with increasing propane injection rate, with some scatter observed at higher injection rates.

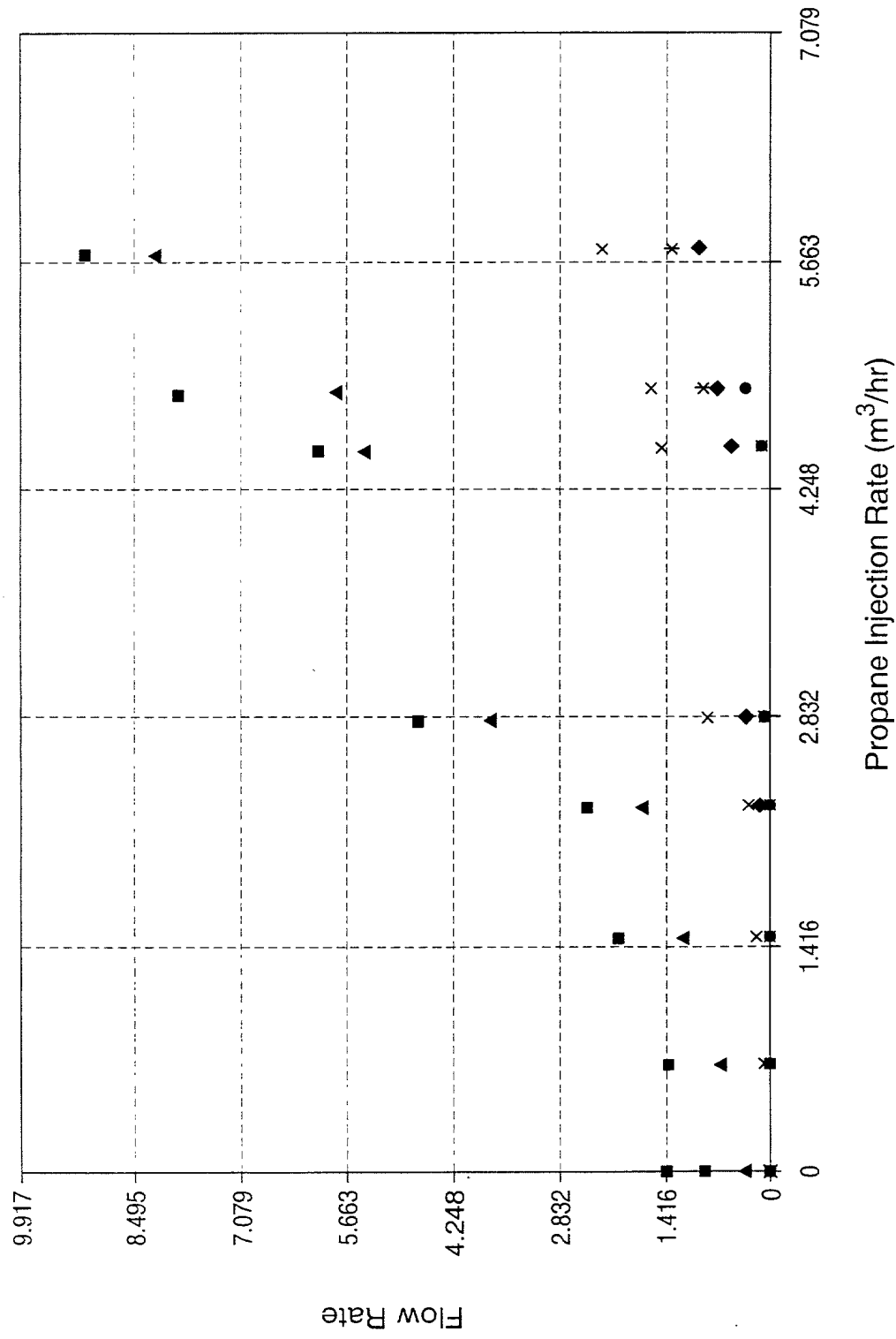
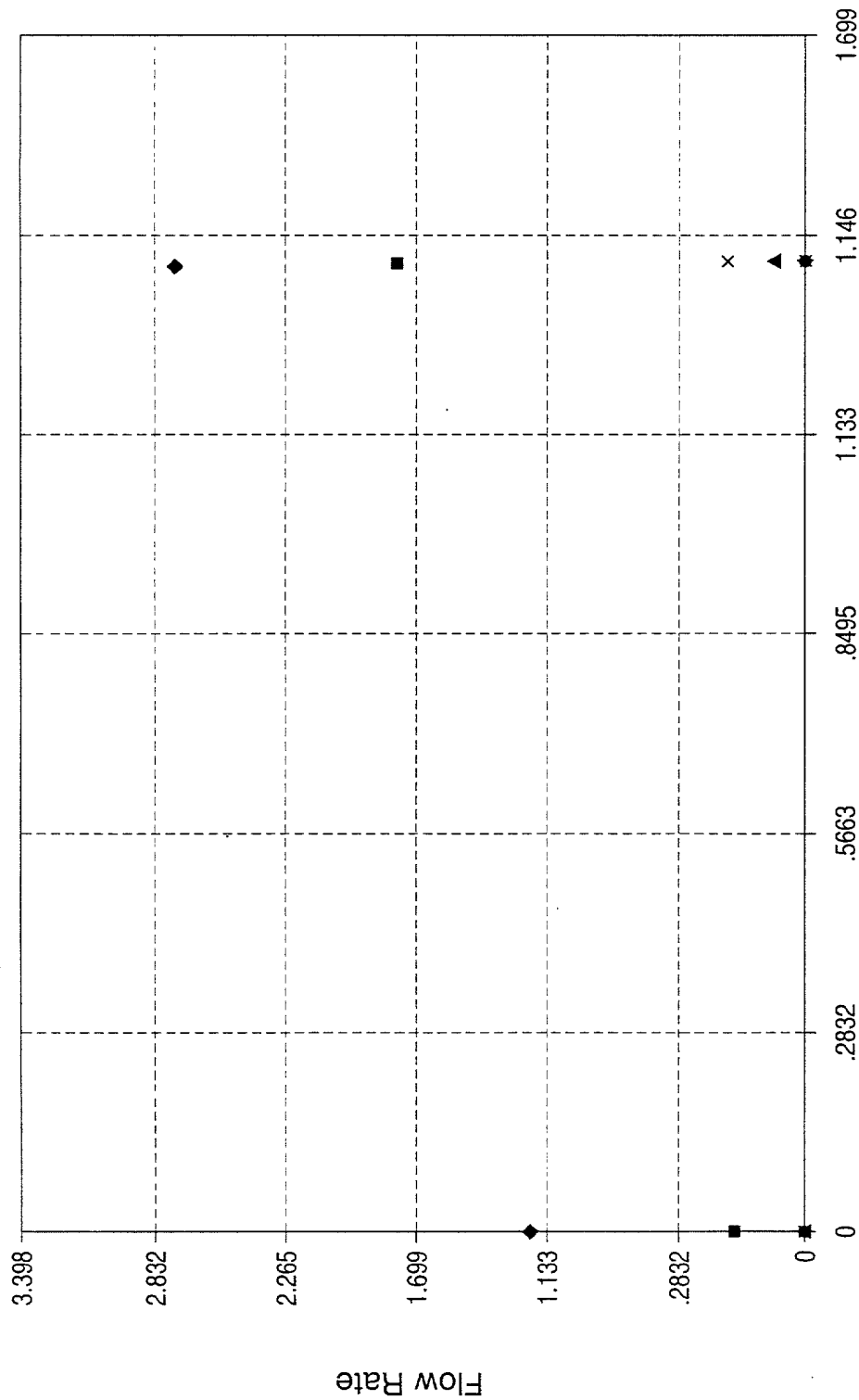


FIG. 155





Butane Injection Rate (m³/hr)

■ 3970 ▲ 3972 ◆ 3974 × 3976 \* 3978 ● 3979

FIG. 156

Copyright © 1999 by John Wiley & Sons, Inc. All rights reserved. No part of this publication may be reproduced, stored in a retrieval system, or transmitted, in any form or by any means, electronic, mechanical, photocopying, recording, or by any information storage and retrieval system, without permission in writing from John Wiley & Sons, Inc.

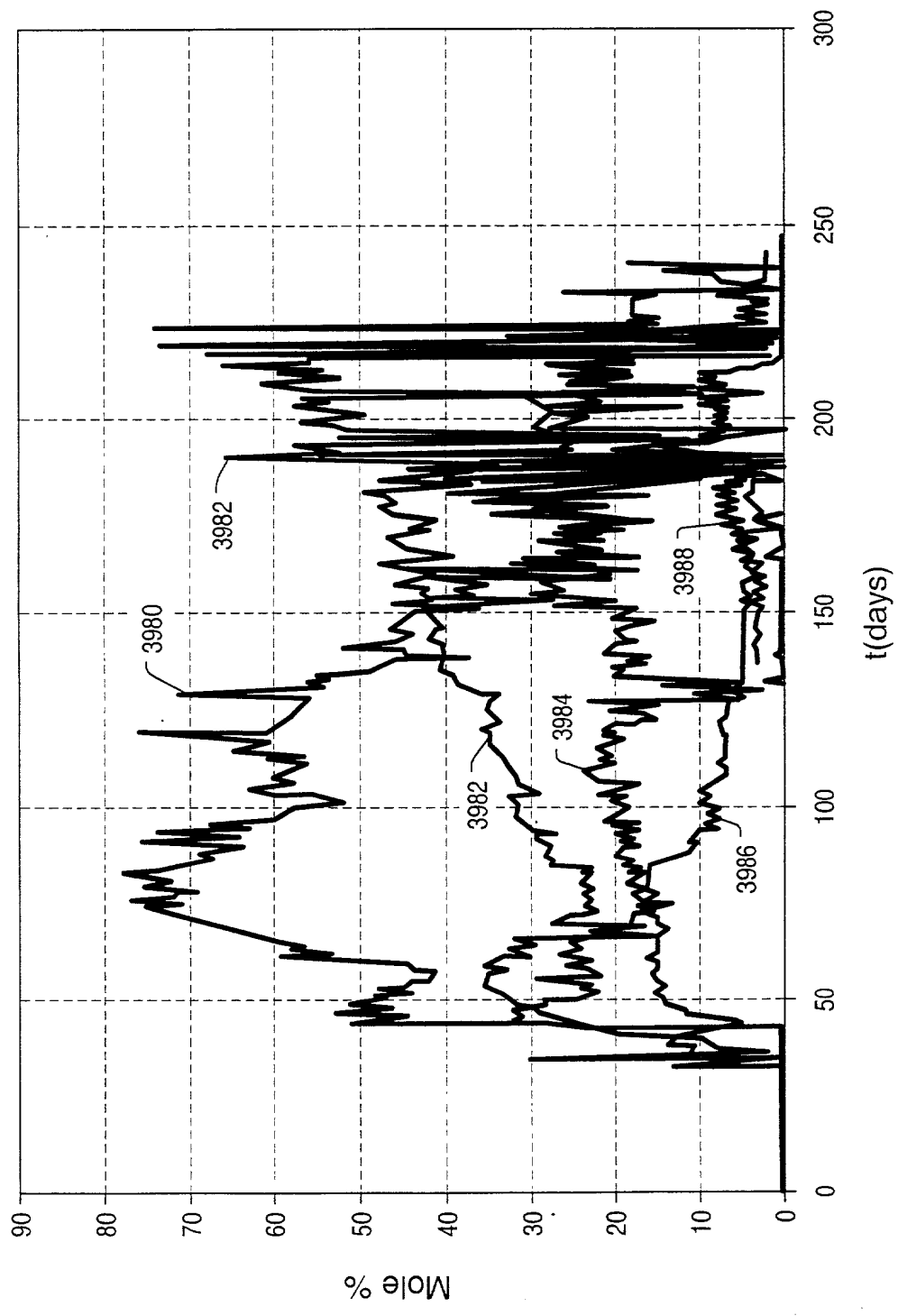


FIG. 157

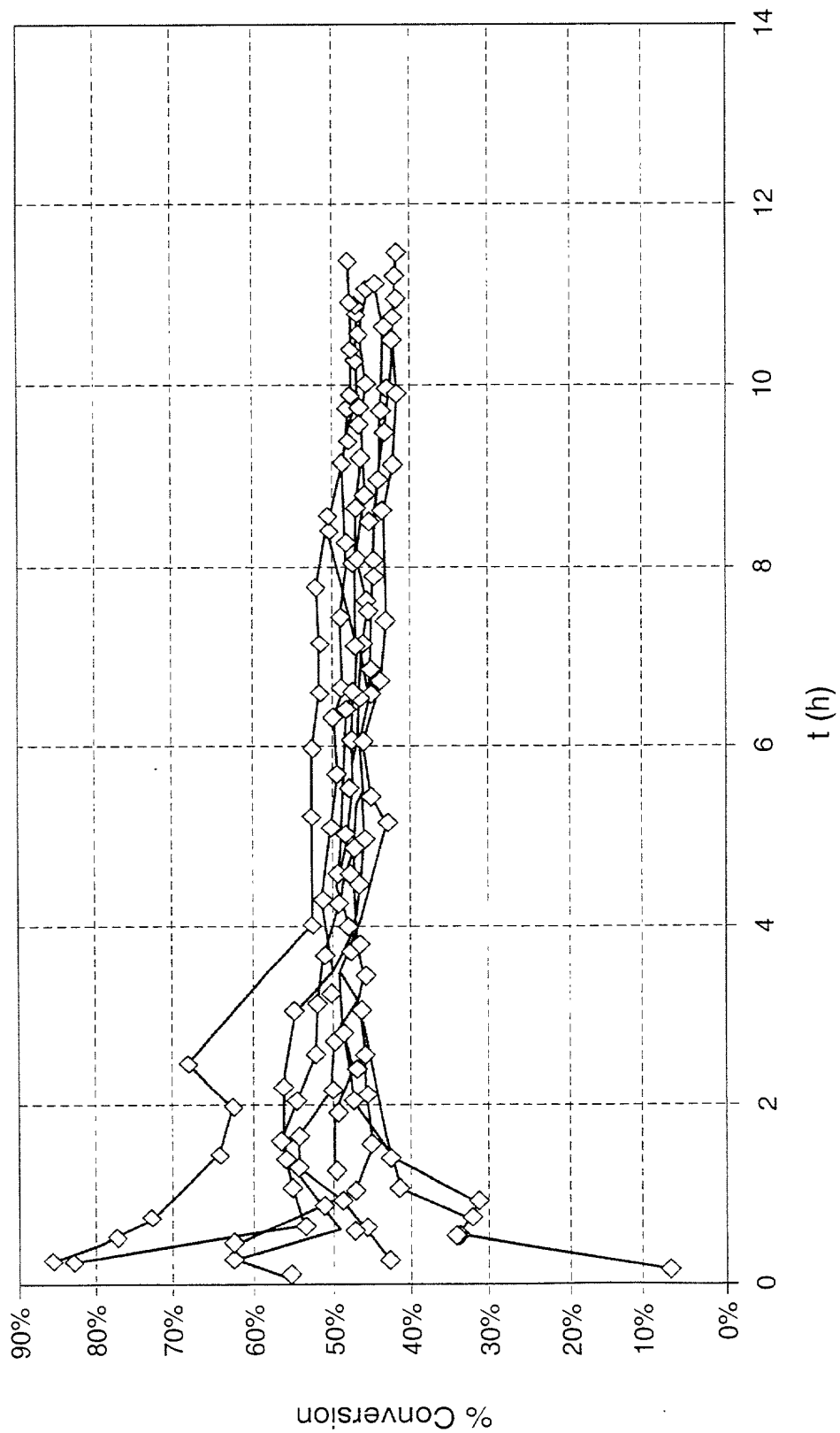


FIG. 158

Figure 159 shows the variation of the dry mole fraction of the gas phase with temperature for the system  $\text{H}_2\text{O}-\text{H}_2\text{SO}_4$  at 100 mm Hg. The curves are labeled 4000, 4002, and 4004.

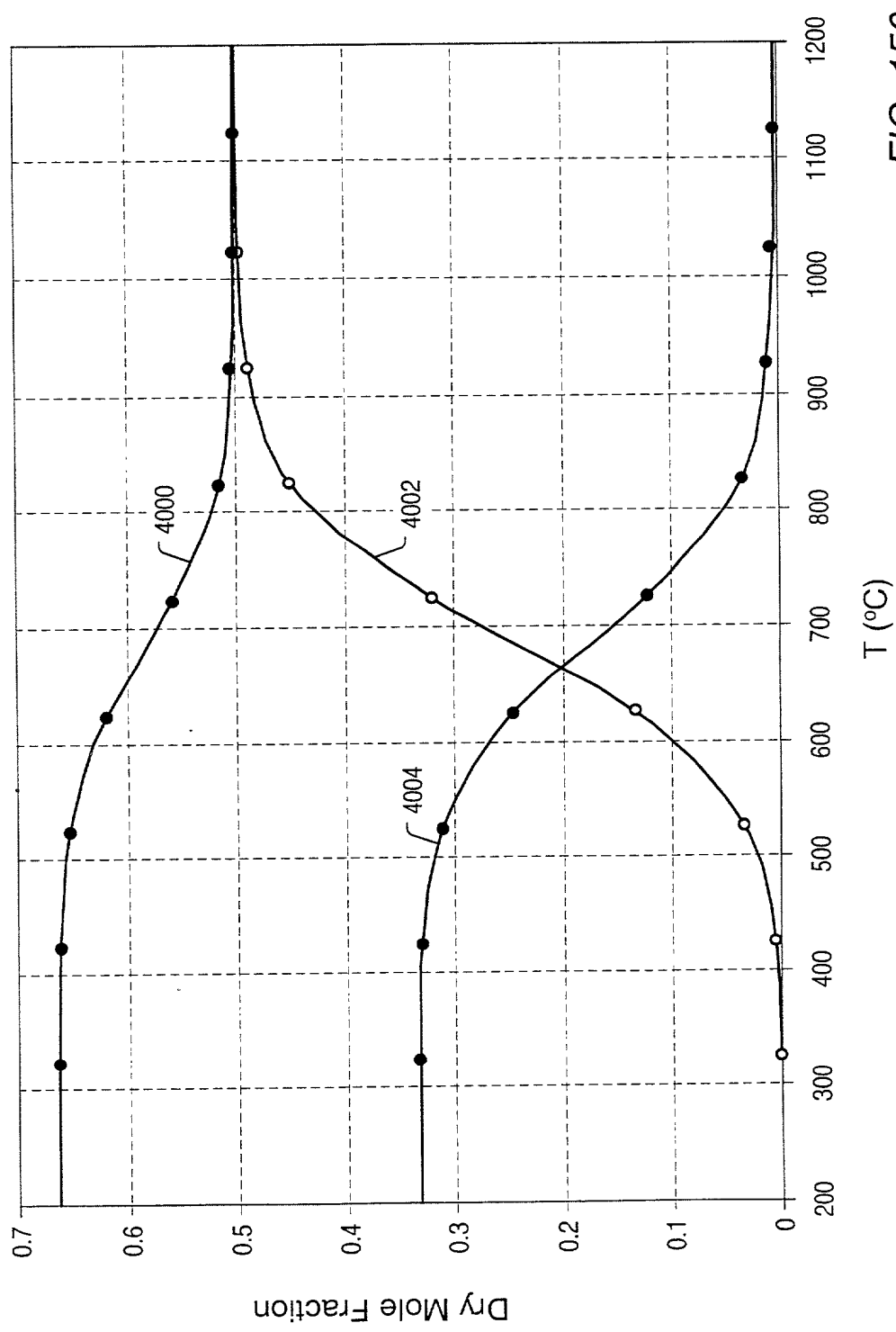


FIG. 159

Copyright © 1994 by John Wiley & Sons, Inc. All rights reserved. No part of this publication may be reproduced, stored in a retrieval system, or transmitted, in any form or by any means, electronic, mechanical, photocopying, recording, or by any information storage and retrieval system, without permission in writing from John Wiley & Sons, Inc.

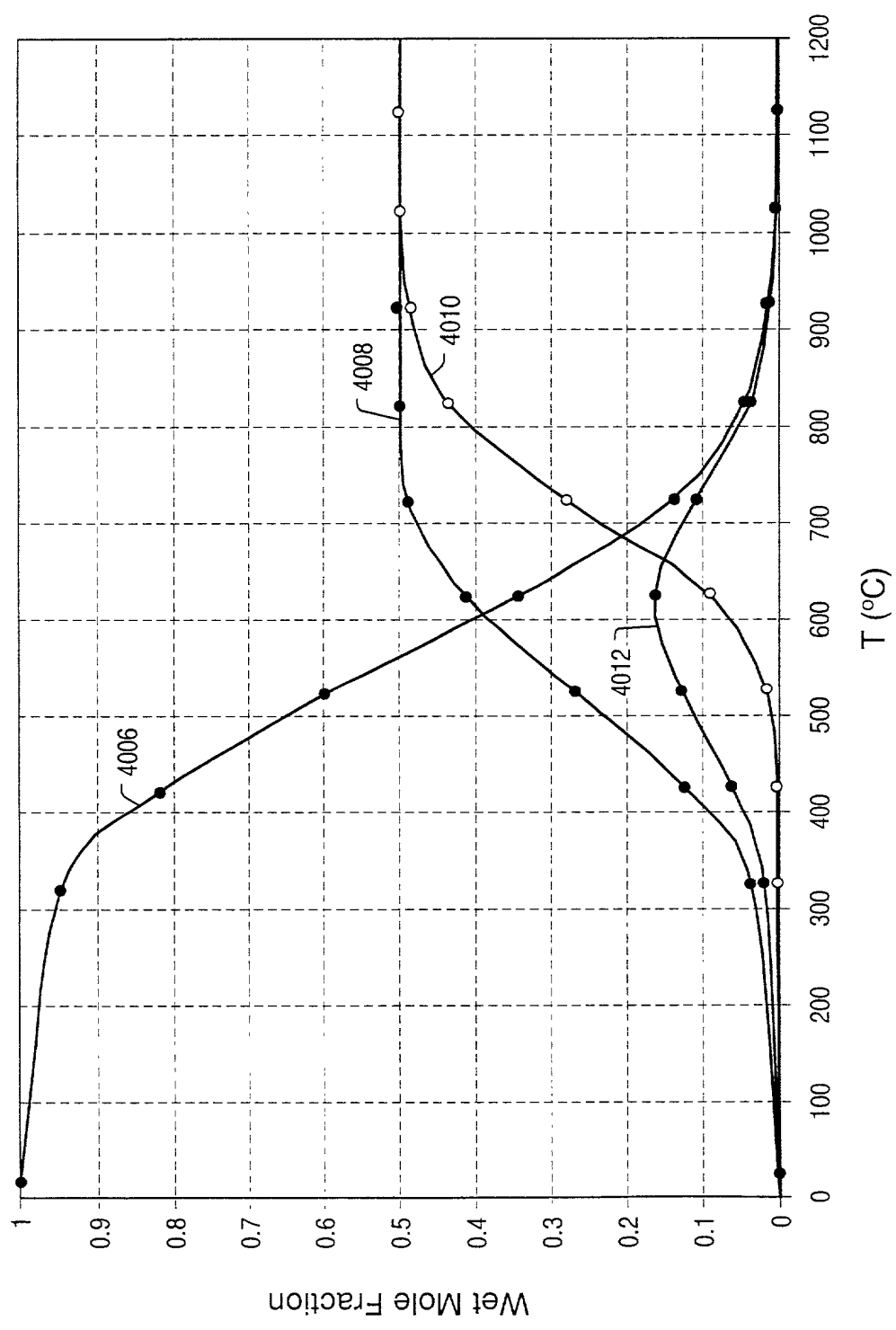


FIG. 160

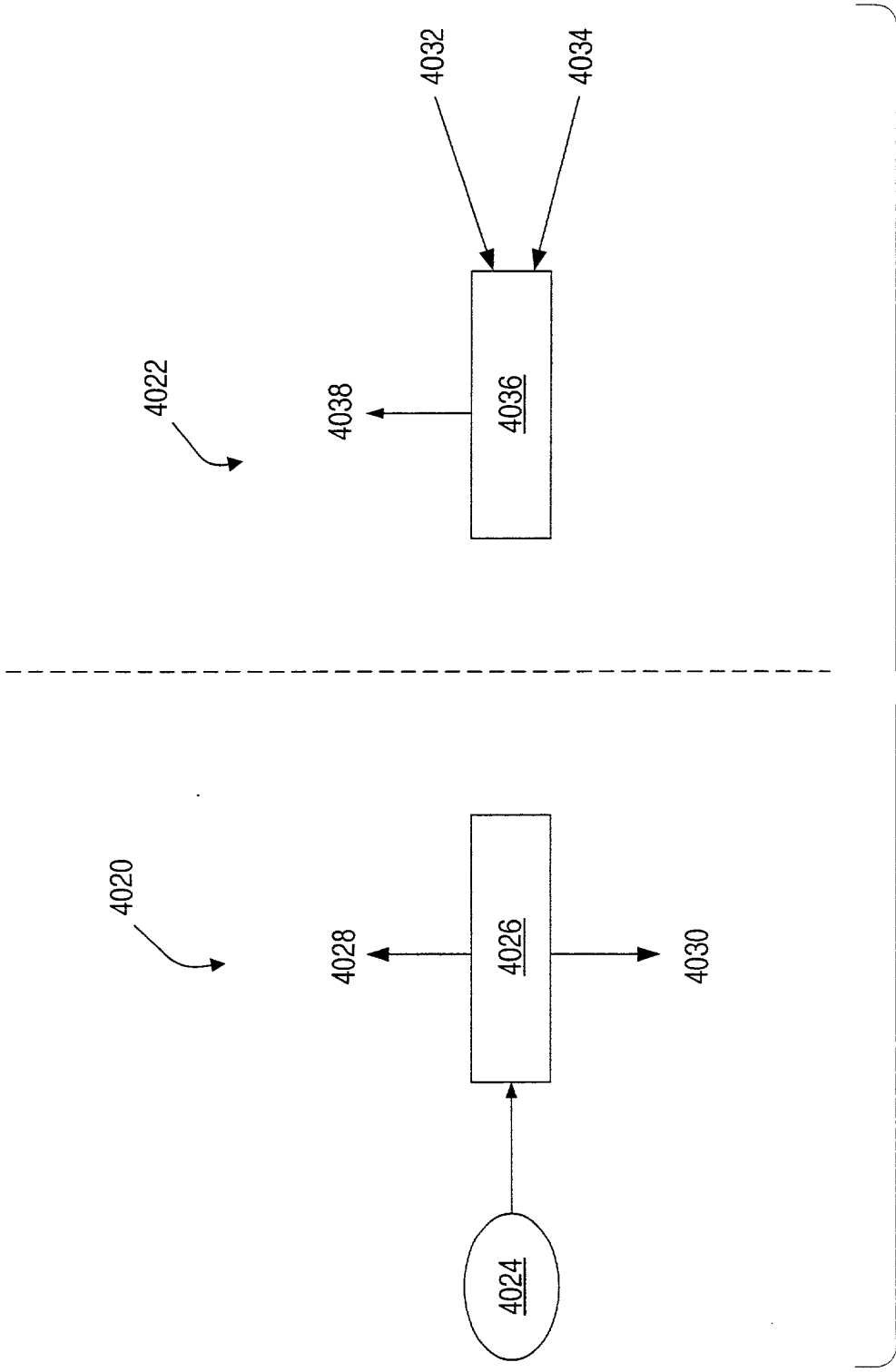


FIG. 161

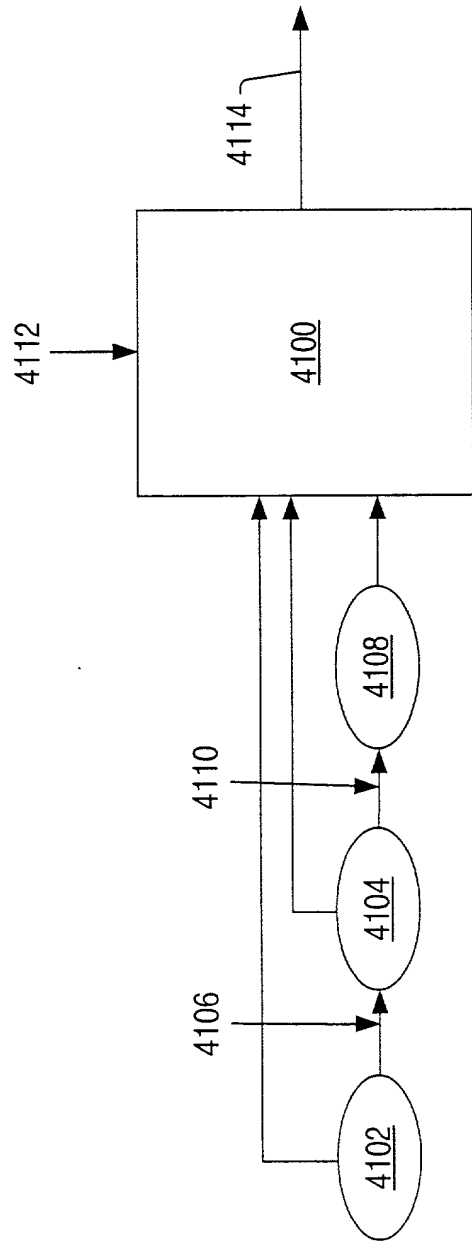


FIG. 162

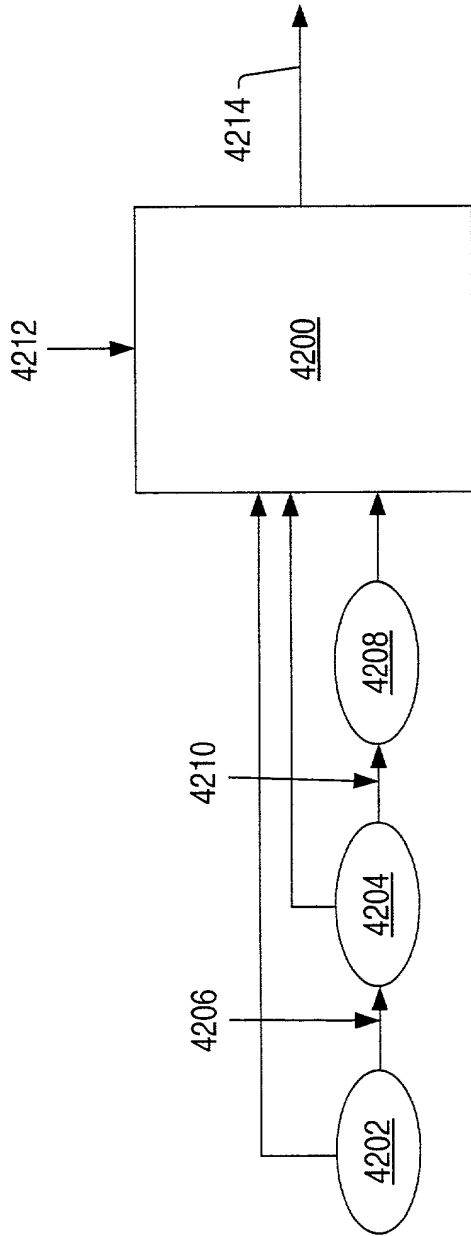


FIG. 163



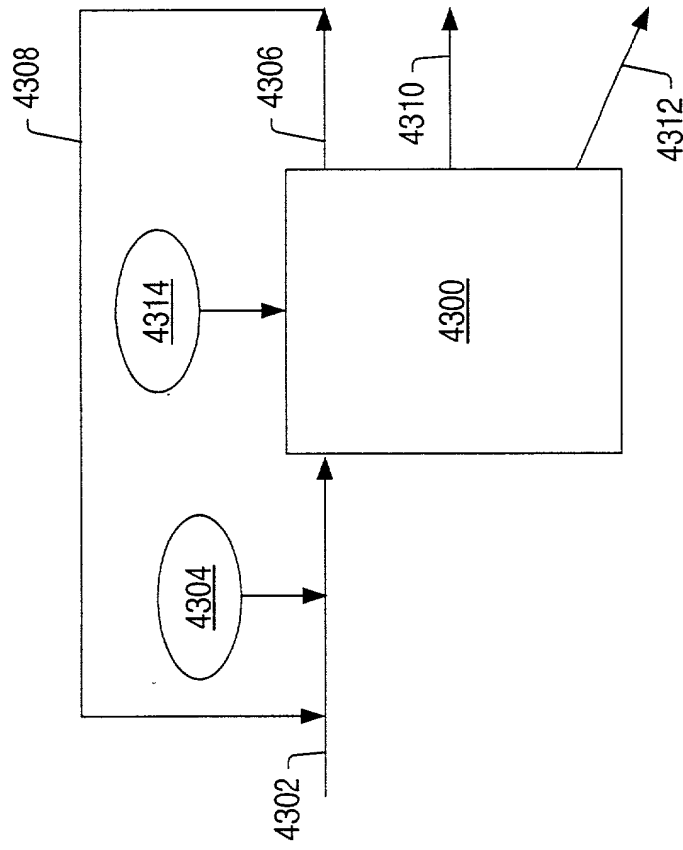


FIG. 164

184.33  
 163.85  
 143.37  
 122.89  
 102.41  
 81.92  
 61.44  
 40.96  
 20.48  
 0.000

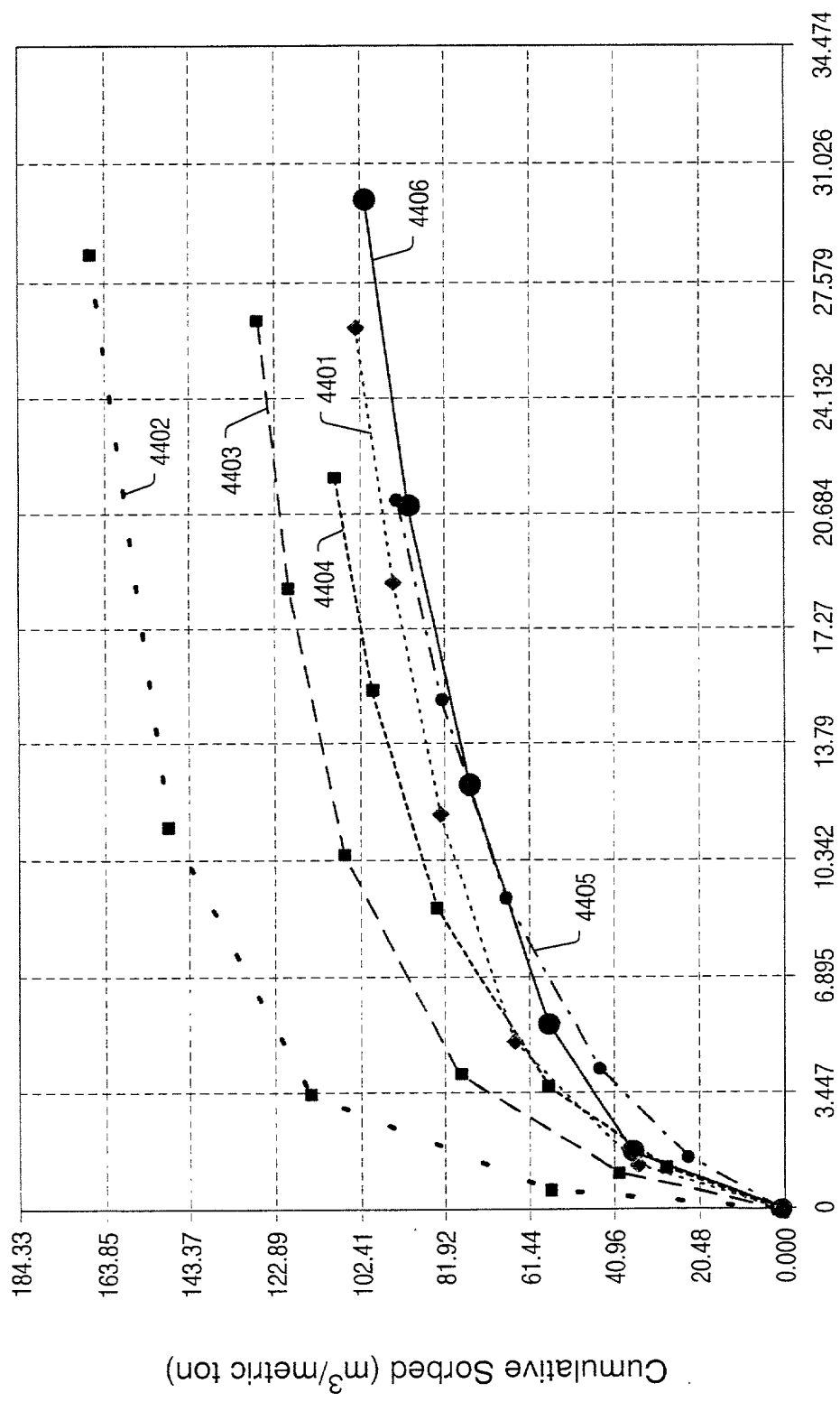


FIG. 165

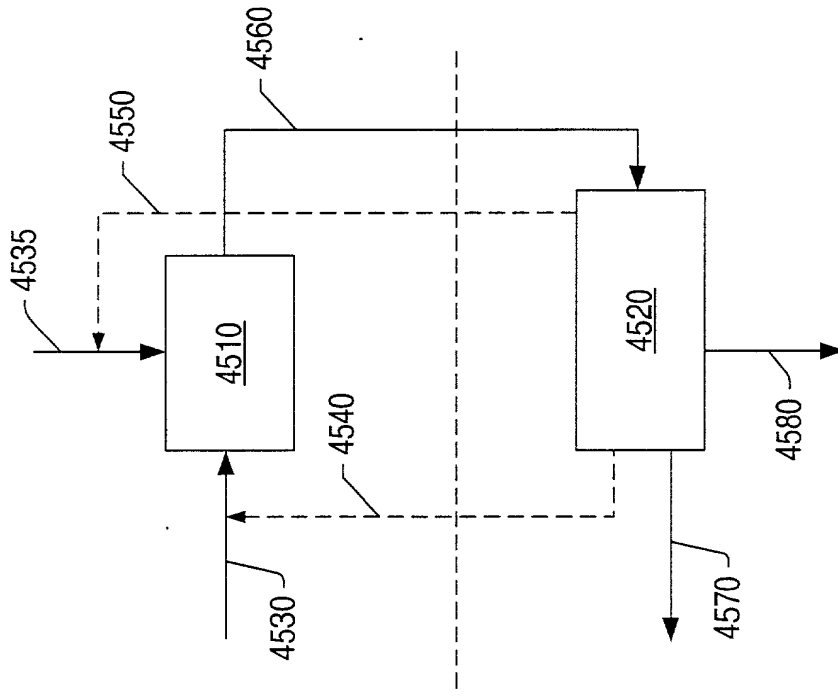


FIG. 166

$\frac{d\phi}{dt} = \frac{d\phi}{dt} \left( \frac{d\phi}{dt} \right)_{\text{max}} \left( \frac{d\phi}{dt} \right)_{\text{min}} \left( \frac{d\phi}{dt} \right)_{\text{avg}}$   
 $\frac{d\phi}{dt} = \frac{d\phi}{dt} \left( \frac{d\phi}{dt} \right)_{\text{max}} \left( \frac{d\phi}{dt} \right)_{\text{min}} \left( \frac{d\phi}{dt} \right)_{\text{avg}}$

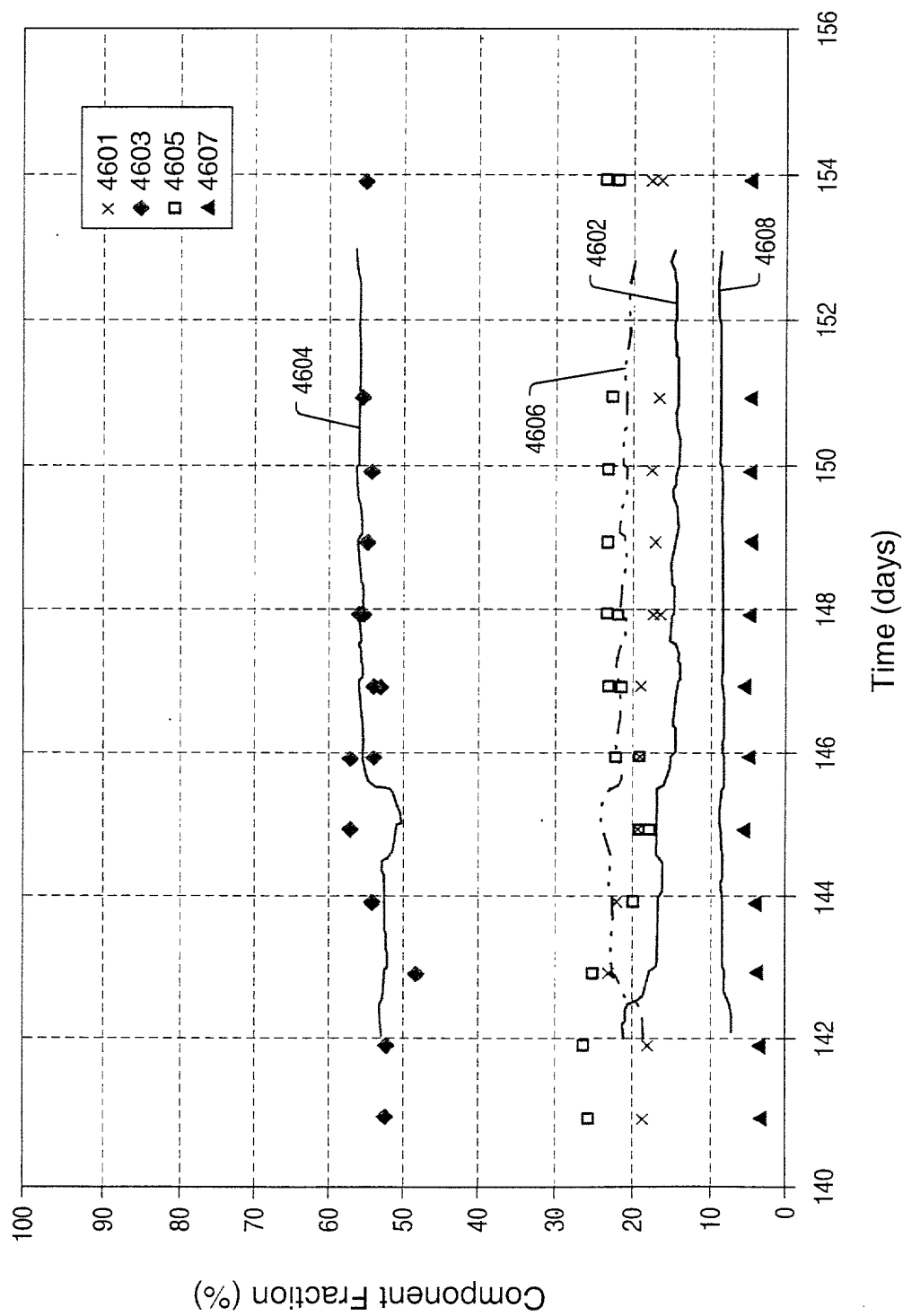


FIG. 167

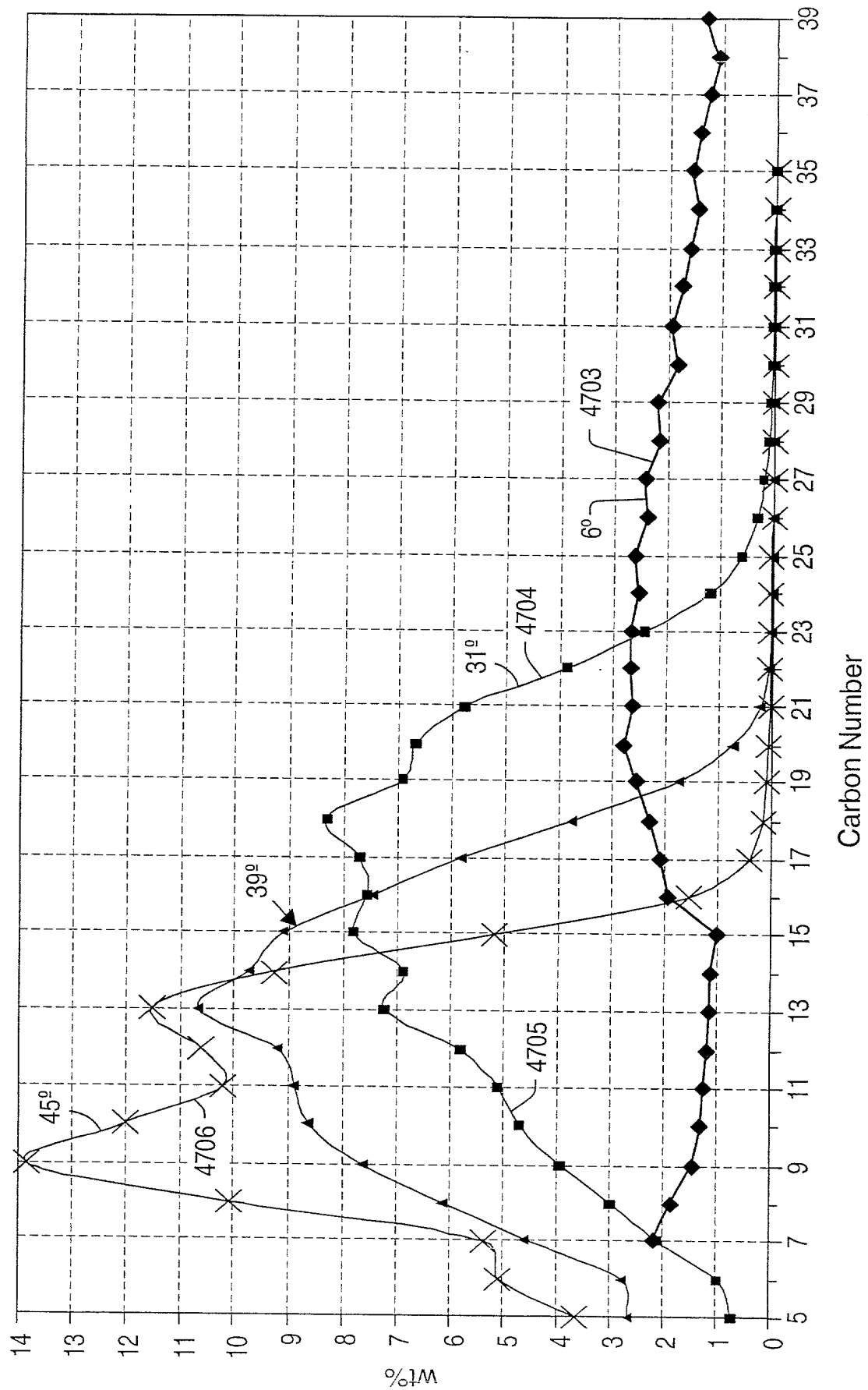


FIG. 168

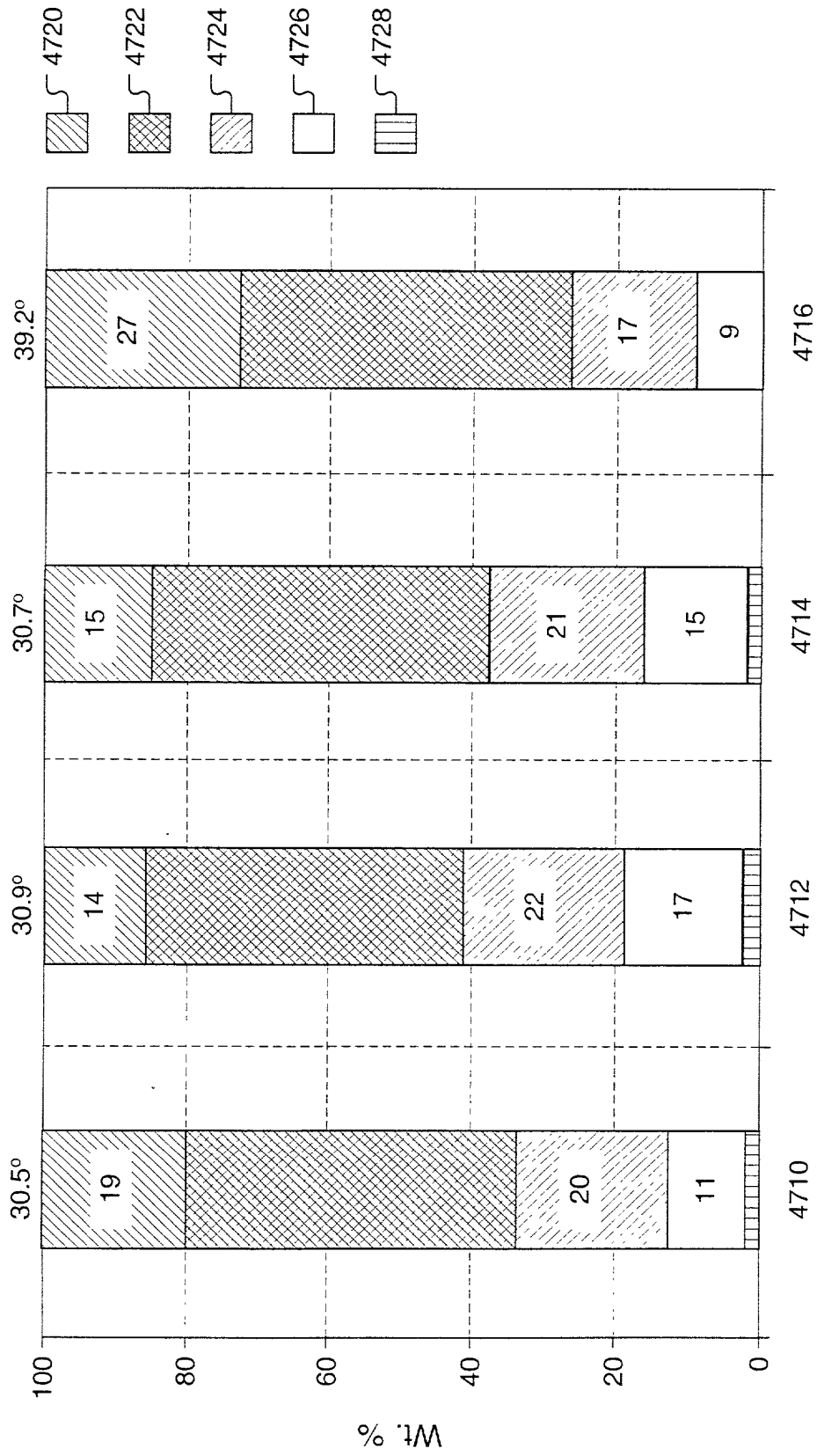


FIG. 169

FIG. 170

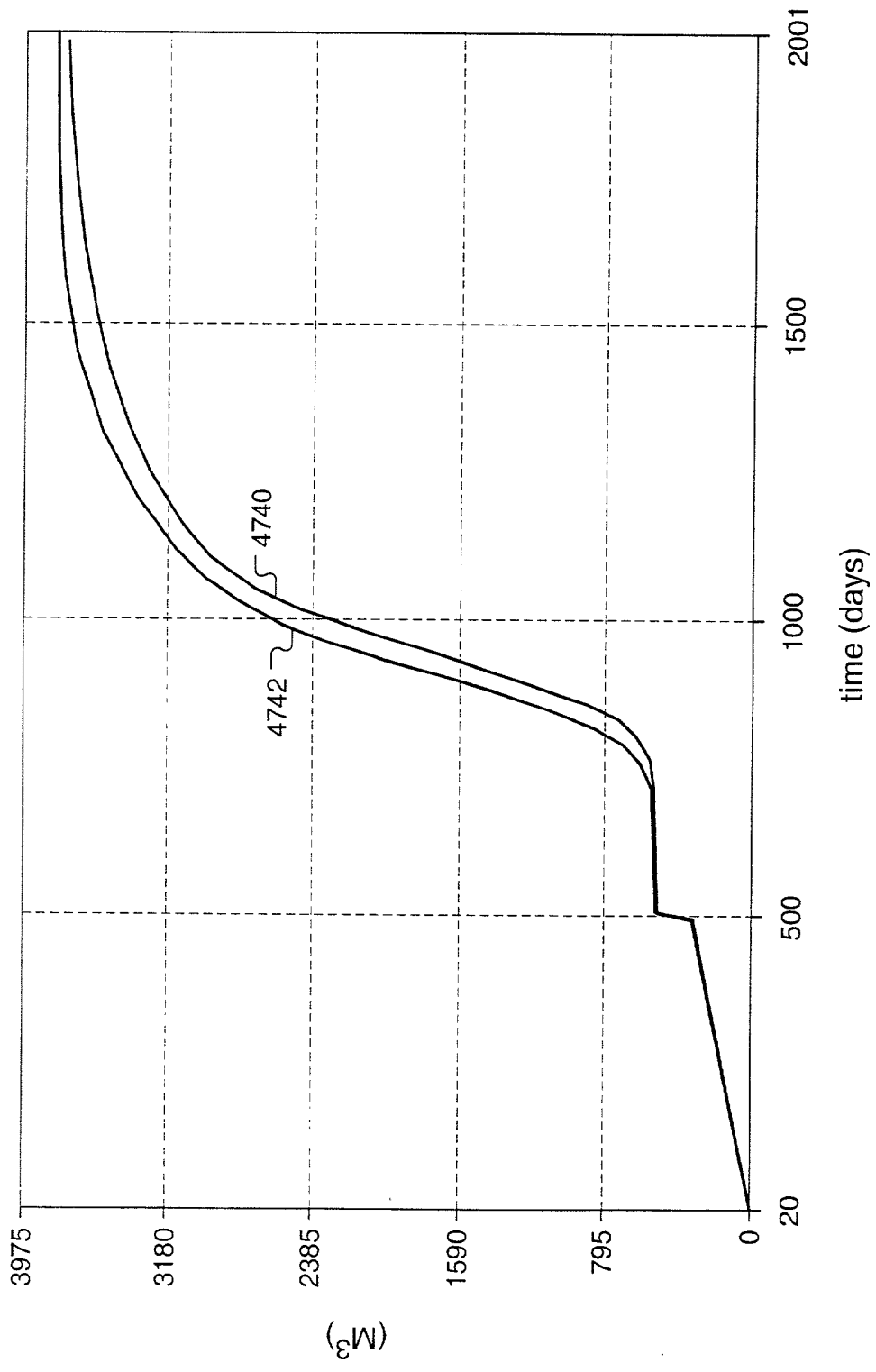


FIG. 170





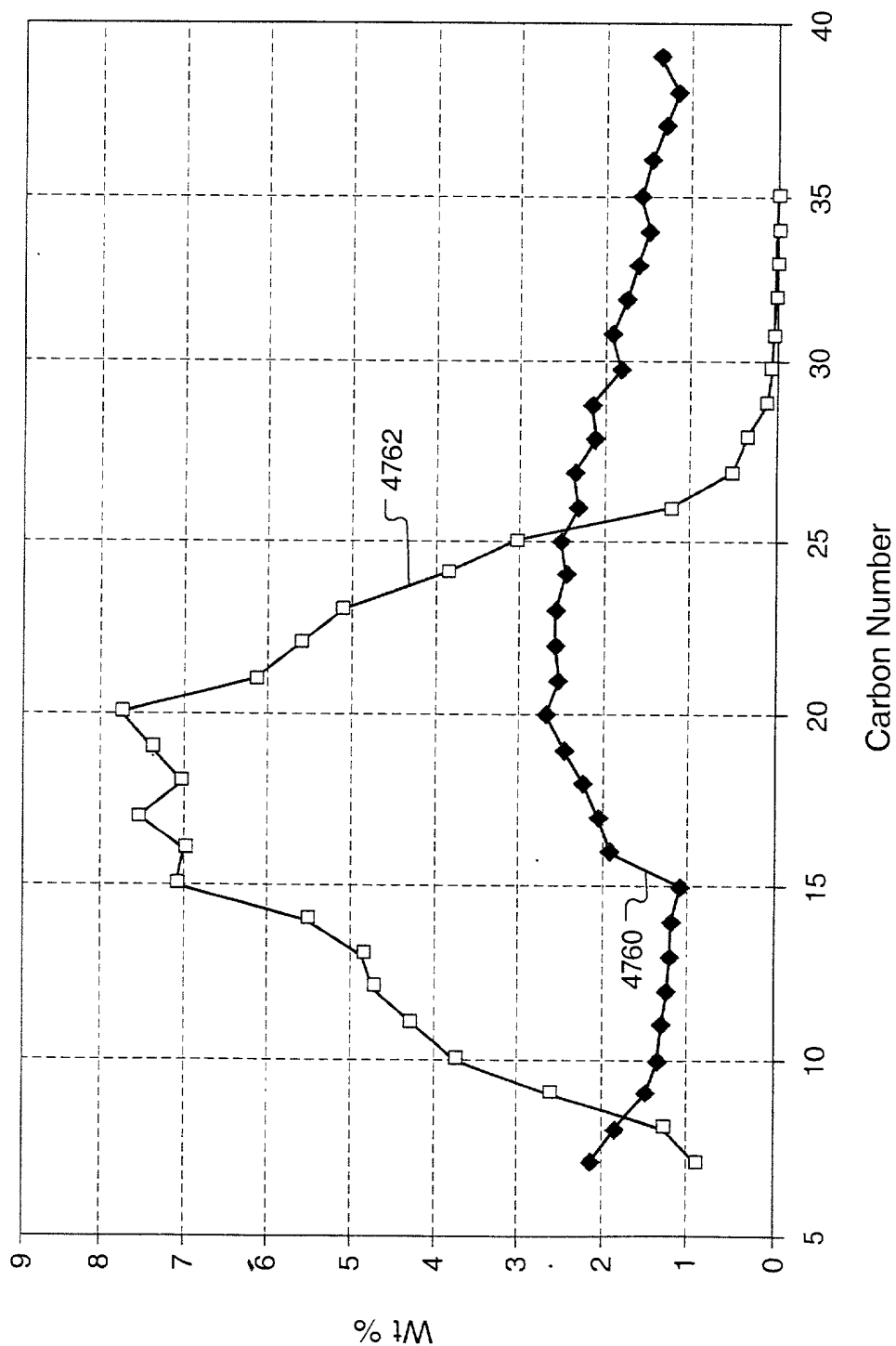


FIG. 172



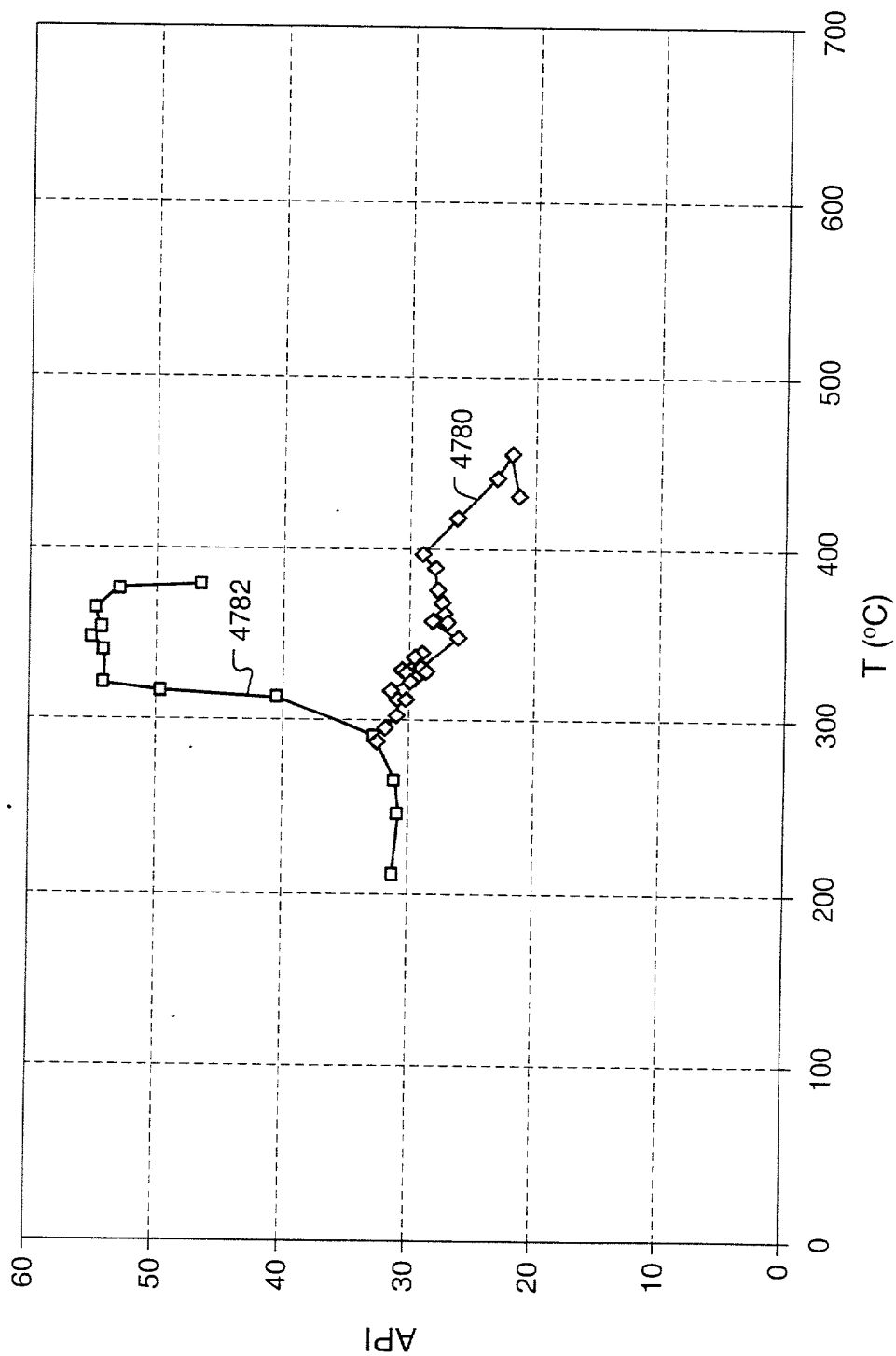
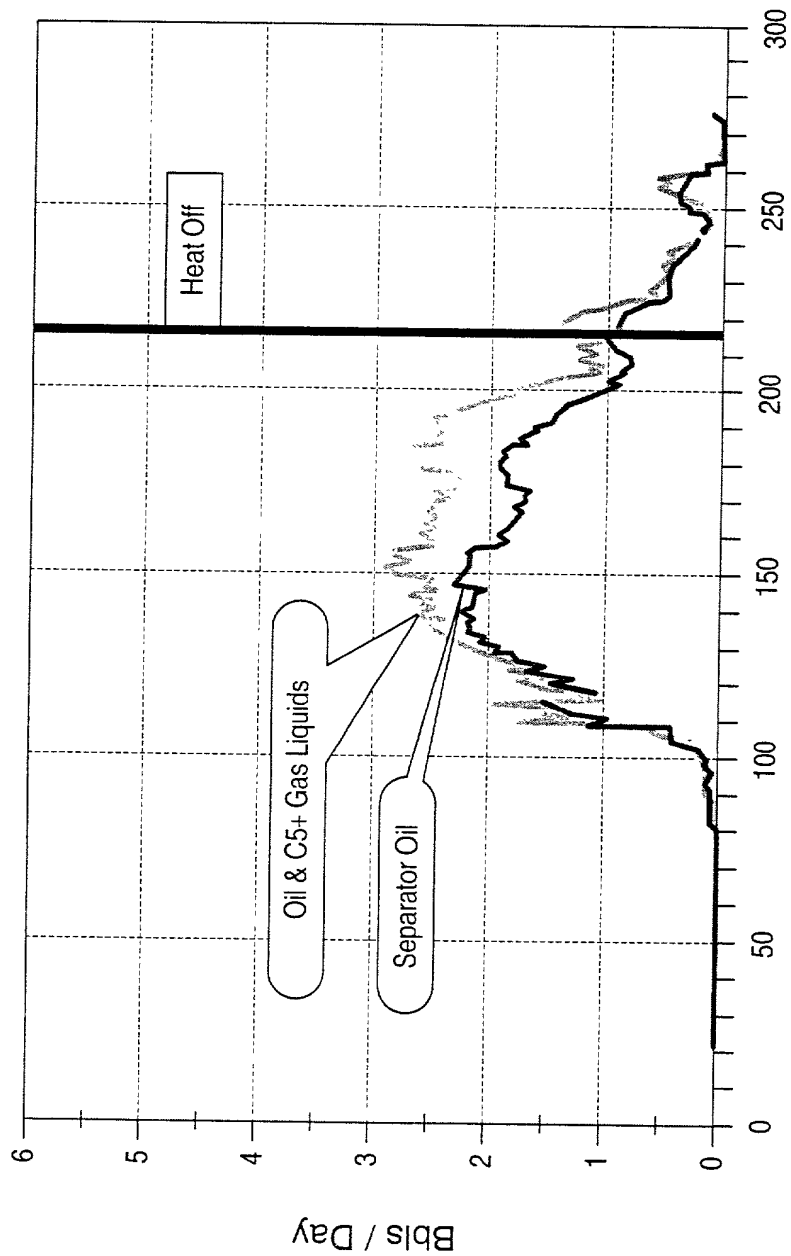


FIG. 174

FIG. 175 is a line graph showing the production of oil and gas liquids from a well over time. The x-axis represents "Days From Start of Heat Injection" from 0 to 300. The y-axis represents "Bbls / Day" from 0 to 6. The graph shows a sharp increase in production starting around day 100, peaking around day 150, and then declining. A vertical line at day 200 is labeled "Heat Off". Two callouts point to the peak: "Oil & C5+ Gas Liquids" and "Separator Oil".



Days From Start of Heat Injection

FIG. 175

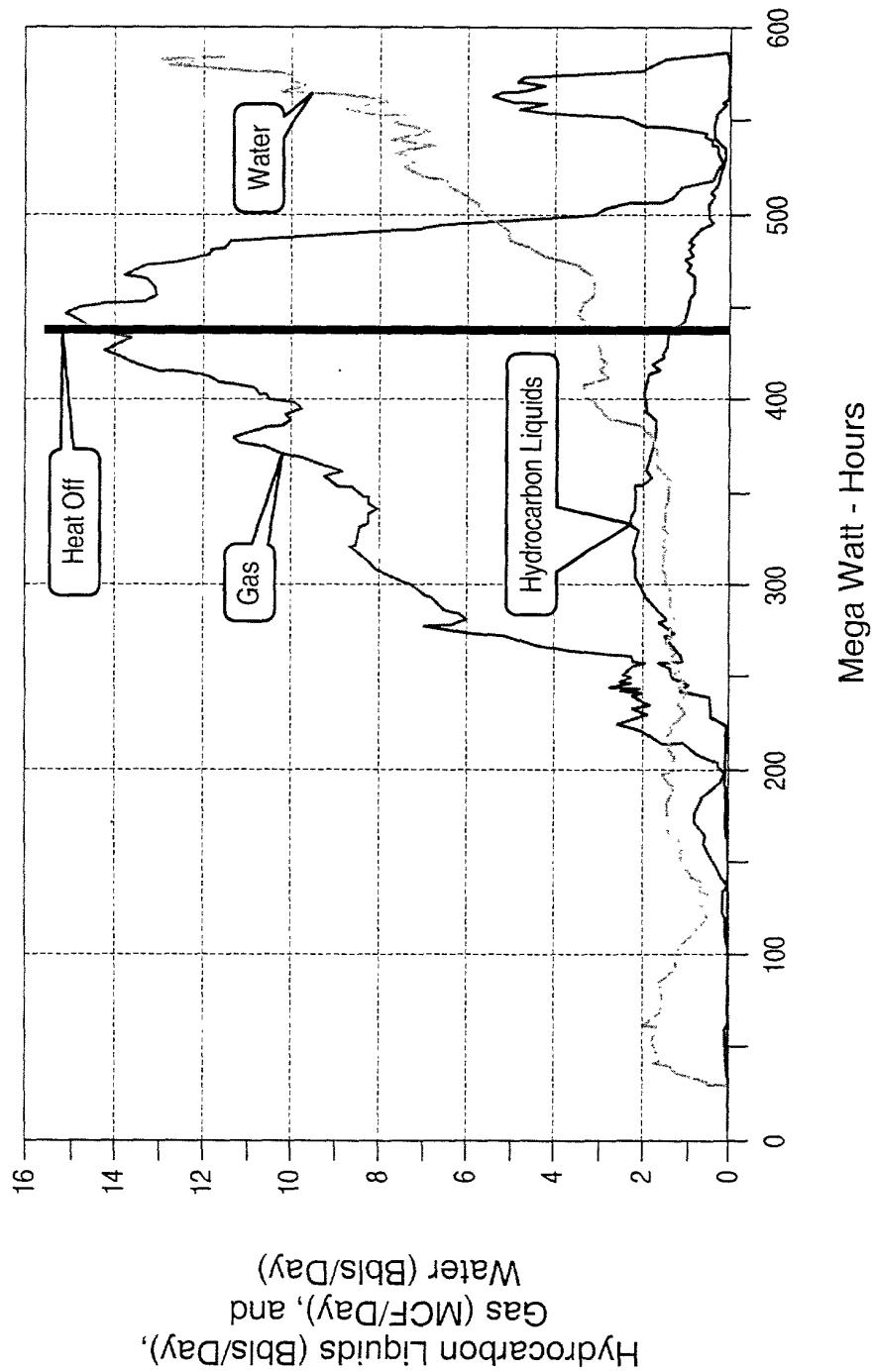


FIG. 176

100% 90% 80% 70% 60% 50% 40% 30% 20% 10% 0%  
 0 100 200 300 400 500 600 700 800 900 1000 1100 1200 1300 1400 1500 1600 1700 1800 1900 2000 2100 2200 2300 2400 2500 2600 2700 2800 2900 3000 3100 3200 3300 3400 3500 3600 3700 3800

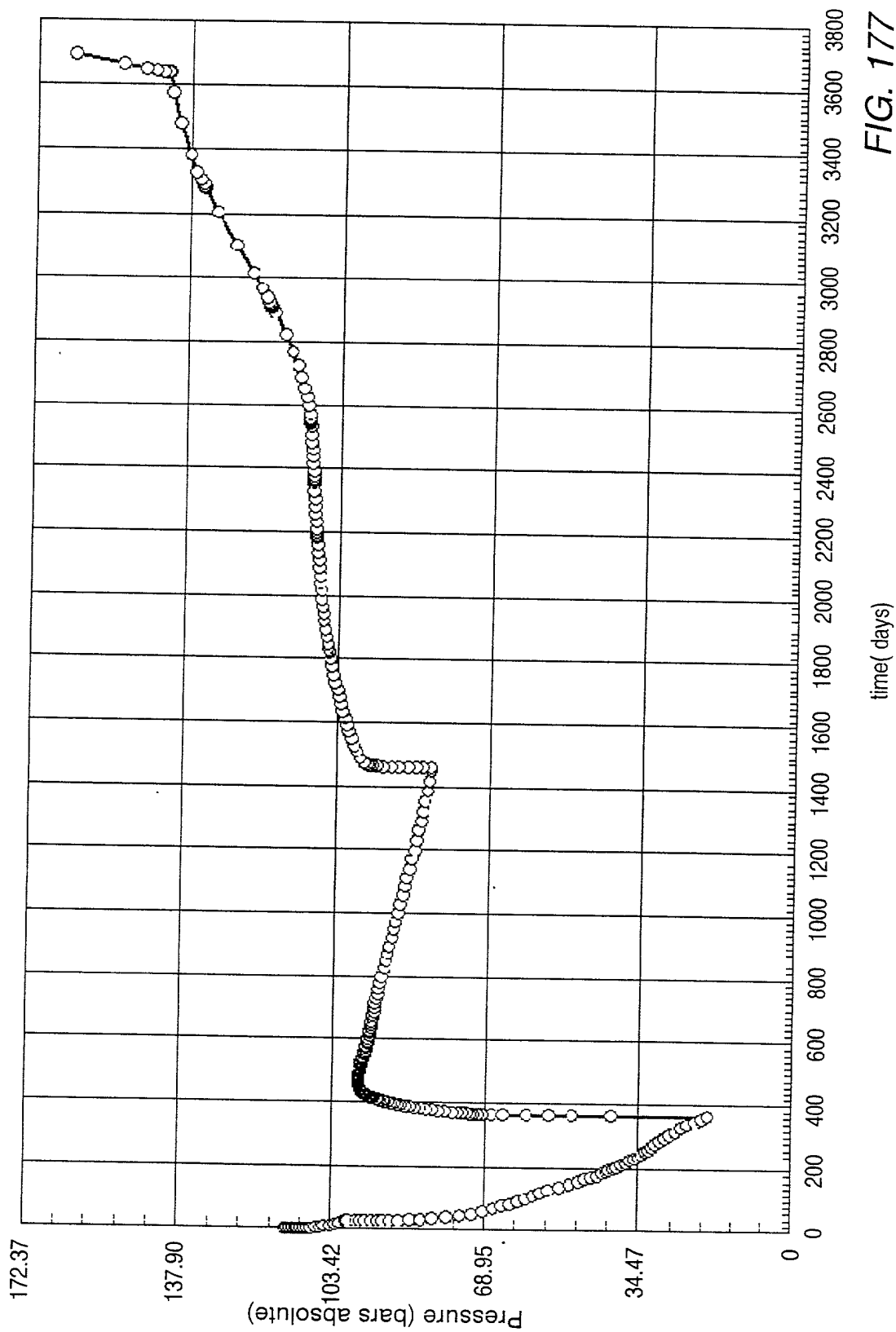


FIG. 177

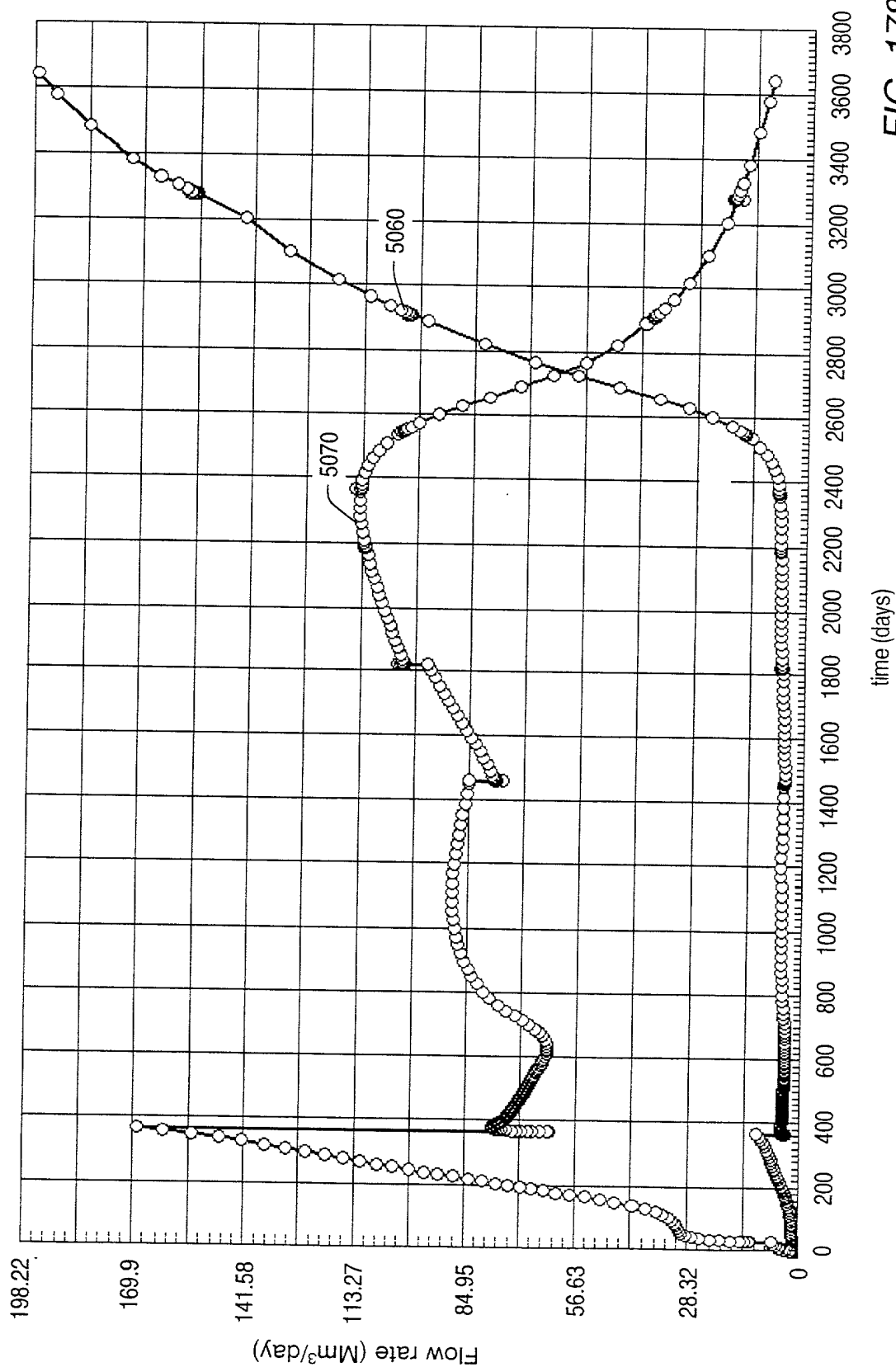


FIG. 178





**FIG. 180**

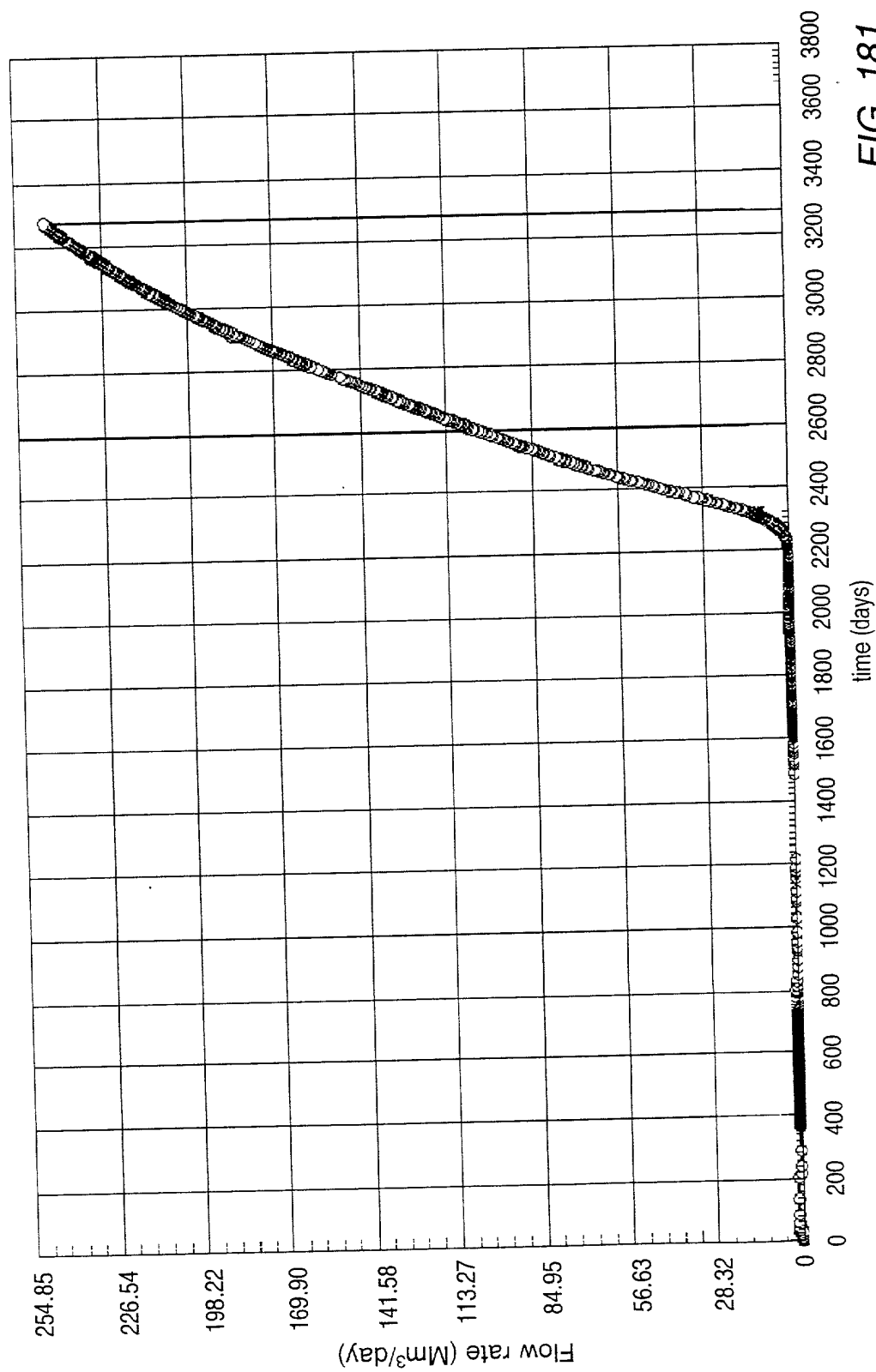


FIG. 181

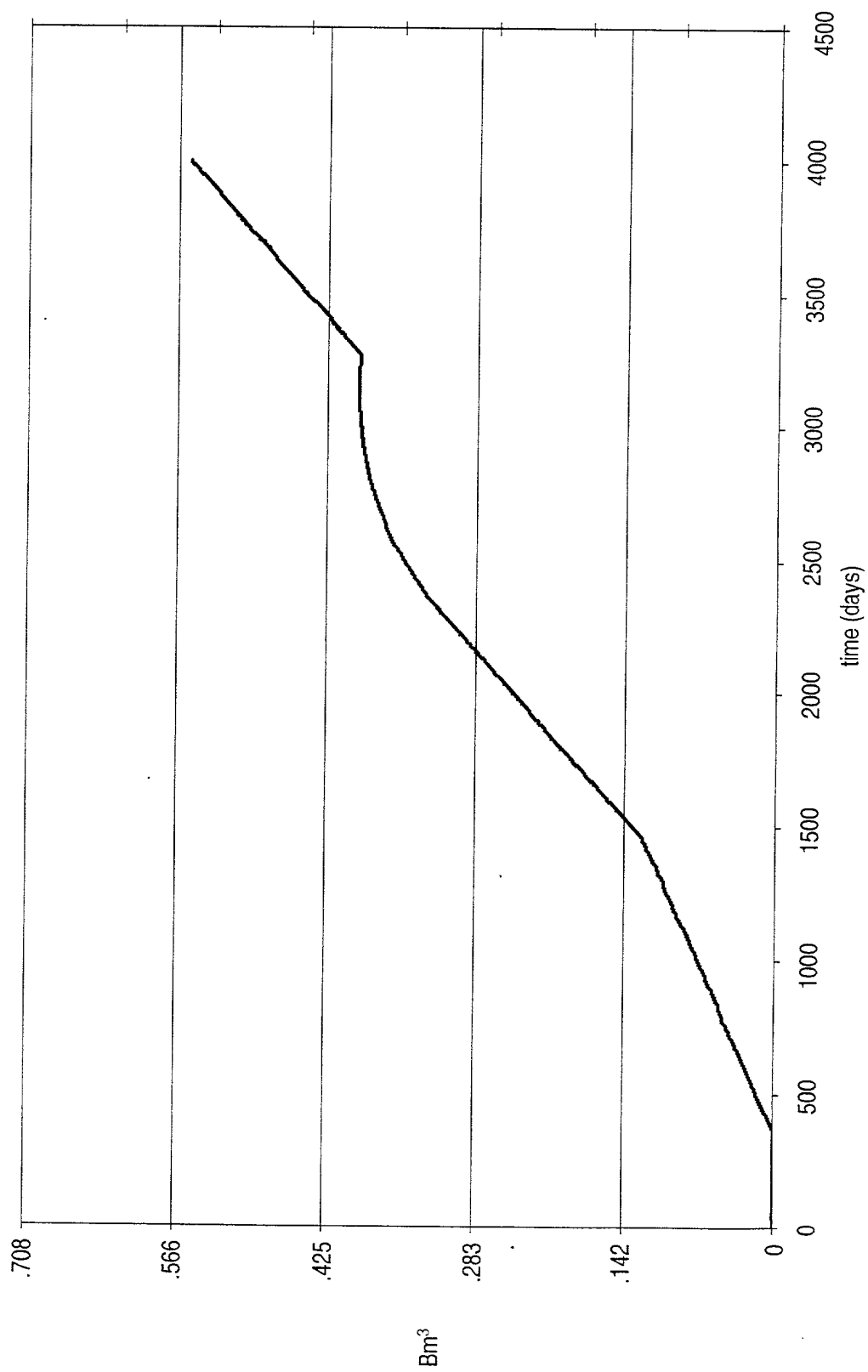


FIG. 182